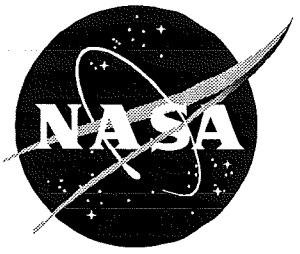

NASA Technical Memorandum 4640

Low-Speed Wind-Tunnel Investigation of the Stability and Control Characteristics of a Series of Flying Wings With Sweep Angles of 50°

Scott P. Fears, Holly M. Ross, and Thomas M. Moul

June 1995

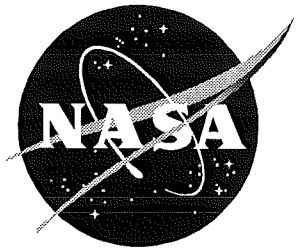

NASA Technical Memorandum 4640

Low-Speed Wind-Tunnel Investigation of the Stability and Control Characteristics of a Series of Flying Wings With Sweep Angles of 50°

Scott P. Fears
Lockheed Engineering & Sciences Company • Hampton, Virginia

Holly M. Ross and Thomas M. Moul
Langley Research Center • Hampton, Virginia

June 1995

Available electronically at the following URL address: http://techreports.larc.nasa.gov/ltrs/ltrs.html

Printed copies available from the following:

NASA Center for AeroSpace Information
800 Elkridge Landing Road
Linthicum Heights, MD 21090-2934
(301) 621-0390

National Technical Information Service (NTIS)
5285 Port Royal Road
Springfield, VA 22161-2171
(703) 487-4650

Summary

A wind-tunnel investigation was conducted in the Langley 12-Foot Low-Speed Tunnel to study the low-speed stability and control characteristics of a series of four flying wings over an extended range of angle of attack (−8° to 48°). Because of the current emphasis on reducing the radar cross section (RCS) of new military aircraft, the planform of each wing was composed of lines swept at a relatively high angle of 50°, and all the trailing-edge lines were aligned with one of the two leading edges. Three arrow planforms with different aspect ratios and one diamond planform were tested. The models incorporated leading-edge flaps for improved longitudinal characteristics and lateral stability and had three trailing-edge flaps that were deflected differentially for roll control, symmetrically for pitch control, and in a split fashion for yaw control. Three top body widths and two sizes of twin vertical tails were also tested on each model. A large aerodynamic database was compiled that could be used to evaluate some of the trade-offs involved in the design of a configuration with a reduced RCS and good flight dynamic characteristics.

The four wings produced similar amounts of lift, but a slight increase in lift occurred as aspect ratio was increased. The configurations were balanced to exhibit neutral longitudinal stability at low angles of attack, and a stable break occurred above maximum lift. The onset of tip separation on the outboard wing panels of the arrow wings caused pitch-up effects for angles of attack near maximum lift, and consequently the stable break on the arrow wings was less pronounced than on the diamond wing. Deflecting the leading-edge flaps improved maximum lift and made the pitching-moment variation with angle of attack more linear throughout the angle-of-attack range.

When deflected symmetrically for pitch control, trailing-edge flaps with a rearward-swept hinge line were more effective than comparably sized flaps with a forward-swept hinge line. In general, the nose-down flap effectiveness decayed at the higher angles of attack because the combination of nose-down flap deflection and high angle of attack caused the flow to separate from the tops of the flaps. As a result, the nose-down flap effectiveness was less linear with deflection angle than the nose-up control. Although the longitudinal stability level of a final design might have to be adjusted, all these configurations could be statically trimmed at angles of attack up to maximum lift by using more than one set of flaps. However, additional control power may be needed to provide a control margin for dynamic situations such as maneuvering or countering turbulence. An additional limit on the trim capability of these wings may be imposed by the need to budget the amount of flap deflection available for each type of control (pitch, roll, or yaw).

When the vertical tails were not used, each of the wings exhibited essentially neutral directional stability. Each wing was laterally stable for angles of attack below maximum lift, but a region of lateral instability existed near maximum lift on most of the configurations. The lateral instabilities became larger when aspect ratio was increased or when top bodies were added to the wings. Both directional and lateral stability were improved by adding twin vertical tails, and lateral stability was improved by deflecting the leading-edge flaps.

The trailing-edge flaps were deflected differentially for roll control and were split on one side for yaw control. Differential deflections of the middle flaps were generally effective over a larger range of angle of attack than either the inboard or outboard flaps. When split, the side force produced by the flaps was highly dependent on the sweep of the flap hinge line. On the forward-swept flaps, the side force produced a yawing-moment increment that opposed the yawing-moment increment produced by the drag on the flap. In contrast, the side force generated by split deflection of the rearward-swept flaps produced yawing-moment increments in the same direction as the drag, and therefore the rearward-swept flaps provided more effective yaw control than the forward-swept flaps. Deflections of all-moving twin vertical tails provided yaw control below maximum lift that became more effective as the wing aspect ratio decreased.

Introduction

Recent advances in low-observables technology, which increase the effectiveness and survivability of military aircraft, have strongly influenced most new designs. When attempting to achieve low observability, some or all of the aircraft signatures (radar, infrared, visual, or acoustic) may be considered, depending on mission requirements. One primary method of reducing radar observability is to decrease the radar cross section (RCS) of the aircraft by appropriately tailoring the external contours of the configuration. However, when these reduced-RCS shaping constraints are emphasized, the resulting aircraft may have an unconventional forebody shape, wing planform, or tail geometry. Each of these design features can have a large influence on the stability and control characteristics of the configuration; thus, a potential conflict exists between achieving a reduced RCS and achieving good flight dynamic characteristics. If the aircraft is a fighter, effective maneuverability during close-in engagements will require good stability and control characteristics for angles of attack up to and beyond maximum lift. As a result, designers will be required to balance the attributes of maneuverability and

low observability to create a fighter that will be successful in both close-in and beyond-visual-range engagements. For other types of aircraft, the stability and control requirements may be less stringent, and the designs may be more strongly influenced by low-observability considerations.

This study consists of an investigation of flying wing candidates for aircraft with reduced RCS. The wing planforms have highly swept leading and trailing edges, and the trailing edges are aligned with one of the two leading edges (fig. 1). The wings are divided into three groups corresponding to the sweep angles of the leading and trailing edges (50°, 60°, and 70°). Each group consists of a diamond planform and three arrow planforms of different aspect ratios (fig. 2). As a result of the high sweep angles, some of the planforms are somewhat unconventional in appearance.

This report presents the results of a static low-speed wind-tunnel investigation of the group of flying wings with sweep angles of 50°. The results for the wings with sweep angles of 60° are reported in reference 1, and the results for the wings with sweep angles of 70° are reported in reference 2. Tests were conducted to determine the low-speed stability and control characteristics of the basic wing planforms over a wide range of angle of attack. In addition, a number of different control concepts, a broad matrix of control settings, differences in top body width, and variations in vertical tail size were also tested. The data obtained on these wing planforms contribute to an aerodynamic database that could be used in defining some of the trade-offs associated with designing for both reduced RCS and good stability and control characteristics.

Symbols

All longitudinal forces and moments are referred to the stability-axis system, and all lateral-directional forces and moments are referred to the body-axis system (fig. 1). The longitudinal location of the moment reference center (MRC) varied among the different wings. This position was chosen such that each configuration would have neutral longitudinal stability at low angles of attack when all the controls were undeflected (table I). The MRC vertical position was fixed at 1.87 in. (4.9 percent of root chord) below the wing horizontal plane on all the configurations. The total planform area (table I) was used to nondimensionalize the force and moment data.

b wingspan, ft

C_D drag coefficient, $\frac{\text{Drag force}}{\bar{q}S}$

C_L lift coefficient, $\frac{\text{Lift force}}{\bar{q}S}$

C_l rolling-moment coefficient, $\frac{\text{Rolling moment}}{\bar{q}Sb}$

C_m pitching-moment coefficient, $\frac{\text{Pitching moment}}{\bar{q}S\bar{c}}$

C_n yawing-moment coefficient, $\frac{\text{Yawing moment}}{\bar{q}Sb}$

C_Y side-force coefficient, $\frac{\text{Side force}}{\bar{q}S}$

$\bar{c}$ mean aerodynamic chord (based on entire planform), ft

$\bar{q}$ free-stream dynamic pressure, lb/ft^2

S reference area (based on entire planform), ft^2

X,Y,Z longitudinal, lateral, and vertical body axes, respectively

α angle of attack, deg

β angle of sideslip, deg

ΔC_l incremental rolling-moment coefficient, C_l, control deflected – C_l, control undeflected

ΔC_n incremental yawing-moment coefficient, C_n, control deflected – C_n, control undeflected

ΔC_Y incremental side-force coefficient, C_Y, control deflected – C_Y, control undeflected

$\delta_{a,\text{IB}}$ differential deflection angle of inboard trailing-edge flaps based on equal and opposite deflection, positive with trailing edge down on right wing, measured normal to hinge line, deg

$\delta_{a,\text{MID}}$ differential deflection angle of middle trailing-edge flaps based on equal and opposite deflection, positive with trailing edge down on right wing, measured normal to hinge line, deg

$\delta_{a,\text{OB}}$ differential deflection angle of outboard trailing-edge flaps based on equal and opposite deflection, positive with trailing edge down on right wing, measured normal to hinge line, deg

δ_{bf} symmetric deflection angle of body flaps, positive with trailing edge down, measured normal to hinge line, deg

$\delta_{f,\text{IB}}$ symmetric deflection angle of inboard trailing-edge flaps, positive with trailing edge down, measured normal to hinge line, deg

$\delta_{f,\text{MID}}$ symmetric deflection angle of middle trailing-edge flaps, positive with trailing edge down, measured normal to hinge line, deg

$\delta_{f,\text{OB}}$ symmetric deflection angle of outboard trailing-edge flaps, positive with trailing edge down, measured normal to hinge line, deg

δ_{LEF} leading-edge flap deflection angle, positive with leading edge down, measured normal to hinge line, deg

δ_r symmetric vertical tail deflection angle, positive with trailing edge left, deg

$\delta_{s,MID}$ split deflection angle of middle trailing-edge flaps, positive when deployed on left wing, measured normal to hinge line, deg

$\delta_{s,OB}$ split deflection angle of outboard trailing-edge flaps, positive when deployed on left wing, measured normal to hinge line, deg

Derivatives:

C_{l_β} lateral stability parameter, $\frac{\partial C_l}{\partial \beta}, \frac{(C_l)_{\beta=5} - (C_l)_{\beta=-5}}{10°}$, per deg

C_{n_β} directional stability parameter, $\frac{\partial C_n}{\partial \beta}, \frac{(C_n)_{\beta=5} - (C_n)_{\beta=-5}}{10°}$, per deg

C_{Y_β} side-force parameter, $\frac{\partial C_Y}{\partial \beta}, \frac{(C_Y)_{\beta=5} - (C_Y)_{\beta=-5}}{10°}$, per deg

Abbreviations:

MRC moment reference center

RCS radar cross section

Model Description

Four flying-wing models (three arrow-wing planforms and one diamond planform) with leading- and trailing-edge sweep angles of 50° (fig. 2) were tested. Given the relatively high sweep angle, initial sizing analysis indicated that arrow wings with aspect ratios between 2.0 and 3.0 could produce viable configurations. As a result, aspect ratios of 3.0 (Wing 9), 2.5 (Wing 10), and 2.0 (Wing 11) were chosen for the arrow planforms (figs. 3 to 5). Unlike the aerodynamic data that were nondimensionalized with the entire planform area, these aspect ratios were computed by using the trapezoidal area shown in figure 2(b). For Wing 9, the three aftmost points on the planform extended back the same distance (fig. 3). During formulation of the remaining planforms, the overall length was held constant, and the trapezoidal areas of Wings 10 and 11 were made approximately equal to that of Wing 9. Consequently, as aspect ratio was decreased on the arrow wings, the span was reduced and the tip chord was increased to maintain approximately the same trapezoidal area. The dimensions of the diamond wing (fig. 6) were dictated by the overall length and the leading- and trailing-edge sweep angles and resulted in an aspect ratio of 1.68. From a geometric point of view, the arrow planforms can be considered to be built up from the diamond planform by the addition of outboard panels having the same sweep angles as the diamond planform (fig. 2). Flat plate models of the basic planforms were constructed from 3/4-in. plywood, and the leading and trailing edges were beveled at a 7° half-angle. Table I shows the geometric characteristics for each wing.

All four wings incorporated leading-edge flaps for improved longitudinal characteristics and increased roll stability at high angles of attack. The chord length of these flaps was the same on all the wings, and the hinge line was located along the leading-edge bevel line (fig. 2). These flaps were tested at deflection angles of 15°, 30°, and 45°. Segmented trailing-edge flaps that were designated inboard (IB), middle (MID), and outboard (OB) were also included on Wings 9, 11, and 12 for roll, pitch, and yaw control (figs. 3, 5, and 6). Wing 10 had only middle and outboard trailing-edge flaps (fig. 4). For the arrow wings, the chord length of the trailing-edge flaps was 30 percent of the length between the leading and trailing edges on the outboard section of the wing. For the diamond wing, the trailing-edge flaps had the same chord length as those on the arrow wing with the lowest aspect ratio (Wing 11). The trailing-edge flaps were deflected symmetrically (–30°, –15°, 15°, and 30°) for pitch control and differentially (–30°) for roll control. Split deflection of these flaps (to be discussed subsequently) was tested as a means to provide yaw control.

To provide supplemental nose-down pitch control, body flaps were tested by using model parts constructed of sheet metal (fig. 7). The body flaps were mounted on the underside of the wing inboard of the trailing-edge flaps. The inboard corners of the undeflected body flaps were positioned on the centerline with their hinge line coinciding with the hinge line of the trailing-edge flaps (fig. 7). Symmetric downward deflections of 52° and 67° were tested on Wings 9, 10, and 11, but only the 67° deflection was tested on Wing 12. The sheet metal part modeled the bottom surface of a beveled body flap (fig. 8). Because these models had a trailing-edge bevel half-angle of 7°, the 60° bend in the sheet metal part represented a 67° deflection of the simulated beveled flap (fig. 8).

As noted previously, split deflection of the trailing-edge flaps to provide yaw control was tested. In this concept, a given flap would separate into top and bottom halves such that the top half would deflect upward and the bottom half would deflect downward. These deflections would be made on either the right or left wing only, thereby creating an unbalanced drag force and an

associated yawing moment. During these tests, sheet metal pieces were mounted on the underside of the wing beneath the middle or outboard trailing-edge flaps to represent the lower half of a split deflection. The upper half was simulated by deflecting the trailing-edge flap upward at the same angle (fig. 9). The tested deflection angles (37°, 67°, and 82°) were measured similar to the body flap deflection angles. For these tests, the split trailing-edge flaps were tested on the right wing.

Three top body shapes were tested on the upper surface of each wing in conjunction with a single bottom body that covered the balance (fig. 10). Some testing was done without a top body, but the bottom body was always on the wing to shield the balance from the airflow. The length and height of the top bodies were kept constant, but the width was varied to obtain the three top shapes (wide, medium, and narrow). The resulting cross-sectional shapes were semielliptical for the wide and narrow bodies and semicircular for the medium body (fig. 10). When installed, the front tip of the top bodies was 5 in. (13.1 percent of the root chord) aft of the leading edge of the wing, and the rear tip was the same distance forward of the wing trailing edge. The front tip of the bottom body was also 5 in. behind the leading edge, and the rear tip was 11.02 in. (28.8 percent of the root chord) forward of the wing trailing edge.

Two sets of vertical tails (small and medium) were tested (fig. 11). The planform of each tail was a 30°-60°-90° triangle with the leading edge swept 60° (fig. 12). The tails were sized such that the medium tail had twice the area of the small tail (table I). They were mounted in a twin tail configuration with zero cant and toe angle and were deflected as all-moving tails for directional control about a vertical axis located at one-half the vertical tail root chord. On some reduced-RCS aircraft (F-117, YF-22, and YF-23), the tails are canted to reduce their contributions to the total aircraft RCS. However, during this study, the tails were tested without cant so that the maximum levels of directional stability and control available from the triangular planforms could be determined. The vertical tails were longitudinally positioned on the wing so that the aftmost points of the undeflected tails were at the wing trailing edge (fig. 13).

Test Techniques and Conditions

The aerodynamic testing was performed in the Langley 12-Foot Low-Speed Tunnel. The model and balance were mounted in the test section on a sting and C-strut arrangement (fig. 14). The tests were conducted at a free-stream dynamic pressure of 4 lb/ft^2, which corresponds to a test Reynolds number of 0.70×10^6 for Wing 9, 0.75×10^6 for Wing 10, 0.80×10^6 for Wing 11, and 0.78×10^6 for Wing 12 based on the mean aerodynamic chord of each wing. A six-component internally mounted strain gauge balance was used to measure the aerodynamic loads. The static force and moment data were measured over an angle-of-attack range of −8° to 48° and over a sideslip range of −15° to 15°. The data at sideslip angles of −5° and 5° were used to calculate the lateral-directional stability derivatives (C_{l_β}, C_{n_β}, and C_{Y_β}) by means of a linear calculation between these two angles. Flow upwash corrections were included during the angle-of-attack calibration, but no corrections were made for flow sidewash, wall effects, or test section blockage.

Results and Discussion

Longitudinal Stability Characteristics

The longitudinal stability characteristics of the four flying wings are presented in the following figures:

Wing planform. Comparisons of the longitudinal characteristics of the four wings with various leading-edge flap deflections and top bodies are presented in figures 15 to 18. The data show a typical effect of increasing the span and aspect ratio of a wing. As the aspect ratio was increased, the lift curve slope increased, resulting in larger levels of lift for most of the test angle-of-attack range. With the leading-edge flaps deflected 45°, maximum levels of lift coefficient between approximately 0.90 and 1.05 were produced at an angle of attack of roughly 32°. When the leading-edge flaps were not deflected, the diamond wing exhibited significantly different stalling characteristics than the arrow wings. For the arrow wings, maximum lift occurred at an angle of attack of approximately 24°. The diamond wing exhibited the onset of separation at a lower angle of attack (20° with the top body off and 16° with the wide top body on), and maximum lift occurred at a higher angle of attack (36° with the top body off and 32° with the wide top body on).

As mentioned previously, the moment reference centers (figs. 3 to 6 and table I) were chosen so that each configuration with the wide top body (fig. 17) would have neutral longitudinal stability at angles of attack near 0° when all the controls were undeflected. As a result, the pitching-moment characteristics of each of the wings exhibited a neutral level of longitudinal stability for angles of attack below maximum lift, but above maximum lift a stable break occurred that became more pronounced as aspect ratio was decreased. For the arrow wings, larger aspect ratios were obtained by adding outboard wing panels of increasing size to the basic diamond shape. These additional components of the planforms with the higher aspect ratios caused the arrow wings to experience pitch-up effects that reduced the magnitude of the stable break. Previous studies have shown that the onset of tip separation on the outboard portions of swept wings can result in a reduction in longitudinal stability that is sometimes called pitch-up (refs. 3 and 4), which may be more pronounced when the outboard portions of the swept wings are farther behind the moment reference center.

Top bodies. The effects of the various top bodies (fig. 10) on the longitudinal characteristics of the different wings are shown in figures 19 to 26. The primary effect of adding a top body was a small reduction in maximum lift. This lift reduction became larger as the width of the top body was increased. The top bodies had minimal effects on the pitching-moment characteristics of these wings.

Leading-edge flaps. The effects of deflections of the leading-edge flaps on the longitudinal characteristics of the different wings are shown in figures 27 to 34. Data are shown for the four planforms with the top body removed in figures 27 to 30 and with the wide top body on in figures 31 to 34. For the arrow wings, the data show some typical effects of leading-edge flap deflections. Deflections of these flaps increased the angle of attack for maximum lift (ref. 5). This effect became more prevalent as aspect ratio was increased. Because of the previously discussed differences in the stall behavior of the arrow and diamond wings, leading-edge flap deflections produced much smaller changes in maximum lift on the diamond wing than on the arrow wings. At the lower angles of attack, these deflections resulted in lift losses on all the wings because they caused the flow to separate from the lower surface of the wing. On an actual aircraft, these lift losses would be minimized by appropriately scheduling the leading-edge flap deflections with angle of attack.

In addition to lift, the pitching-moment characteristics of each of the wings were also significantly affected by deflecting the leading-edge flaps. These deflections increased the low-angle-of-attack longitudinal stability level and reduced the effects of the stable break that occurred above maximum lift. As a result, the variation of pitching moment with angle of attack was more linear on each configuration when the leading-edge flaps were deflected. On the arrow wings, both the maximum lift and nose-down pitching moments were increased at the larger deflection angles.

Vertical tails. Figures 35 to 39 show the effects of adding the twin vertical tails (figs. 12 and 13) on the longitudinal characteristics of the four configurations with the narrow top body on. The addition of the vertical tails caused a small reduction in lift coefficient near maximum lift for each of the wings. This lift reduction was possibly due to the tails interfering with the leading-edge vortical flow on the upper surfaces of the wings, causing these vortices to burst earlier. A flow field investigation (flow visualization, laser Doppler velocimeter, pressure measurements, etc.) would be required to make this determination. Adding the twin vertical tails had negligible effect on the pitching-moment characteristics of these wings.

Longitudinal Control Characteristics

The longitudinal control characteristics of the four flying wings are presented in the following figures.

Inboard trailing-edge flaps. The longitudinal control effectiveness of symmetric deflections of the inboard trailing-edge flaps for Wings 9, 11, and 12 is shown in figures 40 to 42. Because of the way the configurations were designed, Wing 10 did not have inboard trailing-edge flaps. Deflections of the inboard flaps produced small pitching moments that were largest on Wing 11 and smallest on Wing 9. These differences in effectiveness were due primarily to the differences in flap size and longitudinal moment arm between the different configurations. At the lower angles of attack, trailing-edge-down deflections (subsequently called nose-down deflections because they produce nose-down pitching-moment increments) were generally more effective than trailing-edge-up (nose-up) deflections. At the higher angles of attack, the effectiveness of the flaps reversed. The nose-up deflections became more effective, and the nose-down effectiveness was significantly reduced. The linearity of these controls with deflection angle can be inferred from the intermediate deflection angles tested on Wings 11 and 12. With the exception of the low-angle-of-attack nose-up control on Wing 11, a 15° deflection provided almost as much control effectiveness as a 30° deflection, and these flaps therefore did not provide linear control effectiveness. Considering the reduction in nose-down effectiveness that occurred at the higher angles of attack, the large flow-turning angle resulting from the combination of a large nose-down deflection and a high angle of attack most likely caused the flow over the tops of the control surfaces to separate, making the flaps less effective at these conditions.

Middle trailing-edge flaps. Figures 43 to 46 show the longitudinal control effectiveness of symmetric deflections of the middle trailing-edge flaps. Because they had longer longitudinal moment arms and larger areas, the middle flaps were more effective for Wings 9 and 10 than they were for Wings 11 and 12. A comparison of the effectiveness of the middle flaps shows that the pitch control effectiveness appeared to depend on whether the hinge line was swept forward or rearward. The forward-swept middle flaps on Wings 11 and 12 behaved similarly to the inboard flaps. The foward-swept flaps were more effective than the rearward-swept flaps (Wings 9 and 10) in the nose-down direction at low angles of attack, and they were more effective in the nose-up direction at the higher angles of attack. Also, the nose-down effectiveness of these flaps decreased significantly at the higher angles of attack. In contrast, the rearward-swept flaps on Wings 9 and 10 were equally effective in the nose-up and nose-down directions at low angles of attack, and the nose-down effectiveness did not decrease as significantly at the higher angles of attack. Also, the control effectiveness of the rearward-swept flaps on Wing 10 was more linear with deflection angle than that of the forward-swept flaps on Wings 11 and 12. These results could possibly be related to the deflected flaps interacting with any spanwise flow occurring on the swept wings.

Inboard and middle trailing-edge flaps. The longitudinal control effectiveness produced when the inboard and middle trailing-edge flaps were deflected symmetrically is shown for Wings 9, 11, and 12 in figures 47 to 51. At low angles of attack, the multiple deflections produced similar effectiveness in both the nose-up direction and the nose-down direction. However, as noted previously for the individual deflections, the flaps lost effectiveness in the nose-down direction at the higher angles of attack, and a nose-down control reversal occurred for Wing 12. Intermediate multiple deflections were tested for Wings 11 and 12, and these results suggested that the nose-up control was more linear with deflection angle than the nose-down control, especially at the higher angles of attack. These results were due in part to the previously discussed combination of a maximum nose-down deflection and a high angle of attack, which caused the flow over the tops of the flaps to separate, and the effectiveness of the flaps was thereby reduced for these conditions. For Wings 11 and 12, deflecting the leading-edge flaps 45° did not have a significant effect on the control effectiveness produced by

multiple deflections of the inboard and middle trailing-edge flaps.

All these configurations could be statically trimmed to angles of attack between 16° and 26° by using the inboard and middle trailing-edge flaps together. Above these angles of attack, the wings lacked the necessary nose-up control required for trim. If the longitudinal stability was decreased slightly, these configurations could be statically trimmed to higher angles of attack approaching the region of maximum lift. If dynamic factors are considered, additional pitch control power may be needed to provide a control margin for use during situations such as maneuvering or countering turbulence (ref. 6). An additional limit on the trim capability of these wings may be imposed by the need to budget the amount of flap deflection available for each type of control (pitch, roll, or yaw). If some portion of the total flap travel must be reserved for roll or yaw control, the remaining amount available for pitch control will be less than the maximum, and the trim capability will be correspondingly reduced.

Outboard trailing-edge flaps. On Wings 10 and 11, the outboard trailing-edge flaps were deflected symmetrically (figs. 52 and 53). For Wing 10, deflections of the outboard flaps produced small pitching moments similar in character to those produced by the inboard flaps that also had a forward-swept hinge line. For Wing 11, the outboard flaps were ineffective. On both wings, the outboard flaps did not produce as large a lift or pitching-moment increment as the similarly sized middle flaps (figs. 4 and 5 and table I). The reduced pitch-control effectiveness was due to a combination of reduced aerodynamic loading (smaller C_L increment produced by deflection) and a shorter longitudinal moment arm on the outboard flaps.

Middle and outboard trailing-edge flaps. Because Wing 10 was designed without inboard trailing-edge flaps, it was tested with its middle and outboard flaps deflected symmetrically together (figs. 54 and 55). As with the combinations of deflections tested on the other wings, these multiple deflections produced comparable effectiveness in the nose-up and nose-down directions at the lower angles of attack. However, as noted previously for the individual deflections, the flaps lost effectiveness in the nose-down direction at the higher angles of attack. Intermediate multiple deflections were tested, and these results suggest that the longitudinal control was relatively linear with deflection angle with the exception of the nose-down control at the higher angles of attack. With the leading-edge flaps deflected 45°, Wing 10 could be statically trimmed to an angle of attack of 24°. If this configuration was rebalanced to be less longitudinally stable, it could be statically trimmed over the test angle-of-attack range, but additional analysis would be required to determine whether a sufficient dynamic pitch-control margin existed (ref. 6).

Maximum nose-down control. In addition to the trailing-edge flaps, each configuration also had body flaps on the bottom surface of the wing (fig. 8) that were intended to provide supplemental nose-down pitch control. The body flaps were tested in combination with nose-down deflections of the trailing-edge flaps, and the data are presented in figures 56 to 59. Deflections of the body flaps provided small nose-down pitching moments at the lower angles of attack for the arrow wings. Deflecting the body flaps beyond 52° to 67° did not increase effectiveness, and a control reversal actually occurred for the 67° deflection on Wing 10. For the diamond wing, the body flaps were much more effective than they were for the arrow wings, and their effectiveness was comparable to that of the trailing-edge flaps.

Lateral-Directional Stability Characteristics

The lateral-directional stability characteristics of the four flying wings are presented in the following figures.

Sideslip. The lateral-directional force and moment coefficients of the four wings with the wide top body on are presented in figures 60 to 75 as a function of sideslip angle at various angles of attack and leading-edge flap settings. When the leading-edge flaps were undeflected, the coefficients were generally linear functions of sideslip angle at angles of attack of 0°, 12°, 32°, and 48°. At the intermediate angles of attack of 16° and 20°, where some portion of the wings was most likely experiencing separated flow, the variations in the lateral-directional coefficients with sideslip were nonlinear. When the leading-edge flaps were deflected 45°, the flow over the wings was most likely improved at the intermediate angles of attack, and the lateral-directional coefficients generally became more linear at angles of attack of 16° and 20°.

Wing planform. Comparisons of the lateral-directional stability characteristics (computed between sideslip angles of −5° and 5°) of the four wings with various leading-edge flap deflections and top bodies are presented in figures 76 to 79. Note that the data are for the configurations without vertical tail surfaces, and therefore each of the wings possessed essentially neutral values of directional stability (C_{n_β}) throughout the test angle-of-attack range.

Each of the wings was laterally stable (negative C_{l_β}) at the lower angles of attack. However, the lateral stability was reduced at angles of attack near maximum lift, and most of the configurations were laterally unstable for part of this range of angle of attack. This phenomenon is a well-documented characteristic of highly swept wings that is due primarily to asymmetric breakdown of the wing leading-edge vortices at sideslip conditions (ref. 7). Changes in wing planform had a significant effect on the magnitude of the lateral instabilities. In general, increases in aspect ratio resulted in larger levels of lateral instability, and the diamond wing was typically more laterally stable than the arrow wings in this angle-of-attack range. These results indicate that the outboard panels added to the basic diamond planform to create the higher aspect ratios caused the observed reductions in lateral stability for the arrow wings.

Top bodies. The effects of the various top bodies (fig. 10) on the lateral-directional stability characteristics of the four wings are shown in figures 80 to 87. With the leading-edge flaps undeflected, Wing 9 was tested with each of the top bodies (fig. 80), and Wings 10, 11, and 12 were tested with the top body off and with the wide top body on (figs. 81 to 83). Each of the top bodies (wide, medium, and narrow) was tested on the wings when the leading-edge flaps were deflected 45° (figs. 84 to 87).

With the exception of Wing 12, additions of the top bodies had minimal impact on the directional stability of the four wings. For Wing 12 (fig. 87), adding the various top bodies caused small destabilizing increments in C_{n_β} throughout the test angle-of-attack range.

The effects of adding the top bodies on lateral stability were more pronounced. When the leading-edge flaps were undeflected, the lateral instabilities that occurred near maximum lift were increased significantly by adding the top bodies. For Wing 9, these increases in lateral instability became larger as the width of the top body was increased (fig. 80). When the leading-edge flaps were deflected 45°, the results were less consistent. In general, the configurations with the narrow top body had the highest levels of lateral instability, but these lateral instabilities were at the higher angles of attack above maximum lift. These changes in lateral stability indicated that the top bodies had an effect on the separation patterns of the flow on the upper surfaces of the wings.

Leading-edge flaps. The effects of leading-edge flap deflections on the lateral-directional stability characteristics of the four wings are shown in figures 88 to 95. Data are shown for the four planforms with the top body

removed in figures 88 to 91 and with the wide top body on in figures 92 to 95. Leading-edge flap deflections had minimal impact on the directional stability of the four wings.

In contrast to directional stability, leading-edge flap deflections significantly affected lateral stability for both the body-off and wide-body-on configurations. As stated in the section "Longitudinal Stability Characteristics" (p. 4), leading-edge flap deflections increased the angle of attack at maximum lift. Similarly, when the top body was off, the 45° deflection caused the lateral instabilities present near maximum lift to also occur at higher angles of attack. With the wide-body-on, a deflection of 30° eliminated the majority of lateral instability on each of the wings, and a deflection of 45° actually caused lateral instabilities at the higher angles of attack. For this reason, when considering lateral stability, the 30° leading-edge flap deflection was more desirable than the 45° deflection for these wings. The improvements in lateral stability provided by the leading-edge flap deflections would permit these wings to operate over a larger range of angles of attack without encountering regions of lateral instability.

Vertical tails. The effect of the small and medium twin vertical tails (figs. 11 to 13) on the lateral-directional stability characteristics of the four wings with the narrow top body on is shown in figures 96 to 100. Use of the narrow top body for the tails-on testing enabled the tails to be deflected through larger angles before they interfered with the body.

As expected, adding the tails provided directionally stabilizing increments in C_{n_β} on each of the wings for angles of attack below maximum lift, and the medium tails produced larger increments than the small tails. For angles of attack above maximum lift, the tails were located in the low-energy wake above the wings, and they were therefore ineffective. As a result of these improvements in directional stability, each of the configurations with tails was directionally stable for most of the angles of attack tested. As aspect ratio was decreased, the tails produced larger increments in directional stability. The cause for this effect was not determined during this study. Comparison of the data for Wing 9 when the leading-edge flaps were deflected (fig. 97) with the data when the leading-edge flaps were undeflected (fig. 96) shows that deflecting the leading-edge flaps increased the angle-of-attack range over which the vertical tails provided directionally stabilizing increments. This result indicates that the improved flow quality over the tops of the wings, which resulted from deflecting the leading-edge flaps, caused the tails to be more effective.

The effect of the tails on lateral stability were varied between the different configurations. Even though they produced side forces and yawing moments, adding the tails did not significantly change the lateral stability of the arrow wings for angles of attack below 16° (figs. 96 to 99). The presence of the vertical tails probably caused an induced load on the aft sections of the wing because of an end plate effect (ref. 8). This induced load would result in a rolling moment in the opposite direction to the rolling moment generated by the vertical tails in sideslip. Because these two rolling moments are typically of similar magnitudes, they tend to cancel each other so that addition of the tails has minimal effect on the lateral stability at the lower angles of attack. For the diamond wing (fig. 100), the vertical tails increased lateral stability at these angles of attack. The tails produced larger changes in lateral stability on this wing because the induced loads were most likely smaller on the diamond planform. When the leading-edge flaps were deflected (figs. 97 to 100), adding the small vertical tails significantly reduced the lateral instabilities at the higher angles of attack near maximum lift and adding the medium tails eliminated these instabilities on each wing. These beneficial lateral stability effects could possibly be attributed to a favorable interference effect produced by the vertical tails. The tails were most likely obstructing any vortex flow on the upper surfaces of the wings at the higher angles of attack, thereby improving the lateral stability by causing a more symmetric bursting of these vortices. This premise is supported by the previously discussed losses in maximum lift that resulted when the vertical tails were added to the configuration (figs. 35 to 39).

Lateral Control Characteristics

The lateral control characteristics of the four flying wings are presented in the following figures.

The lateral controls tested on these wings consisted of differential deflections of the inboard, middle, and outboard trailing-edge flaps. On each of the wings, the middle and outboard flaps were tested separately and when deflected together. On the diamond wing (Wing 12), the inboard flap was tested separately and deflected together with the middle flap. Figures 101 to 104 show the lateral control effectiveness of differential deflections of the various flaps for each of the wings

when the leading-edge flaps were deflected 45° and the wide top body was used.

For each of the wings, differential deflections of the middle flaps produced levels of roll-control effectiveness comparable to that of the outboard flaps for angles of attack below approximately 8°. As angle of attack was increased above 8°, the effectiveness of the outboard flaps was reduced significantly, and a control reversal occurred at an angle of attack of approximately 18° on Wings 11 and 12. In contrast, the effectiveness of the middle flaps did not decrease as rapidly as angle of attack was increased. As a result, the middle flaps were generally effective over a larger range of angle of attack than the outboard flaps. On the diamond wing (fig. 104), the inboard flaps provided levels of roll-control effectiveness comparable to that of the middle flaps over a large range of angle of attack, despite the shorter moment arm of these flaps about the roll axis. Given the magnitudes of roll-control effectiveness generated by single and multiple deflections, the use of two or more sets of flaps for roll control may be required for these wings to achieve maximum lateral control throughout the test angle-of-attack range.

On the arrow wings, the yawing moments produced by differential deflections of the trailing-edge flaps were generally negligible at low angles of attack, but small adverse yawing moments were typically generated at the higher angles of attack by deflections of the outboard flaps. On the diamond wing, differential deflections of the inboard flaps produced very small proverse yawing moments at the higher angles of attack. However, as with the arrow wings, deflections of the outboard flaps produced adverse yawing moments over the same angle-of-attack range.

Directional Control Characteristics

The directional control characteristics of the four flying wings are presented in the following figures.

Two types of directional controls, split trailing-edge flaps (figs. 7 and 9) and vertical tail deflections (figs. 12 and 13), were tested on these models. As discussed in the section "Model Description" (p. 3), the split trailing-edge flaps were designed to separate into a top half that would deflect upward and a bottom half that would deflect downward at the same angle, and they would be deflected on only one wing at a time. The resulting geometry would result in an unbalanced incremental drag force on the wing that would produce an associated yawing moment. The all-moving twin vertical tails were deflected about an unswept hinge post at the midpoint of the tail root chord.

Split trailing-edge flaps. The control effectiveness of split deflections of the outboard trailing-edge flaps for each of the wings with the wide top body on and the leading-edge flaps deflected 45° is shown in figures 105 to 108. All these deflections were made on the right wing to generate a positive yawing moment. Split deflections of the outboard flaps produced small yawing moments that were similar in magnitude for each of the wings. In addition to the drag forces produced by these deflections, analysis showed that these yawing moments were also strongly influenced by the side forces generated by these devices (fig. 123). The forward sweep of the hinge lines on the outboard flaps caused these surfaces to function as a left rudder deflection when deflected on the right wing. For this reason, split deflections of a surface with a forward-swept hinge line produced rudder-like side forces that generated yawing moments in the opposite direction to the yawing moments generated by the drag on the device, resulting in a lower net yawing moment (fig. 123). For the wing with the highest aspect ratio (Wing 9), split deflections of the outboard flaps produced negligible rolling moments. For the other wings (Wings 10, 11, and 12), split deflections of the outboard

flaps produced proverse rolling moments for most of the angles of attack tested that were due to a spoiler-like loss of lift on the wing on which the flaps were deflected. The magnitudes of these proverse rolling moments increased as the aspect ratio of the configurations was decreased.

Figures 109 to 112 show the control effectiveness of split deflections of the middle trailing-edge flaps for each of the wings with the wide top body on and the leading-edge flaps deflected 45°. As with the outboard flaps, the middle flaps were deflected on the right wing to generate positive yawing moments. Split deflections of the middle flaps on Wings 9 and 10 (figs. 109 and 110) produced yawing moments much larger than those produced by split deflections of the outboard flaps on these wings (figs. 105 and 106). These larger yawing moments primarily resulted from the difference in the sweep of the hinge lines between the middle and outboard flaps. In contrast to the forward sweep on the outboard flaps, the rearward sweep of the middle flaps on Wings 9 and 10 caused split deflections of these flaps to produce side forces in the opposite direction of those produced by comparable deflections of the outboard flaps. These side forces produced yawing moments in the same direction as the yawing moments produced by the drag forces, resulting in higher net yawing moments (fig. 123). The data for different deflection angles on Wings 9 and 10 (figs. 109 and 110) shows that the −67° deflection angle produced larger yawing moments than the −37° deflection angle at low angles of attack, but this control effectiveness was not always linear with deflection angle. The data for Wing 10 shows that the −82° deflection produced only slightly more yawing moment than the −67° deflection. Because the hinge lines of the middle flaps on Wings 11 and 12 were swept forward, these flaps were less effective, as were the outboard flaps on these wings. For Wings 9 and 10, negligible rolling moments were produced below an angle of attack of approximately 12°, and adverse rolling moments were generated above this angle of attack that were generally independent of deflection angle. Like the outboard flaps, the forward-swept middle flaps on Wings 11 and 12 generally produced rolling moments toward the wing on which the flap was split because of a spoiler-like loss of lift on that wing.

Vertical tails. Figures 113 to 117 show the control effectiveness of the small twin vertical tails on each of the wings with the narrow top body on. Deflections of the small tails produced yaw-control effectiveness that was relatively invariant for angles of attack below approximately 8°. As angle of attack was increased above 8°, the yaw-control effectiveness decreased as the tails became shielded by the wing and body, and the tails were essentially ineffective for angles of attack above approximately 32°. The tails became more effective as the aspect ratio of the configuration was decreased. As mentioned previously in the discusion of the effect of the vertical tails on lateral-directional stability (p. 9), the cause of this was not determined during this study. The −30° deflection of the small tails produced approximately twice the yaw control effectiveness of the −10° deflection on each of the wings, indicating that the yaw-control effectiveness of the small tails was not linear for deflections between −10° and −30°. At low angles of attack, deflections of the small tails produced proverse rolling moments on the arrow wings and adverse rolling moments on the diamond wing. On each of the wings, large adverse rolling moments occurred near maximum lift. For Wing 9, comparison of the data when the leading-edge flaps were undeflected (fig. 113) and deflected 45° (fig. 114) shows that leading-edge flap deflections had minimal effect on the yaw-control effectiveness of deflections of the small tails.

The control effectiveness of deflections of the medium twin vertical tails for each of the wings with the narrow top body on is shown in figures 118 to 122. The yaw-control effectiveness produced by deflections of the medium tails was generally larger than that generated by the small tails, but the angles of attack at which the effectiveness began to decrease (approximately 8°) and the tails became ineffective (approximately 36°) were similar to those for the small tails. As with the small tails, the medium tails became more effective as aspect ratio was decreased. The data for deflection angles of −10° and −21° (the lower maximum deflection angle for the medium tails resulted from the larger medium tails interfering with the body at a smaller deflection angle) indicated that the yaw-control effectiveness of the medium tails was linear with deflection angle for deflection angles below 21°. The rolling moments produced by deflections of the medium tails were also similar in character to, but larger in magnitude than, those produced by deflections of the small tails. On the arrow wings, small proverse rolling moments were generally produced at the lower angles of attack, and adverse rolling moments were produced near maximum lift. On the diamond wing, adverse rolling moments were produced throughout the test angle-of-attack range, with larger moments occurring near maximum lift. Comparison of the data when the leading-edge flaps were undeflected (fig. 118) and deflected 45° (fig. 119) on Wing 9 shows that leading-edge flap deflections had minimal effects on the yaw-control effectiveness of deflections of the medium tails.

Conclusions

A wind-tunnel investigation was conducted in the Langley 12-Foot Low-Speed Tunnel to study the low-speed stability and control characteristics of a series of four flying wings over an extended range of angle of

attack. Because of the current emphasis on reducing the radar cross section (RCS) of new military aircraft, the planform of each wing was composed of lines swept at a relatively high angle of 50°, and all the trailing-edge lines were aligned with one of the two leading edges. Three arrow planforms with different aspect ratios and one diamond planform were tested. The models incorporated leading-edge flaps for improved longitudinal characteristics and lateral stability and had trailing-edge flaps in three segments that were deflected differentially for roll control, symmetrically for pitch control, and in a split fashion for yaw control. Three top body widths and two sizes of twin vertical tails were also tested on each model. A large aerodynamic database was compiled that could be used to evaluate some of the trade-offs involved in the design of a configuration with a reduced RCS and good flight dynamic characteristics. The results of this investigation may be summarized as follows:

1. The maximum lift coefficient of the four wings ranged between 0.90 and 1.05 when the leading-edge flaps were deflected 45°. This maximum lift occurred at an angle of attack of about 32°. The moment reference centers were set such that each configuration exhibited neutral longitudinal stability at low angles of attack, but a stable break occurred above maximum lift.

2. Without vertical tail surfaces, each of the wings exhibited essentially neutral directional stability for most of the angles of attack tested. The configurations were laterally stable for angles of attack below maximum lift, but a region of lateral instability existed near maximum lift on most of the configurations. In general, the diamond wing was the most laterally stable of the four wings tested.

3. Increases in aspect ratio resulted in small increases in lift coefficient for this series of wings. The onset of tip separation on the outboard wing panels that were added to the basic diamond planform to create the arrow wings caused the arrow wings to experience pitch-up effects for angles of attack near maximum lift, and consequently the stable break was less pronounced on these wings. These planform additions also caused lateral instabilities near maximum lift that generally became larger as the aspect ratio was increased.

4. When the leading-edge flaps were not deflected, adding top bodies to the wings caused a small reduction in maximum lift and reduced lateral stability near maximum lift. These results indicated that the top bodies affected the separation patterns on the upper surfaces of the wings.

5. Leading-edge flap deflections improved the maximum lift on the arrow wings by increasing the angle of attack where the maximum lift occurred. These deflections also significantly affected the pitching-moment characteristics of each of the wings by increasing the low-angle-of-attack longitudinal stability level and by reducing the effects of the stable break. As a result, each configuration had a more linear variation of pitching moment with angle of attack when the leading-edge flaps were deflected. In addition, a deflection of 30° eliminated the lateral instability on each of the wings.

6. The addition of vertical tails provided expected increases in directional stability and improved lateral stability.

7. Trailing-edge flaps were deflected symmetrically for pitch control on each wing. Flaps with a rearward-swept hinge line were more effective in pitch than comparably sized flaps with a forward-swept hinge line. In general, the nose-down control effectiveness decayed at the higher angles of attack because the combination of a nose-down flap deflection and a high angle of attack caused the flow to separate from the tops of the flaps, and the nose-down control of the flaps was consequently less linear with deflection angle than the nose-up control. Depending on the longitudinal stability level of a final design, all these configurations could be statically trimmed at angles of attack up to maximum lift when using more than one set of flaps. However, dynamic analysis would be required to determine whether an adequate control margin existed for control during maneuvers or stability in gusts. An additional limit on the trim capability of these wings may be imposed by the need to budget the amount of flap deflection available for each type of control (pitch, roll, or yaw).

8. Differential deflections of the trailing-edge flaps were tested for roll control on each wing. The middle flaps were generally effective over a larger range of angle of attack than the inboard or outboard flaps. The magnitude of roll control generated by a given set of flaps indicates that combined deflections of more than one set of flaps may be required for each of these wings to have acceptable roll-control capability throughout the test angle-of-attack range.

9. Split deflections of the middle and outboard trailing-edge flaps were tested for yaw control. When split, the forward-swept outboard trailing-edge flaps were not effective. This result occurred because the yawing moment produced by the side force on these flaps opposed the yawing moment produced by the drag, resulting in a lower net moment. For two of the arrow wings, the middle trailing-edge segments were swept aft, and the yawing moment from the side force and drag on these flaps acted in the same direction, resulting in a large net yawing moment. For this reason, split deflection of the rearward-swept middle flaps is an attractive candidate for yaw control for these two arrow wings.

10. Deflection of all-moving twin vertical tails was also tested for yaw control. The tails provided yaw control below maximum lift that became more effective as the wing aspect ratio was decreased, but they were ineffective above maximum lift, where they became immersed in the low-energy wake of the stalled wing. Significant adverse rolling moments were created near maximum lift by tail deflections.

References

1. Moul, Thomas M.; Fears, Scott P.; Ross, Holly M.; and Foster, John V.: *Low-Speed Wind-Tunnel Investigation of the Stability and Control Characteristics of a Series of Flying Wings With Sweep Angles of 60°*. NASA TM-4649, 1995.

2. Ross, Holly M.; Fears, Scott P.; and Moul, Thomas M.: *Low-Speed Wind-Tunnel Investigation of the Stability and Control Characteristics of a Series of Flying Wings With Sweep Angles of 70°*. NASA TM-4671, 1995.

3. Hom, K. W.; Morris, O. A.; and Hahne, D. E.: Low-Speed Investigation of the Maneuver Capability of Supersonic Fighter Wings. AIAA-83-0426, Jan. 1983.

4. Freeman, Delma C., Jr.: *Low Subsonic Flight and Force Investigation of a Supersonic Transport Model With a Highly Swept Arrow Wing*. NASA TN D-3887, 1967.

5. Talay, Theodore A.: *An Introduction to the Aerodynamics of Flight*. NASA SP-367, 1975.

6. Ogburn, Marilyn E.; Foster, John V.; Nguyen, Luat T.; Breneman, Kevin P.; McNamara, William G.; Clark, Christopher M.; Rude, Dennis D.; Draper, Majorie G.; Wood, Craig A.; and Hynes, Marshall S.: High-Angle-of-Attack Nose-Down Pitch Control Requirements for Relaxed Static Stability Combat Aircraft. *High-Angle-of-Attack Technology*, Volume I, Joseph R. Chambers, William P. Gilbert, and Luat T. Nguyen, eds., NASA CP-3149, Part 2, 1992, pp. 639–658.

7. Johnson, Joseph L., Jr.; Grafton, Sue B.; and Yip, Long P.: Exploratory Investigation of the Effects of Vortex Bursting on the High Angle-of-Attack Lateral-Directional Stability Characteristics of Highly-Swept Wings. *A Collection of Technical Papers—AIAA 11th Aerodynamic Testing Conference*, Mar. 1980, pp. 282–297. (Available as AIAA-80-0463).

8. Queijo, M. J.; and Riley, Donald R.: *Calculated Subsonic Span Loads and Resulting Stability Derivatives of Unswept and 45° Sweptback Tail Surfaces in Sideslip and in Steady Roll*. NACA TN-3245, 1954.

Table I. Model Geometric Characteristics

	Wing 9	Wing 10	Wing 11	Wing 12
Wing:				
Area (reference), in^2	917.86	874.83	813.62	613.05
Area (trapezoidal), in^2	765.46	768.15	769.34	613.05
Span, in.	48.00	43.82	39.20	32.08
Mean aerodynamic chord, in.	22.93	24.52	26.10	25.48
Root chord, in.	38.22	38.22	38.22	38.22
Tip chord, in.	0	0	0	0
Aspect ratio (based on total planform)	2.51	2.19	1.89	1.68
Aspect ratio (based on trapezoidal area)	3.00	2.50	2.00	1.68
Leading-edge sweep, deg	50	50	50	50
Trailing-edge sweep, deg	±50	±50	±50	±50
Dihedral, deg	0	0	0	0
Incidence, deg	0	0	0	0
Moment reference centers:				
Longitudinal (X-axis), percent $\bar{c}$	33.68	31.07	28.76	27.34
Longitudinal (X-axis), in. (back from nose)	18.09	17.17	15.80	13.33
Vertical (Z-axis), in. (below wing centerline)	1.87	1.87	1.87	1.87
Leading-edge flaps:				
Area (per side), in^2	87.38	73.50	56.54	36.73
Span (per side), in.	17.65	15.16	12.11	8.56
Chord, in.	4.67	4.67	4.67	4.67
Trailing-edge flaps:				
Inboard:				
Area (per side), in^2	14.84		33.41	27.28
Span (per side), in.	4.99		7.50	6.77
Chord, in.	5.84		8.55	7.66
Middle:				
Area (per side), in^2	46.49	39.33	33.41	27.28
Span (per side), in.	10.45	8.69	7.50	6.77
Chord, in.	5.84	6.70	8.55	7.66
Outboard:				
Area (per side), in^2	32.83	43.72	33.41	27.28
Span (per side), in.	8.00	9.34	7.50	6.77
Chord, in.	5.84	6.70	8.55	7.66
Body flaps:				
Area (per side), in^2	17.63	26.25	11.11	24.06
Span (per side), in.	5.47	6.73	4.34	6.39
Chord, in.	5.84	6.70	4.67	6.76
Split trailing-edge flaps:				
Middle:				
Area (per side), in^2	46.49	39.33	33.41	27.28
Span (per side), in.	10.45	8.69	7.50	6.77
Chord, in.	5.84	6.70	8.55	7.66
Outboard:				
Area (per side), in^2	32.83	43.72	33.41	27.28
Span (per side), in.	8.00	9.34	7.50	6.77
Chord, in.	5.84	6.70	8.55	7.66

Table I. Concluded

	Wide Top	Medium Top	Narrow Top	Bottom
Bodies:				
Length, in.	28.20	28.20	28.20	22.20
Width, in.	10.40	7.00	4.60	9.50
Height, in.	3.50	3.50	3.50	3.00

	Medium	Small
Vertical tails:		
Area, in^2	50.47	25.27
Root chord, in.	15.27	10.80
Tip chord, in.	0	0
Height, in.	6.61	4.68
Aspect ratio	.87	.87
Leading-edge sweep, deg	60	60
Hinge line location, percent chord	50	50

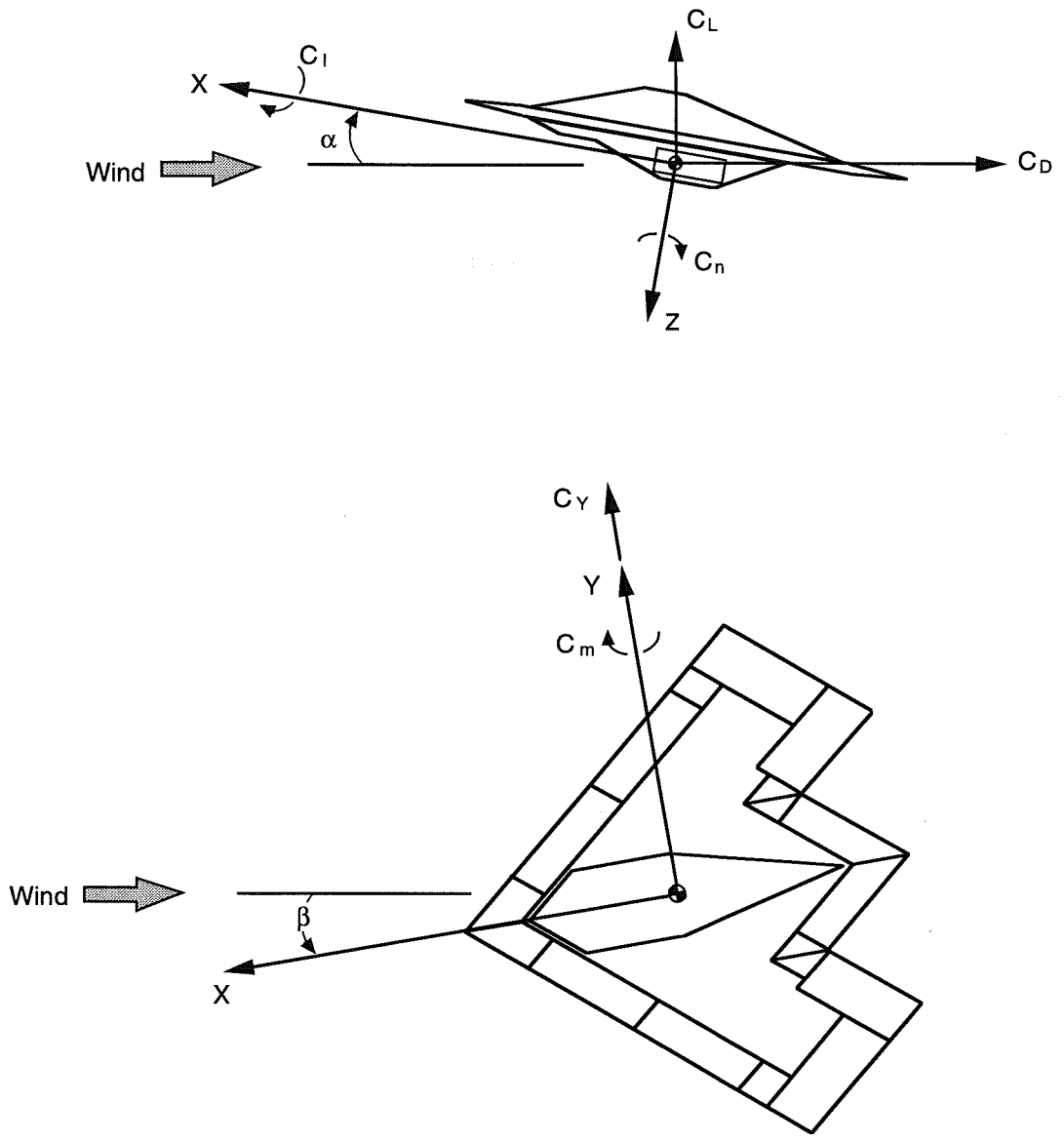

Figure 1. System of axes and angular notation.

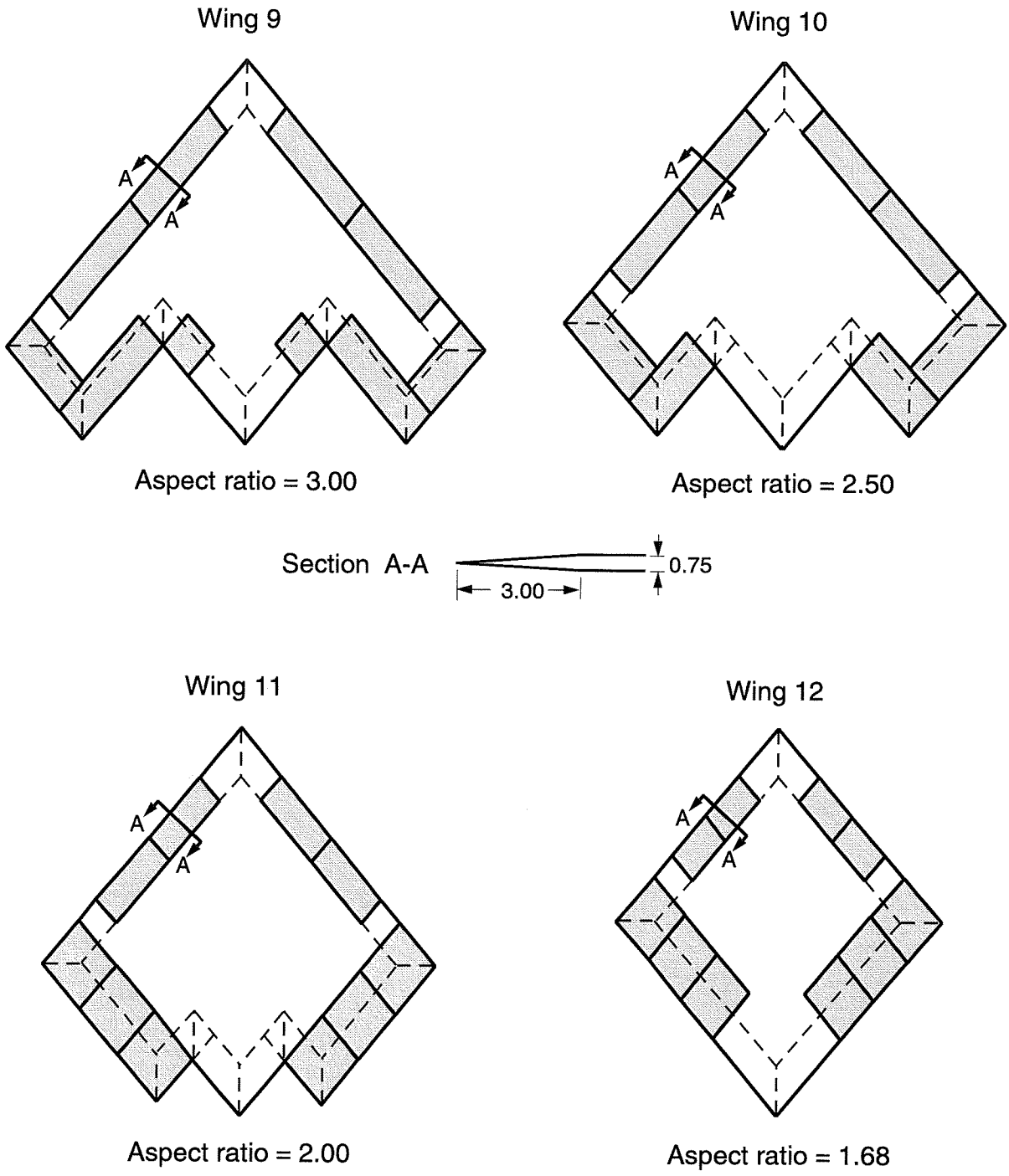

(a) Control surfaces (shaded areas) and bevel lines (dashed lines).

Figure 2. Wing planforms.

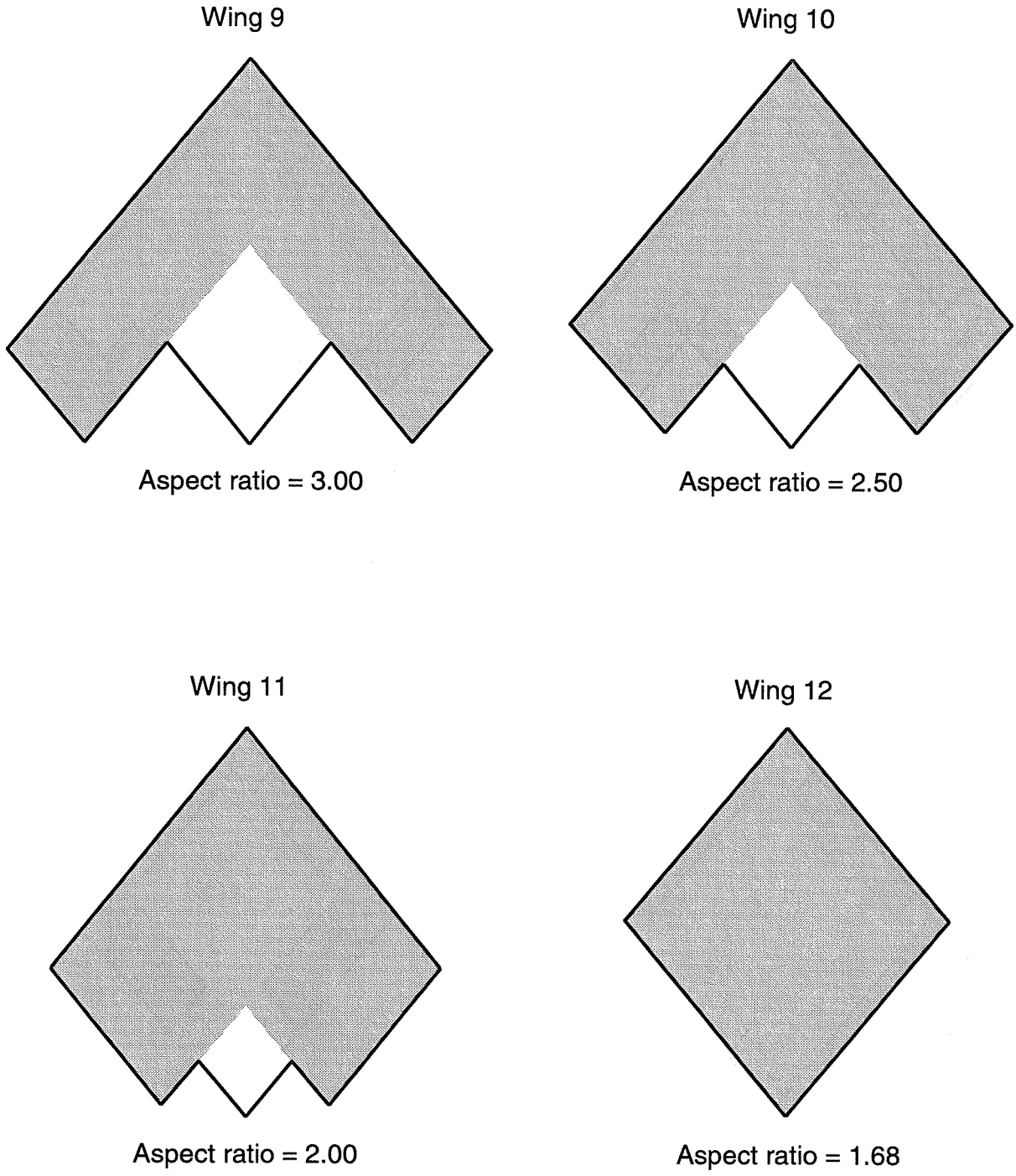

(b) Trapezoidal wing areas (shaded areas).

Figure 2. Concluded.

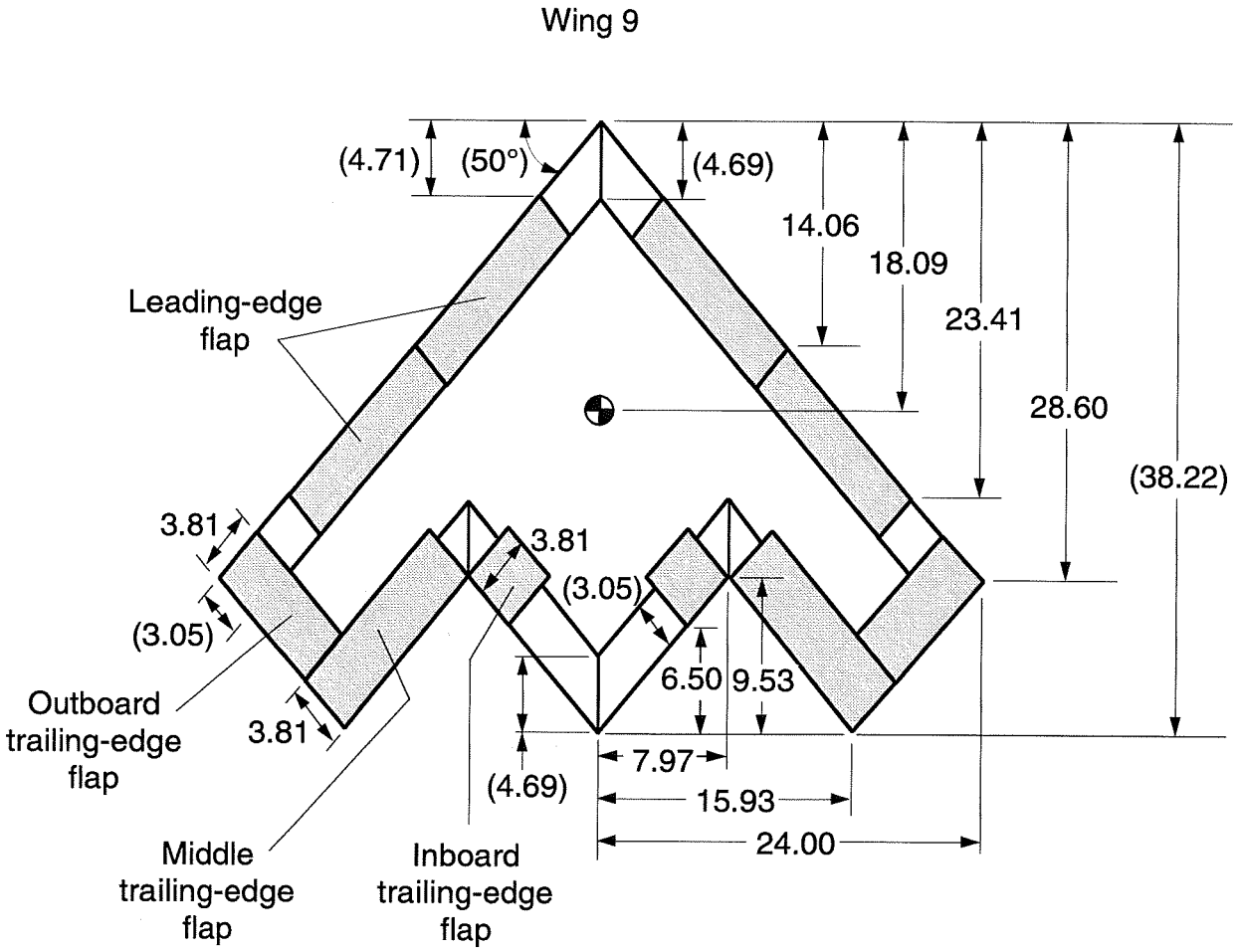

Figure 3. Wing 9. Linear dimensions are in inches. Dimensions in parentheses are common for all wings. Shaded areas indicate control surfaces.

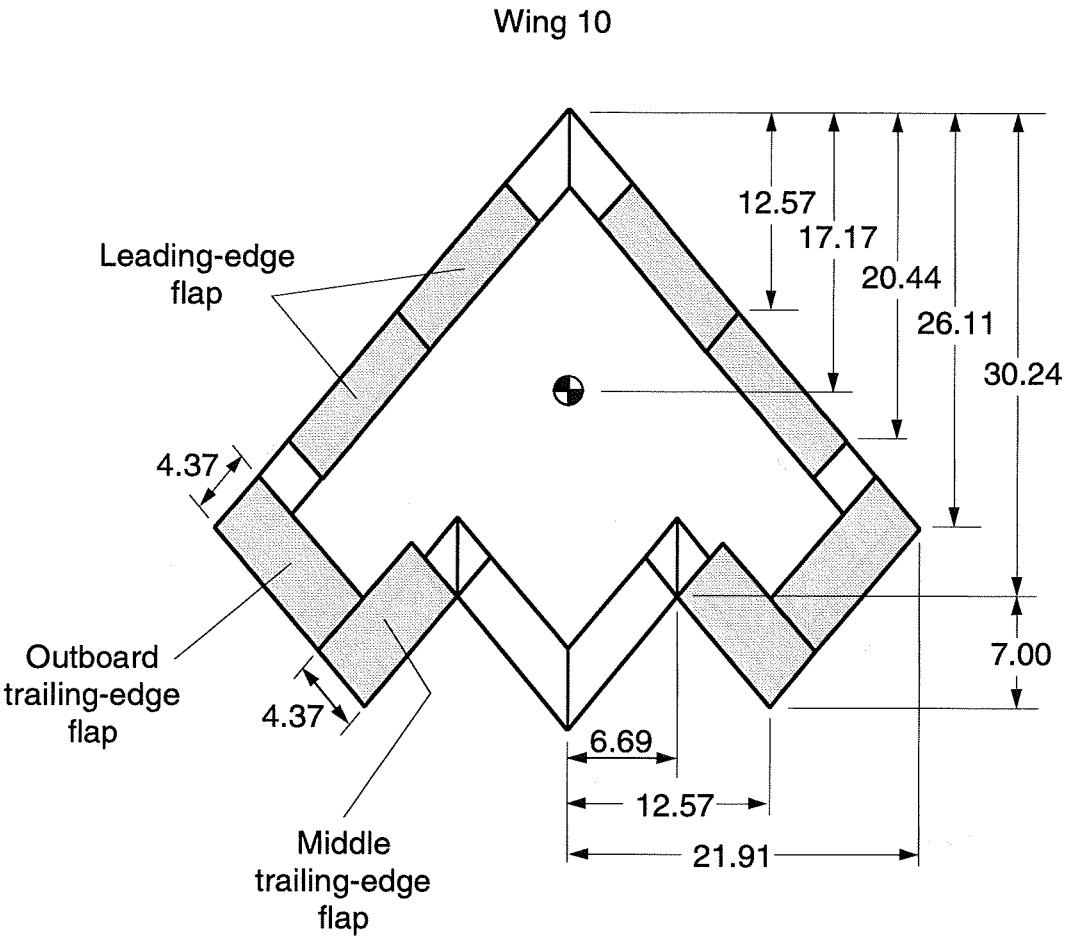

Figure 4. Wing 10. All dimensions are in inches. Shaded areas indicate control surfaces.

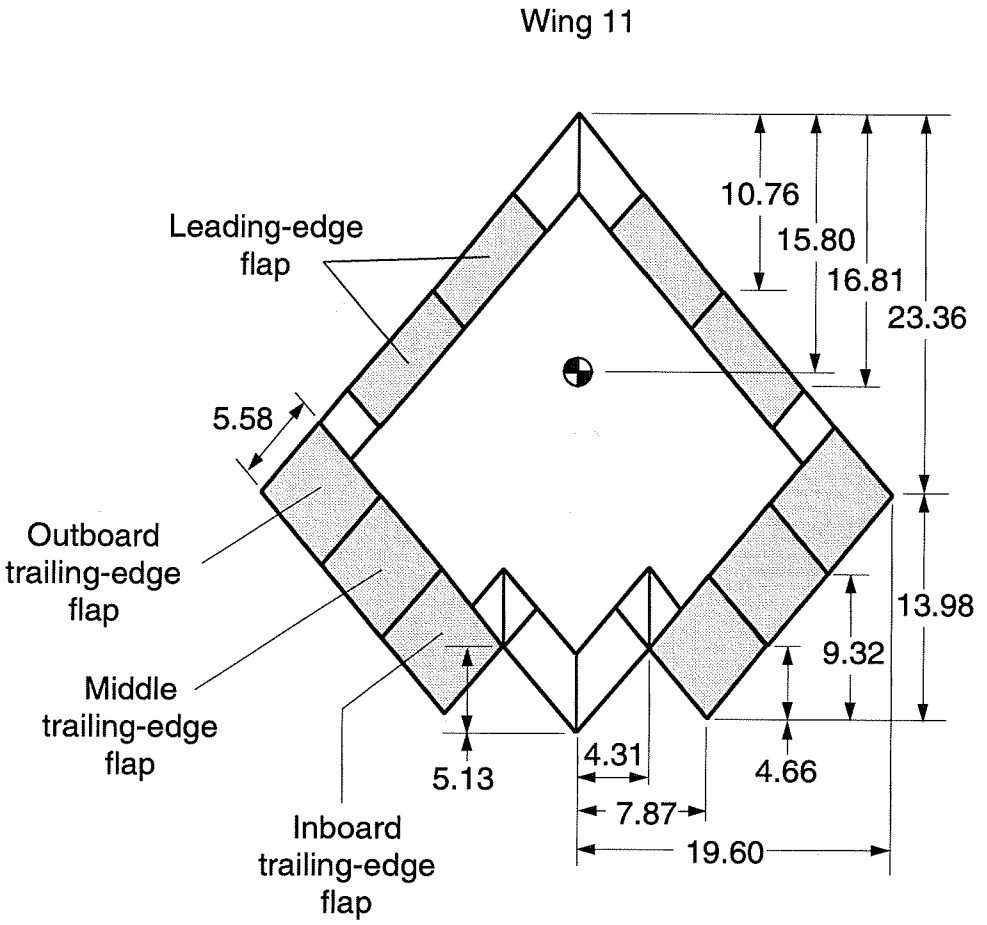

Figure 5. Wing 11. All dimensions are in inches. Shaded areas indicate control surfaces.

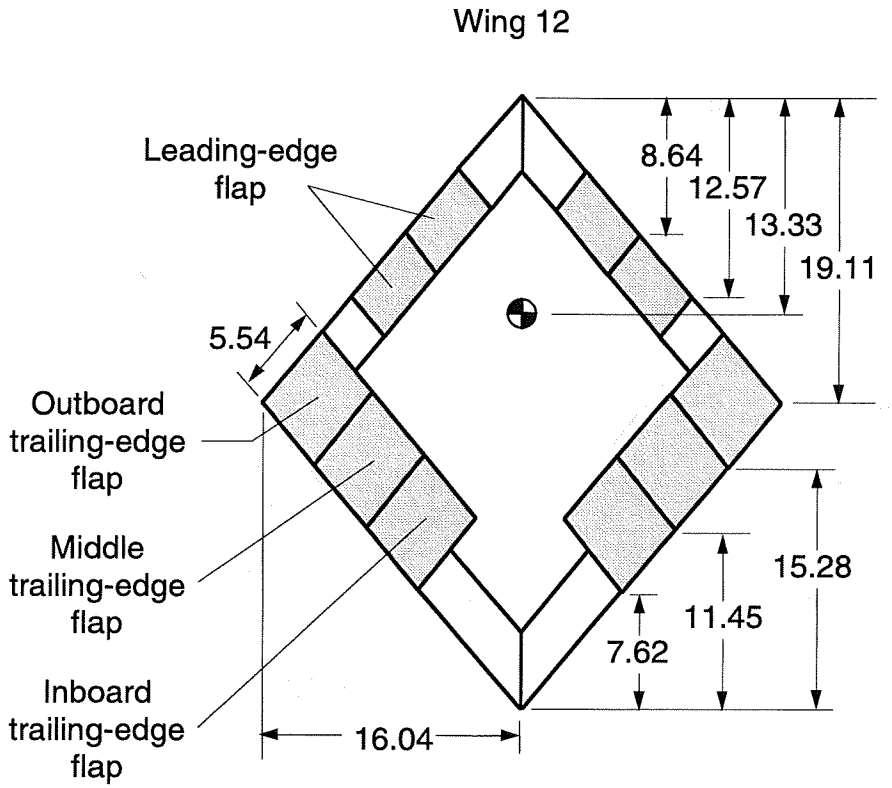

Figure 6. Wing 12. All dimensions are in inches. Shaded areas indicate control surfaces.

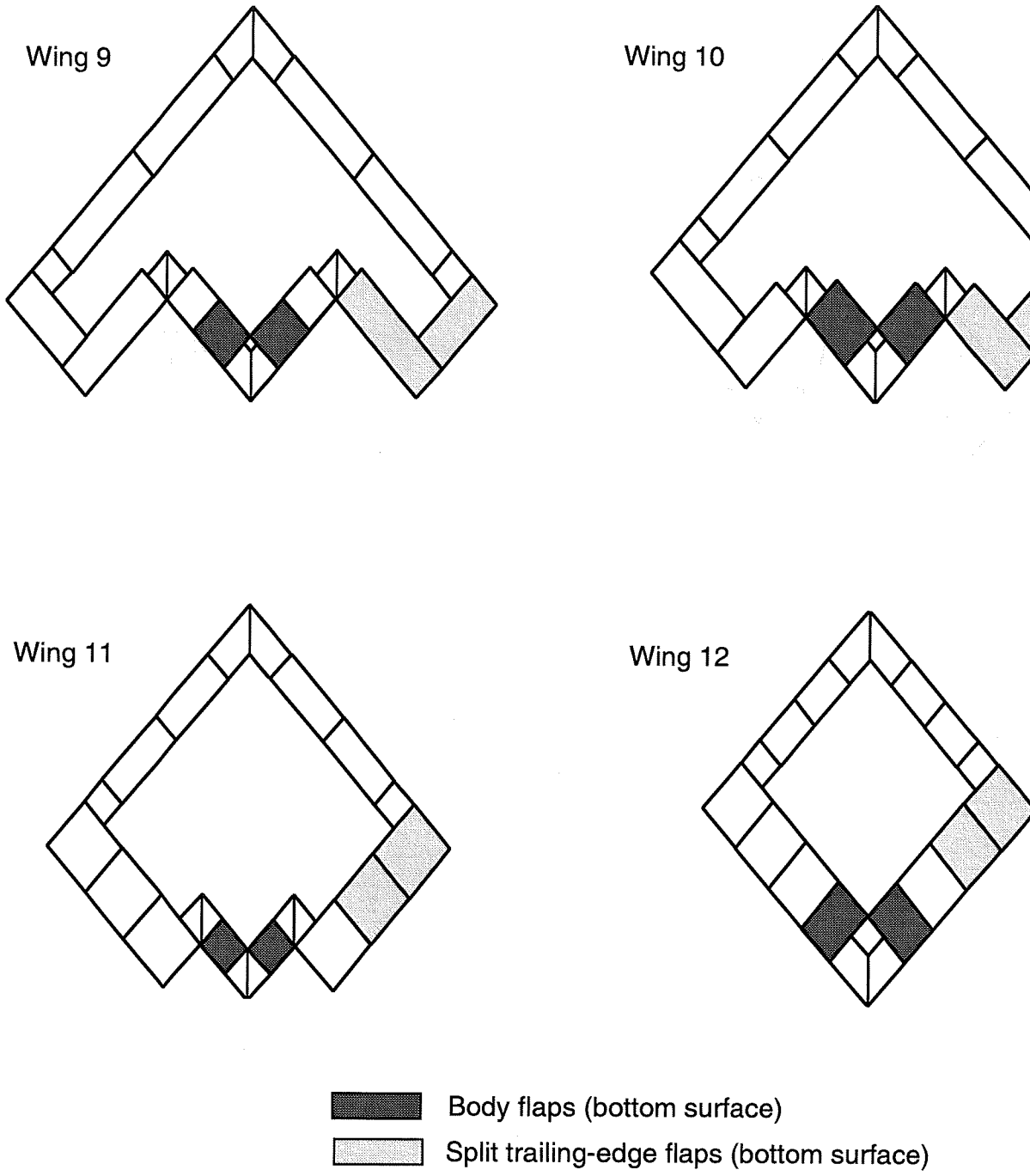

Figure 7. Top view showing locations of undeflected body flaps and split trailing-edge flaps on bottom surfaces of wings.

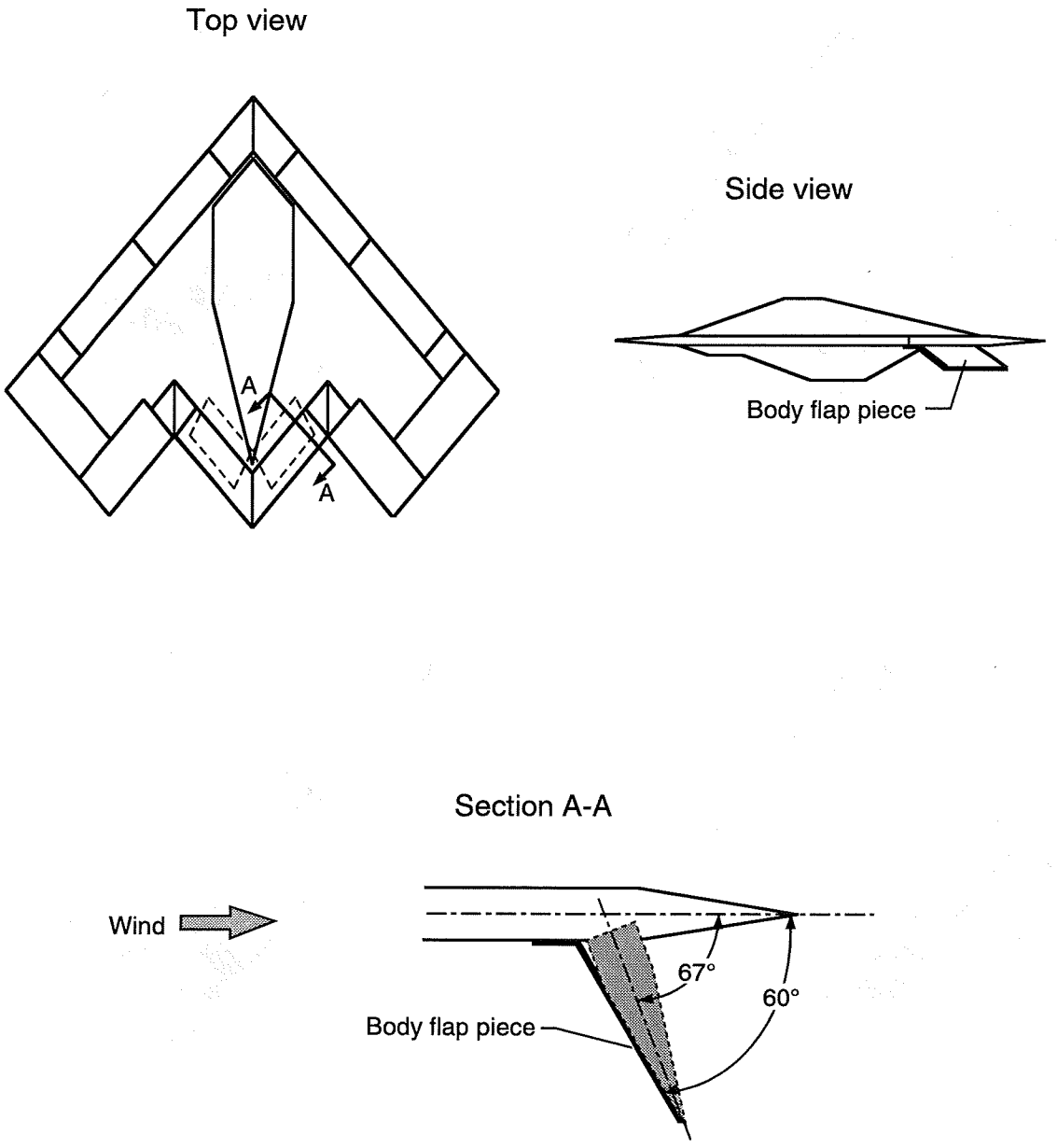

(a) Typical body flap location and mounting for deflection angle of 67°. Shaded area represents simulated flap.

Figure 8. Body flap locations, dimensions, and deflection angles.

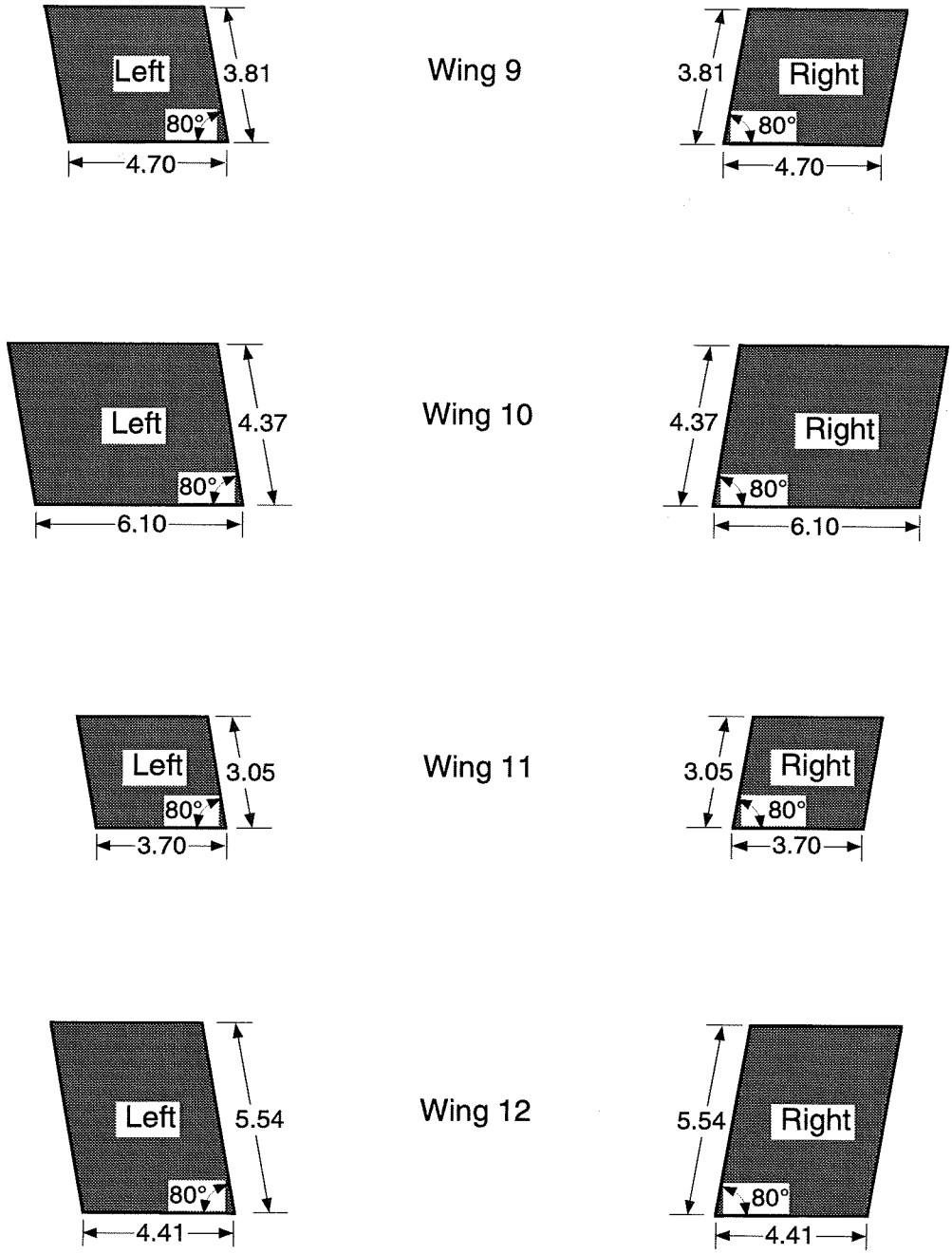

(b) Planforms of body flaps. All dimensions are in inches.

Figure 8. Concluded.

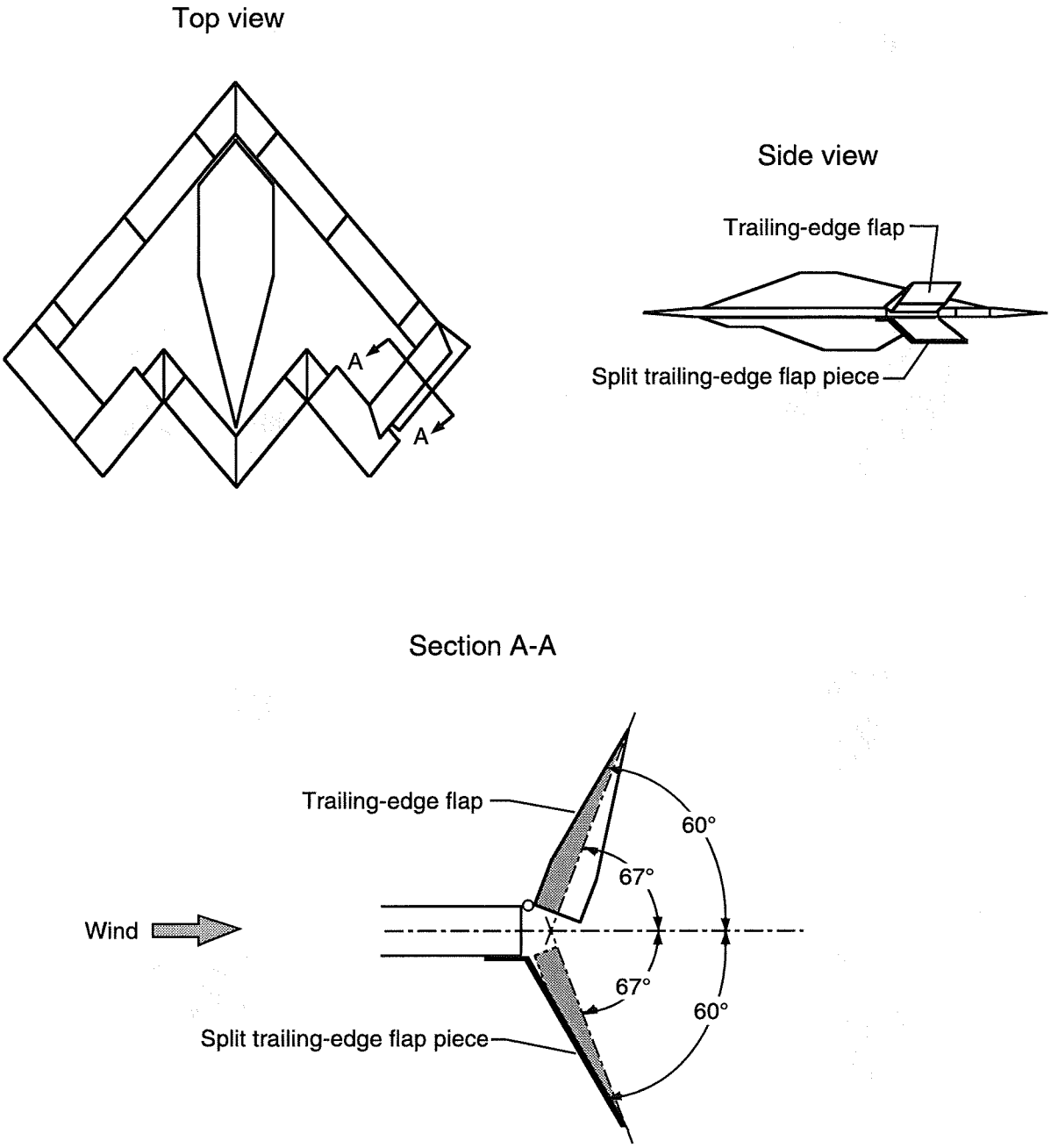

(a) Typical split trailing-edge flap location and mounting for deflection angle of 67°. Shaded areas represent simulated upper and lower halves of split flaps.

Figure 9. Split trailing-edge flap locations, dimensions, and deflection angles.

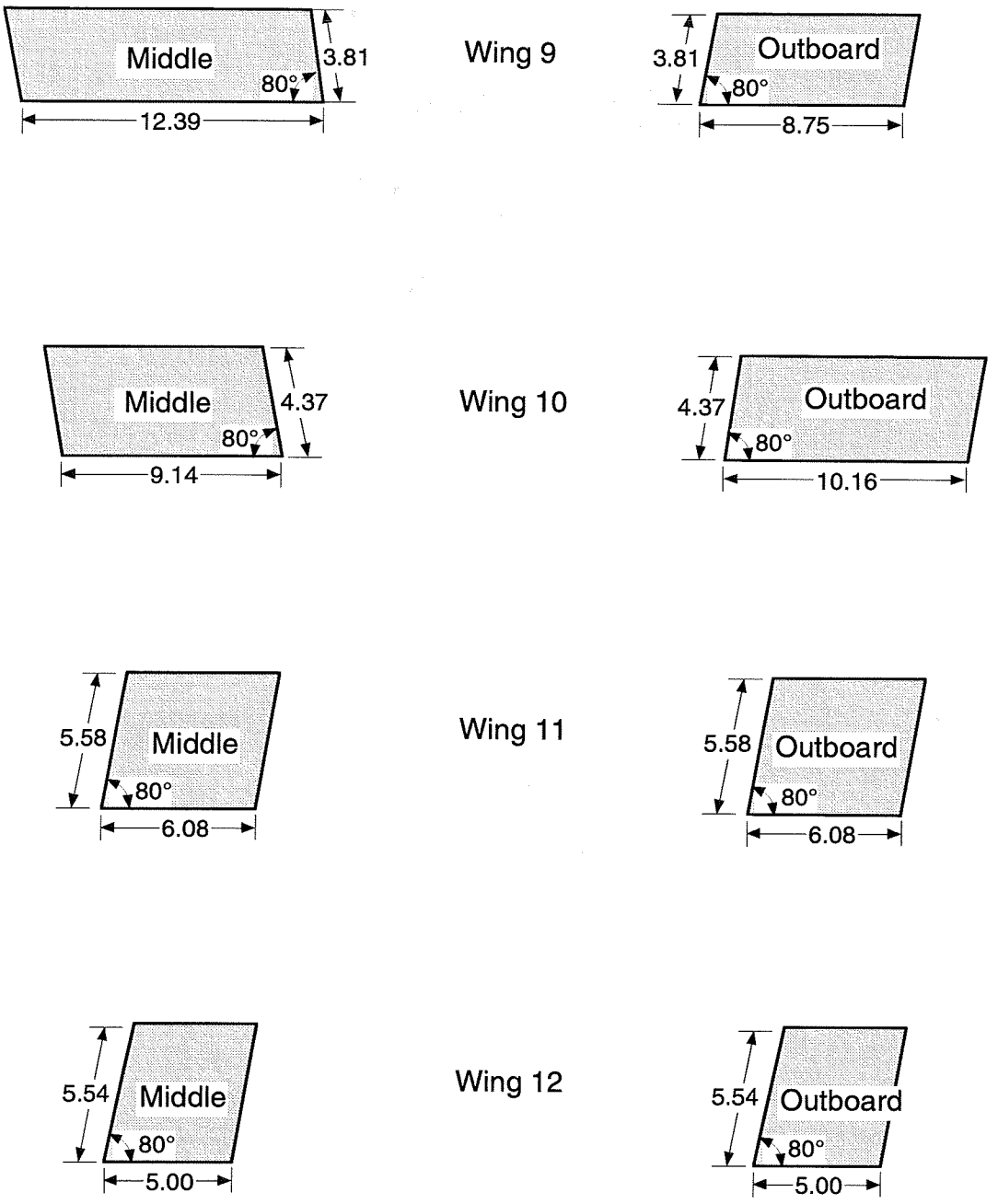

(b) Planforms of split trailing-edge flaps. All dimensions are in inches.

Figure 9. Concluded.

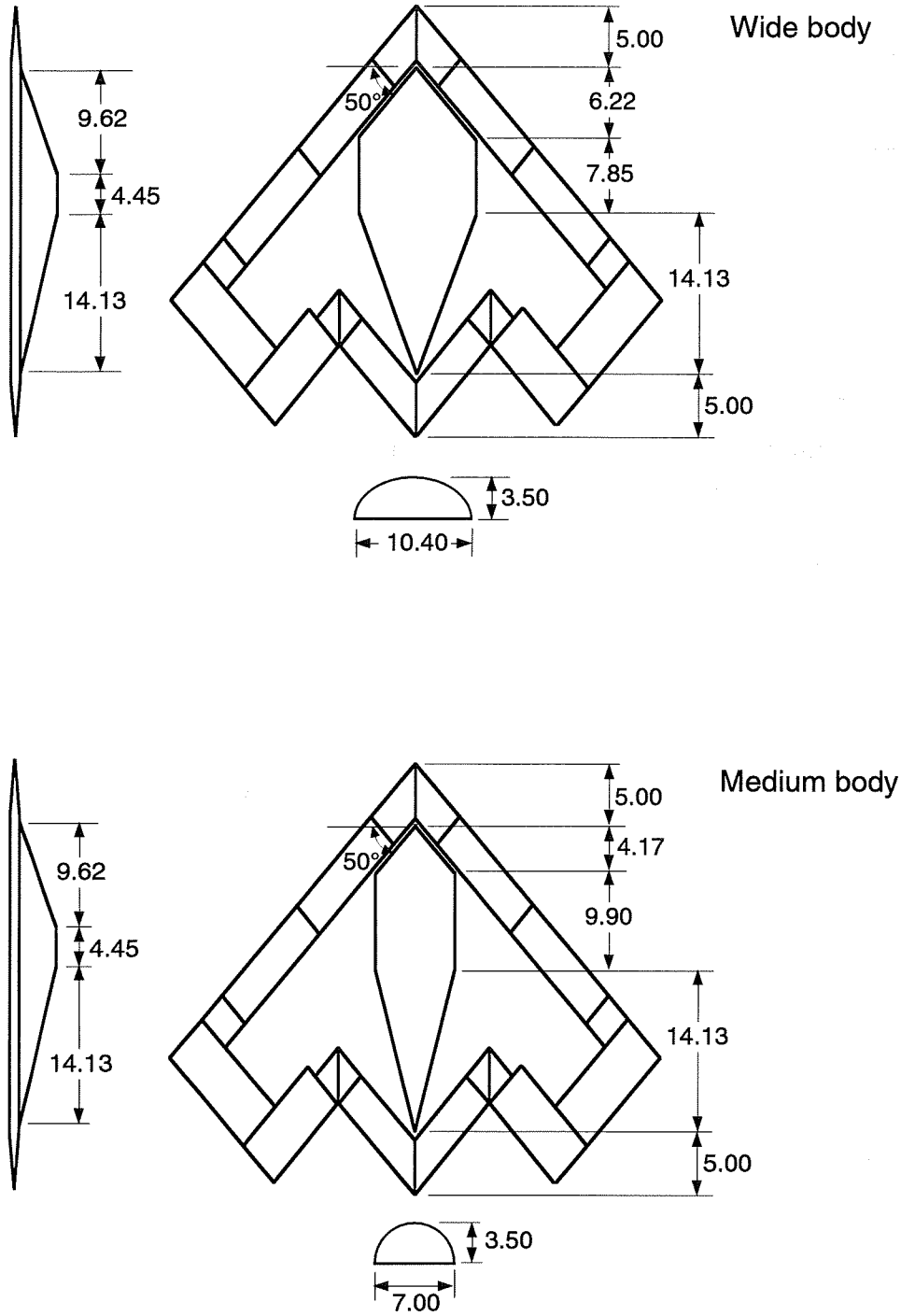

(a) Wide and medium top bodies.

Figure 10. Top bodies and bottom balance cover. All dimensions are in inches.

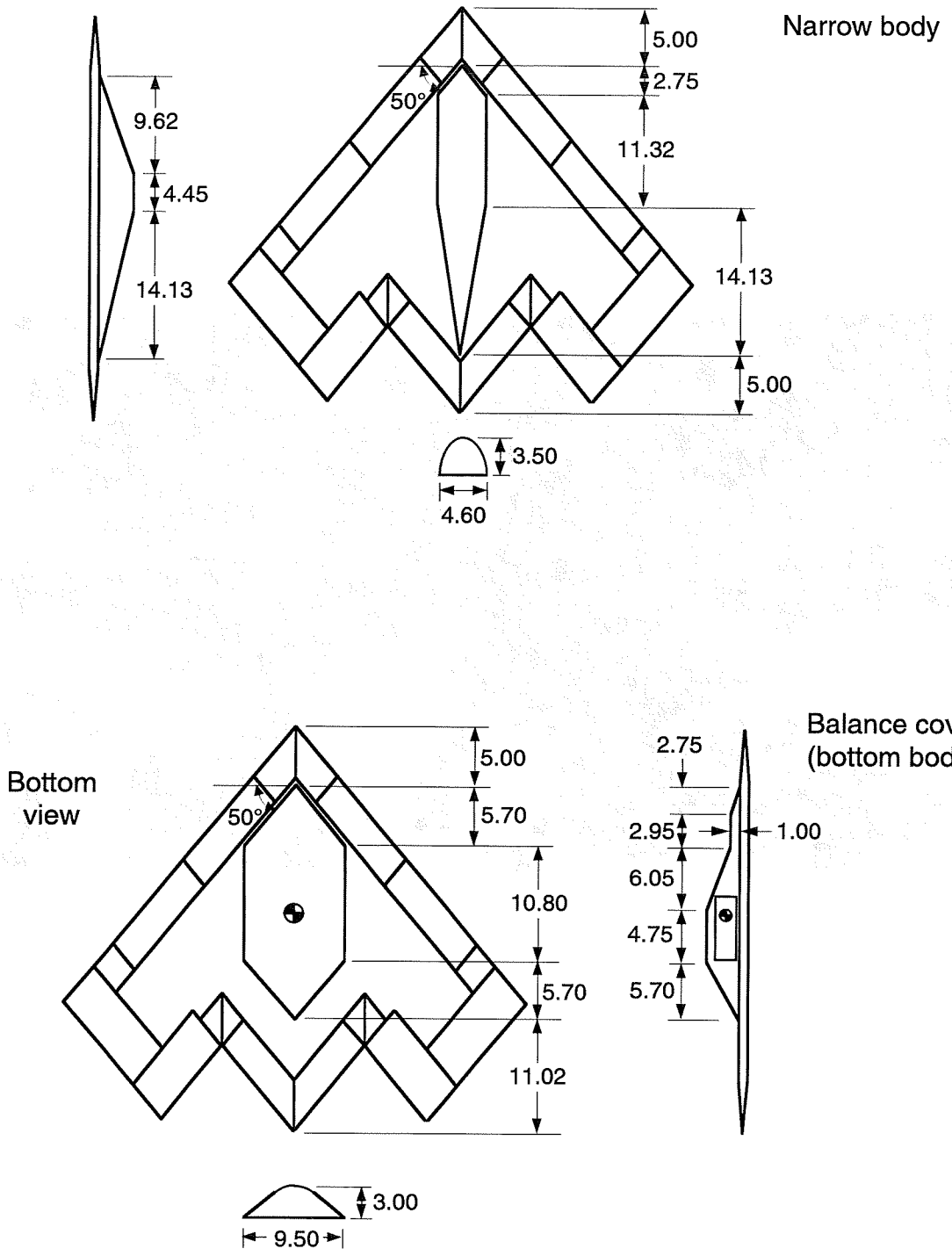

(b) Narrow top body and bottom balance cover.

Figure 10. Concluded.

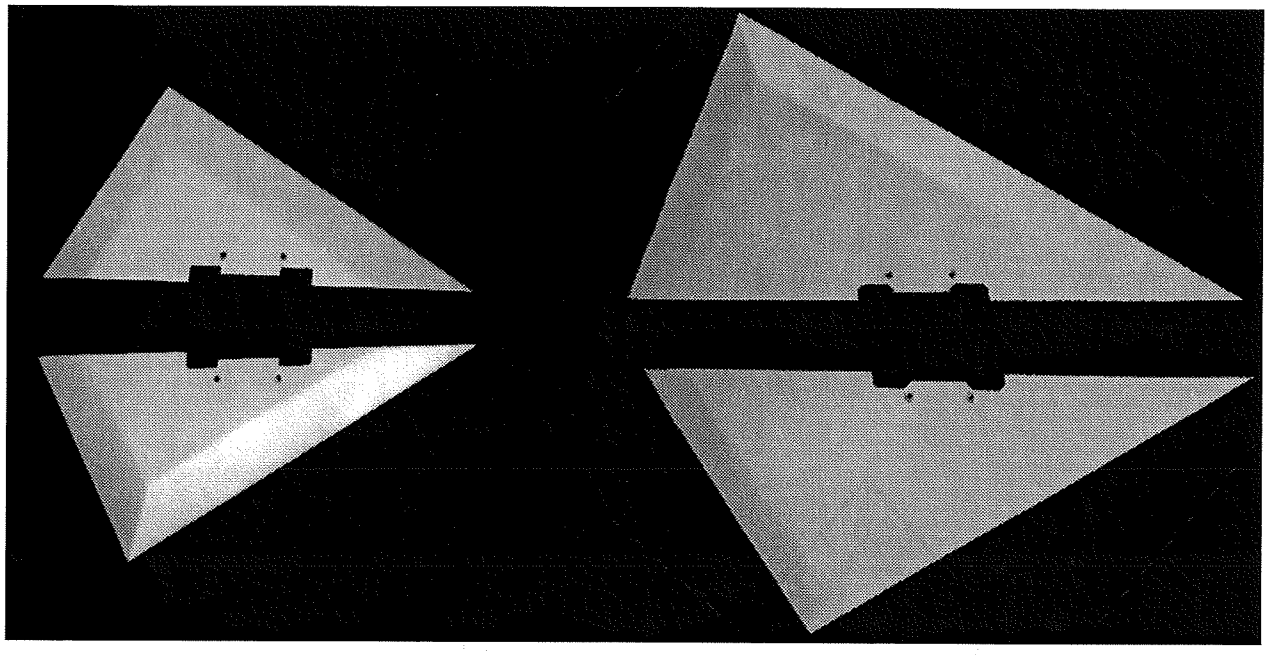

Figure 11. Vertical tails.

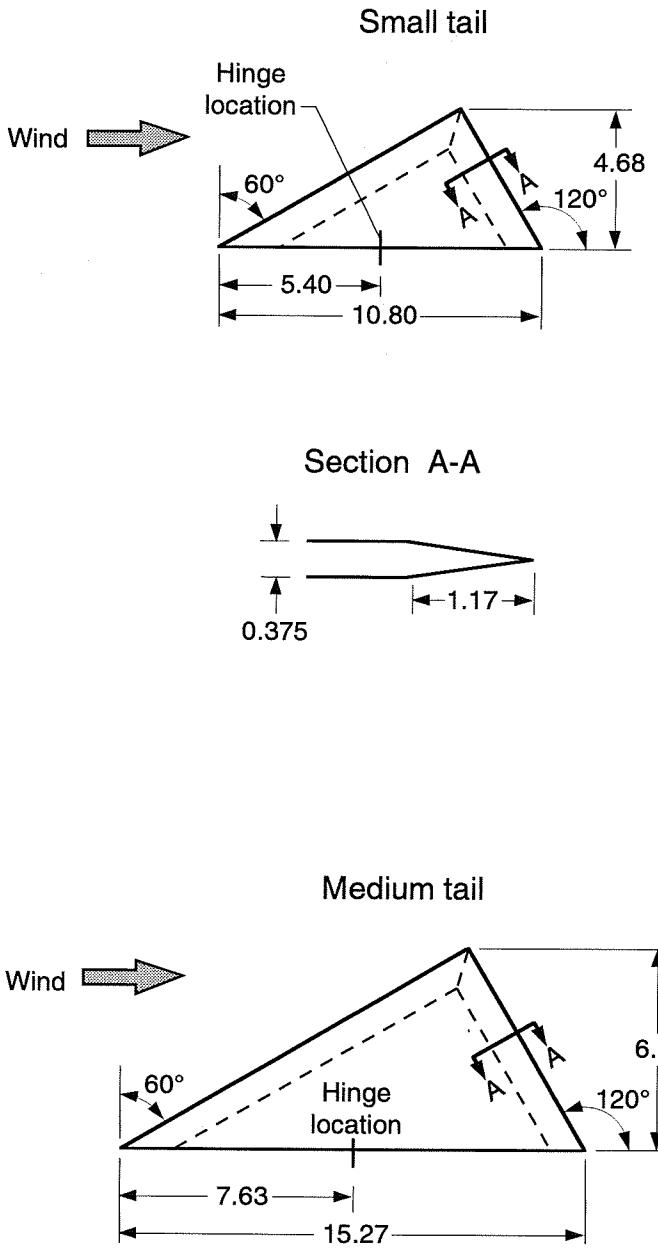

Figure 12. Medium and small vertical tails. All dimensions are in inches. Dashed lines indicate bevel lines.

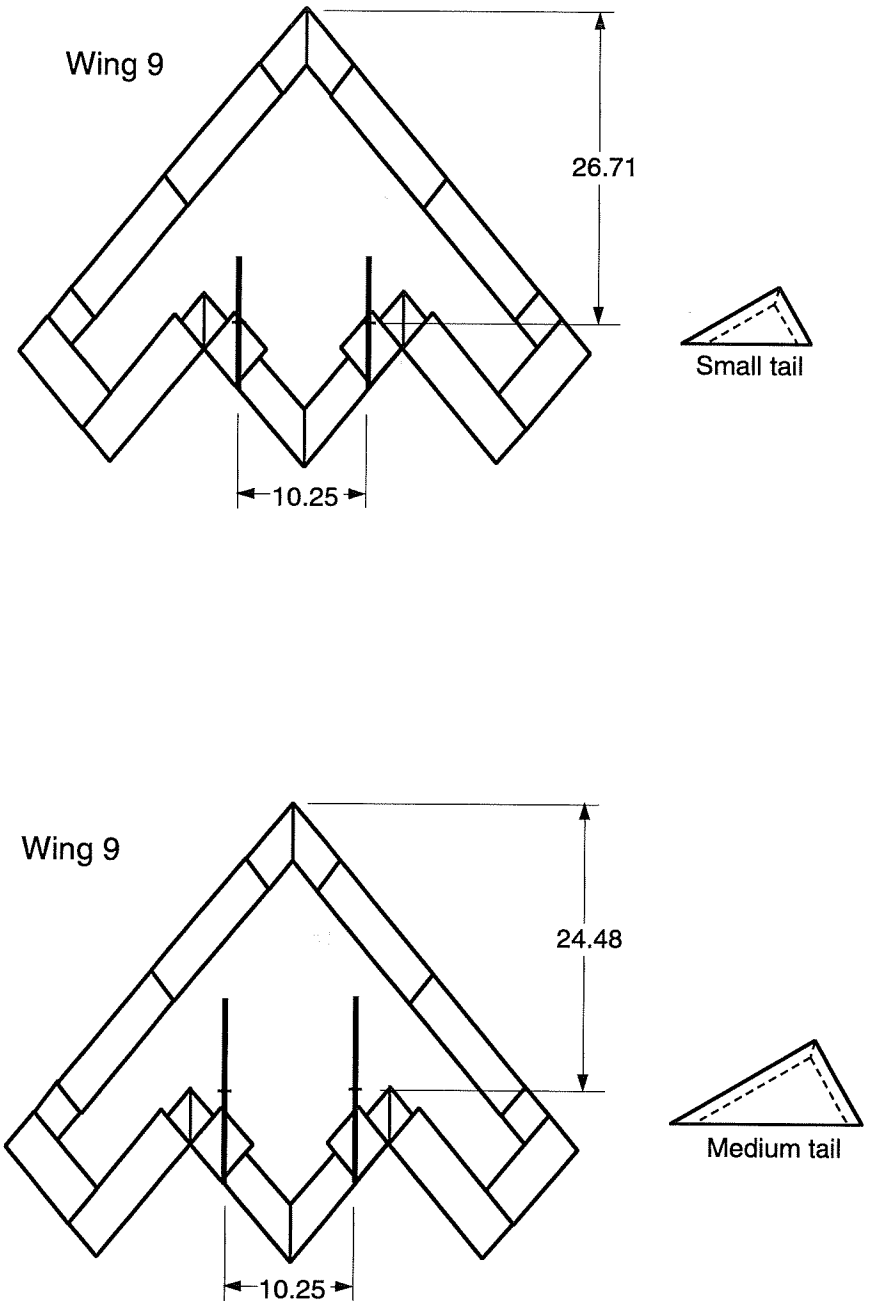

(a) Small and medium tails on Wing 9.

Figure 13. Vertical tail locations. All dimensions are in inches.

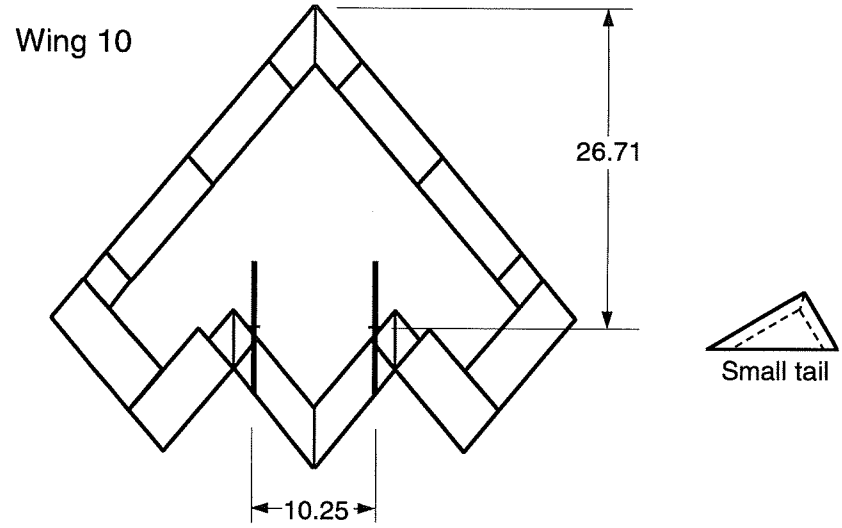

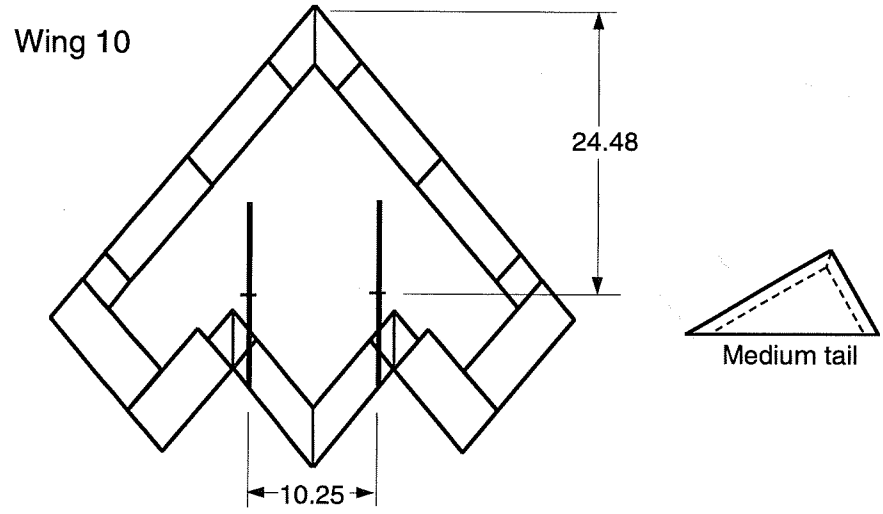

(b) Small and medium tails on Wing 10.

Figure 13. Continued.

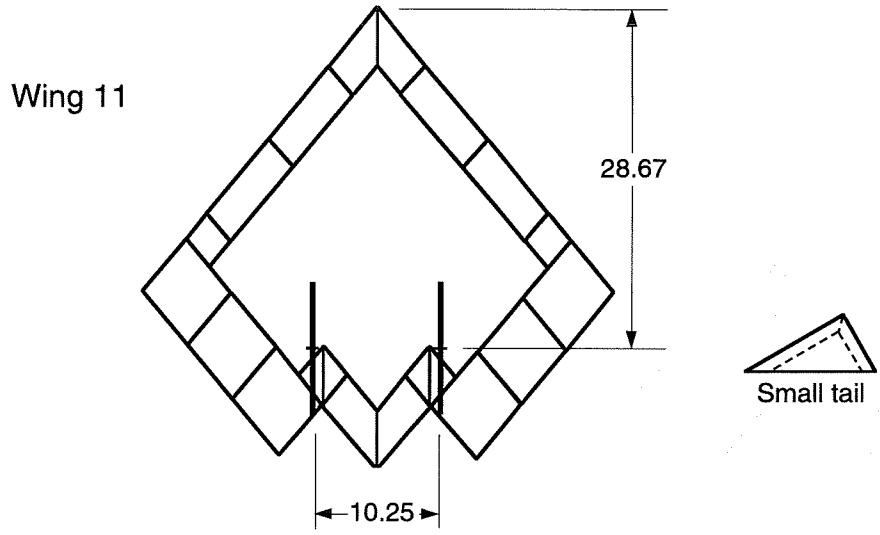

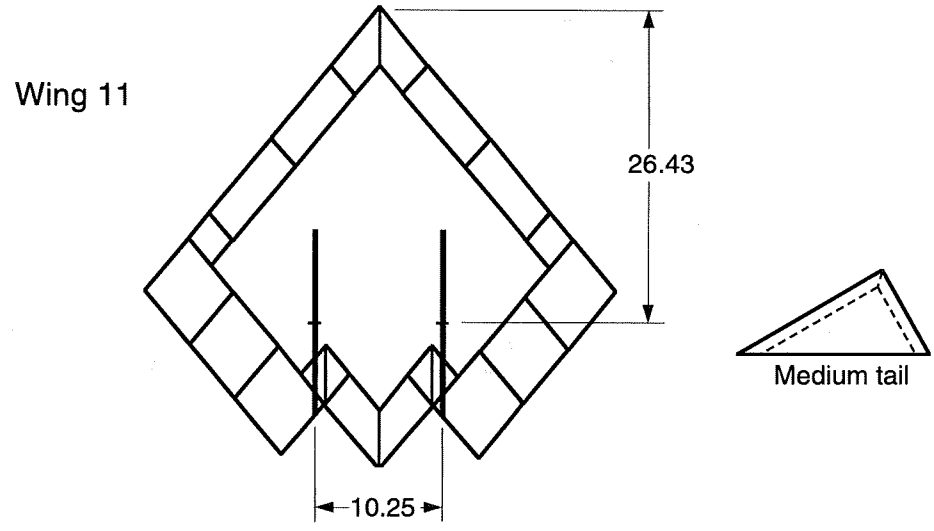

(c) Small and medium tails on Wing 11.

Figure 13. Continued.

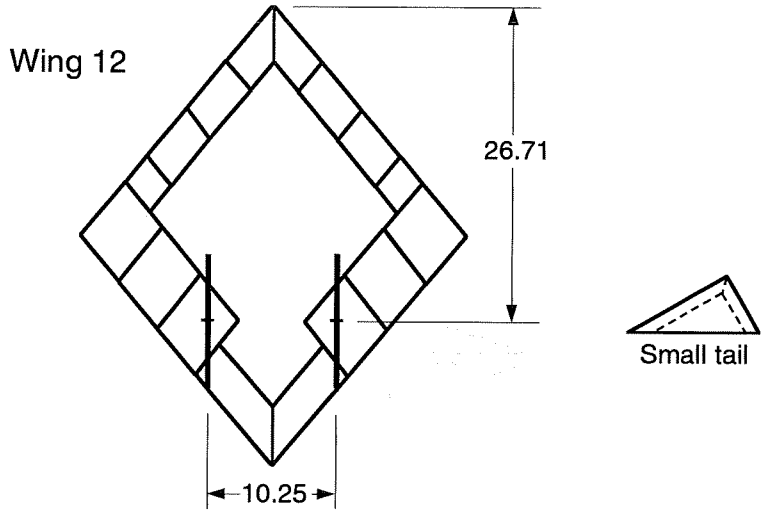

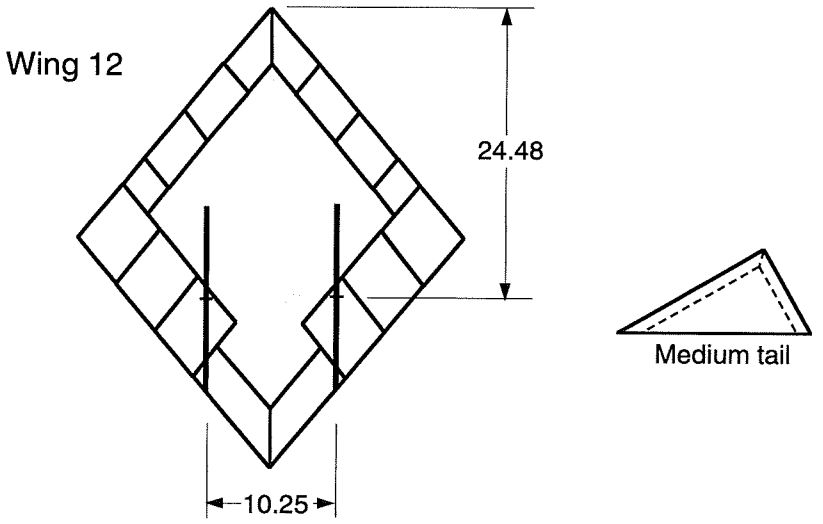

(d) Small and medium tails on Wing 12.

Figure 13. Concluded.

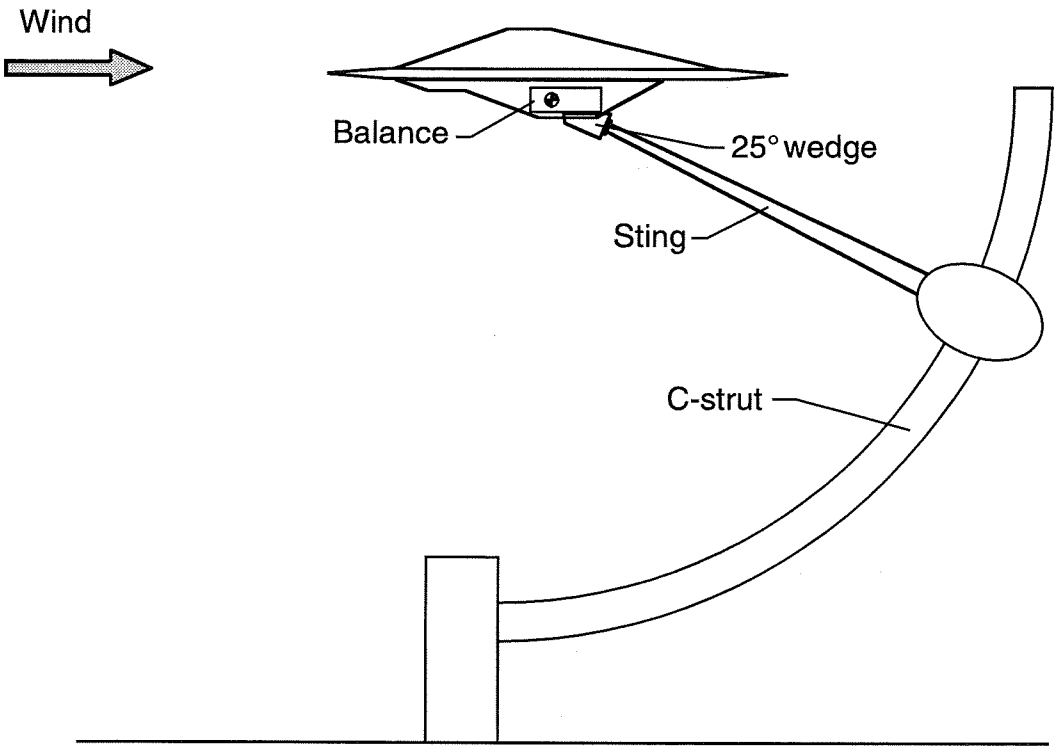

Figure 14. Typical configuration mounted on sting and C-strut arrangement in wind-tunnel test section. Not to scale.

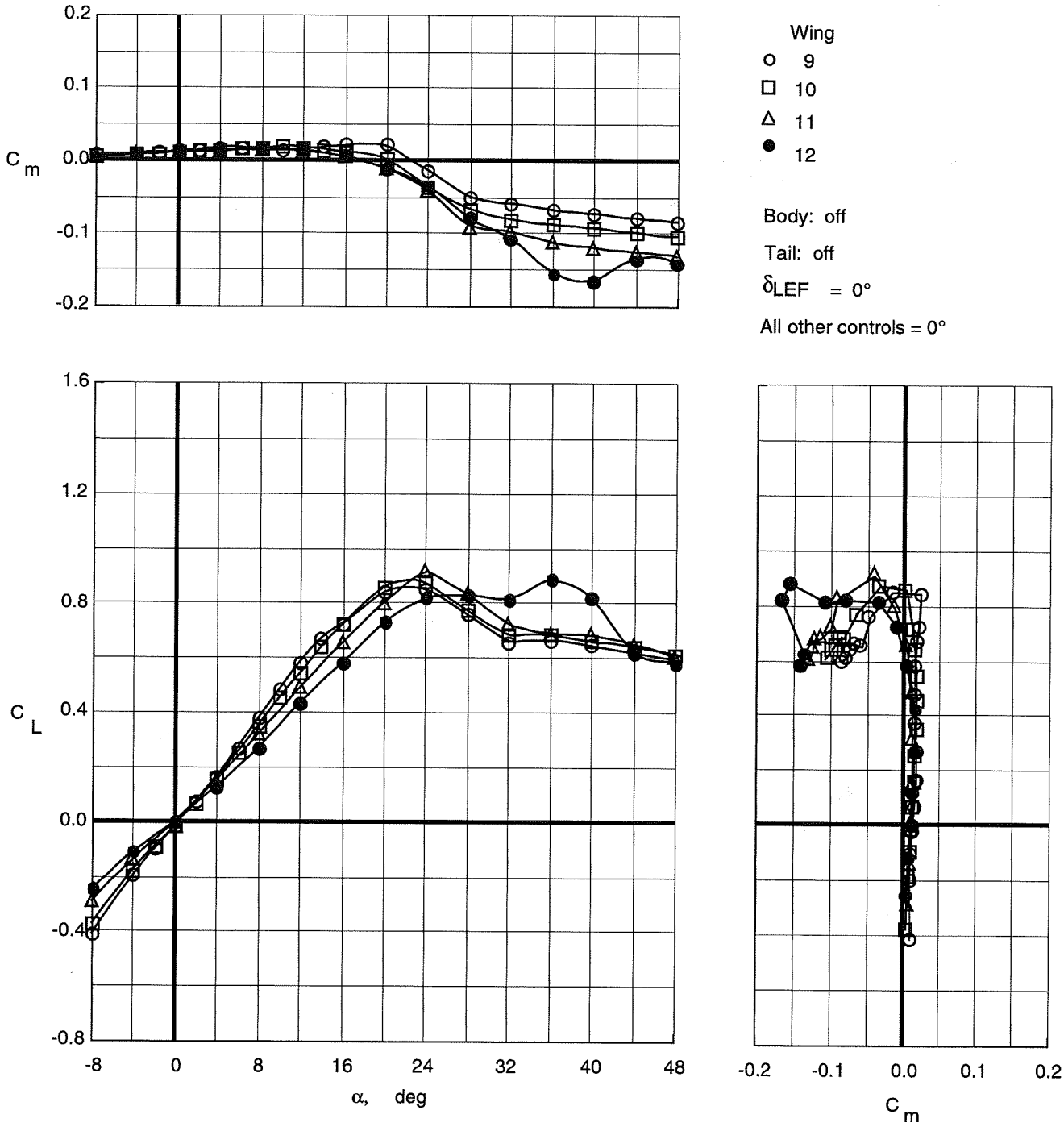

Figure 15. Longitudinal characteristics of wing planforms with top body off.

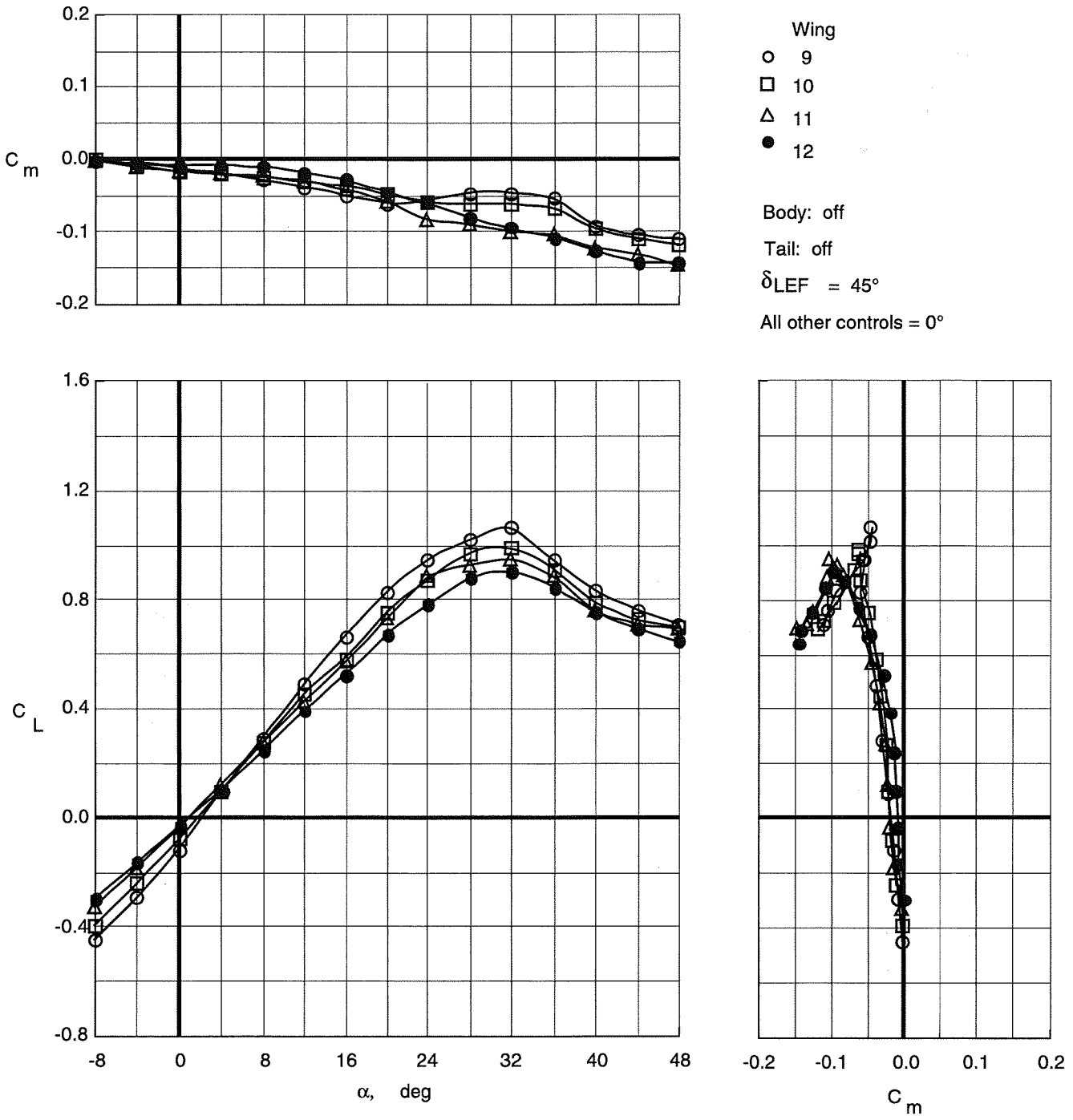

Figure 16. Longitudinal characteristics of wing planforms with top body off and leading-edge flaps deflected.

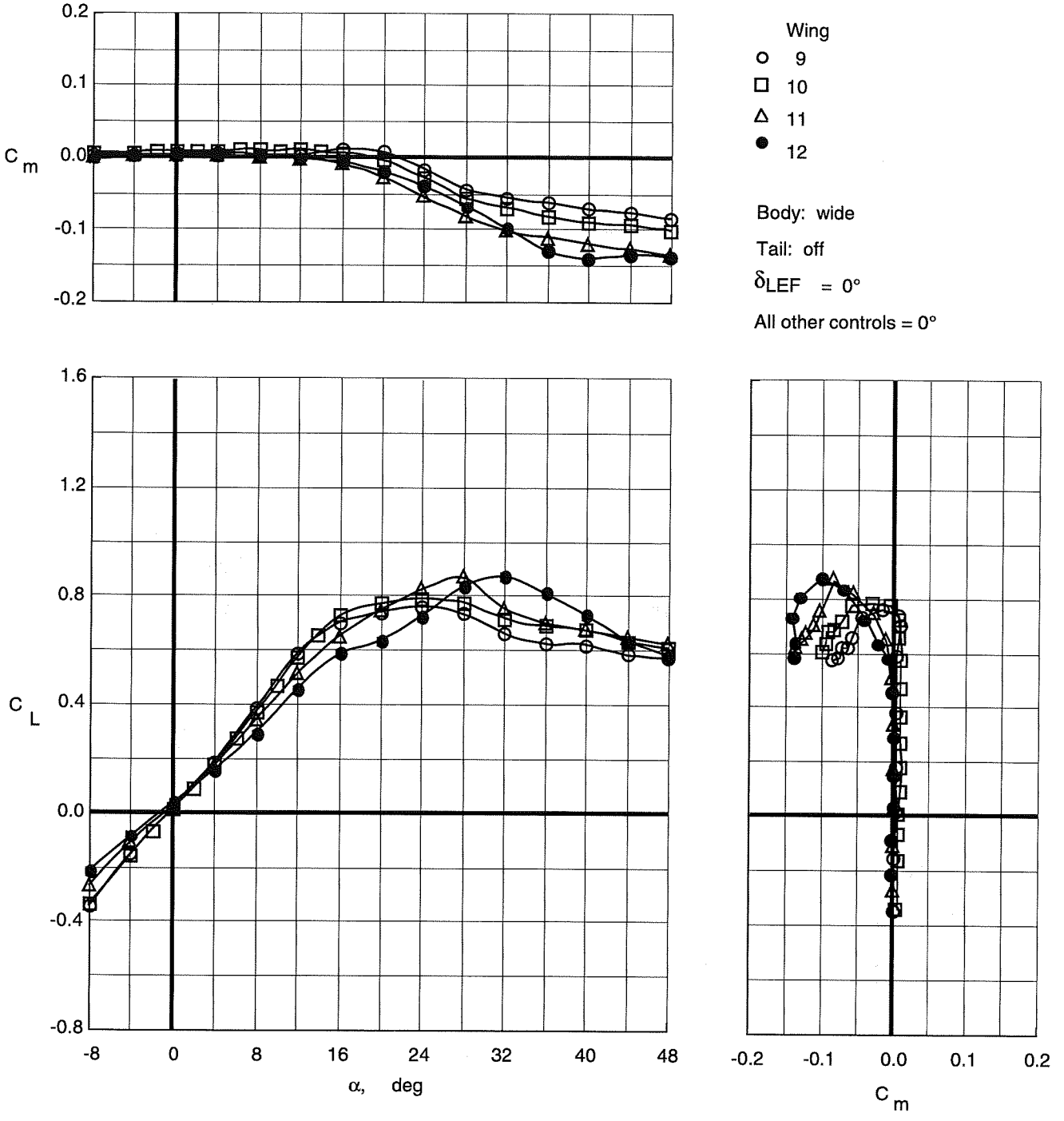

Figure 17. Longitudinal characteristics of wing planforms with wide top body on.

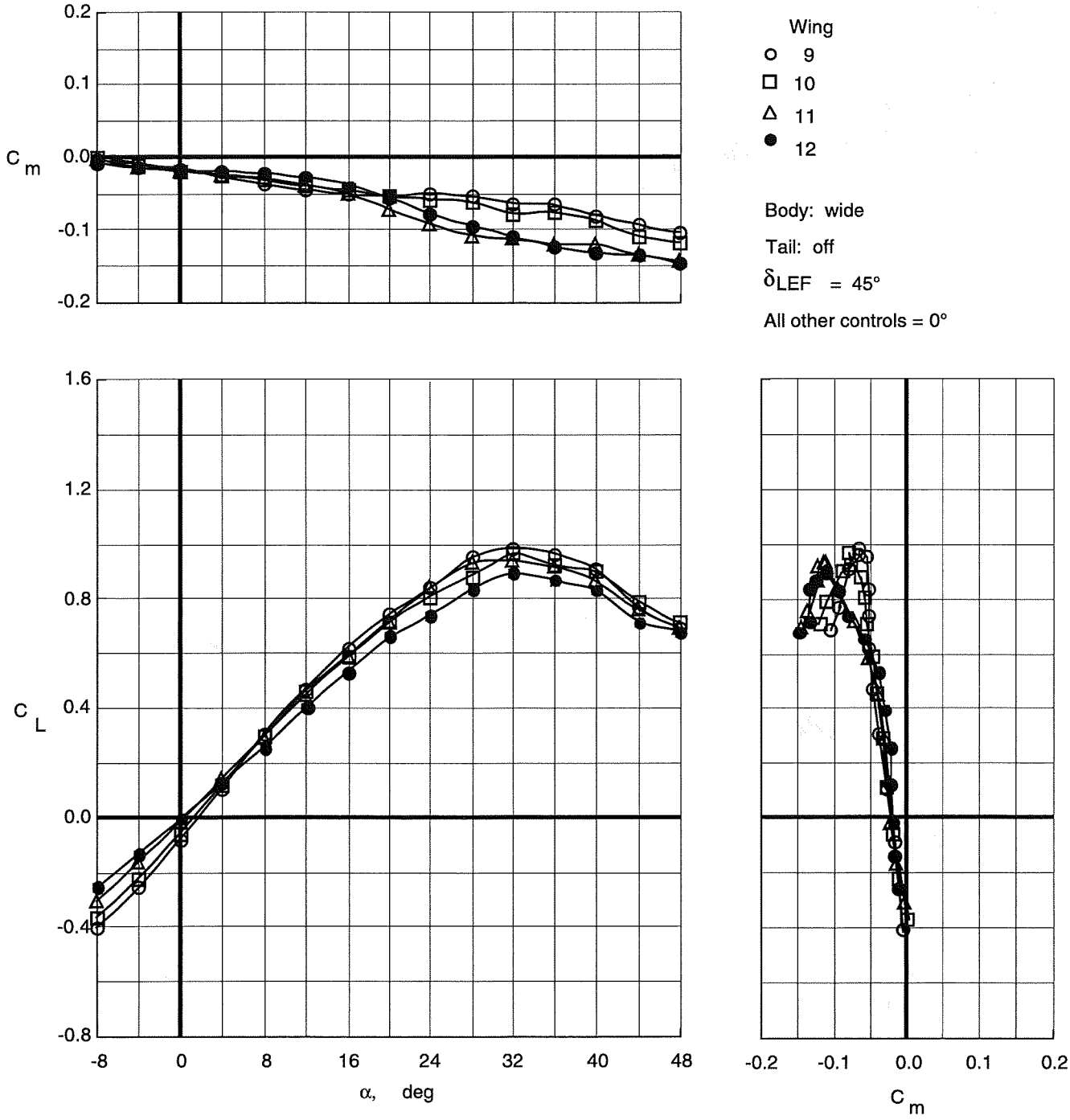

Figure 18. Longitudinal characteristics of wing planforms with wide top body on and leading-edge flaps deflected.

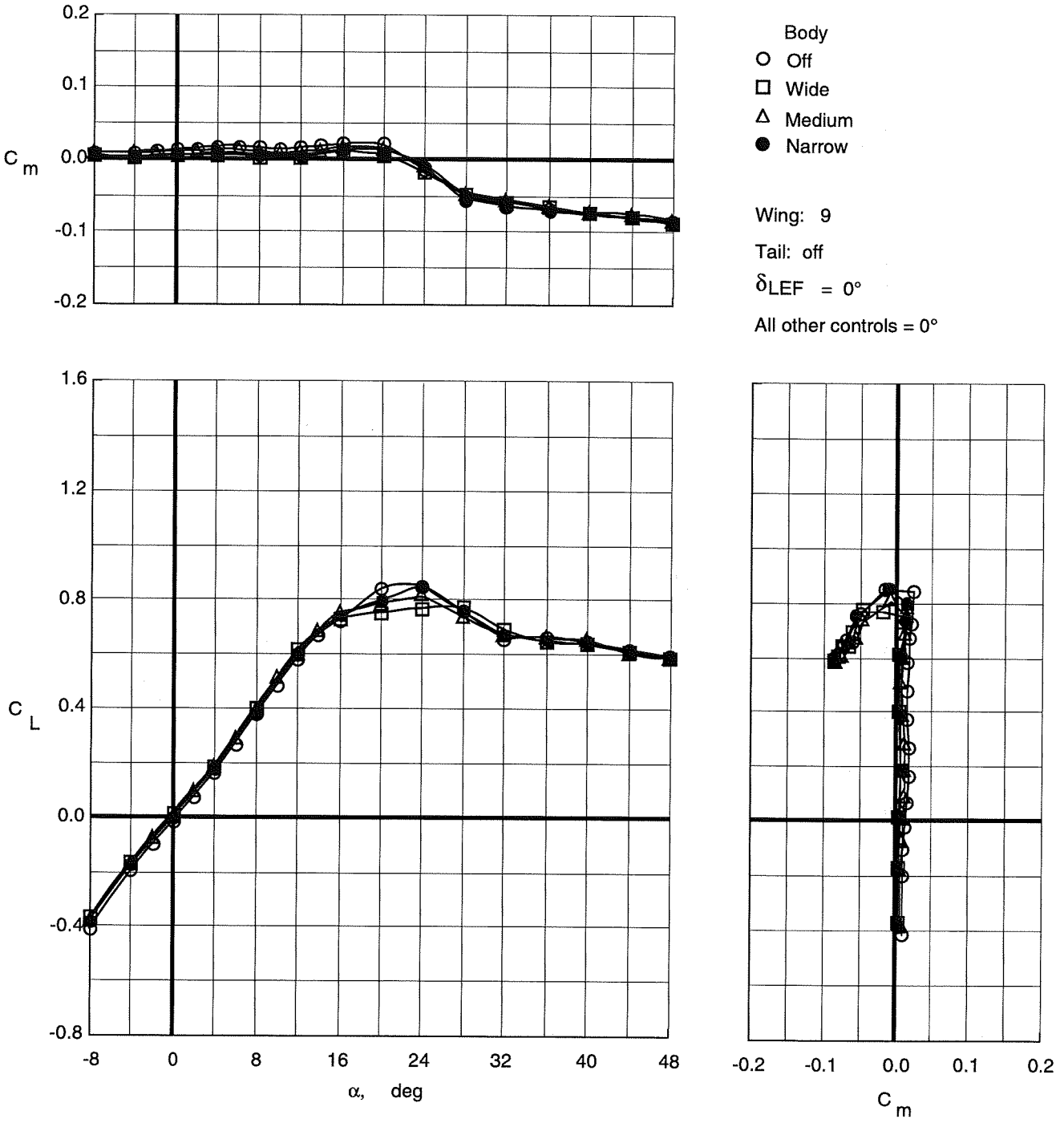

Figure 19. Effect of top body width on longitudinal characteristics of Wing 9.

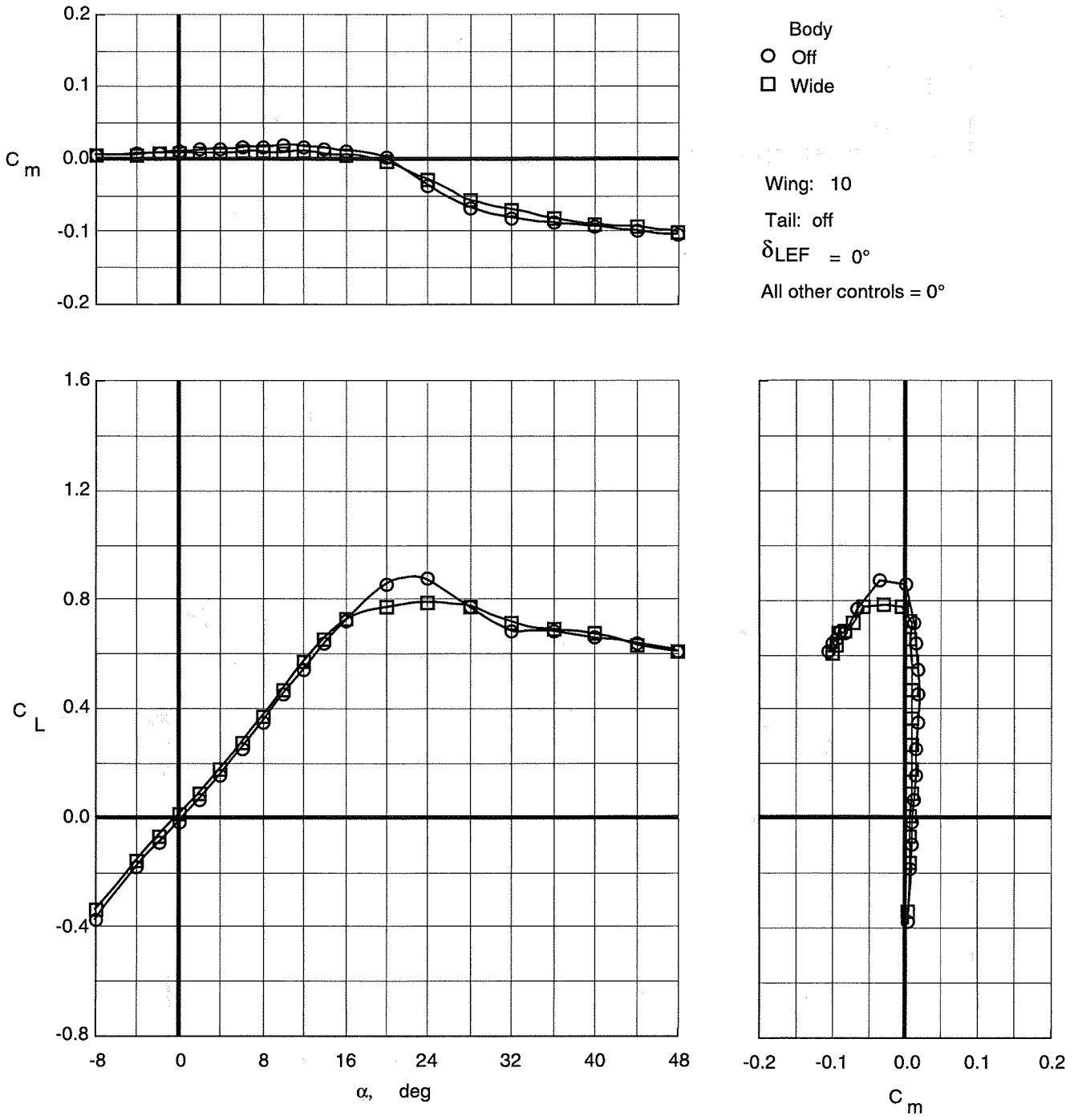

Figure 20. Effect of wide top body on longitudinal characteristics of Wing 10.

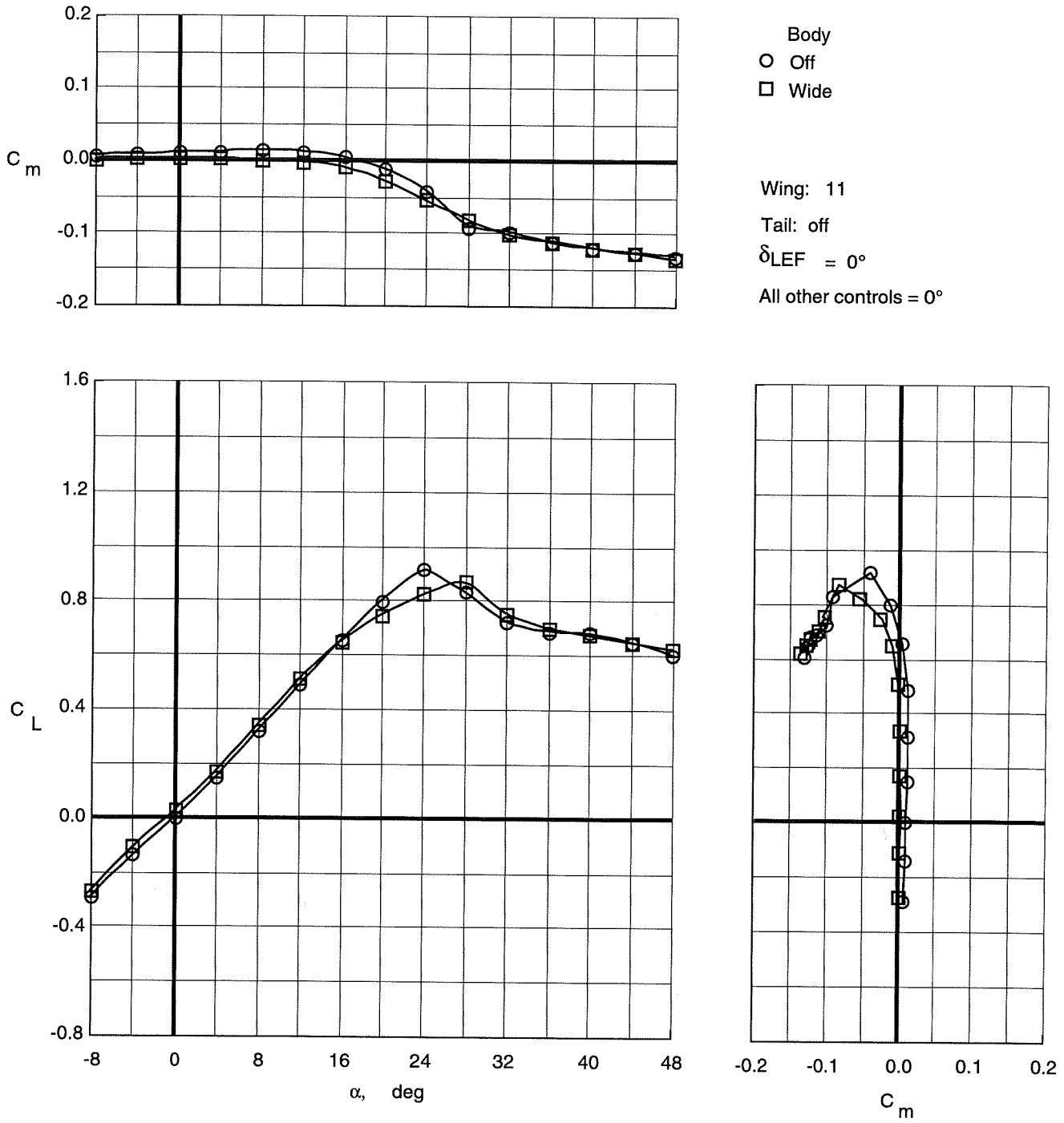

Figure 21. Effect of wide top body on longitudinal characteristics of Wing 11.

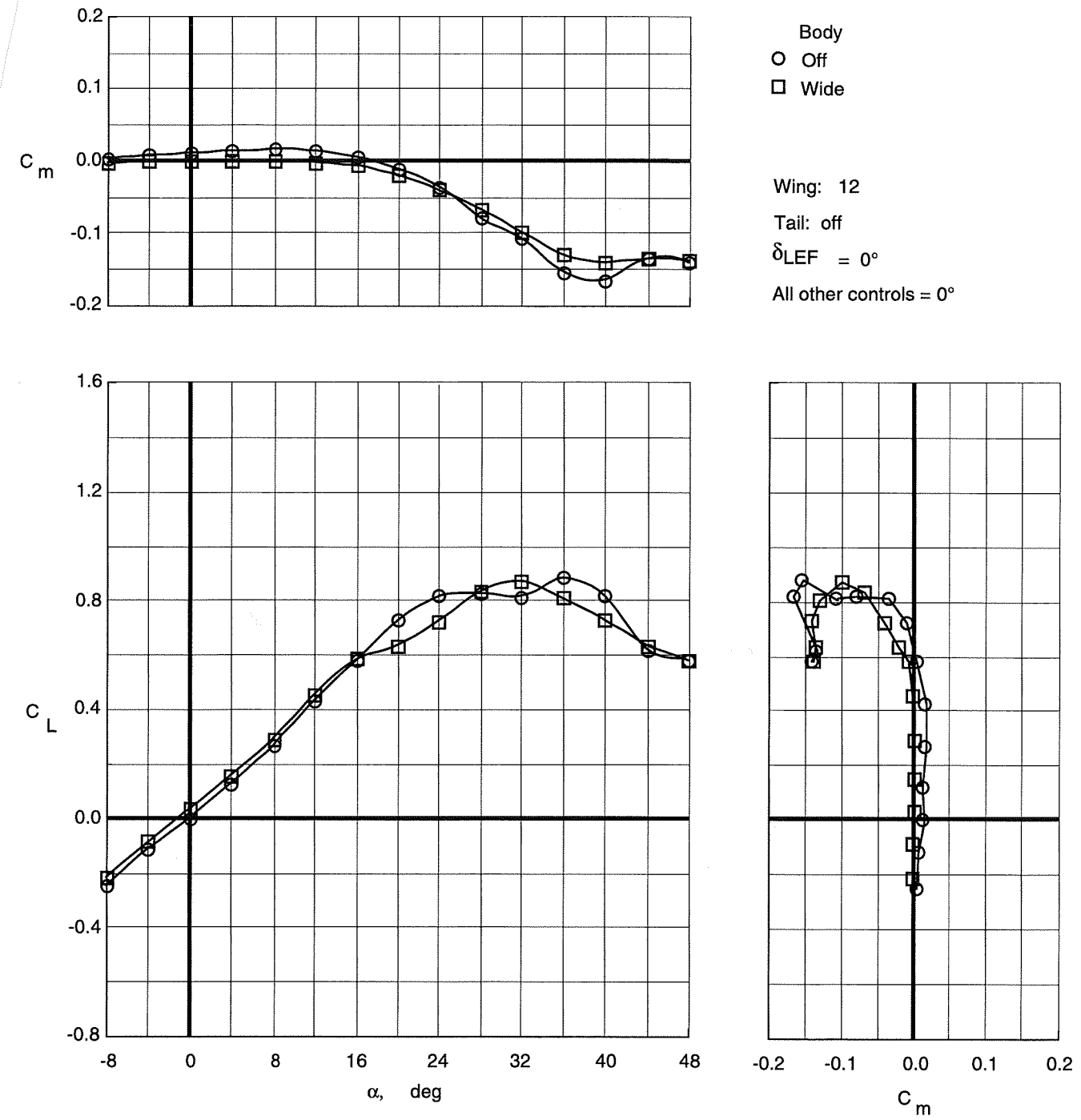

Figure 22. Effect of wide top body on longitudinal characteristics of Wing 12.

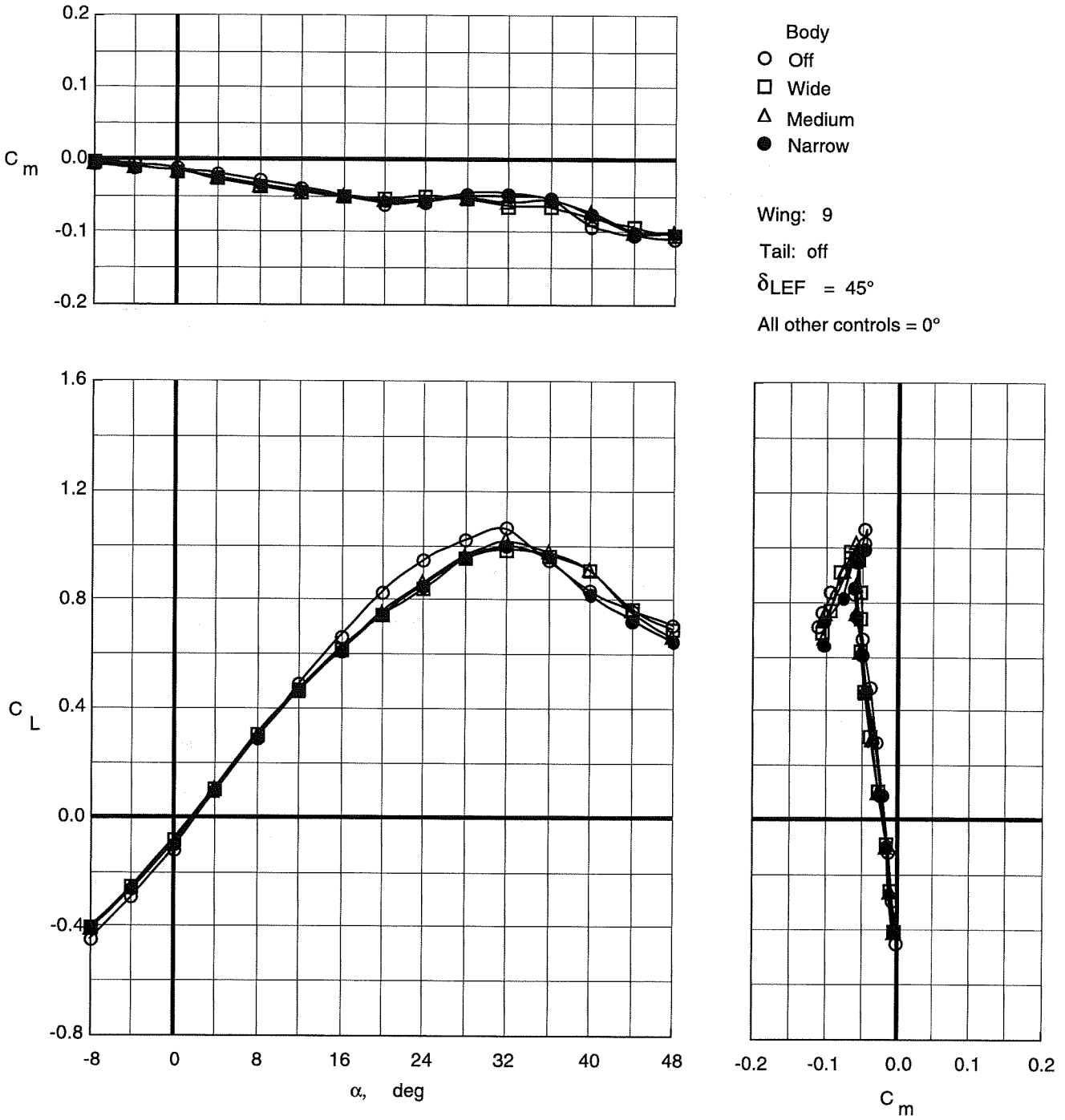

Figure 23. Effect of top body width on longitudinal characteristics of Wing 9 with leading-edge flaps deflected.

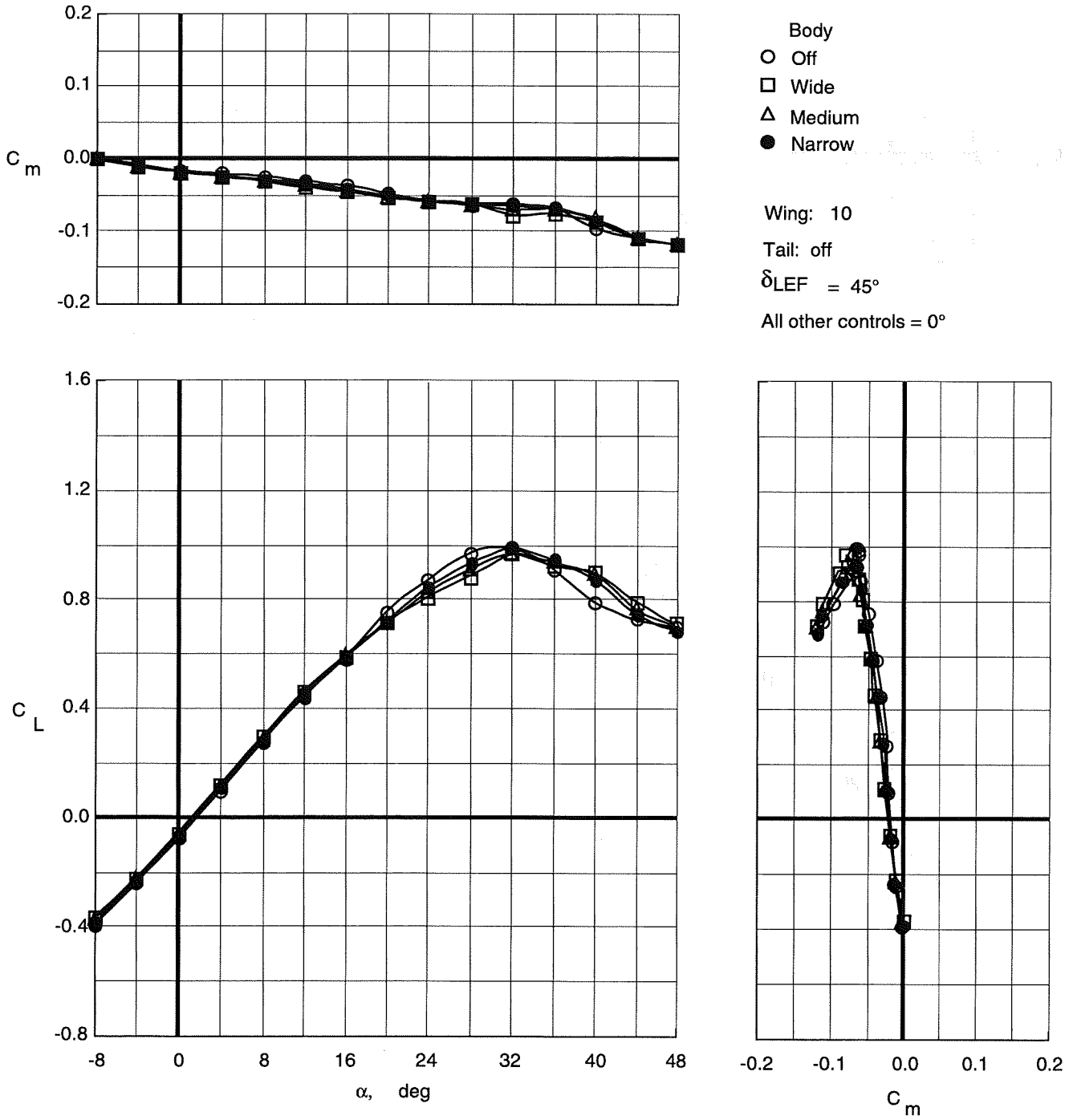

Figure 24. Effect of top body width on longitudinal characteristics of Wing 10 with leading-edge flaps deflected.

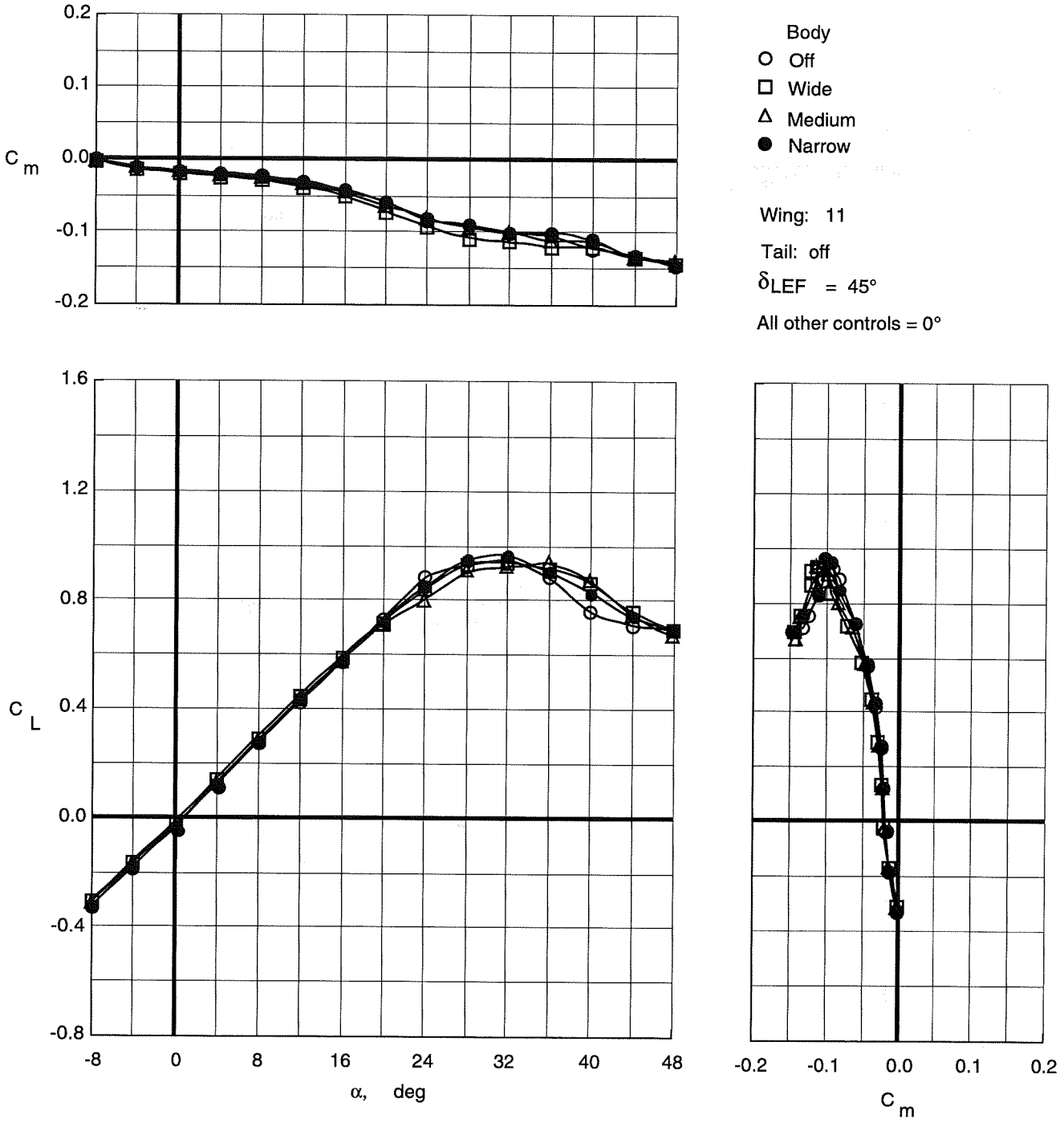

Figure 25. Effect of top body width on longitudinal characteristics of Wing 11 with leading-edge flaps deflected.

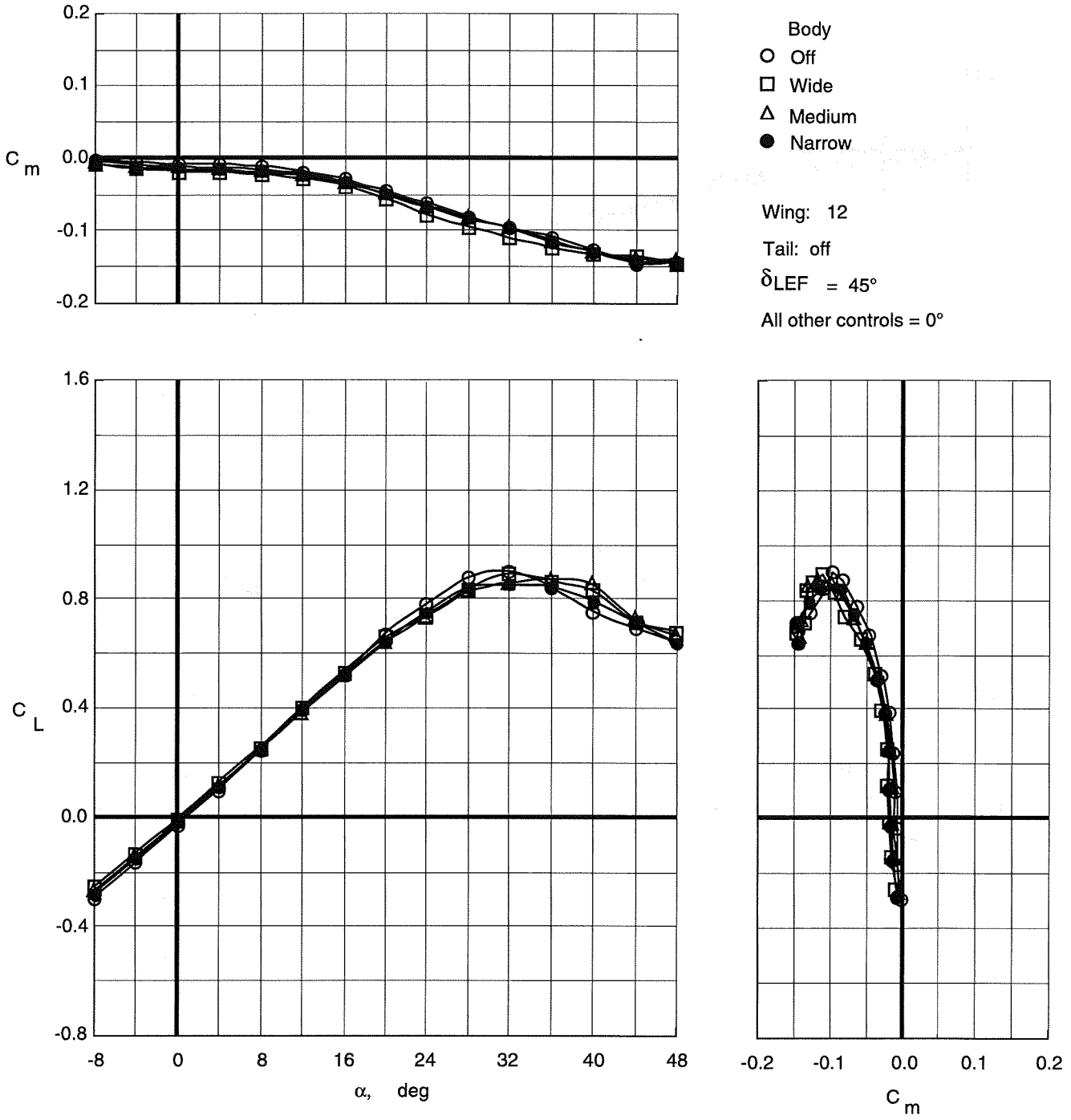

Figure 26. Effect of top body width on longitudinal characteristics of Wing 12 with leading-edge flaps deflected.

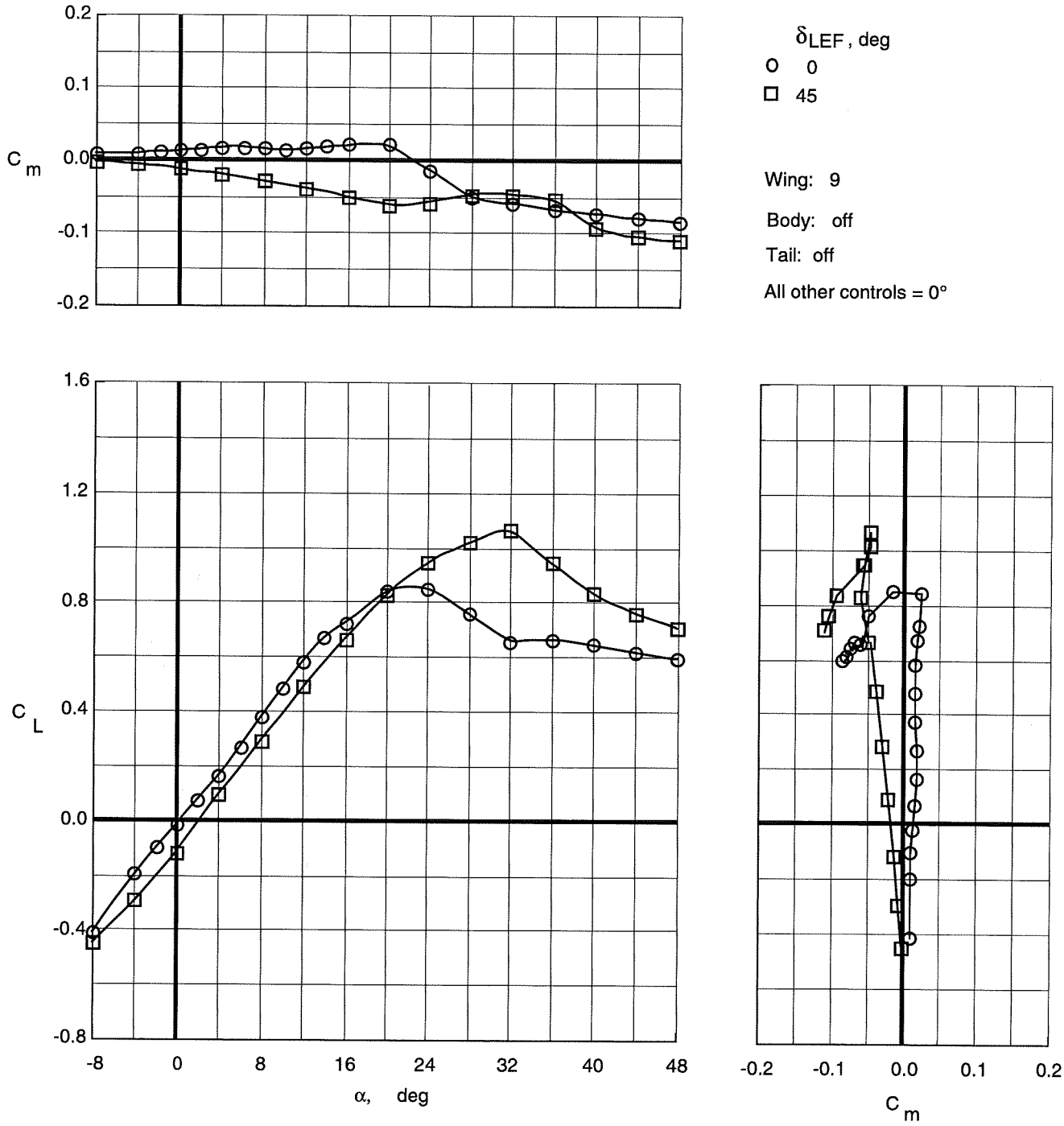

Figure 27. Effect of leading-edge flap deflection on longitudinal characteristics of Wing 9 with top body off.

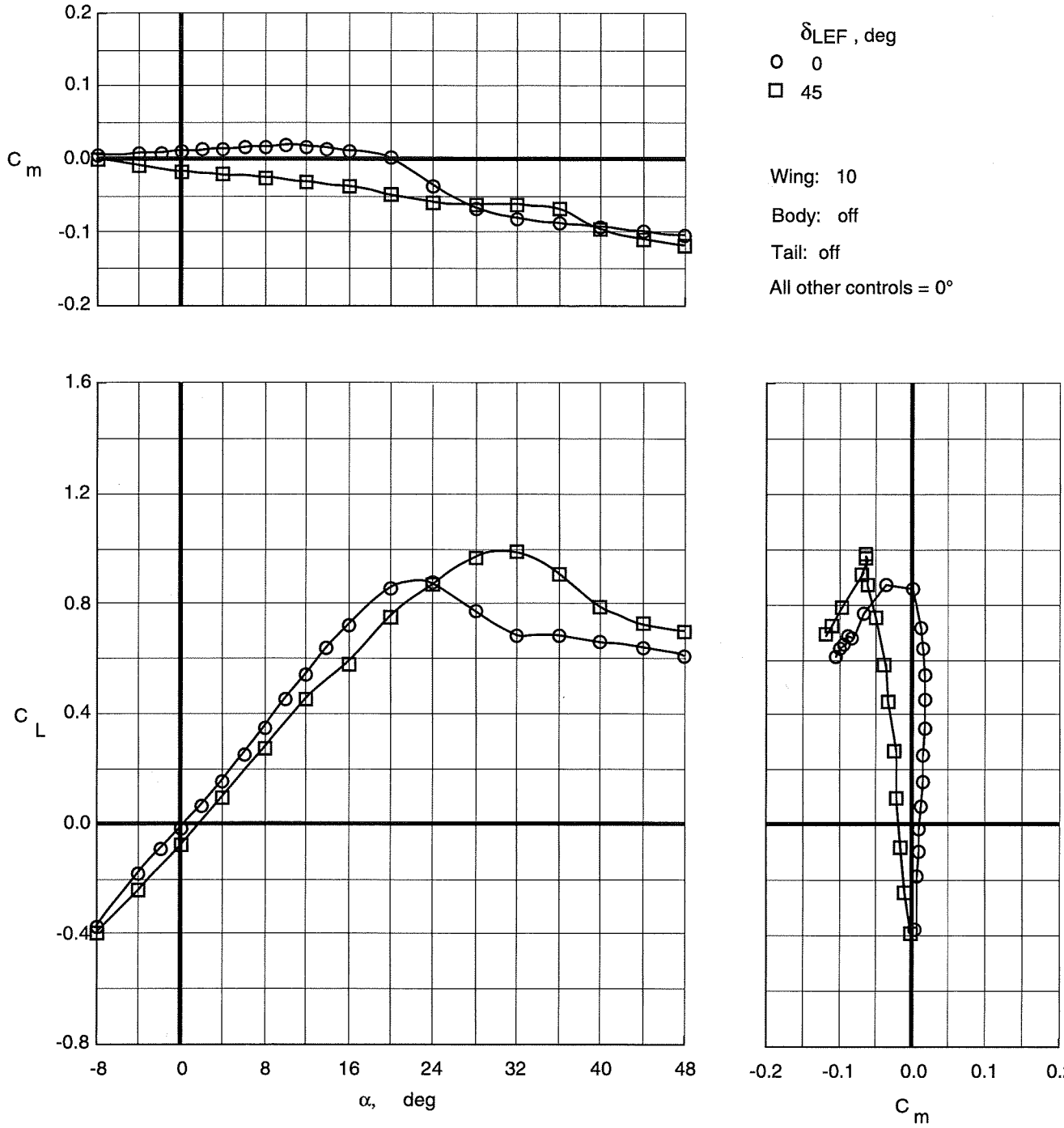

Figure 28. Effect of leading-edge flap deflection on longitudinal characteristics of Wing 10 with top body off.

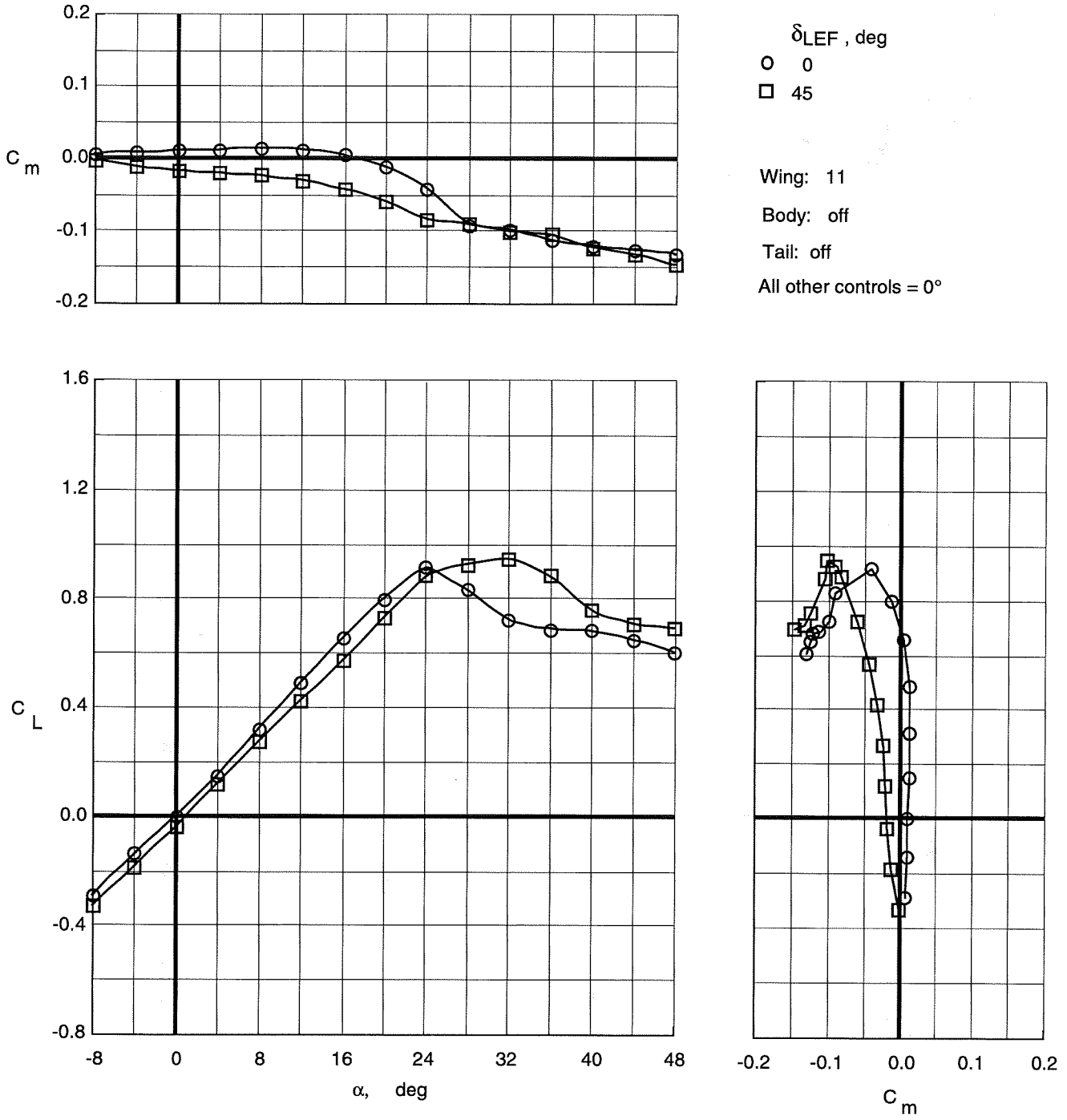

Figure 29. Effect of leading-edge flap deflection on longitudinal characteristics of Wing 11 with top body off.

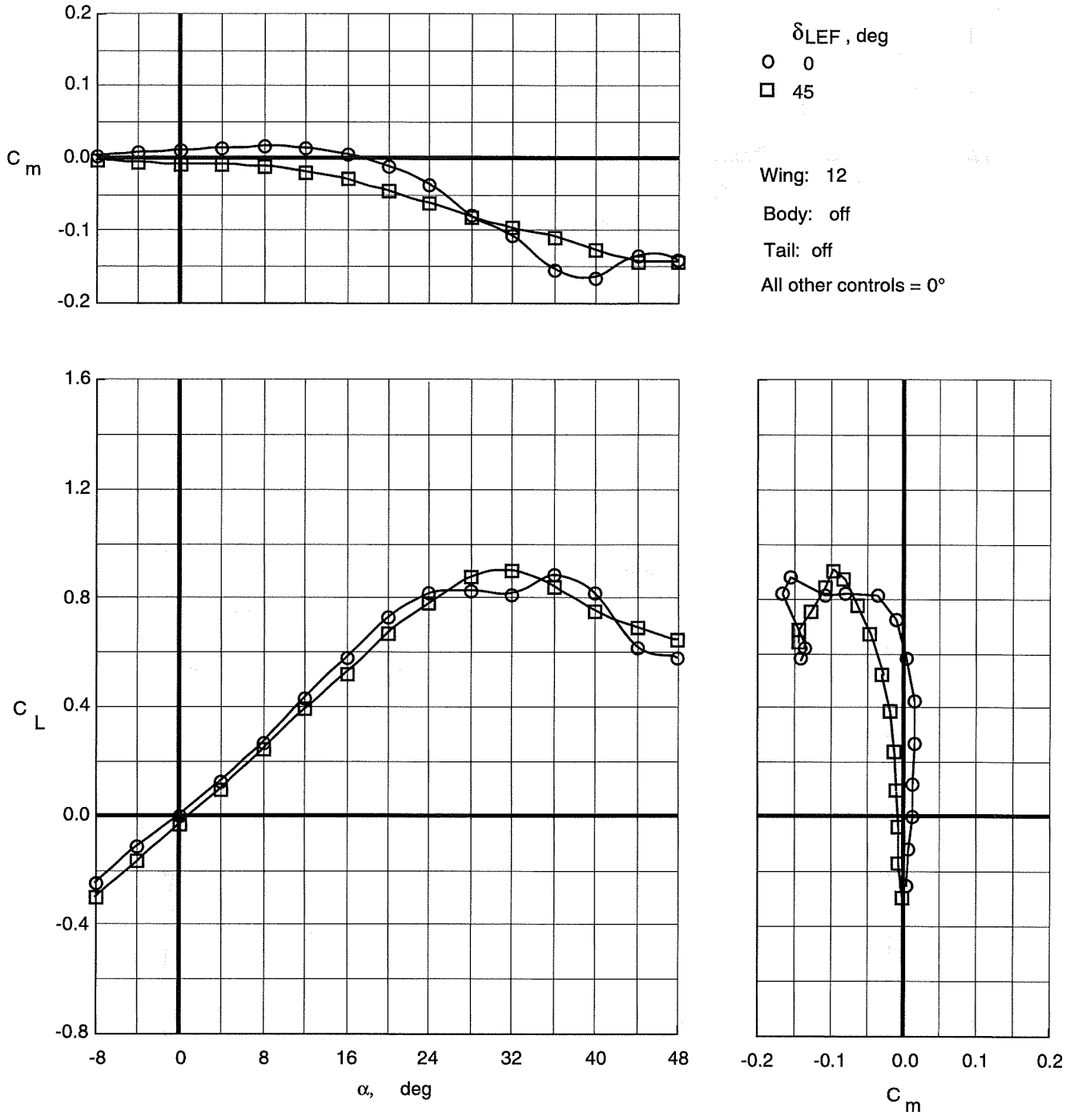

Figure 30. Effect of leading-edge flap deflection on longitudinal characteristics of Wing 12 with top body off.

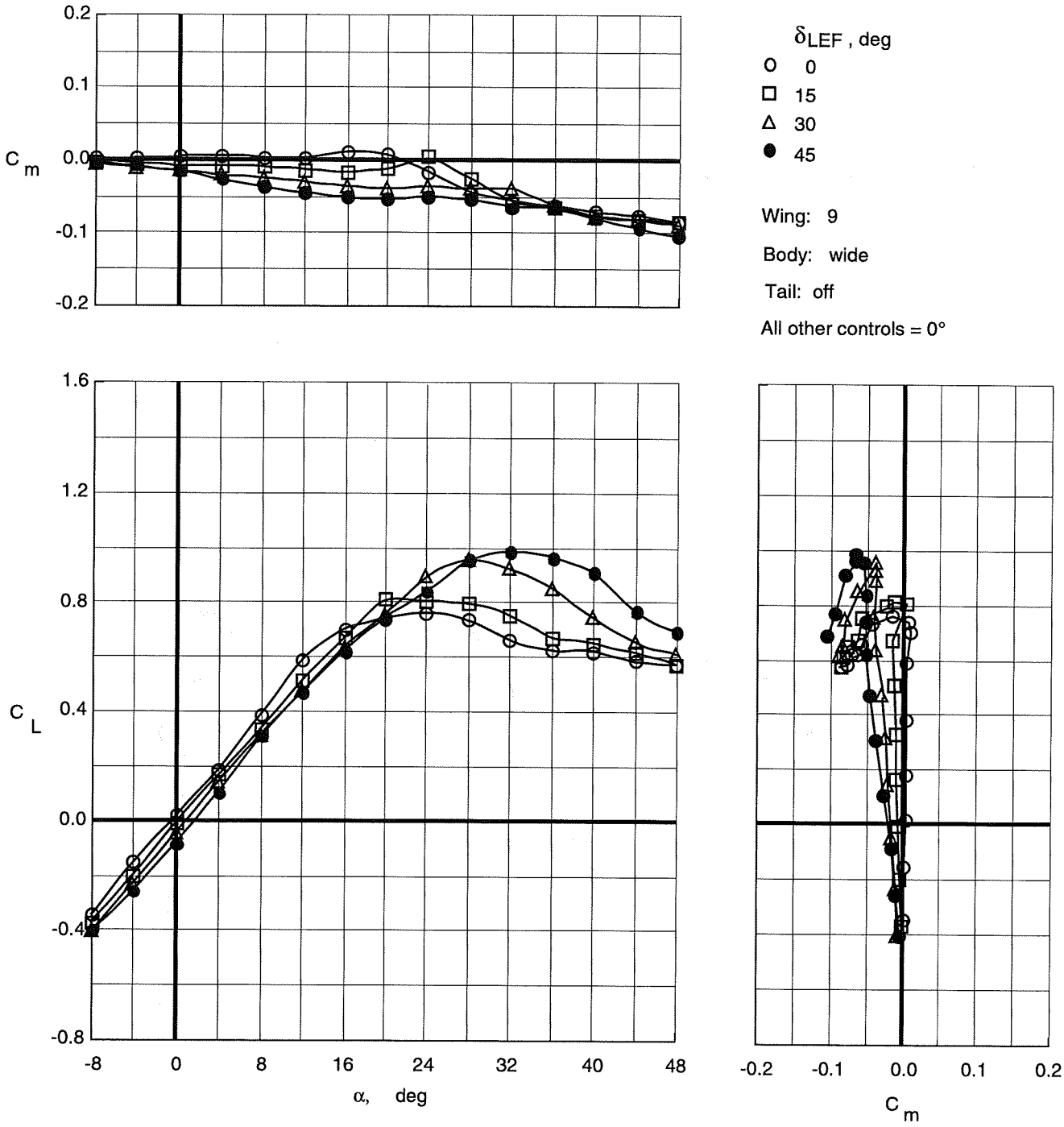

Figure 31. Effect of leading-edge flap deflections on longitudinal characteristics of Wing 9 with wide top body on.

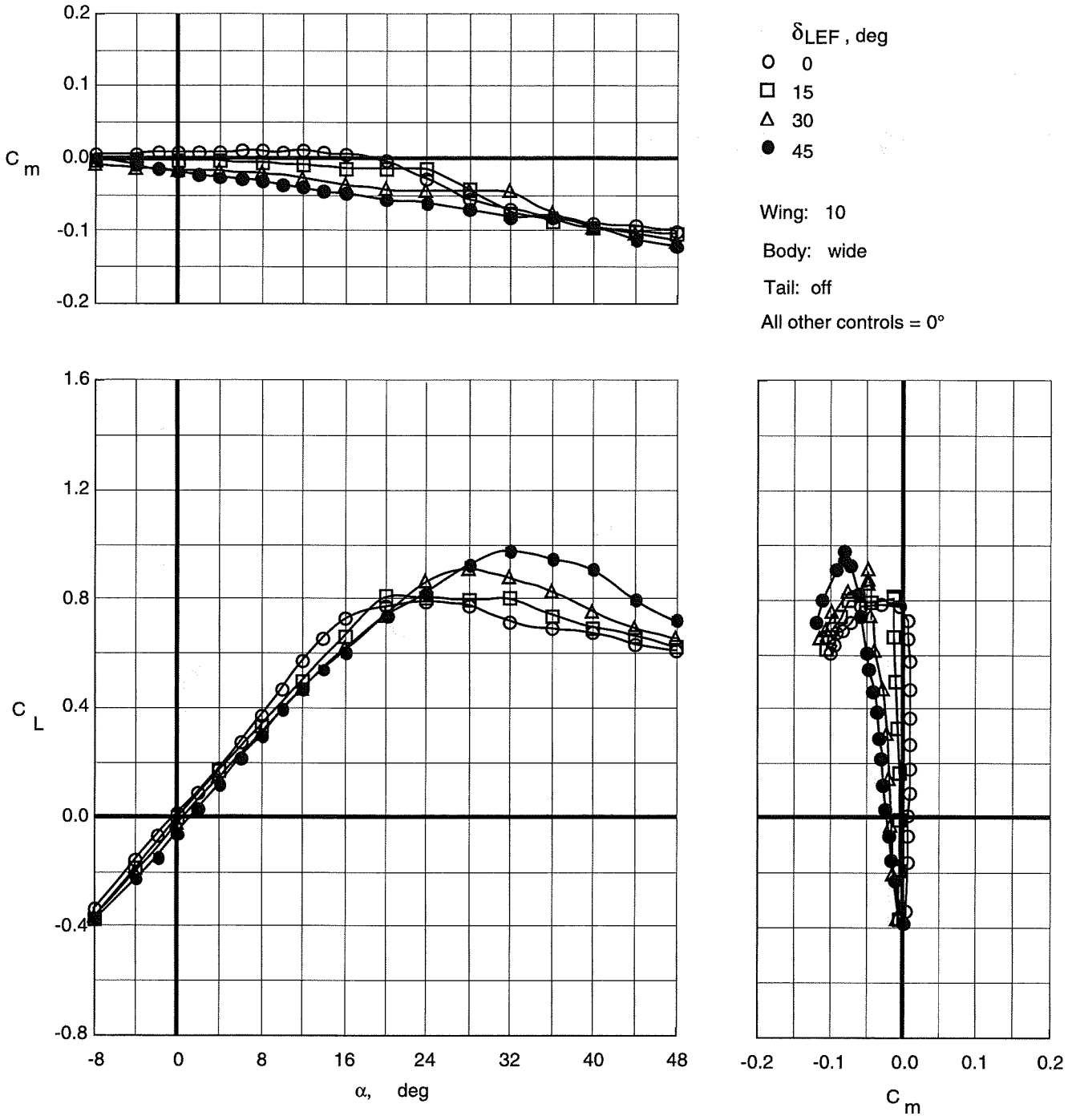

Figure 32. Effect of leading-edge flap deflections on longitudinal characteristics of Wing 10 with wide top body on.

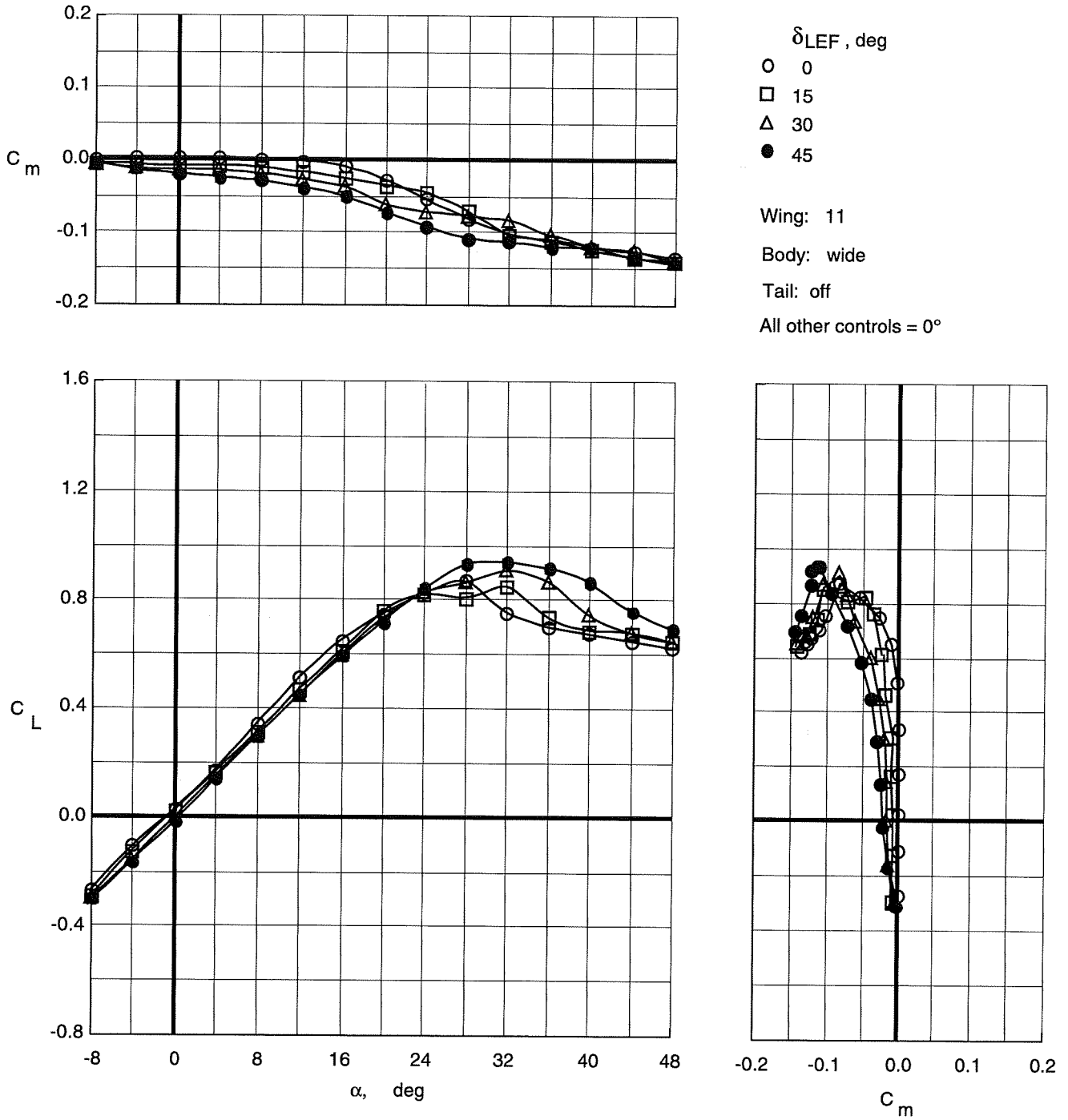

Figure 33. Effect of leading-edge flap deflections on longitudinal characteristics of Wing 11 with wide top body on.

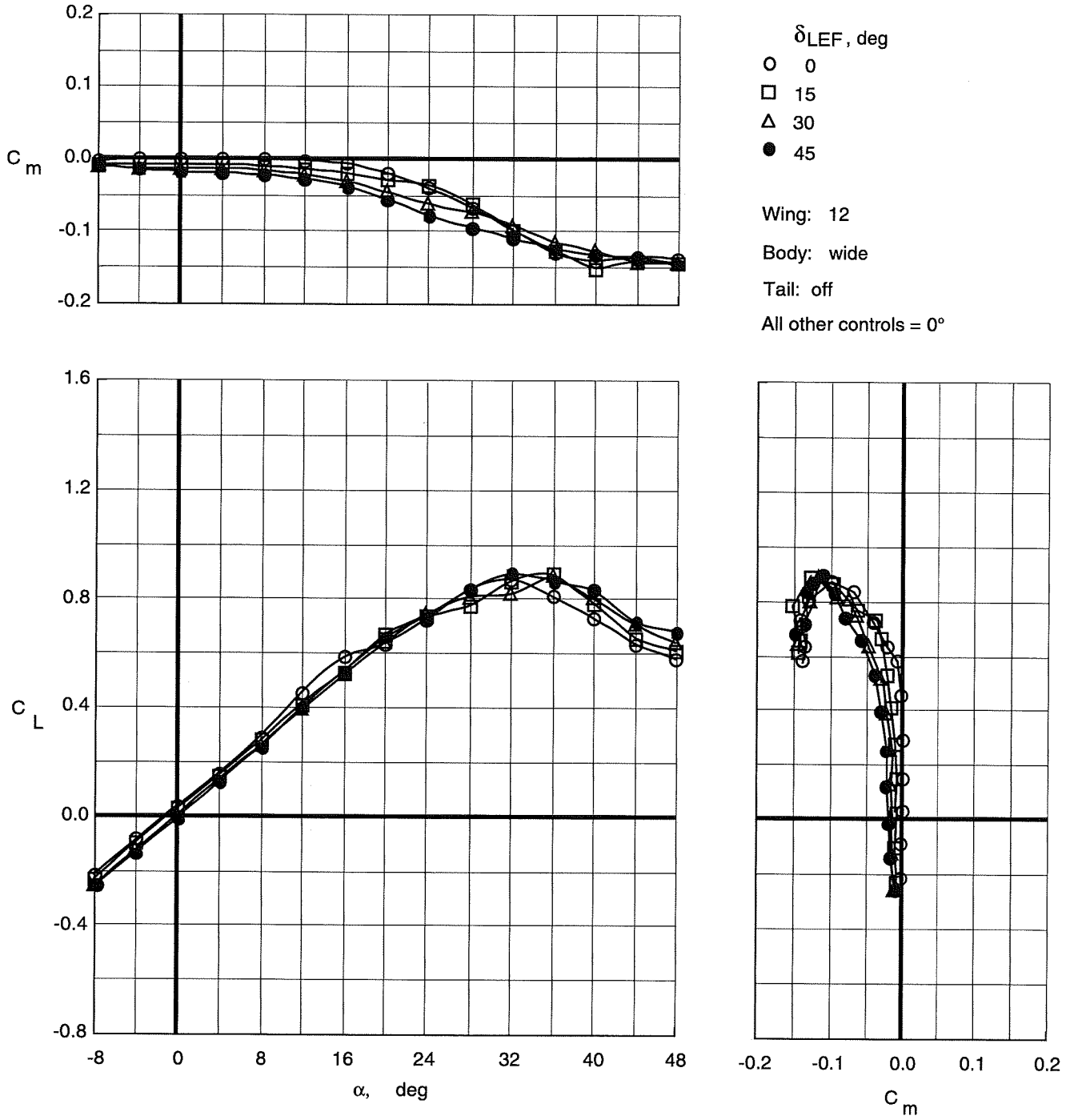

Figure 34. Effect of leading-edge flap deflections on longitudinal characteristics of Wing 12 with wide top body on.

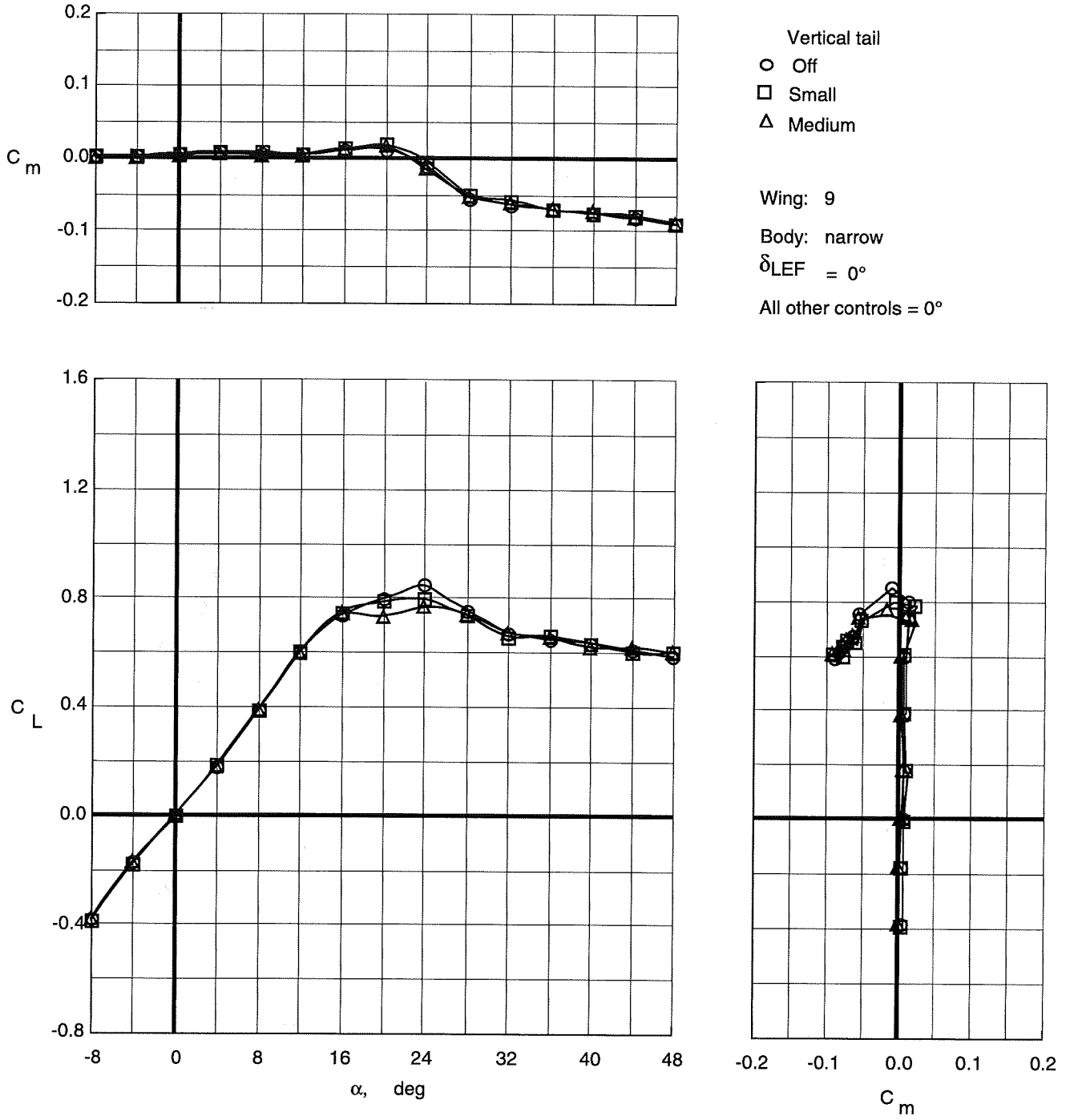

Figure 35. Effect of vertical tail size on longitudinal characteristics of Wing 9 with narrow top body on.

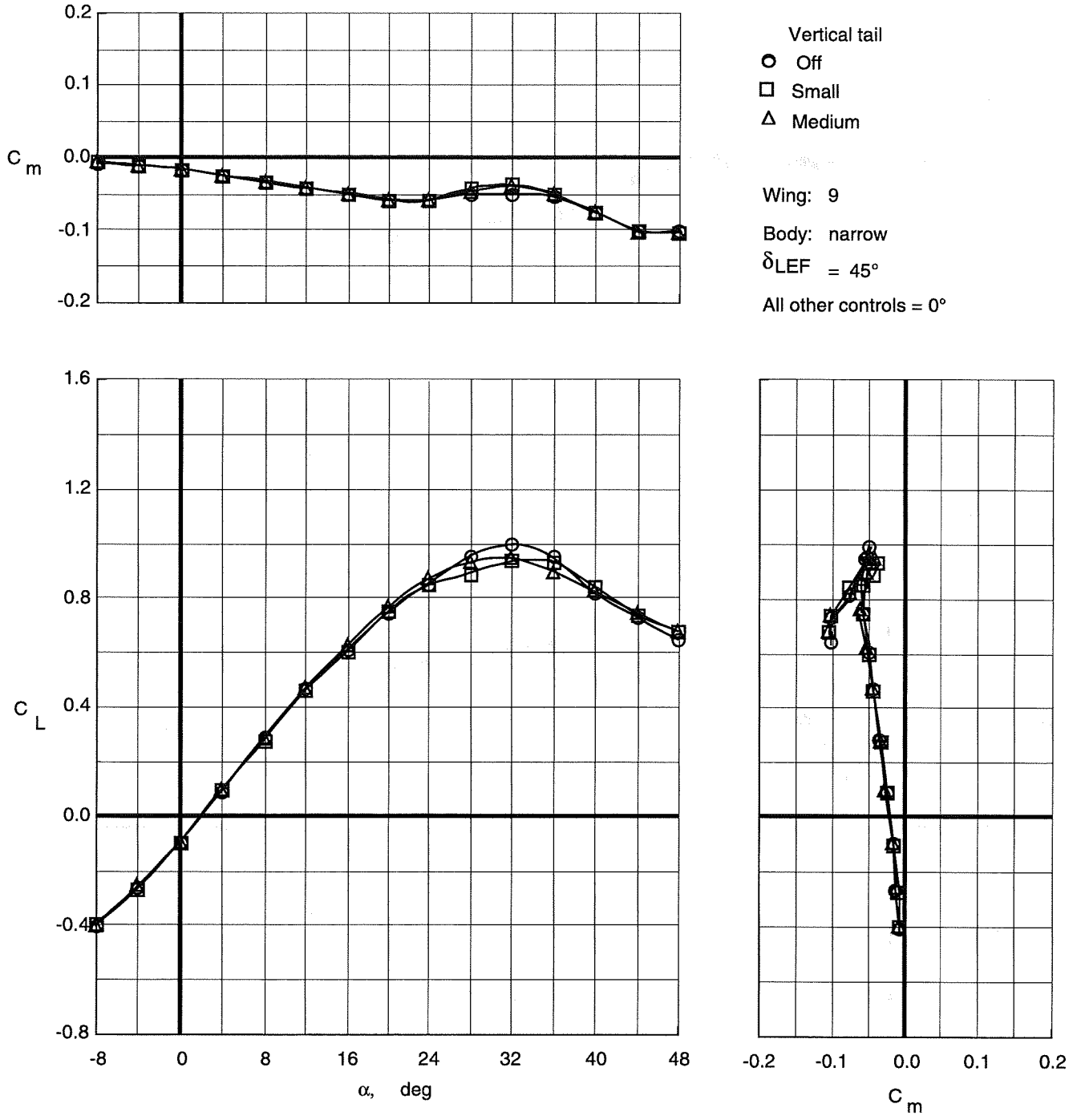

Figure 36. Effect of vertical tail size on longitudinal characteristics of Wing 9 with narrow top body on and leading-edge flaps deflected.

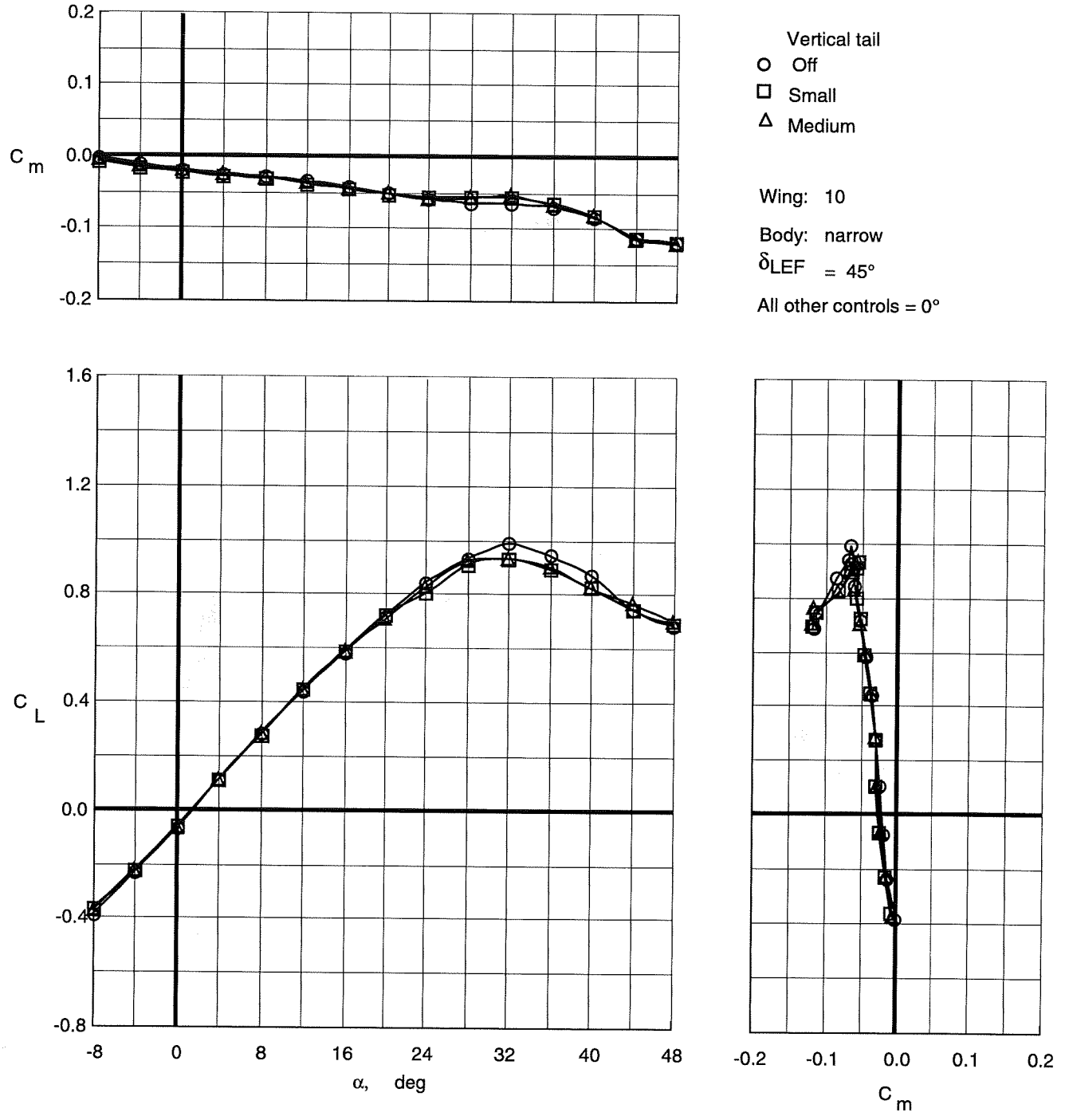

Figure 37. Effect of vertical tail size on longitudinal characteristics of Wing 10 with narrow top body on and leading-edge flaps deflected.

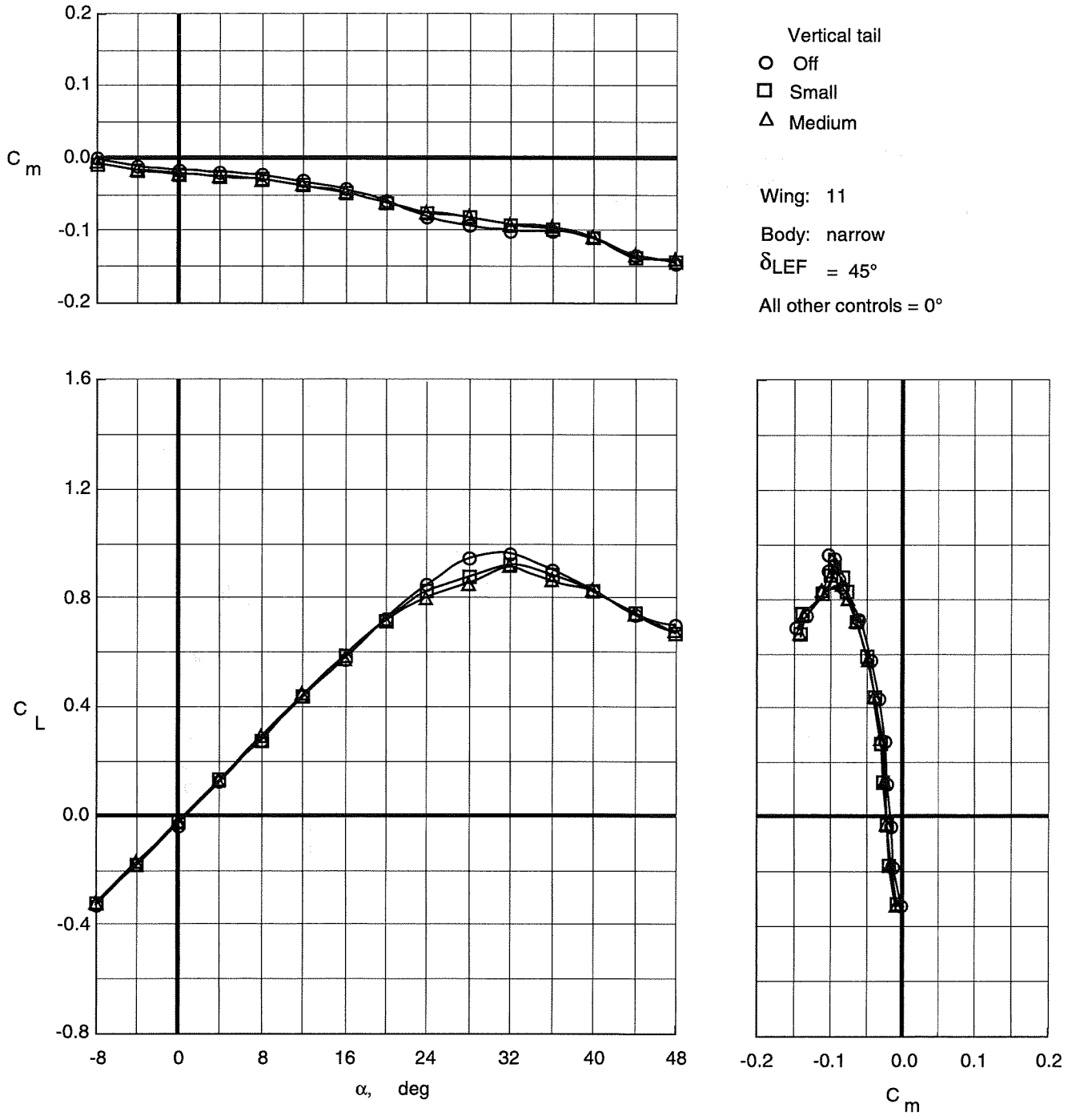

Figure 38. Effect of vertical tail size on longitudinal characteristics of Wing 11 with narrow top body on and leading-edge flaps deflected.

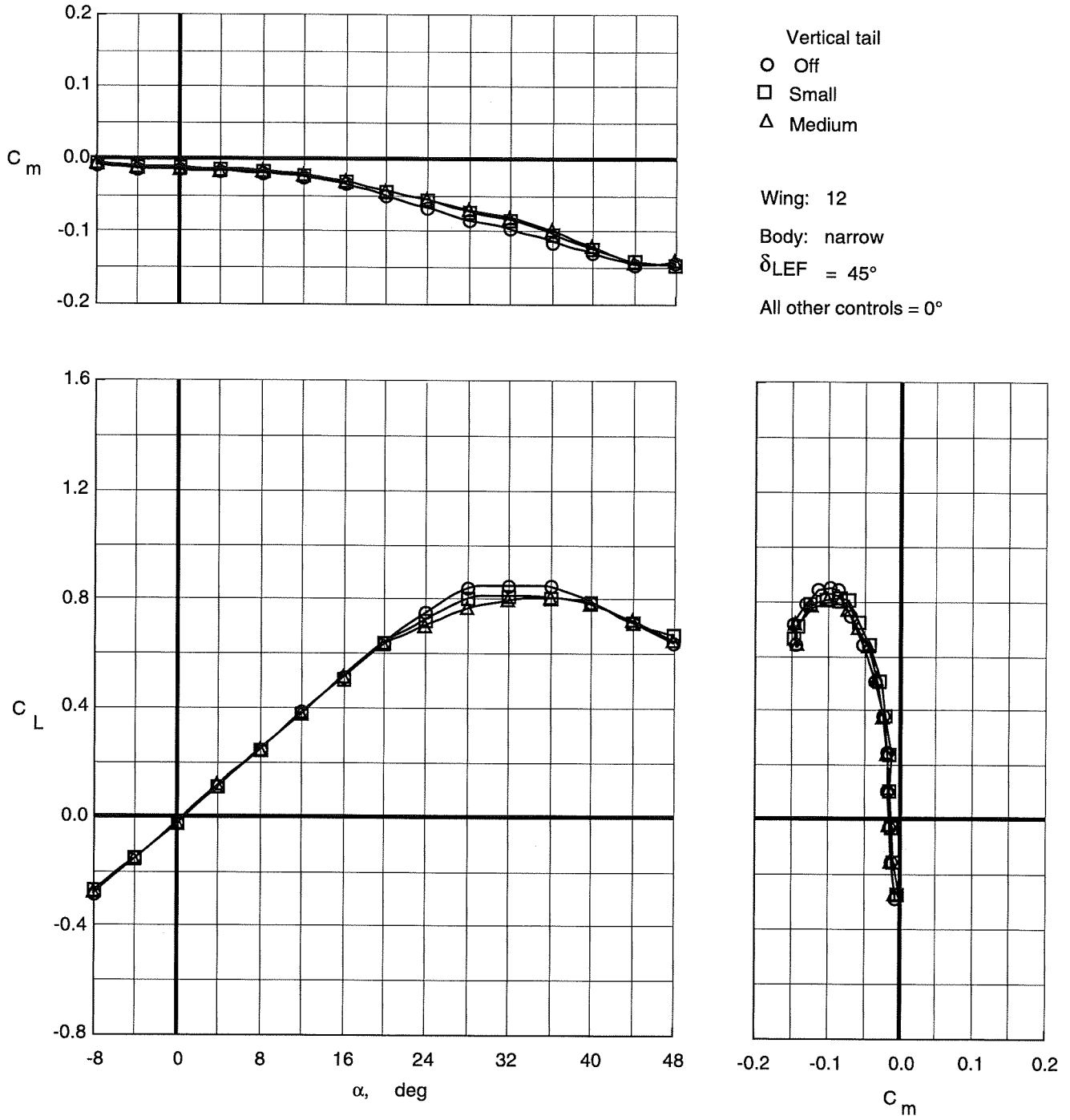

Figure 39. Effect of vertical tail size on longitudinal characteristics of Wing 12 with narrow top body on and leading-edge flaps deflected.

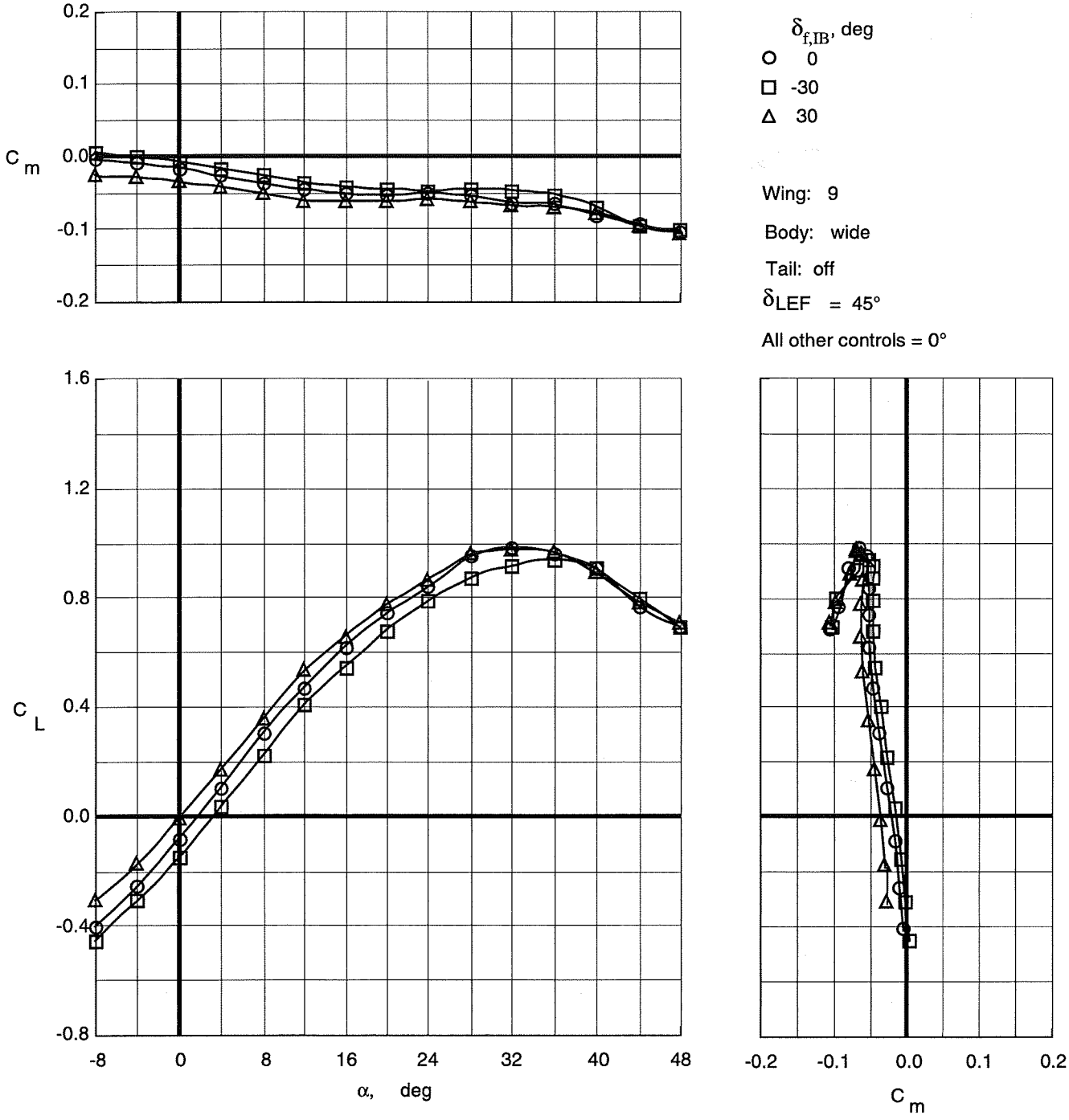

Figure 40. Control effectiveness of symmetric deflections of inboard trailing-edge flaps on Wing 9 with wide top body on and leading-edge flaps deflected.

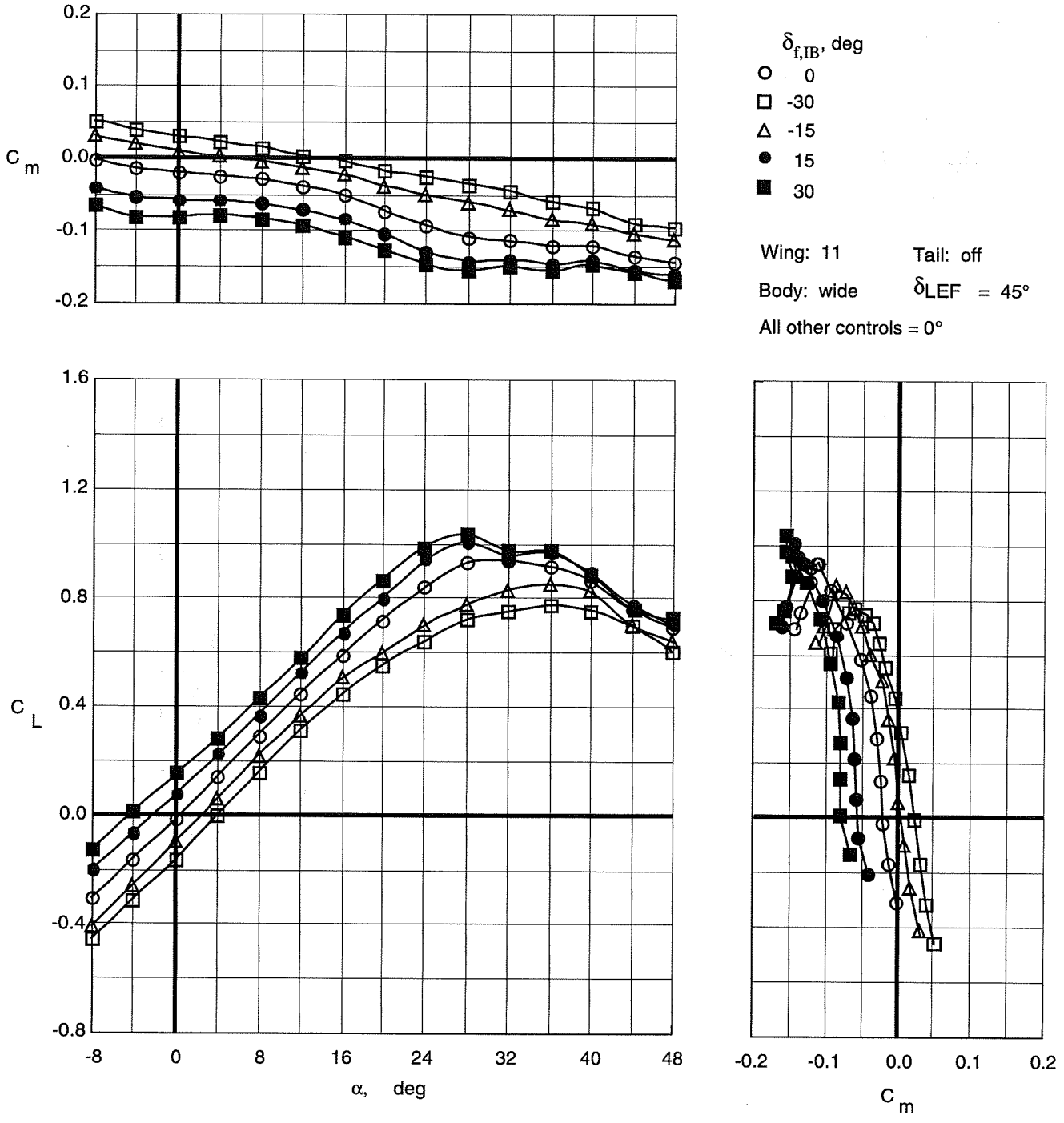

Figure 41. Control effectiveness of symmetric deflections of inboard trailing-edge flaps on Wing 11 with wide top body on and leading-edge flaps deflected.

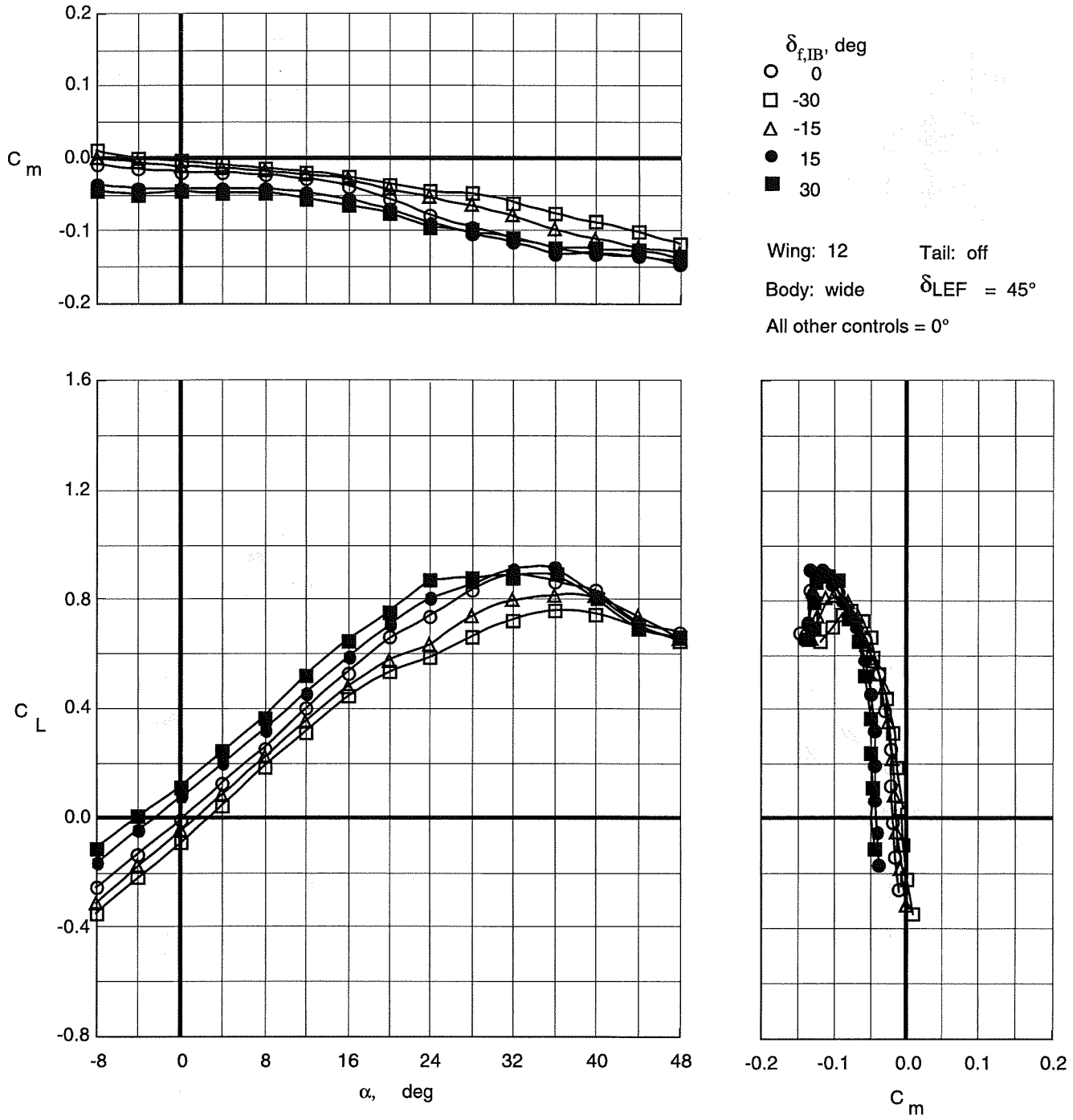

Figure 42. Control effectiveness of symmetric deflections of inboard trailing-edge flaps on Wing 12 with wide top body on and leading-edge flaps deflected.

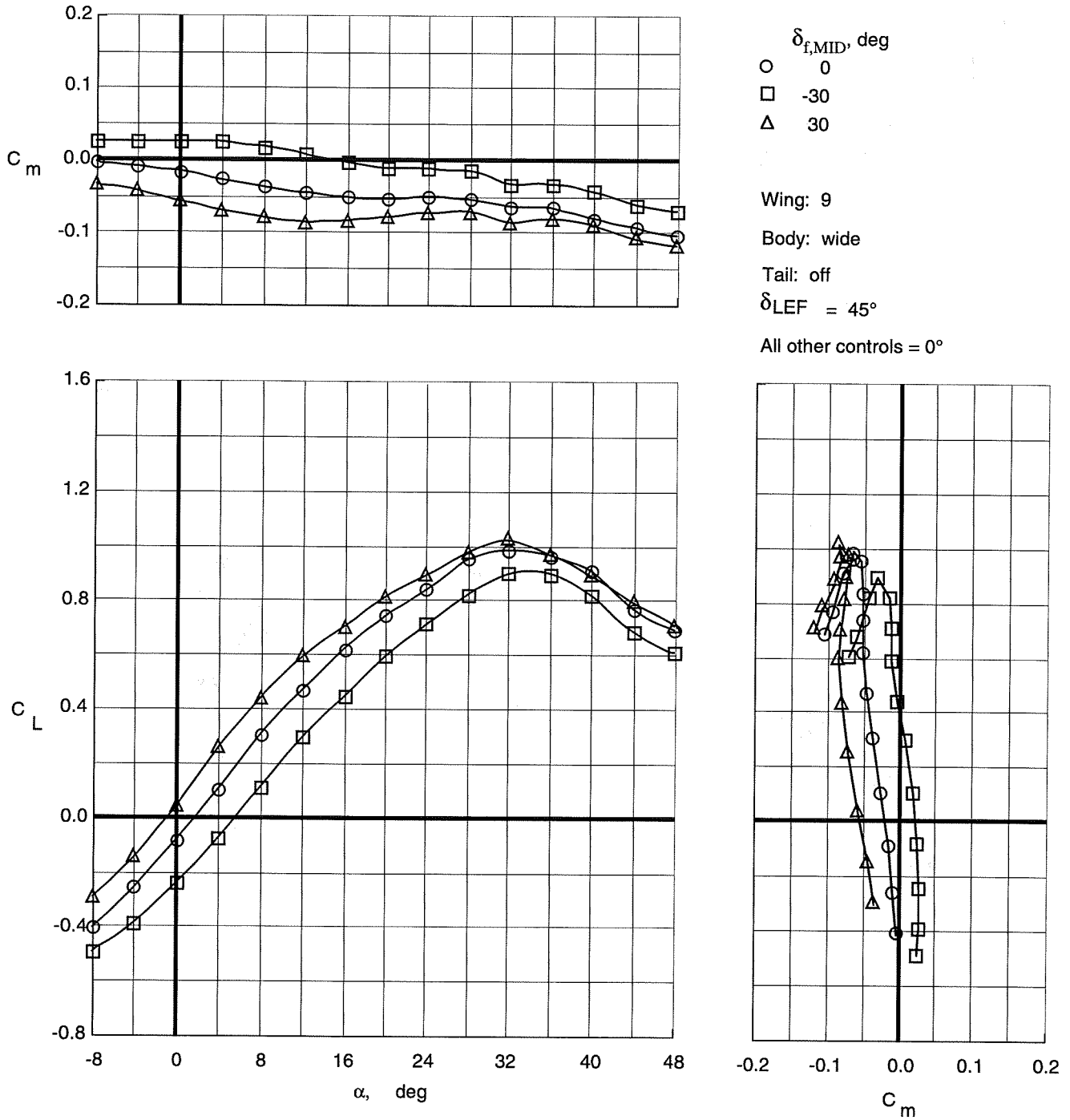

Figure 43. Control effectiveness of symmetric deflections of middle trailing-edge flaps on Wing 9 with wide top body on and leading-edge flaps deflected.

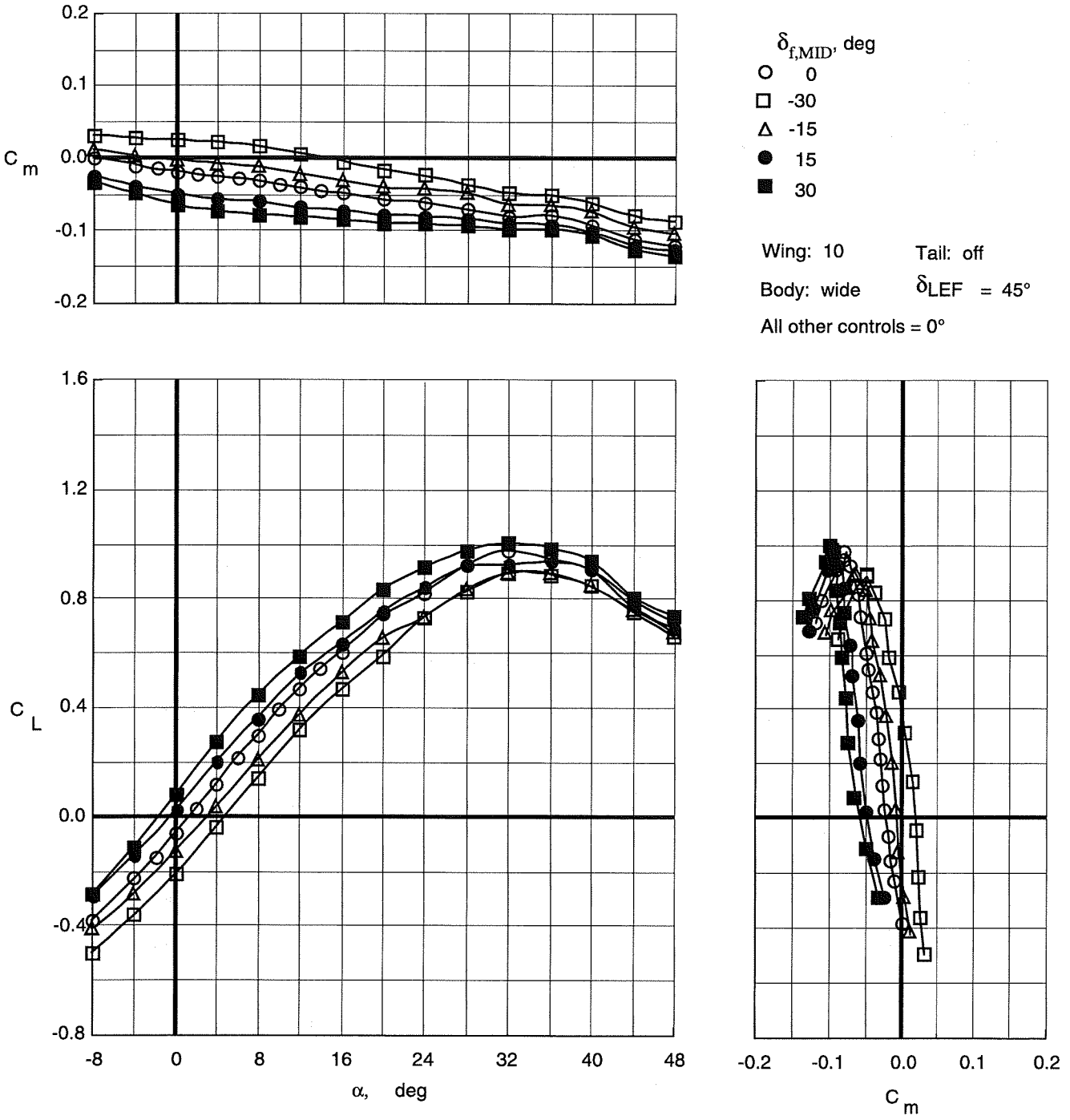

Figure 44. Control effectiveness of symmetric deflections of middle trailing-edge flaps on Wing 10 with wide top body on and leading-edge flaps deflected.

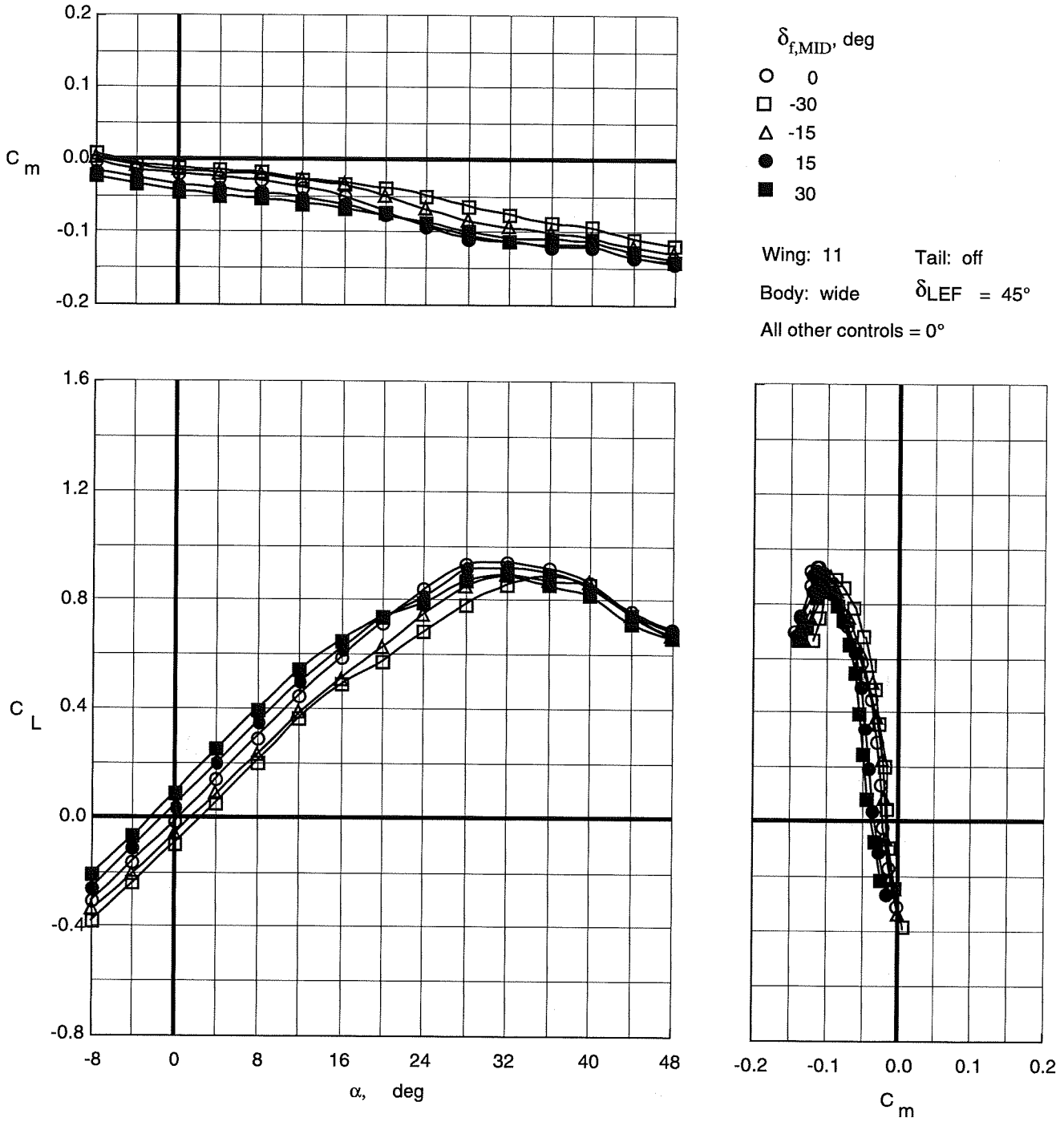

Figure 45. Control effectiveness of symmetric deflections of middle trailing-edge flaps on Wing 11 with wide top body on and leading-edge flaps deflected.

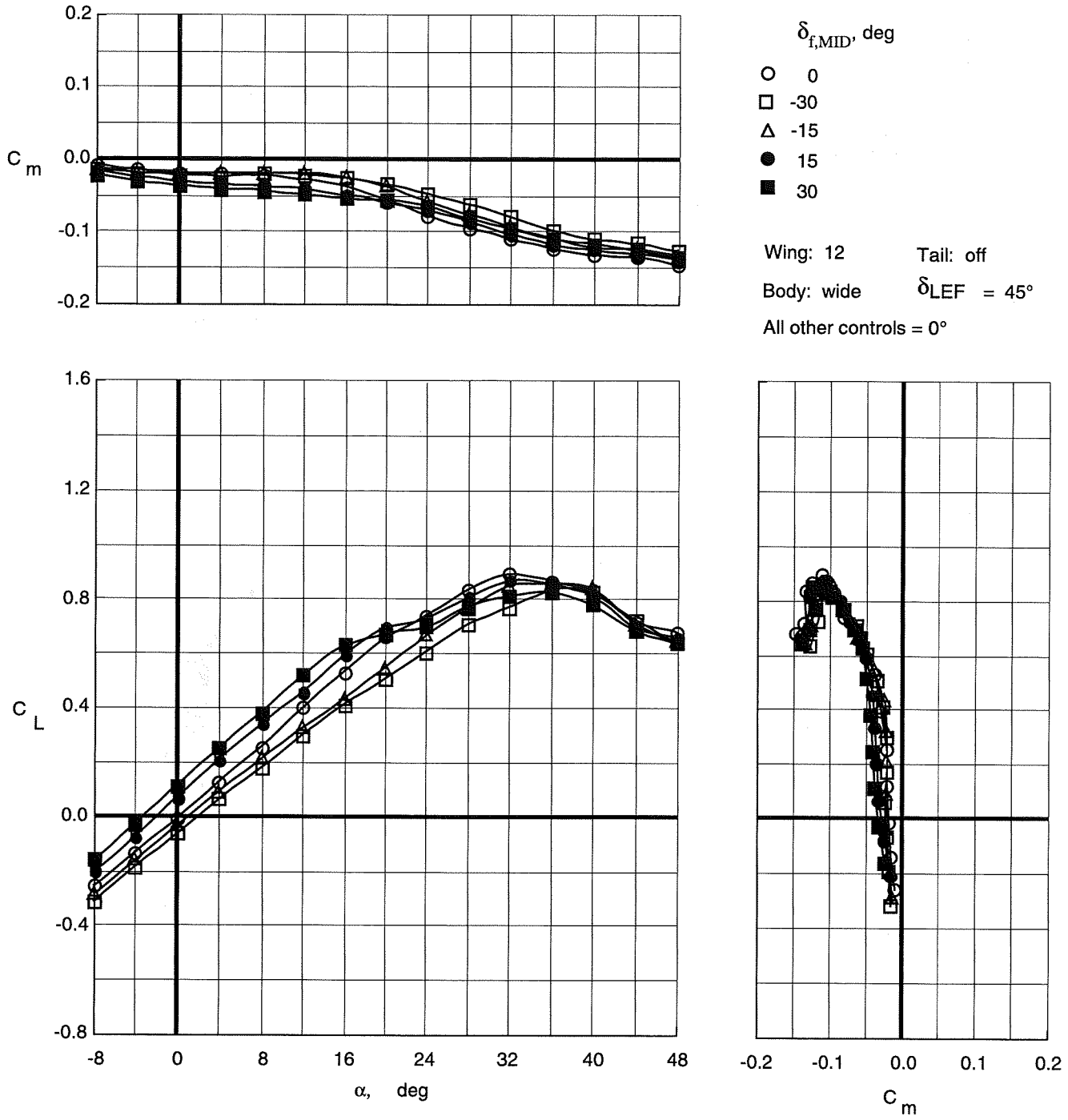

Figure 46. Control effectiveness of symmetric deflections of middle trailing-edge flaps on Wing 12 with wide top body on and leading-edge flaps deflected.

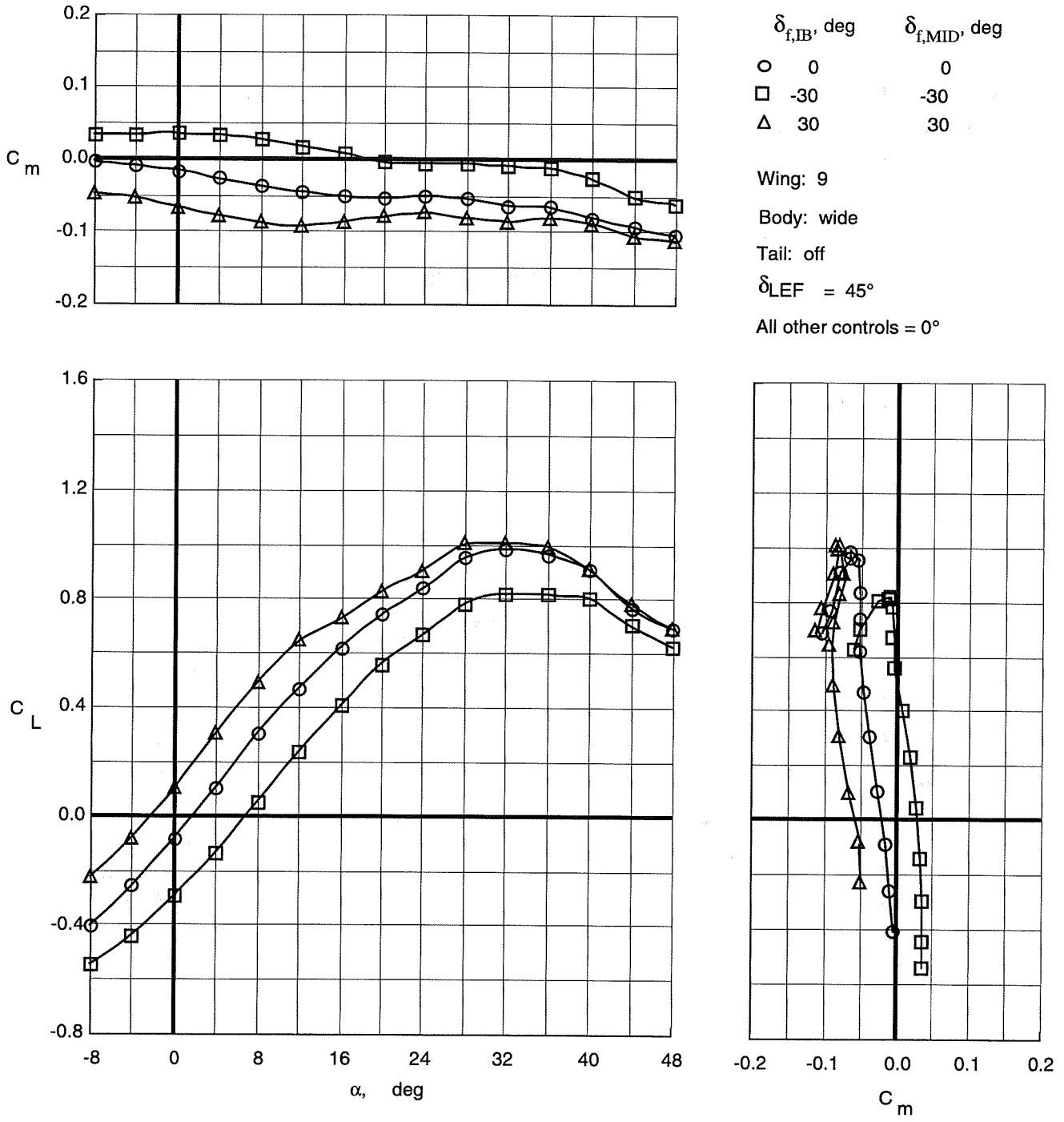

Figure 47. Control effectiveness of symmetric deflections of inboard and middle trailing-edge flaps on Wing 9 with wide top body on and leading-edge flaps deflected.

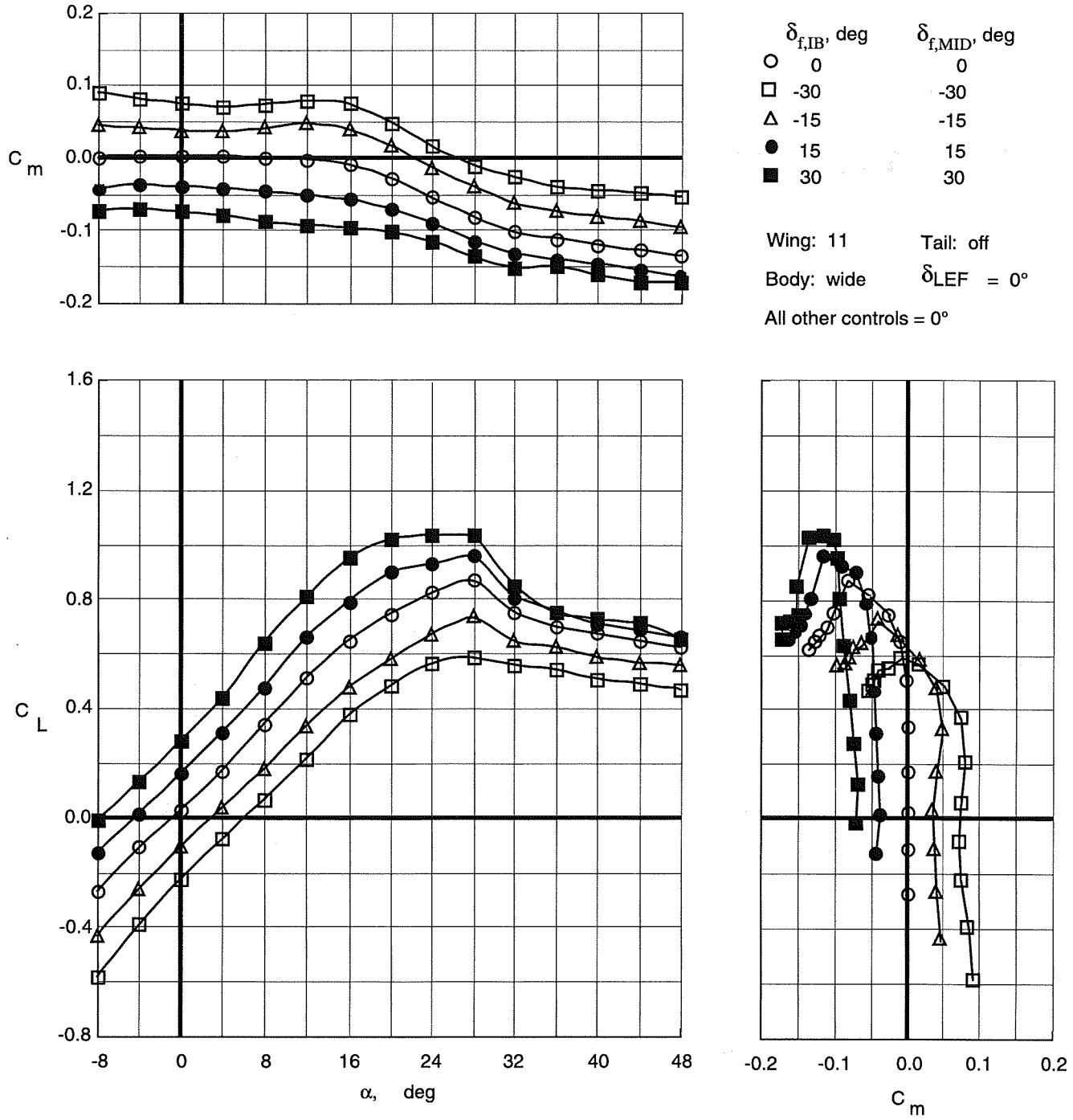

Figure 48. Control effectiveness of symmetric deflections of inboard and middle trailing-edge flaps on Wing 11 with wide top body on.

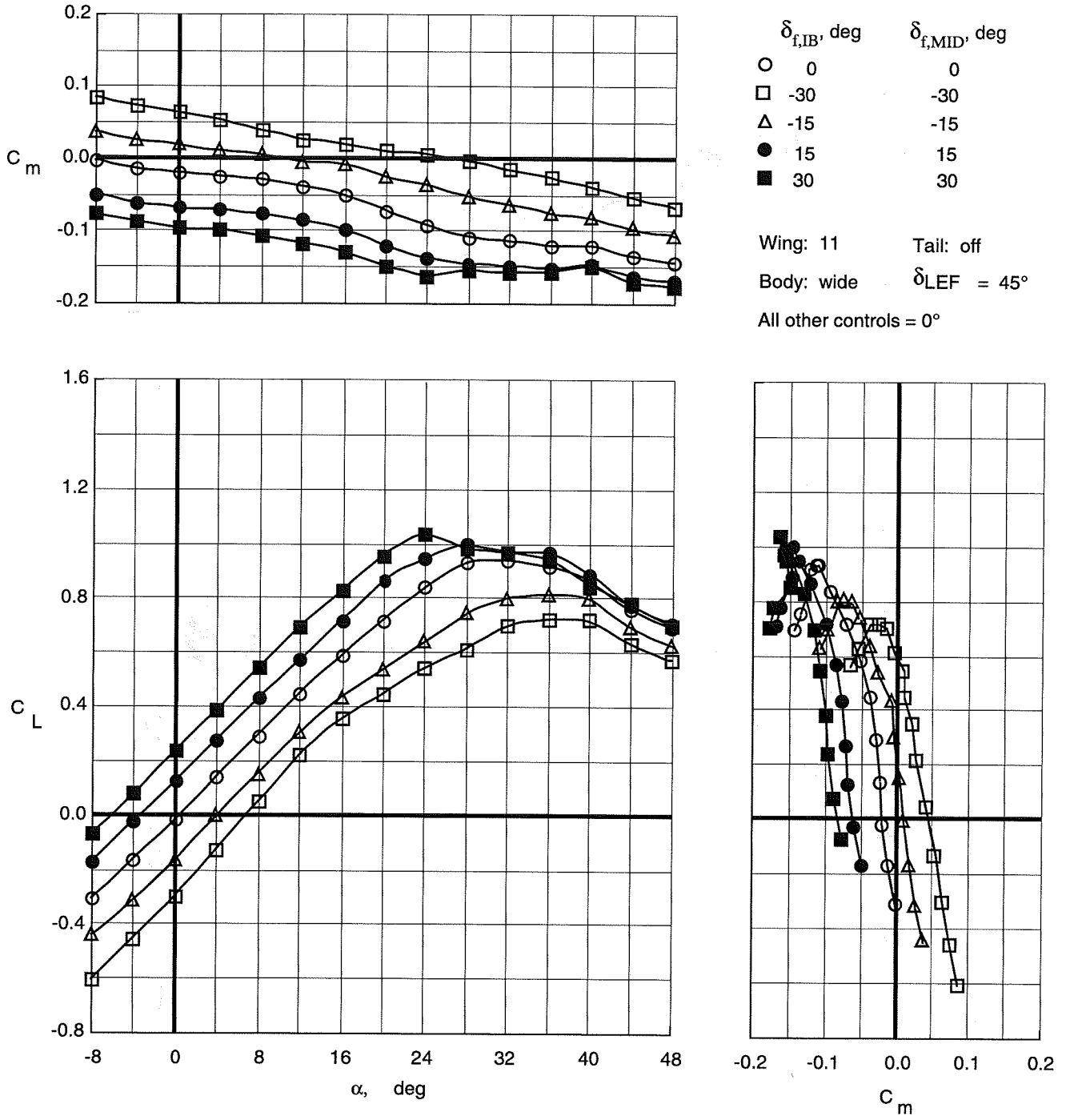

Figure 49. Control effectiveness of symmetric deflections of inboard and middle trailing-edge flaps on Wing 11 with wide top body on and leading-edge flaps deflected.

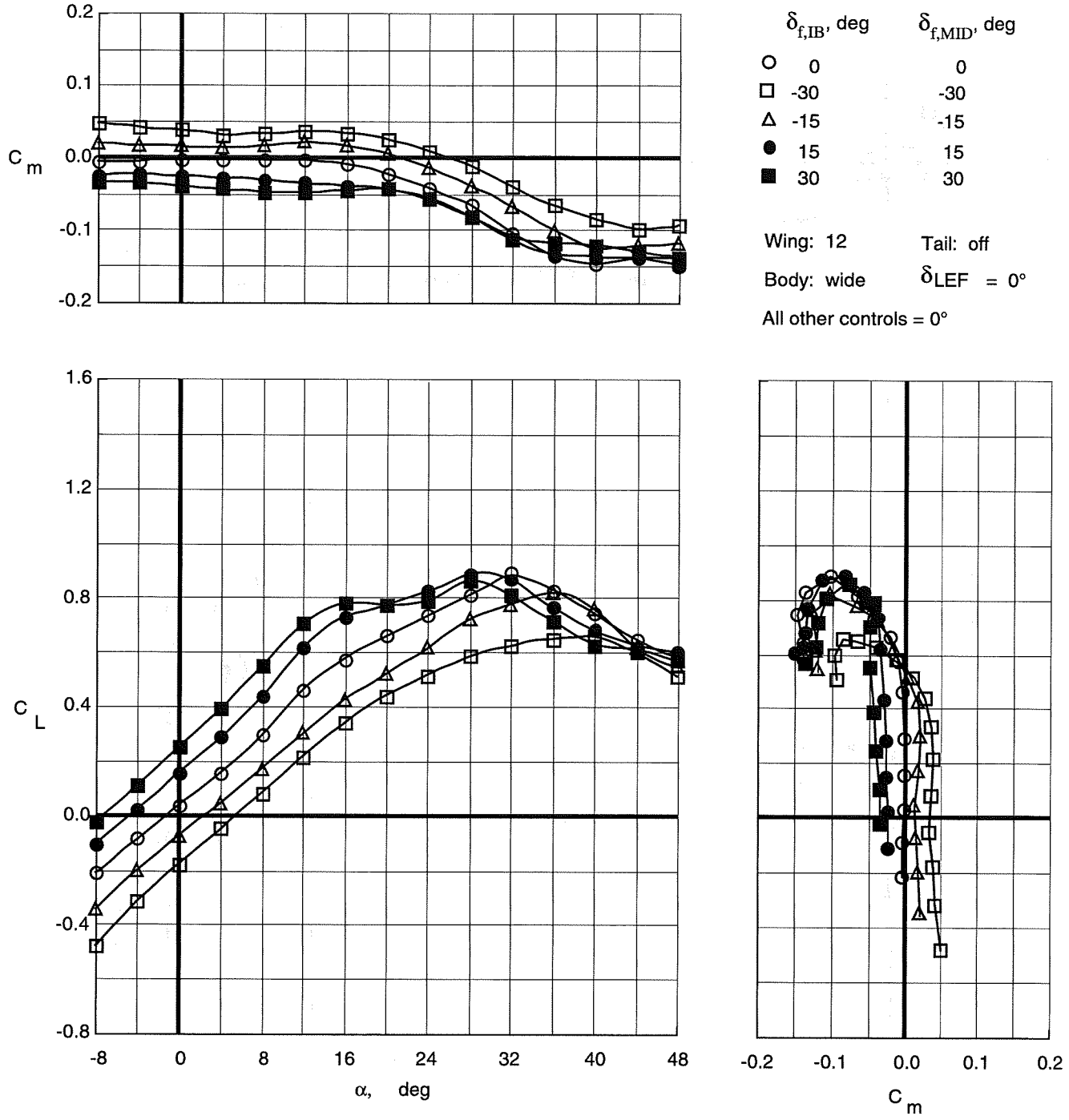

Figure 50. Control effectiveness of symmetric deflections of inboard and middle trailing-edge flaps on Wing 12 with wide top body on.

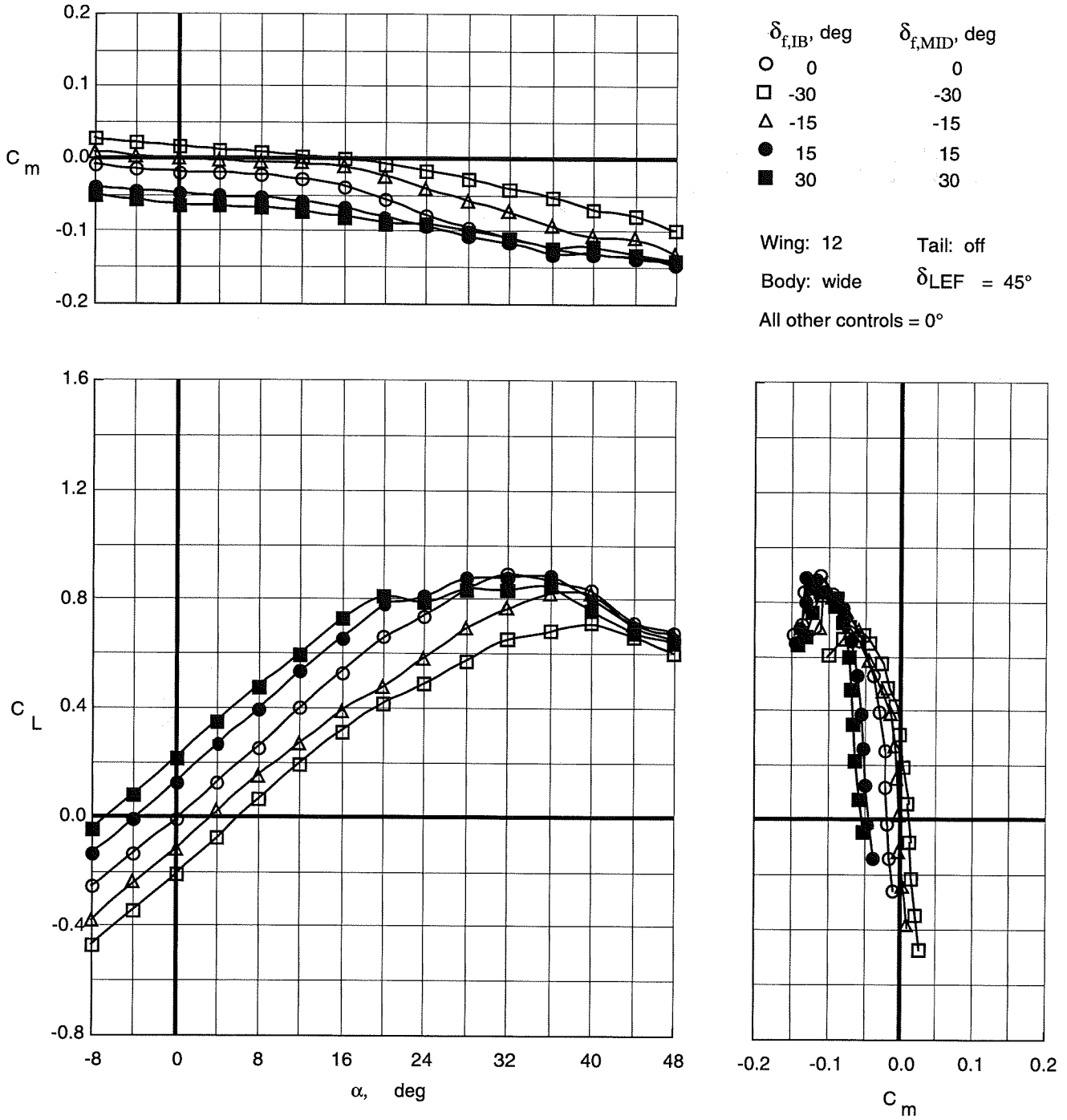

Figure 51. Control effectiveness of symmetric deflections of inboard and middle trailing-edge flaps on Wing 12 with wide top body on and leading-edge flaps deflected.

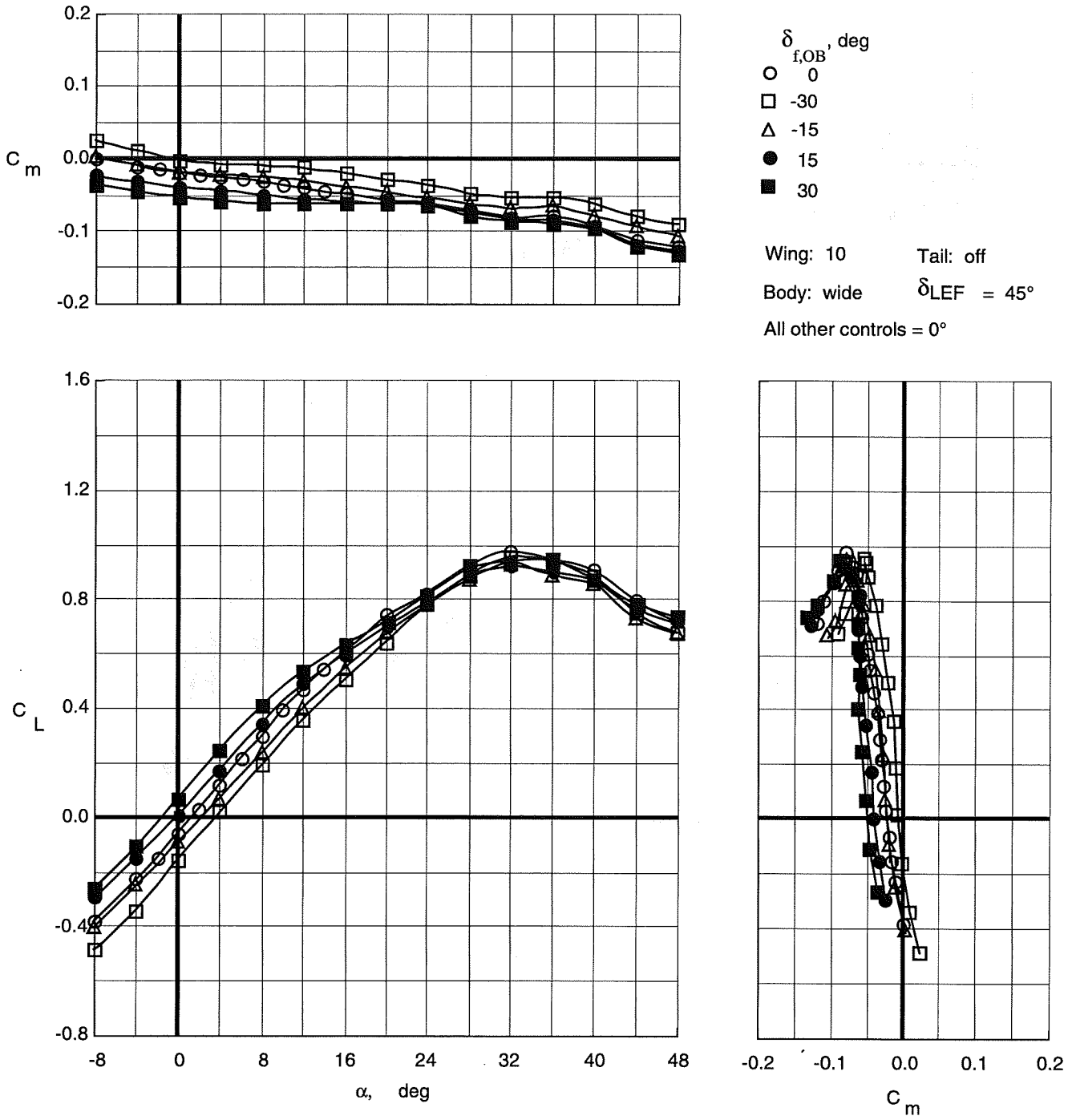

Figure 52. Control effectiveness of symmetric deflections of outboard trailing-edge flaps on Wing 10 with wide top body on and leading-edge flaps deflected.

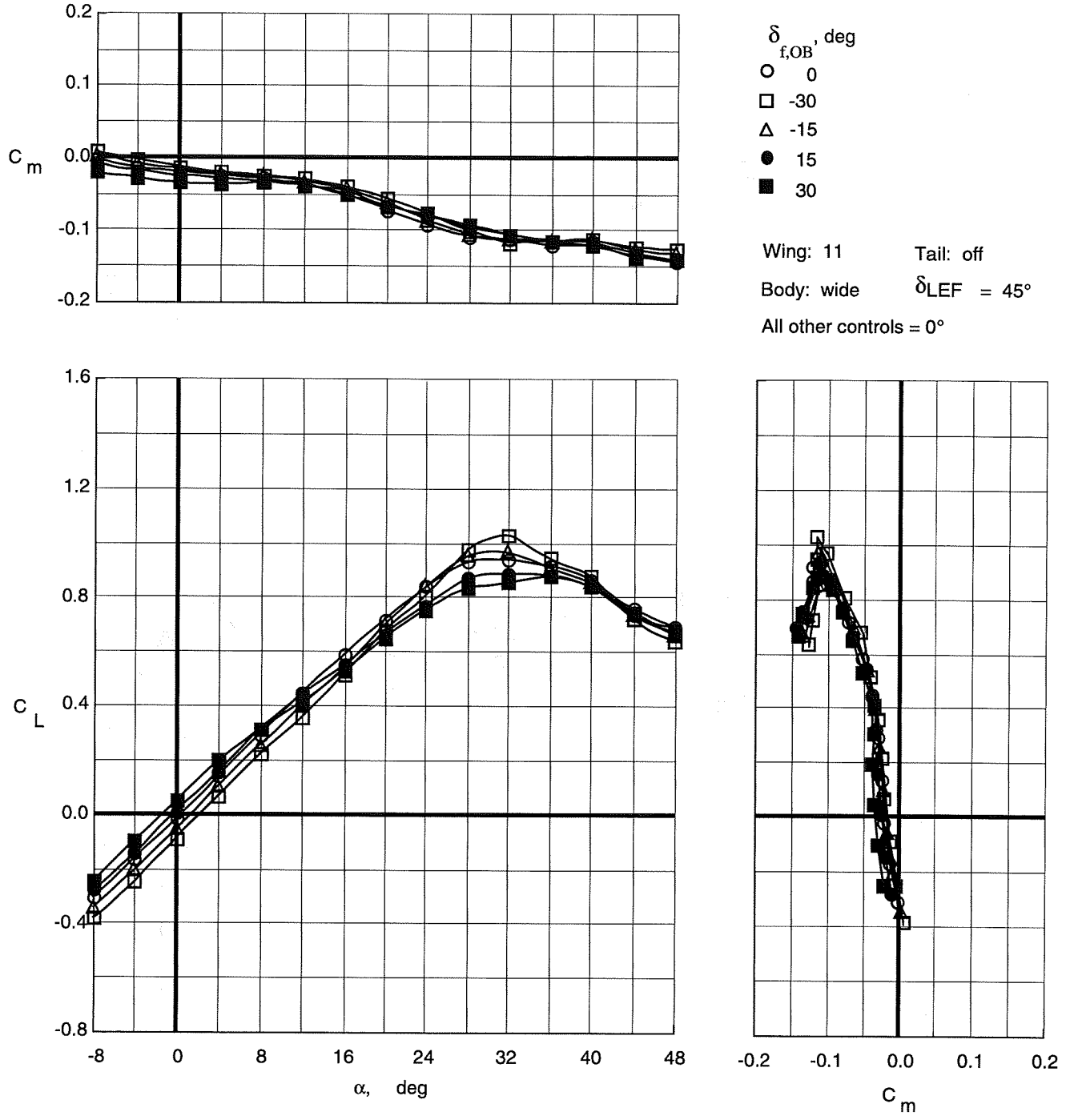

Figure 53. Control effectiveness of symmetric deflections of outboard trailing-edge flaps on Wing 11 with wide top body on and leading-edge flaps deflected.

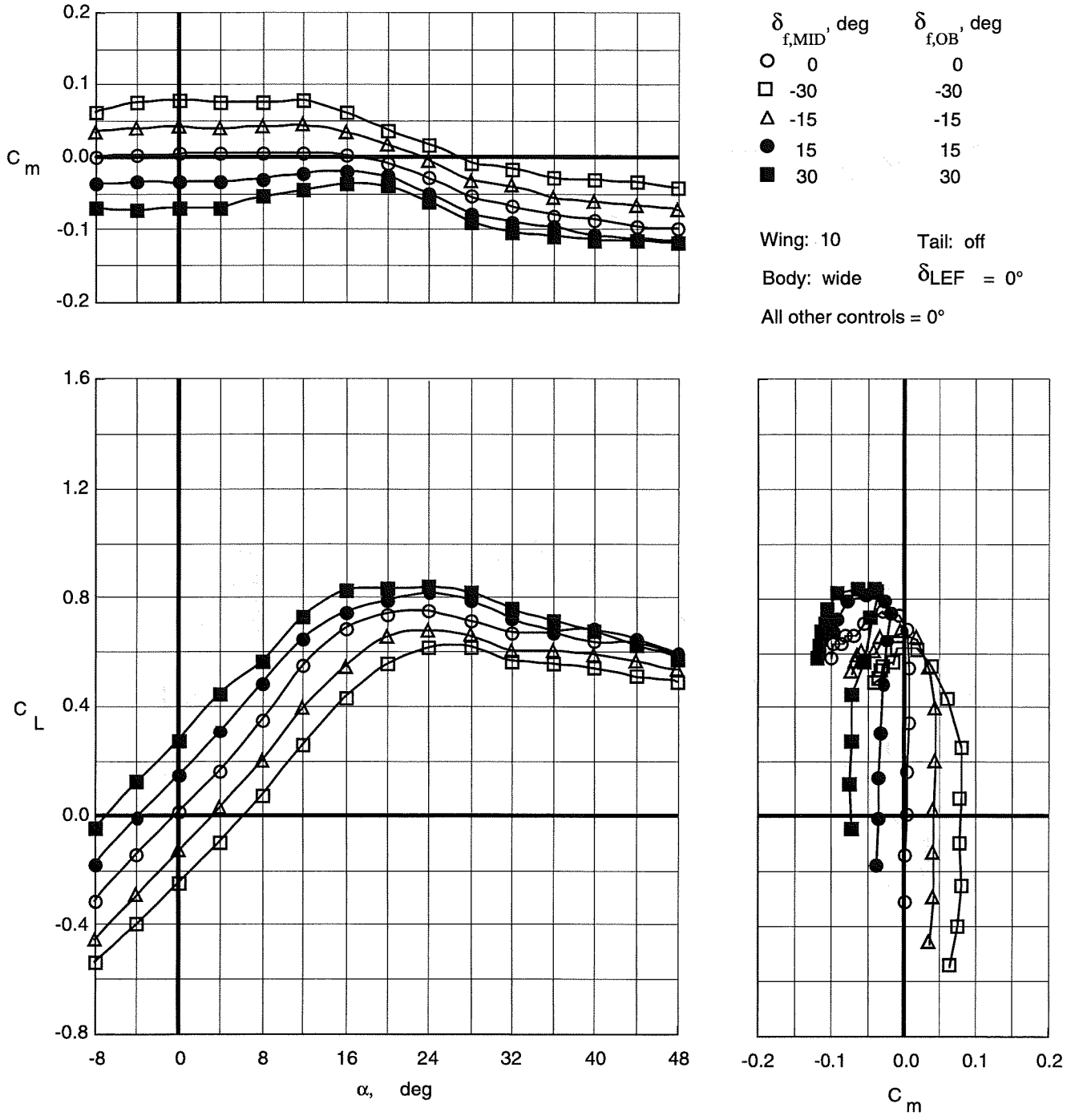

Figure 54. Control effectiveness of symmetric deflections of middle and outboard trailing-edge flaps on Wing 10 with wide top body on.

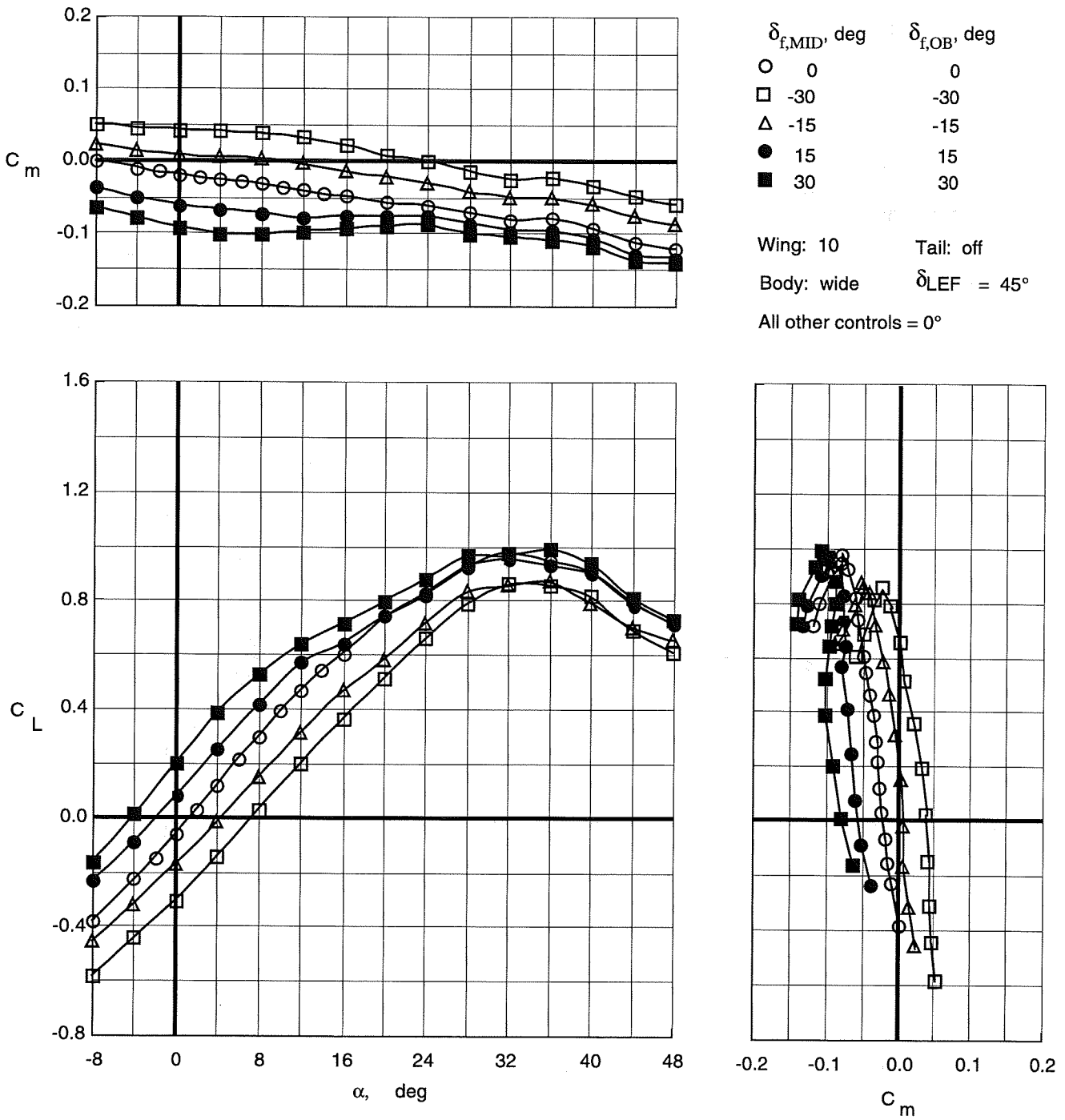

Figure 55. Control effectiveness of symmetric deflections of middle and outboard trailing-edge flaps on Wing 10 with wide top body on and leading-edge flaps deflected.

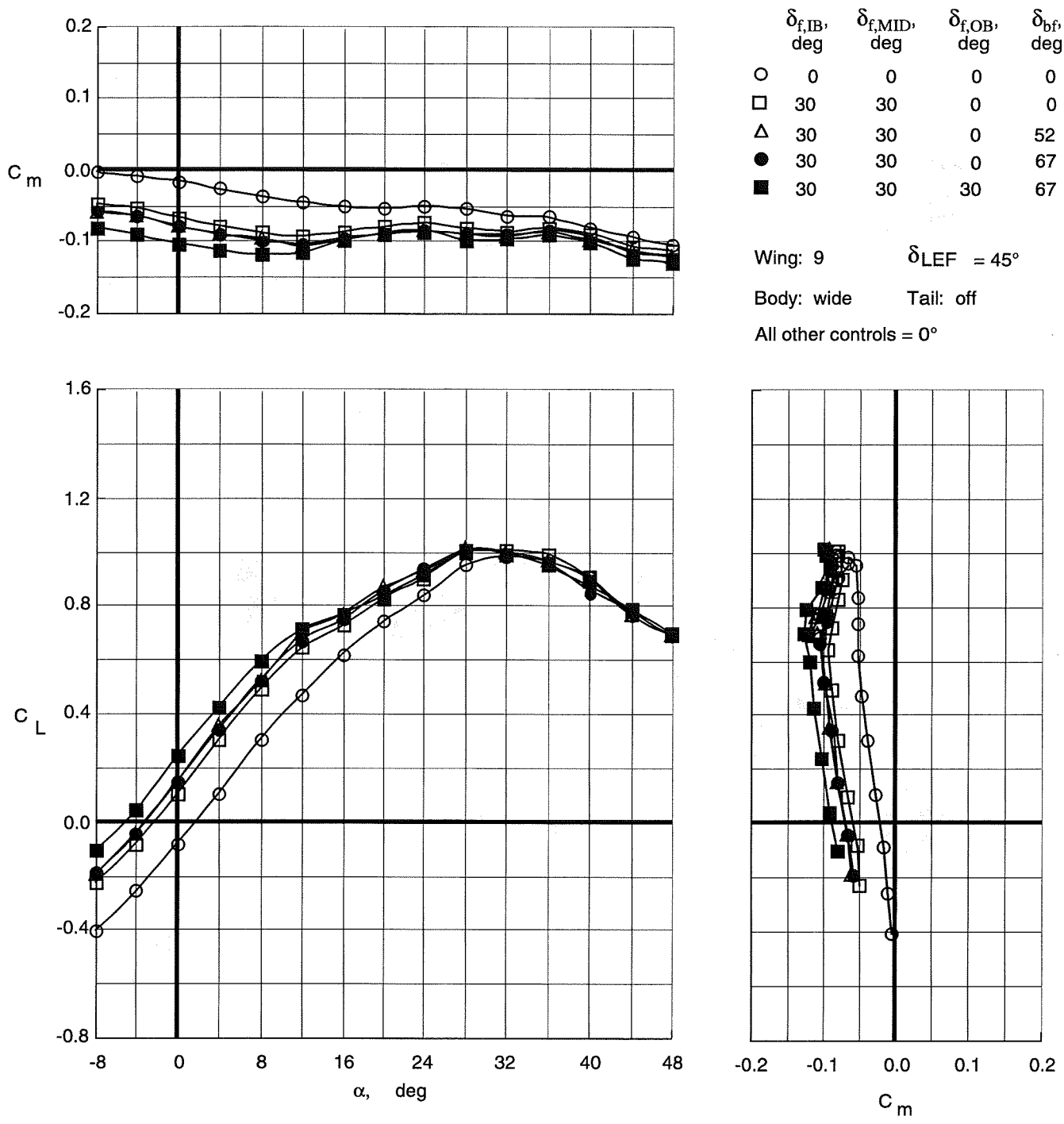

Figure 56. Control effectiveness of symmetric deflections of trailing-edge flaps and body flaps on Wing 9 with wide top body on and leading-edge flaps deflected.

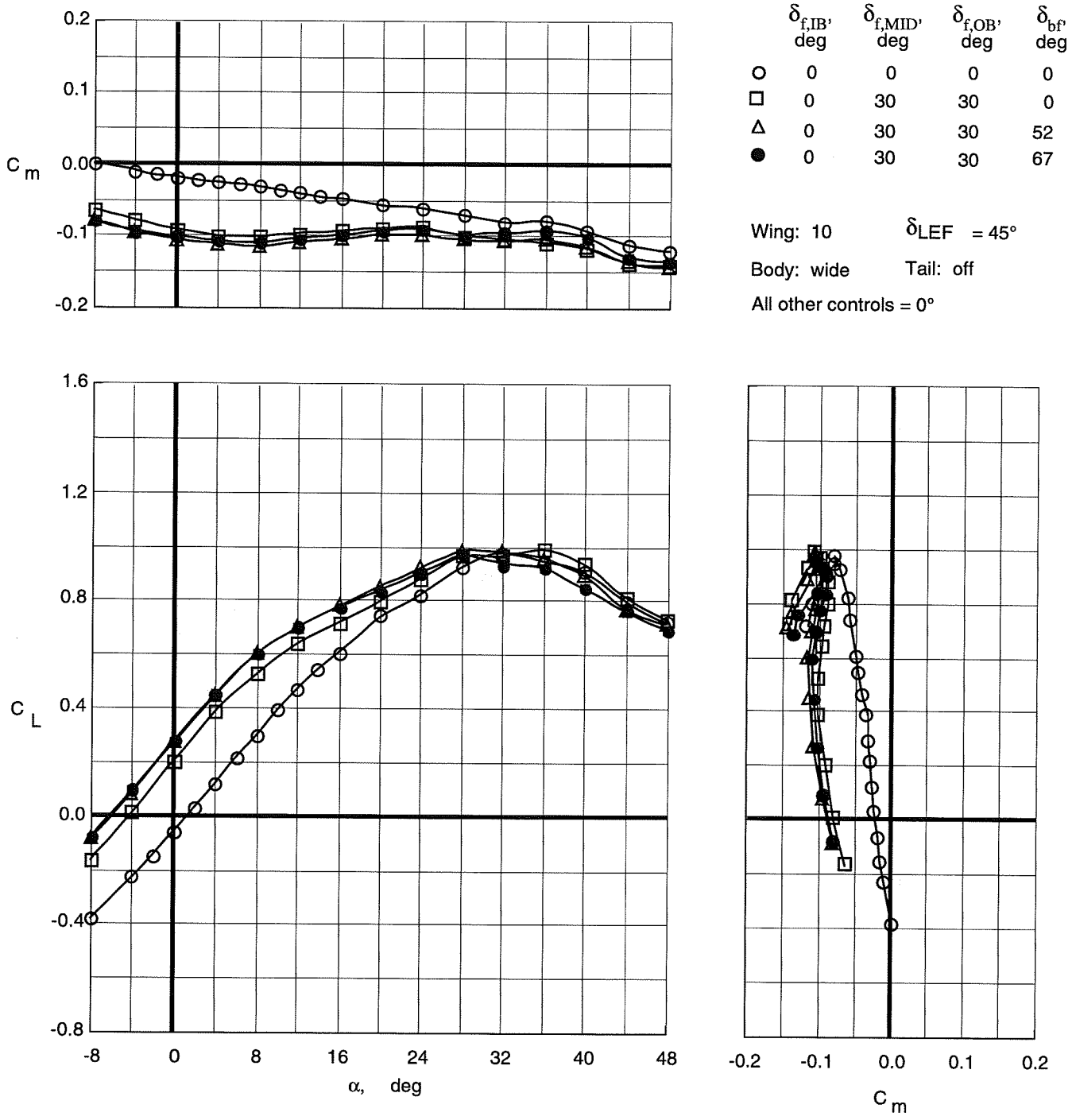

Figure 57. Control effectiveness of symmetric deflections of trailing-edge flaps and body flaps on Wing 10 with wide top body on and leading-edge flaps deflected.

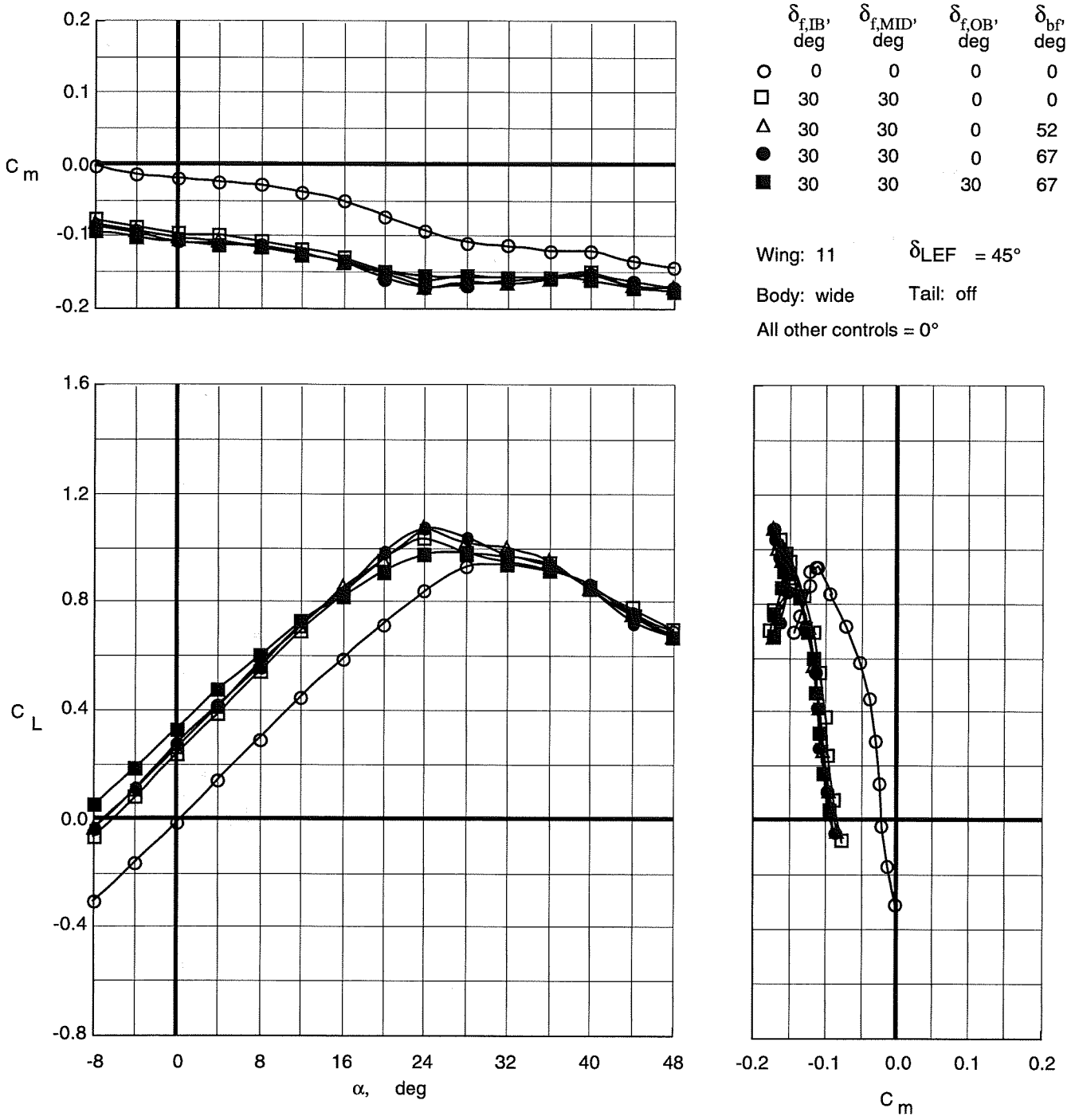

Figure 58. Control effectiveness of symmetric deflections of trailing-edge flaps and body flaps on Wing 11 with wide top body on and leading-edge flaps deflected.

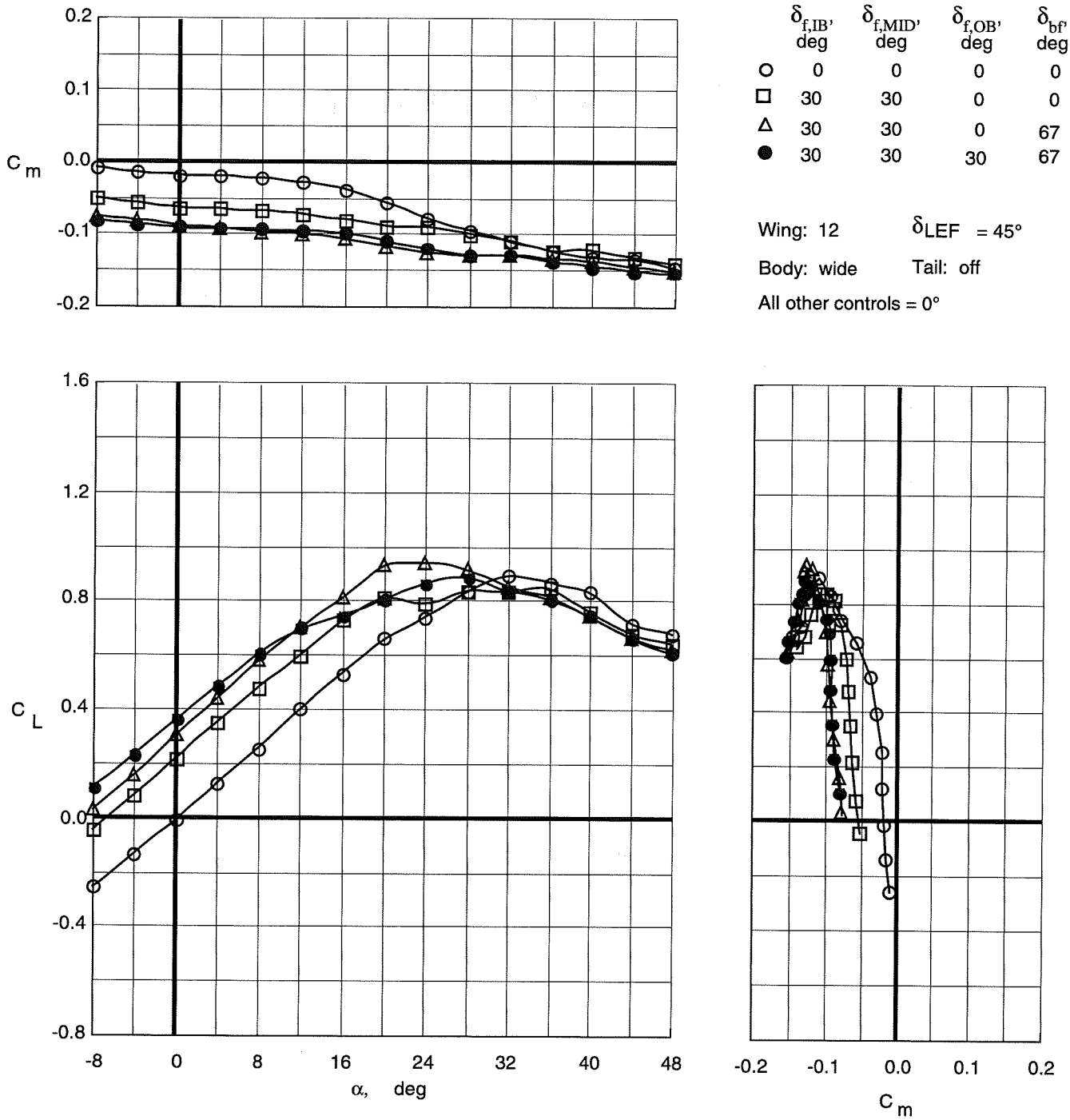

Figure 59. Control effectiveness of symmetric deflections of trailing-edge flaps and body flaps on Wing 12 with wide top body on and leading-edge flaps deflected.

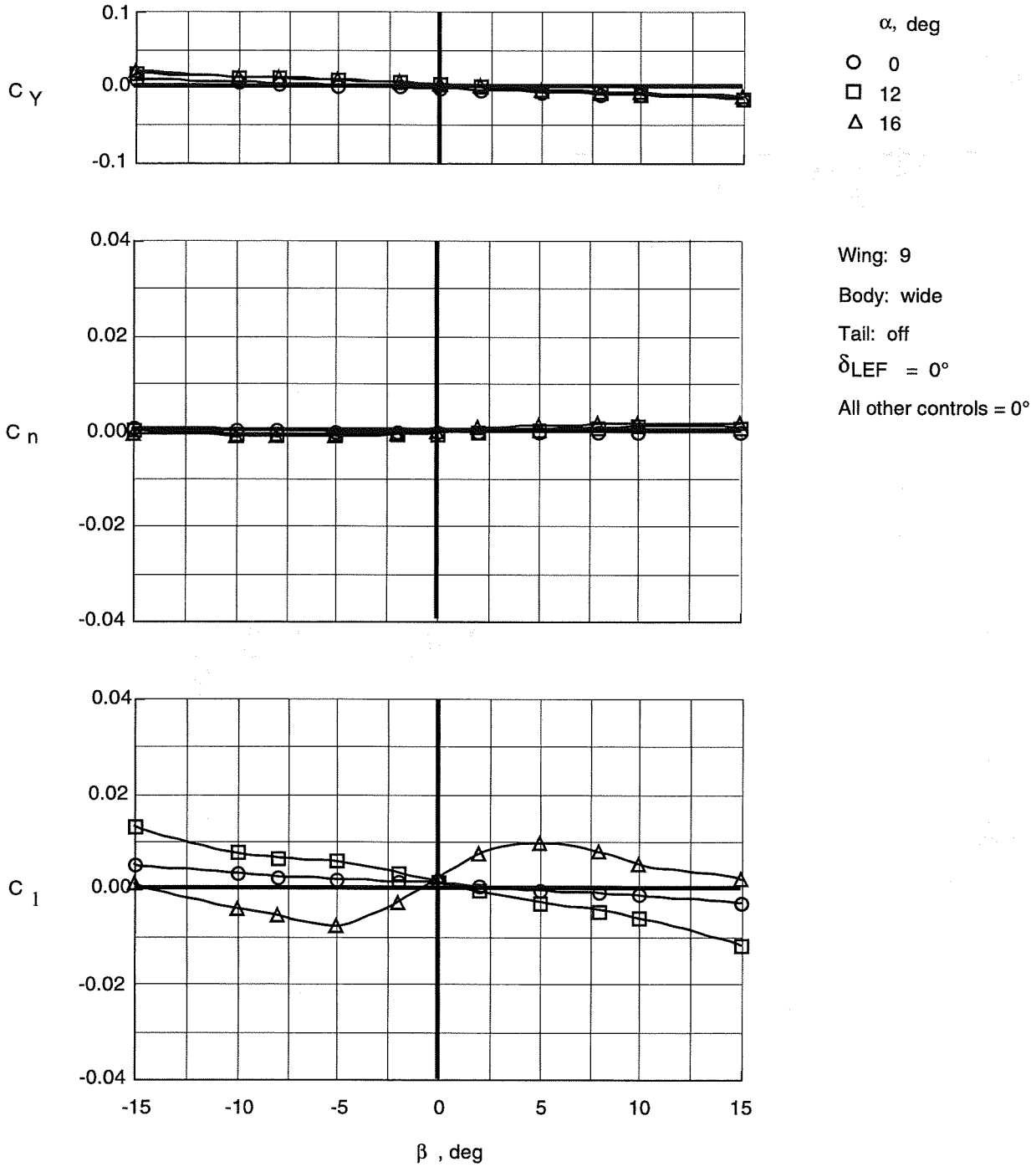

Figure 60. Variation of lateral-directional coefficients with sideslip at low angles of attack for Wing 9 with wide top body on.

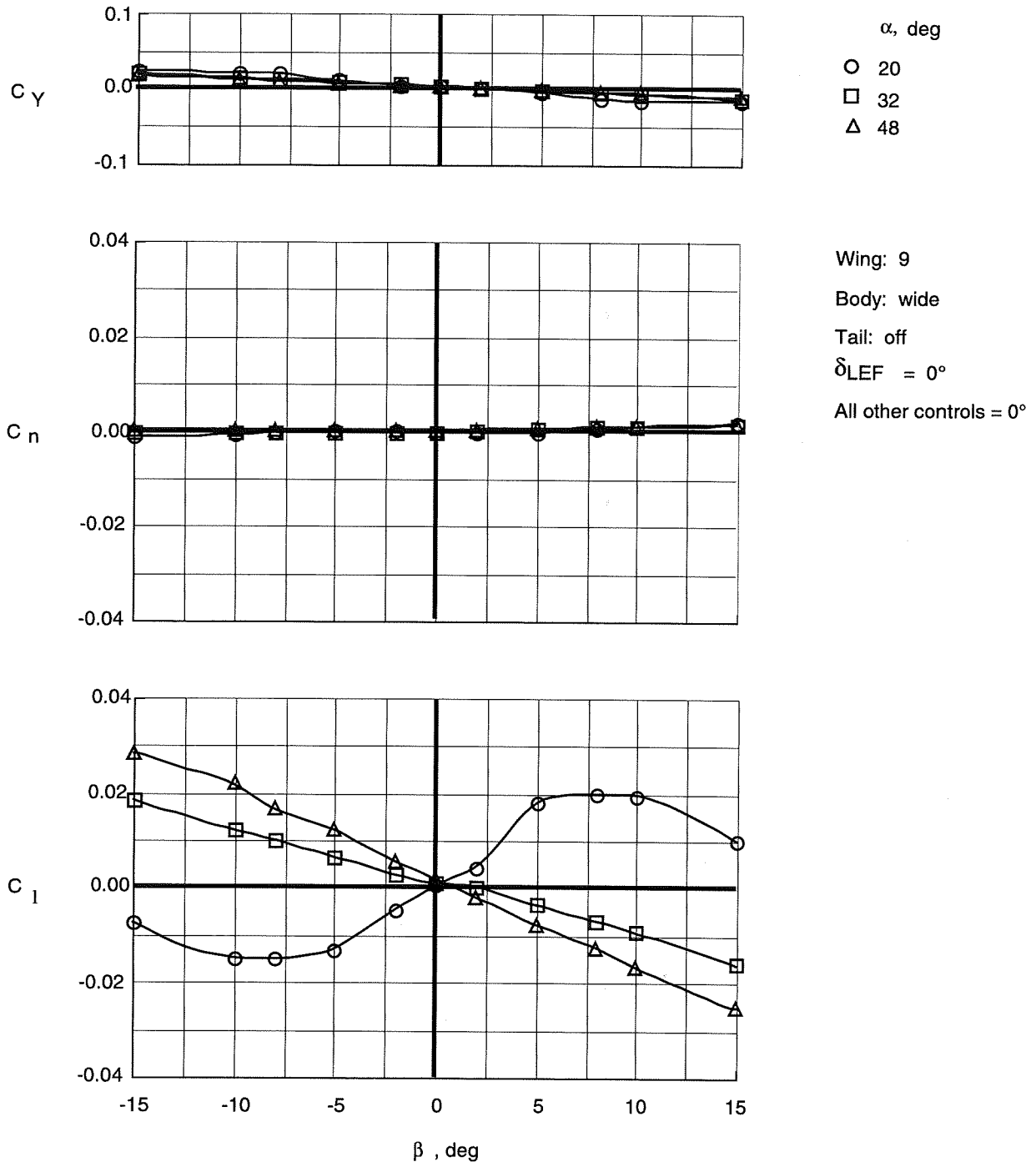

Figure 61. Variation of lateral-directional coefficients with sideslip at high angles of attack for Wing 9 with wide top body on.

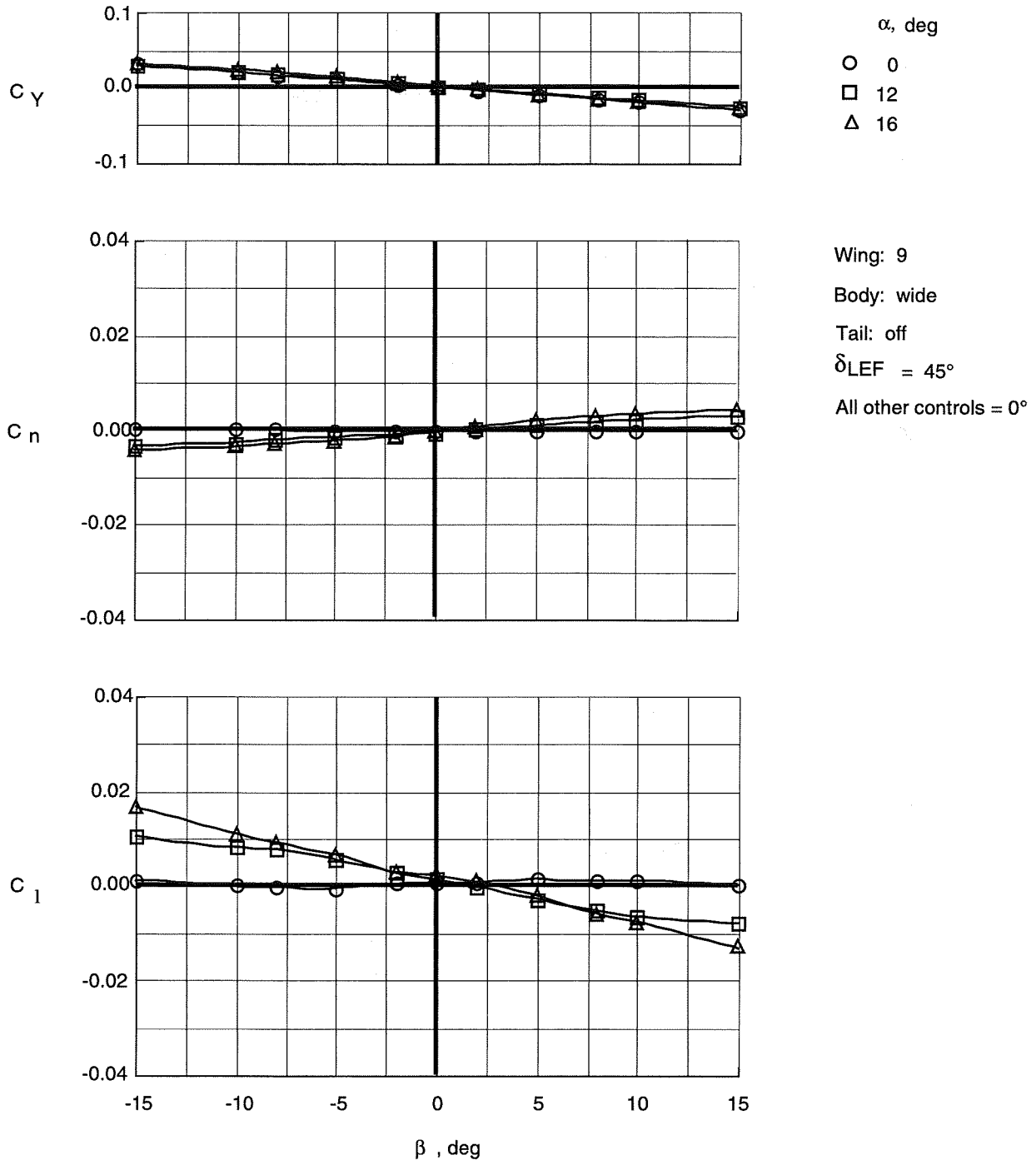

Figure 62. Variation of lateral-directional coefficients with sideslip at low angles of attack for Wing 9 with wide top body on and leading-edge flaps deflected.

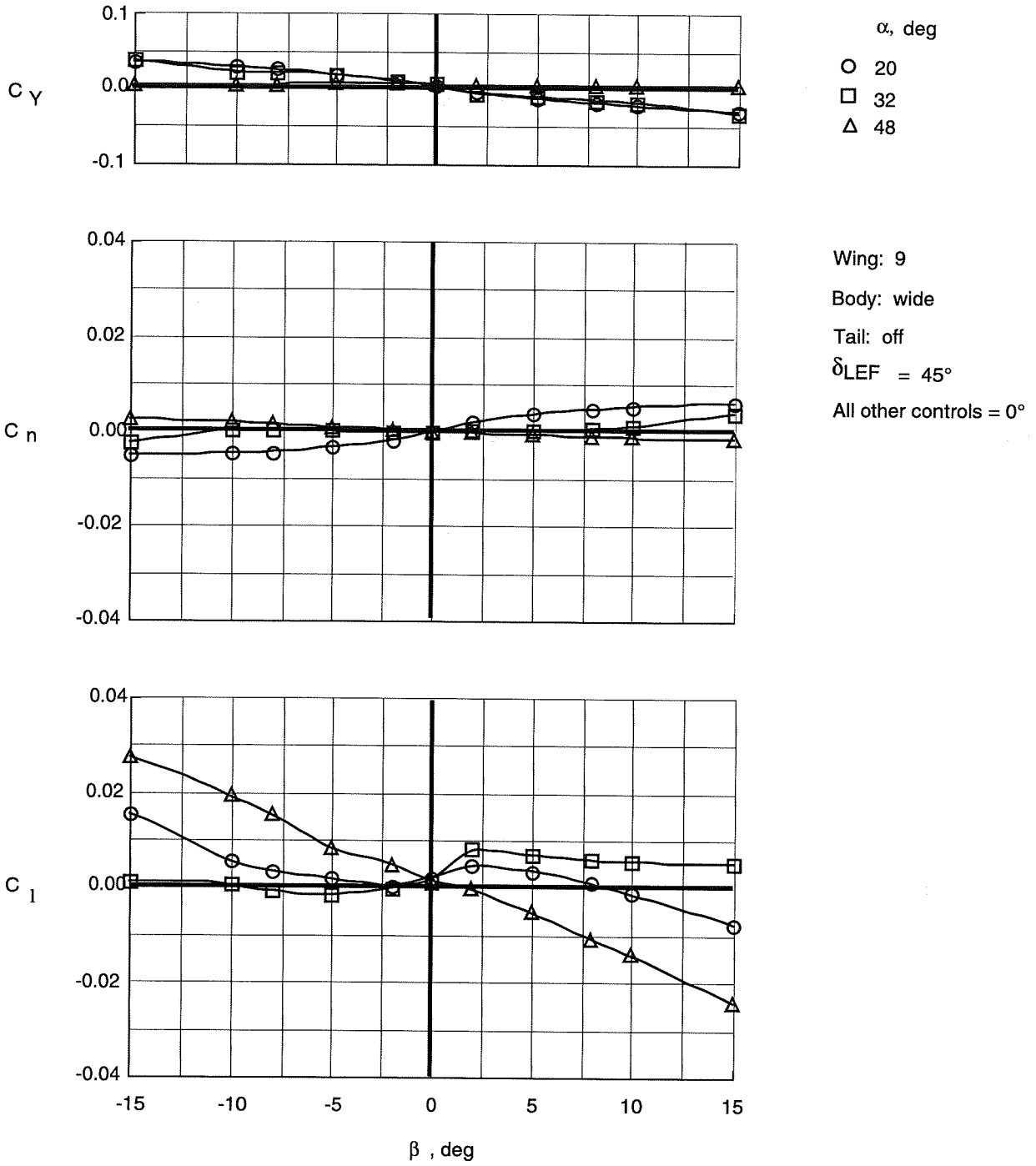

Figure 63. Variation of lateral-directional coefficients with sideslip at high angles of attack for Wing 9 with wide top body on and leading-edge flaps deflected.

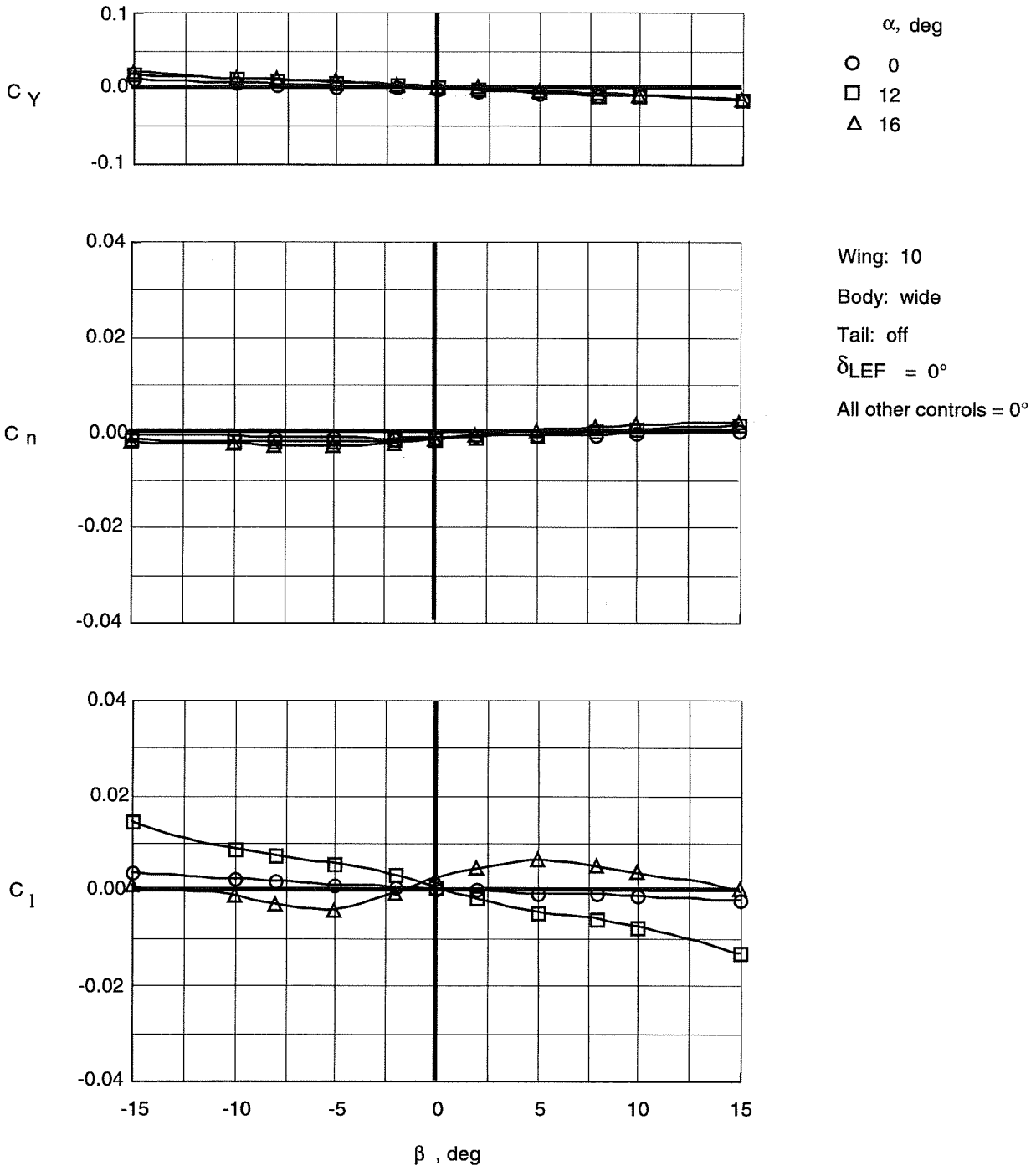

Figure 64. Variation of lateral-directional coefficients with sideslip at low angles of attack for Wing 10 with wide top body on.

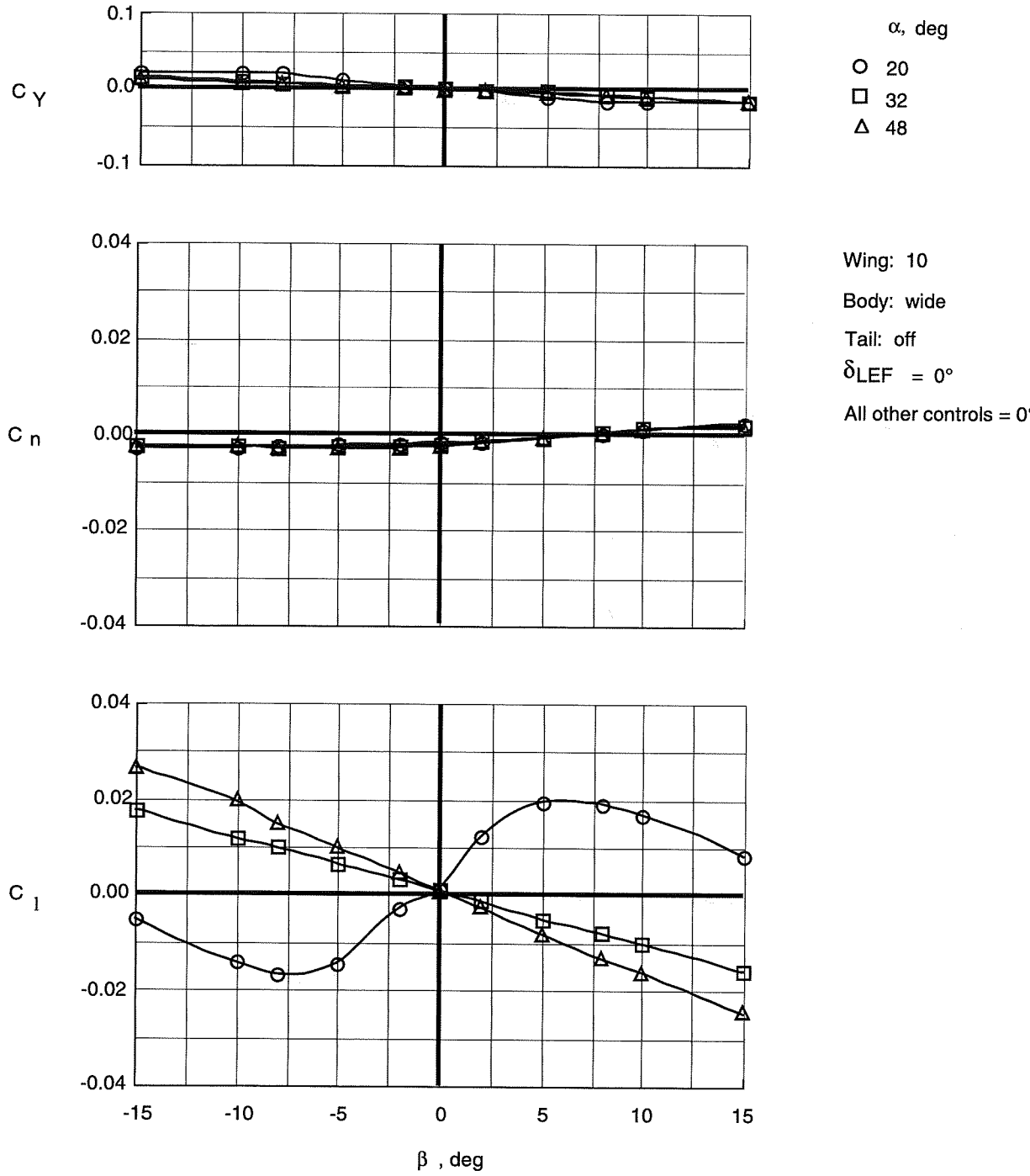

Figure 65. Variation of lateral-directional coefficients with sideslip at high angles of attack for Wing 10 with wide top body on.

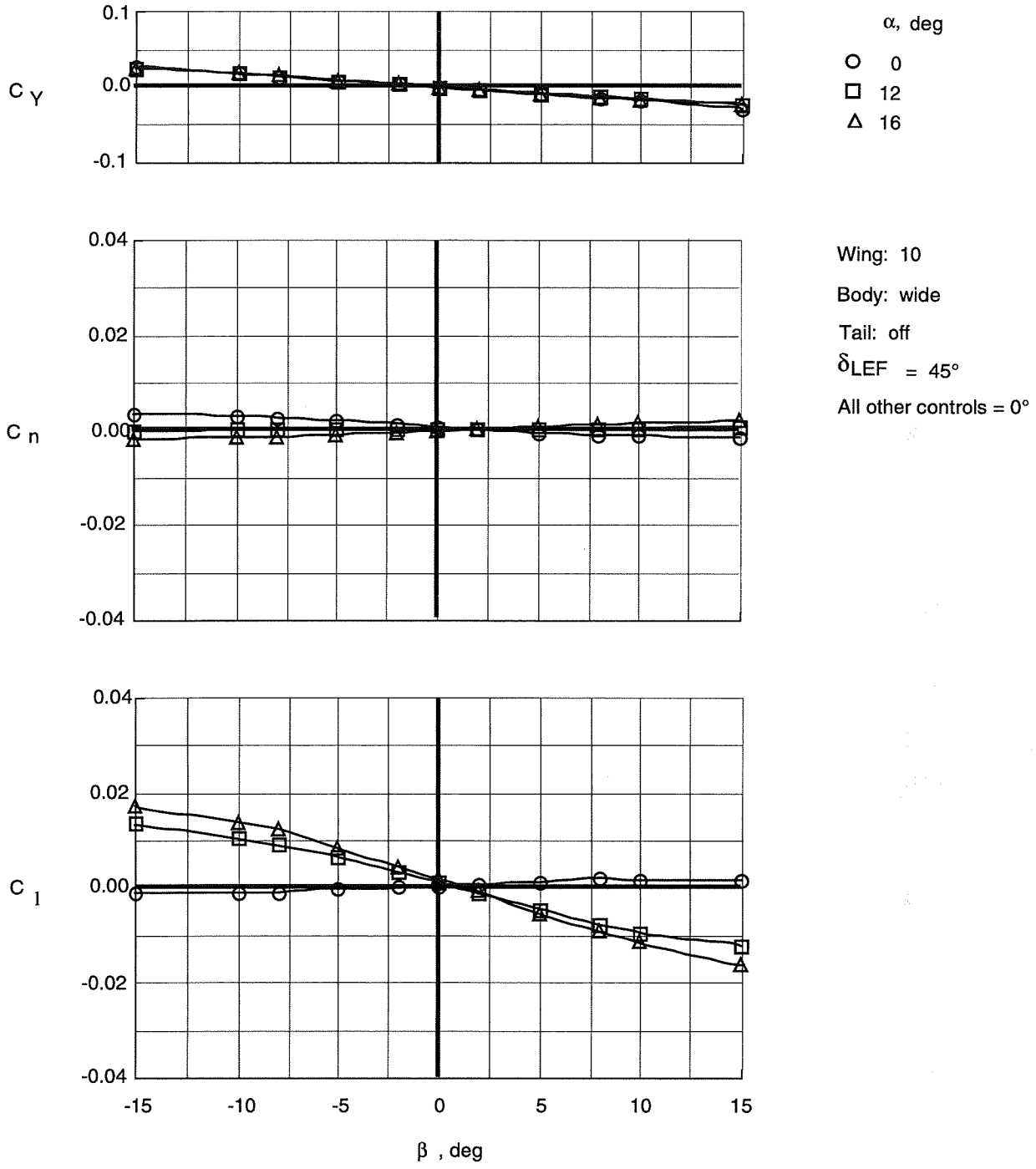

Figure 66. Variation of lateral-directional coefficients with sideslip at low angles of attack for Wing 10 with wide top body on and leading-edge flaps deflected.

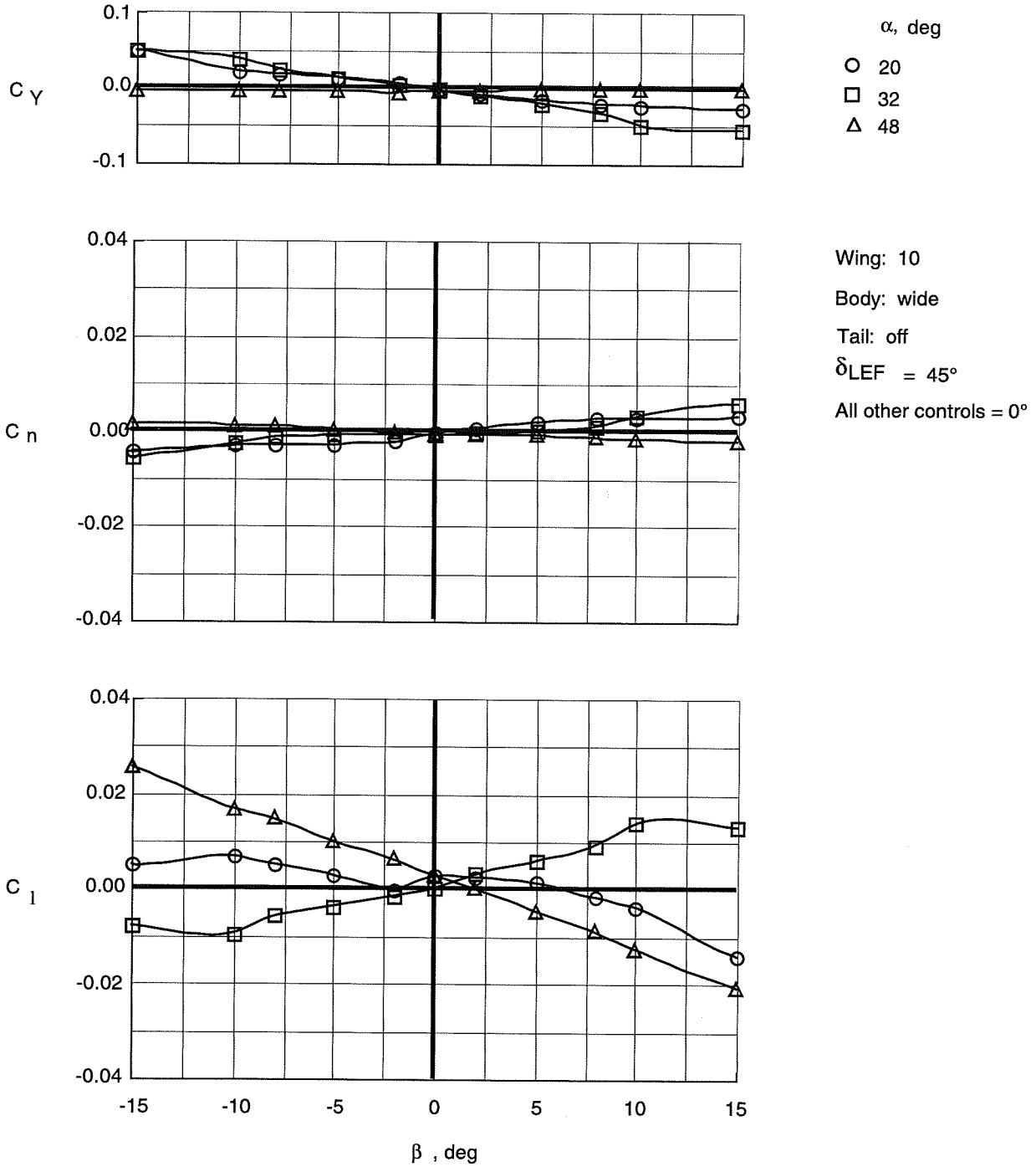

Figure 67. Variation of lateral-directional coefficients with sideslip at high angles of attack for Wing 10 with wide top body on and leading-edge flaps deflected.

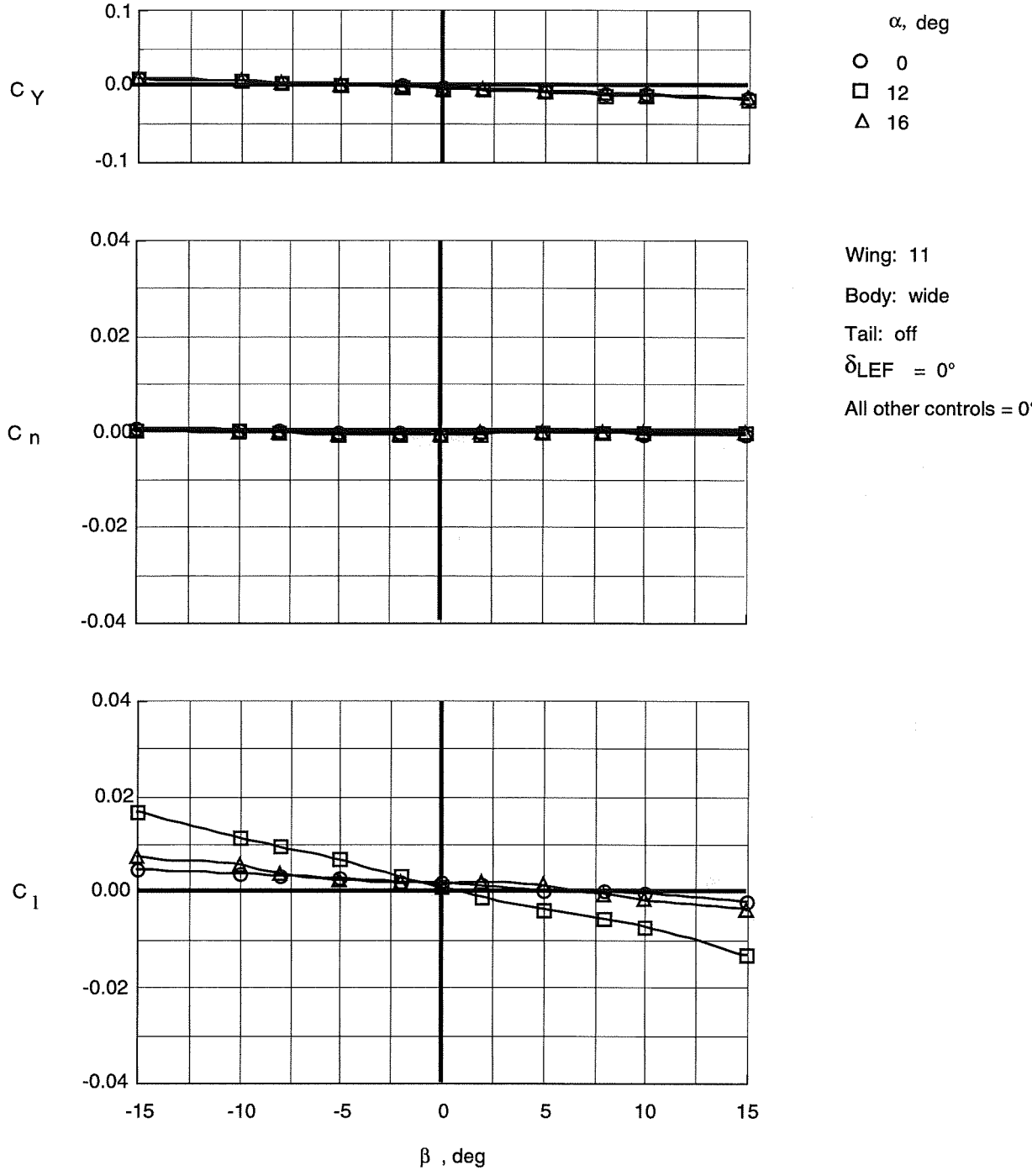

Figure 68. Variation of lateral-directional coefficients with sideslip at low angles of attack for Wing 11 with wide top body on.

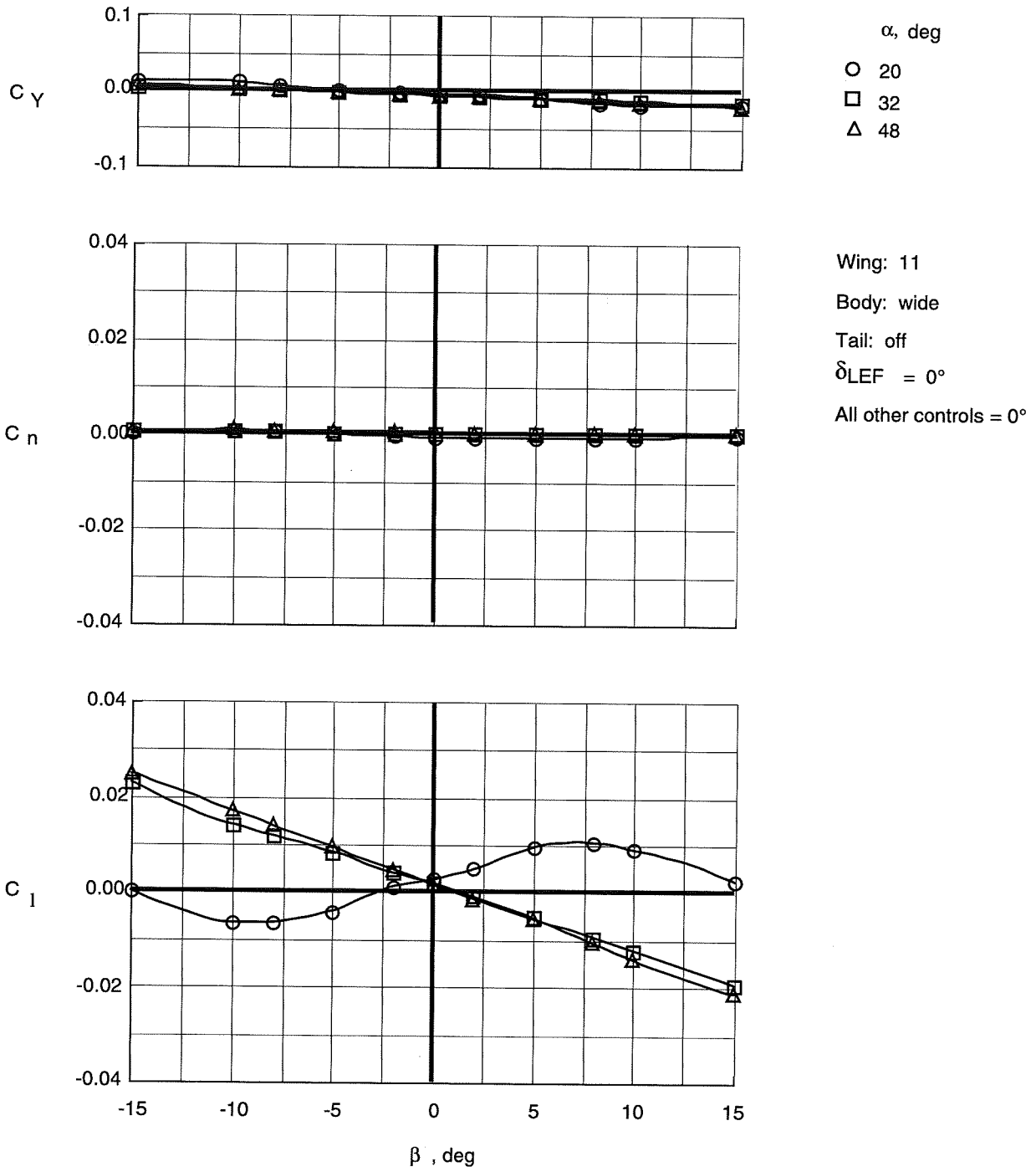

Figure 69. Variation of lateral-directional coefficients with sideslip at high angles of attack for Wing 11 with wide top body on.

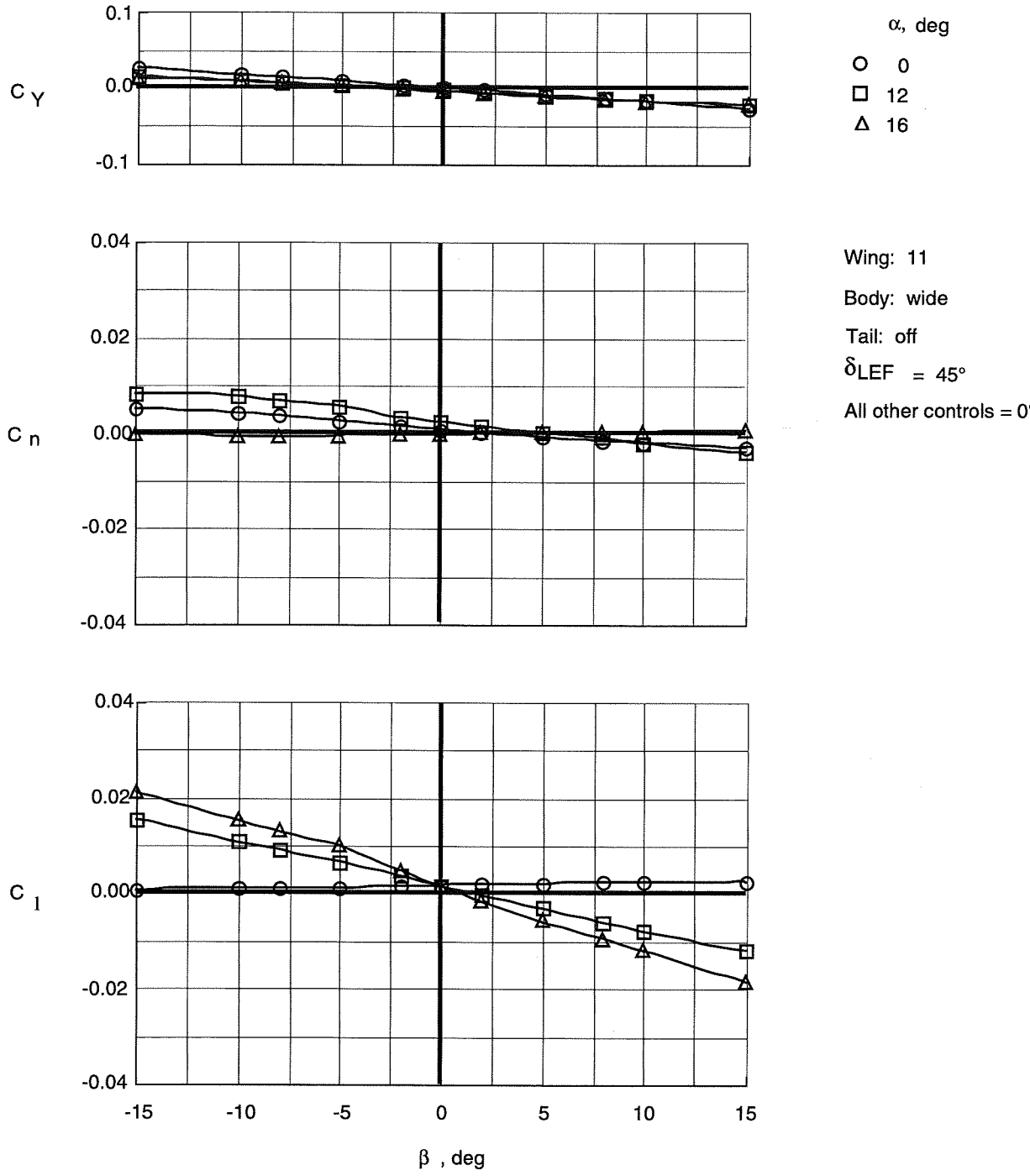

Figure 70. Variation of lateral-directional coefficients with sideslip at low angles of attack for Wing 11 with wide top body on and leading-edge flaps deflected.

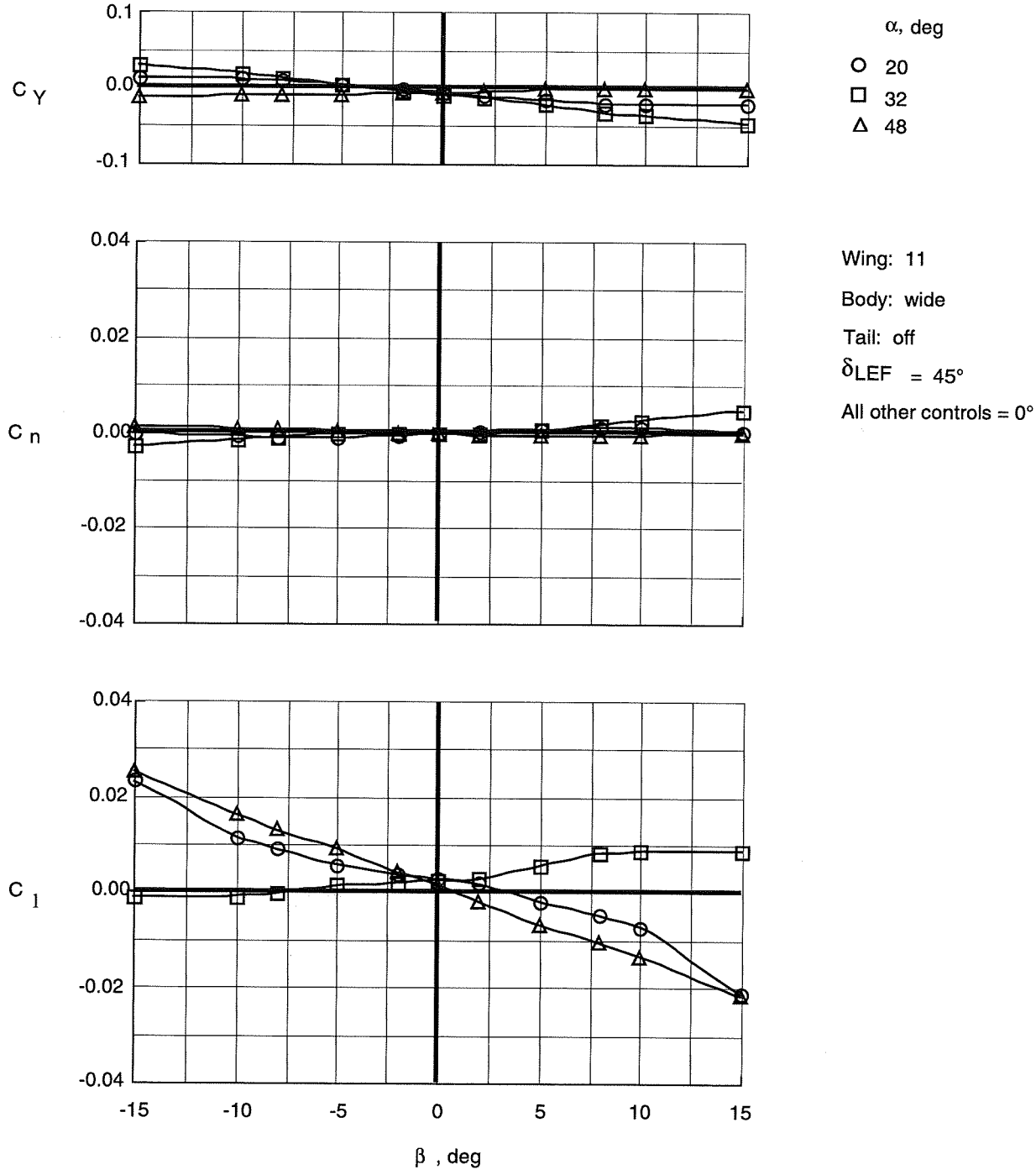

Figure 71. Variation of lateral-directional coefficients with sideslip at high angles of attack for Wing 11 with wide top body on and leading-edge flaps deflected.

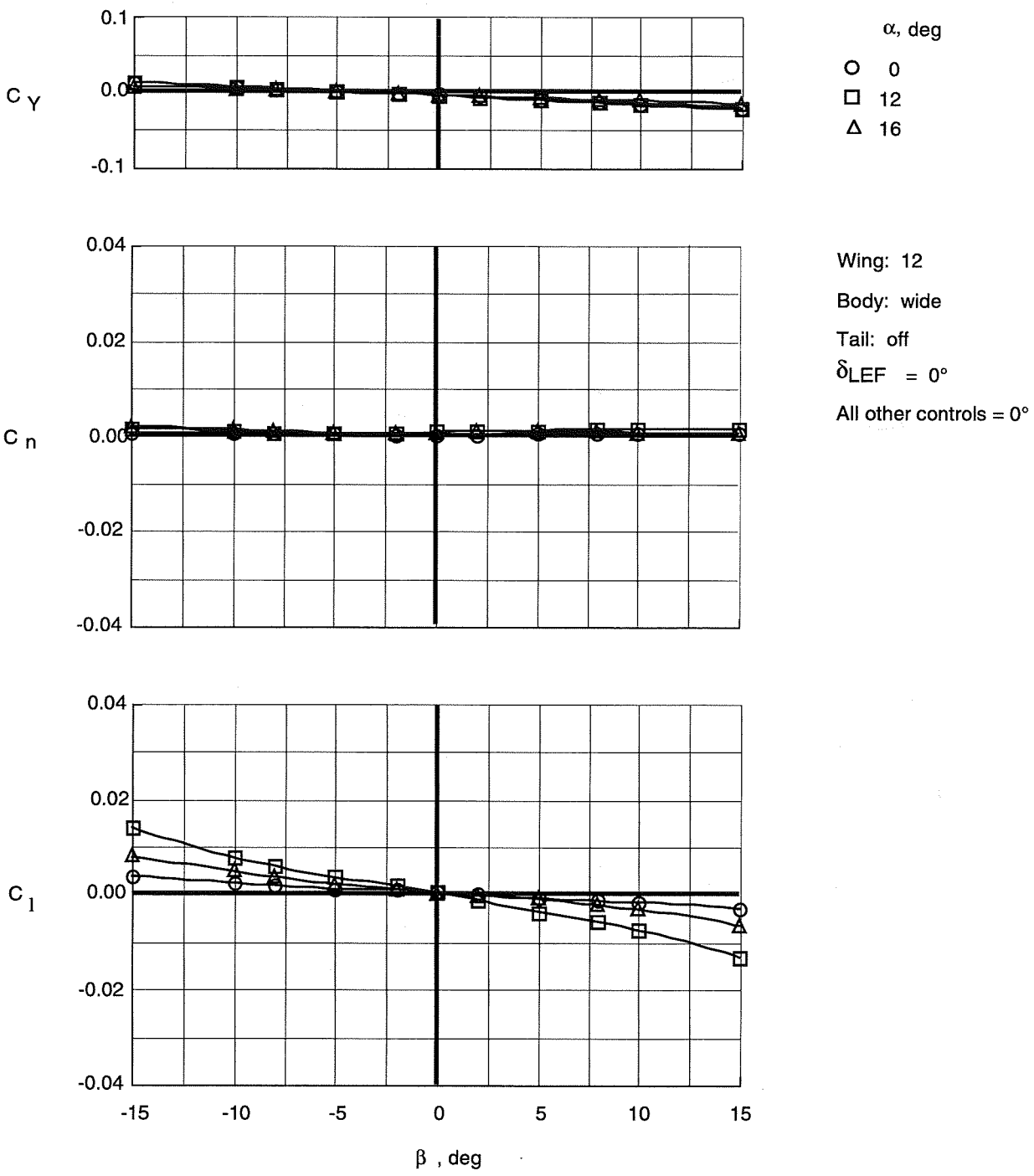

Figure 72. Variation of lateral-directional coefficients with sideslip at low angles of attack for Wing 12 with wide top body on.

C-2

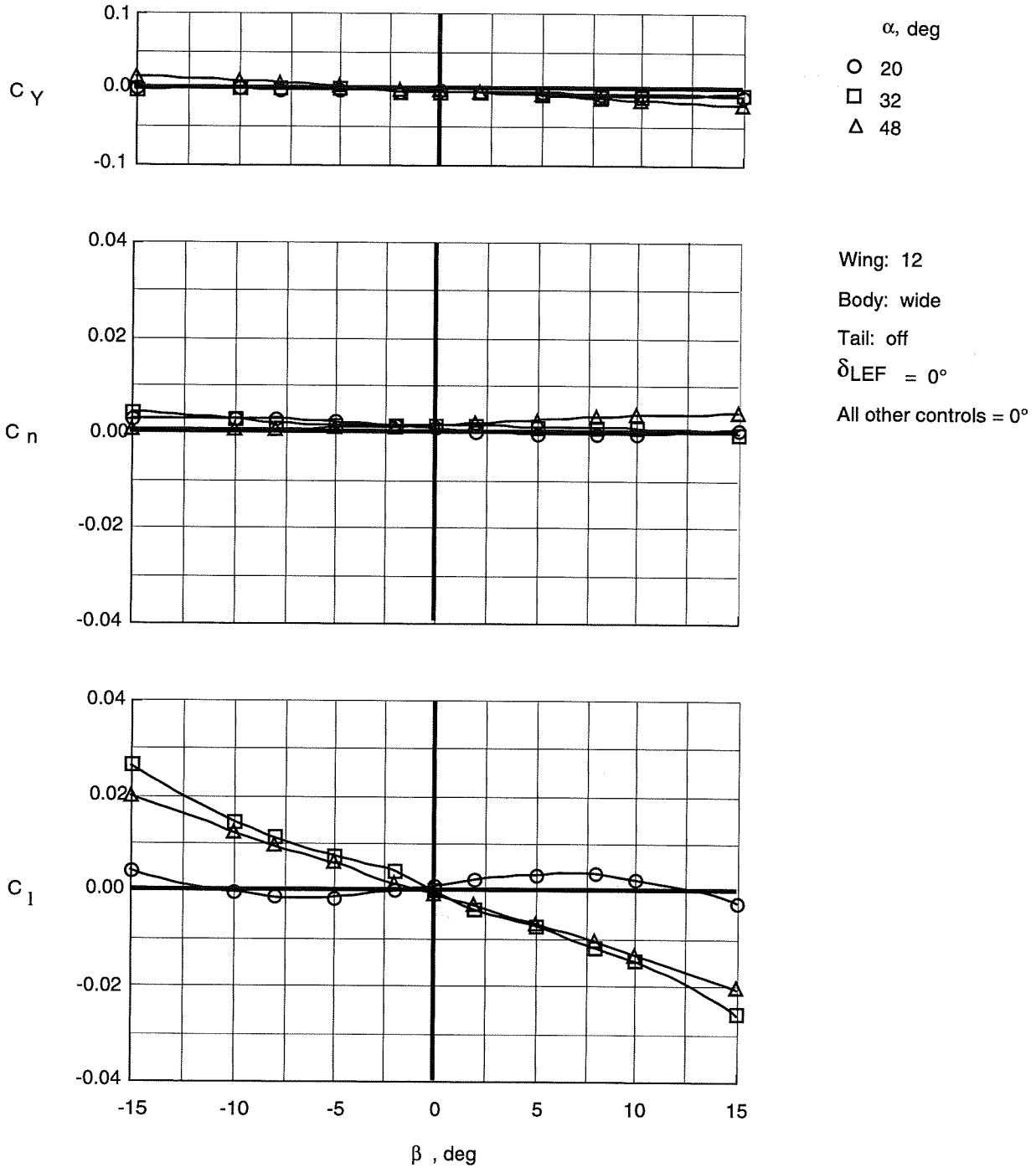

Figure 73. Variation of lateral-directional coefficients with sideslip at high angles of attack for Wing 12 with wide top body on.

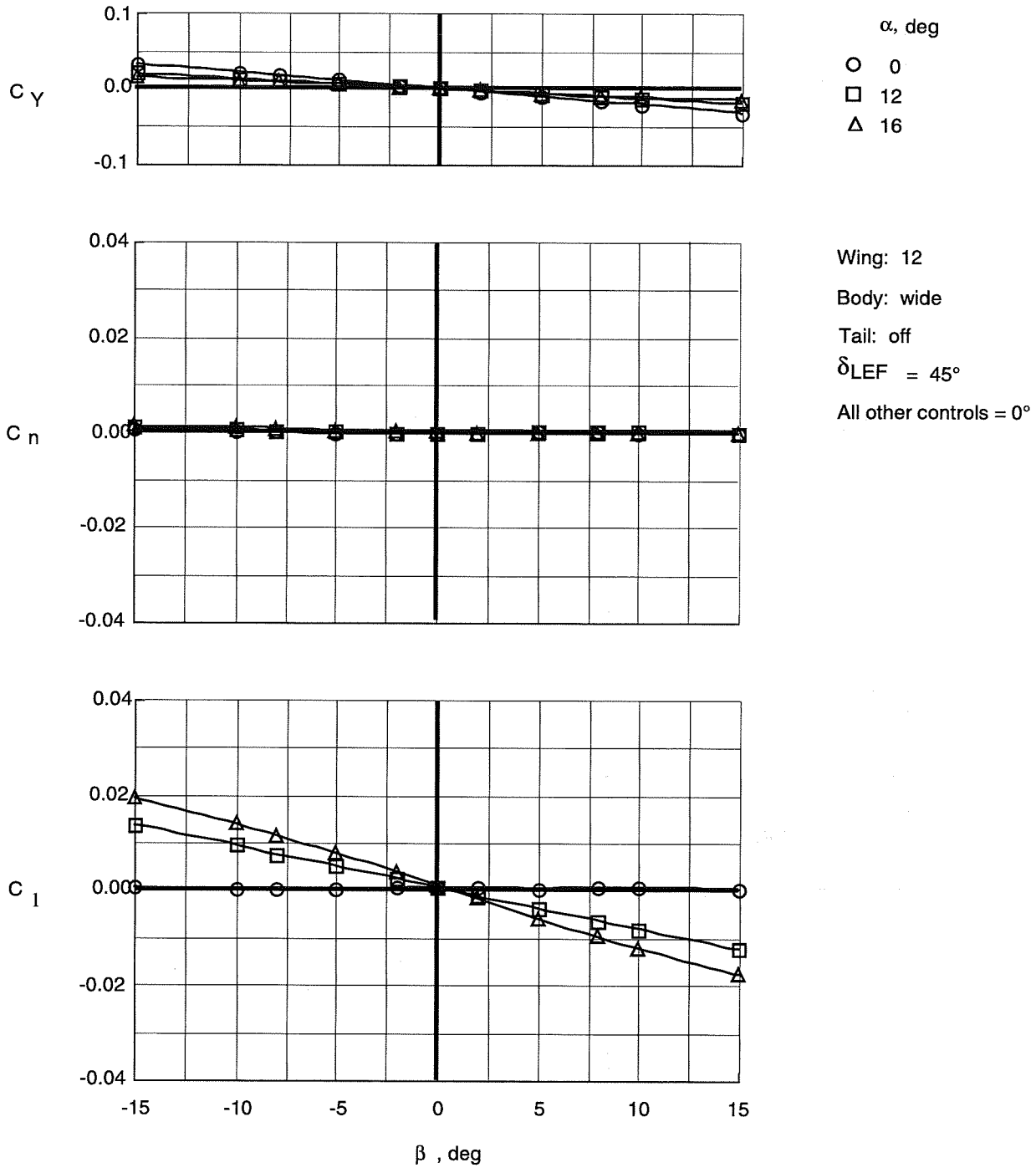

Figure 74. Variation of lateral-directional coefficients with sideslip at low angles of attack for Wing 12 with wide top body on and leading-edge flaps deflected.

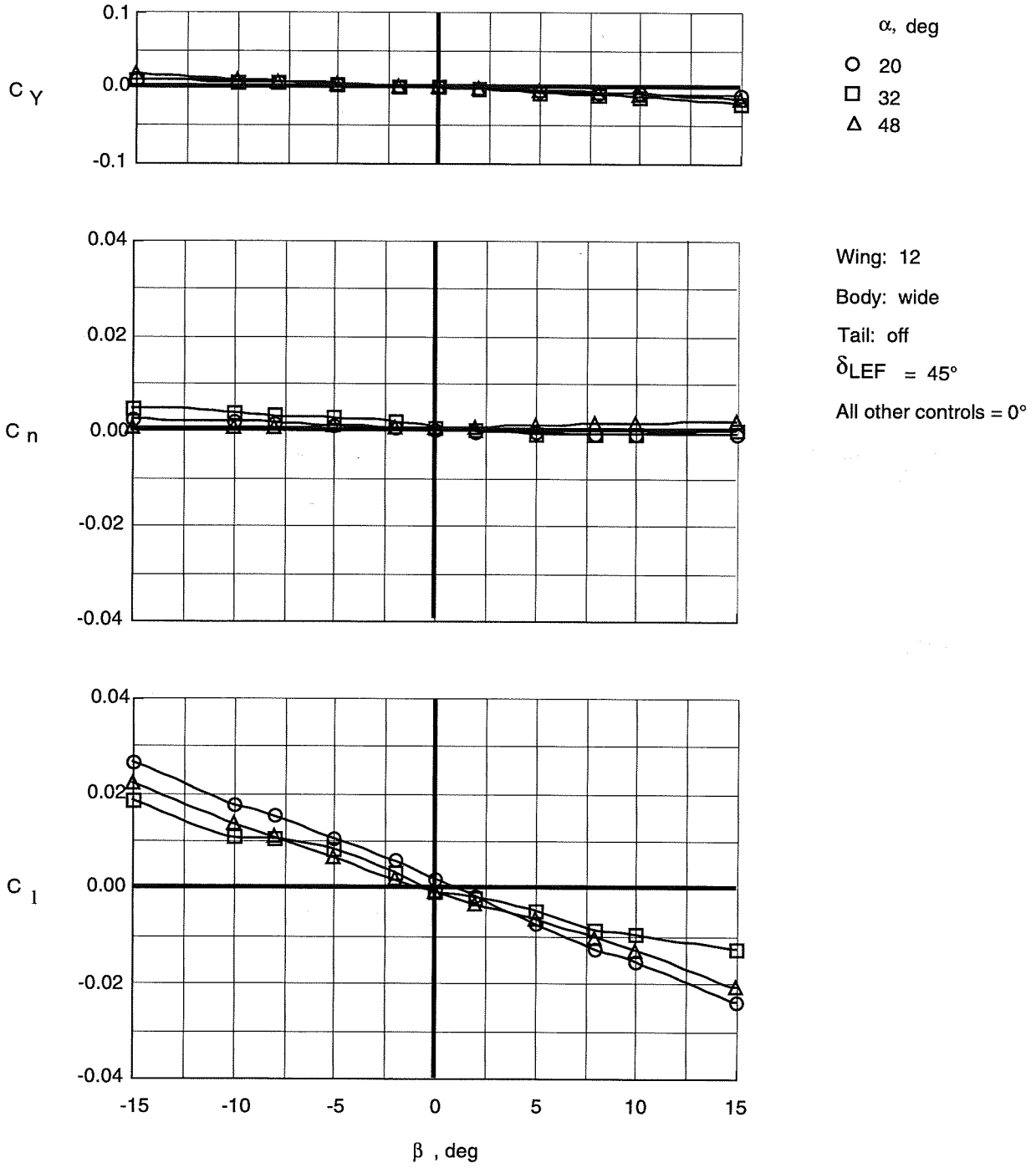

Figure 75. Variation of lateral-directional coefficients with sideslip at high angles of attack for Wing 12 with wide top body on and leading-edge flaps deflected.

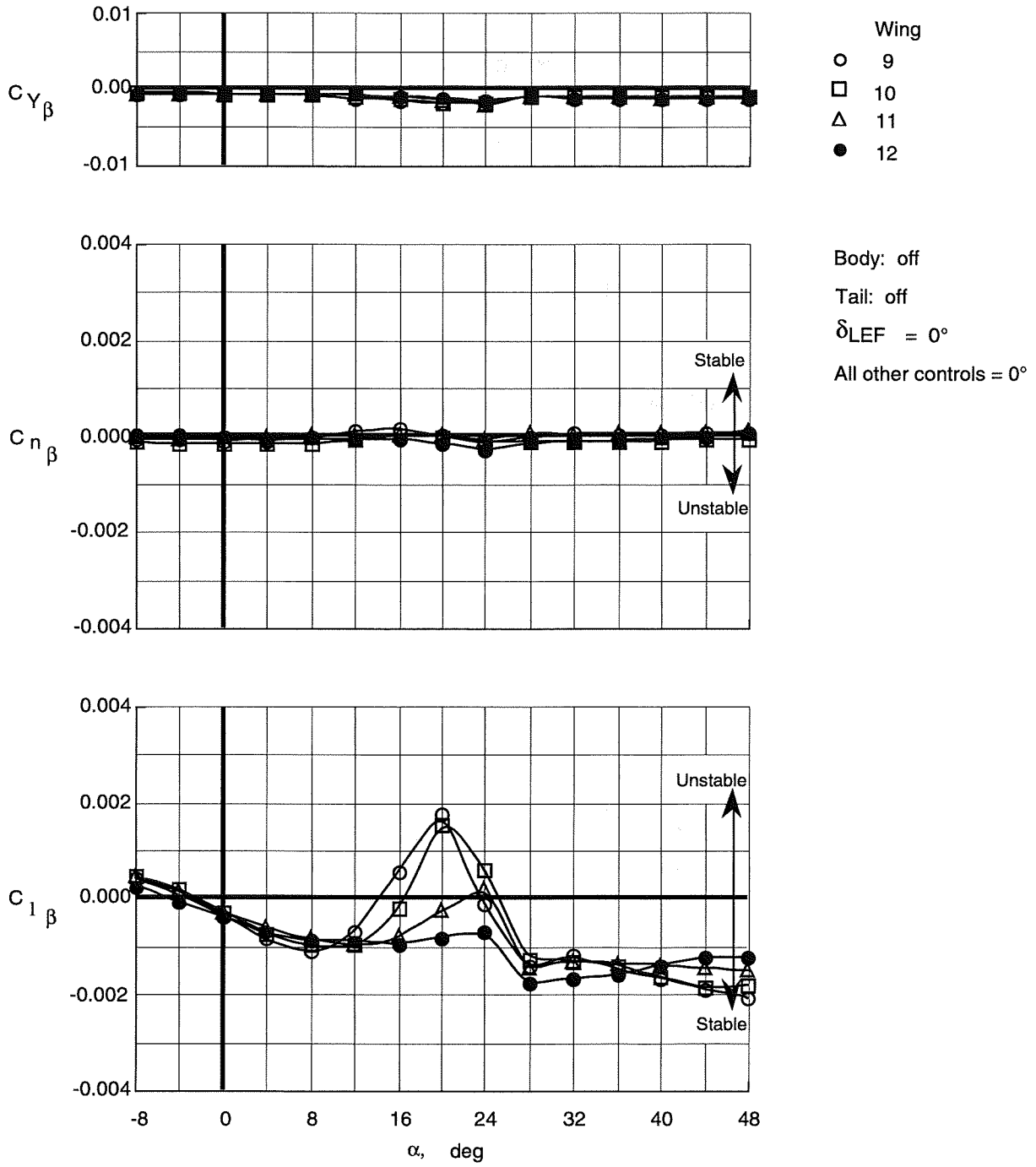

Figure 76. Lateral-directional stability characteristics of wing planforms with top body off.

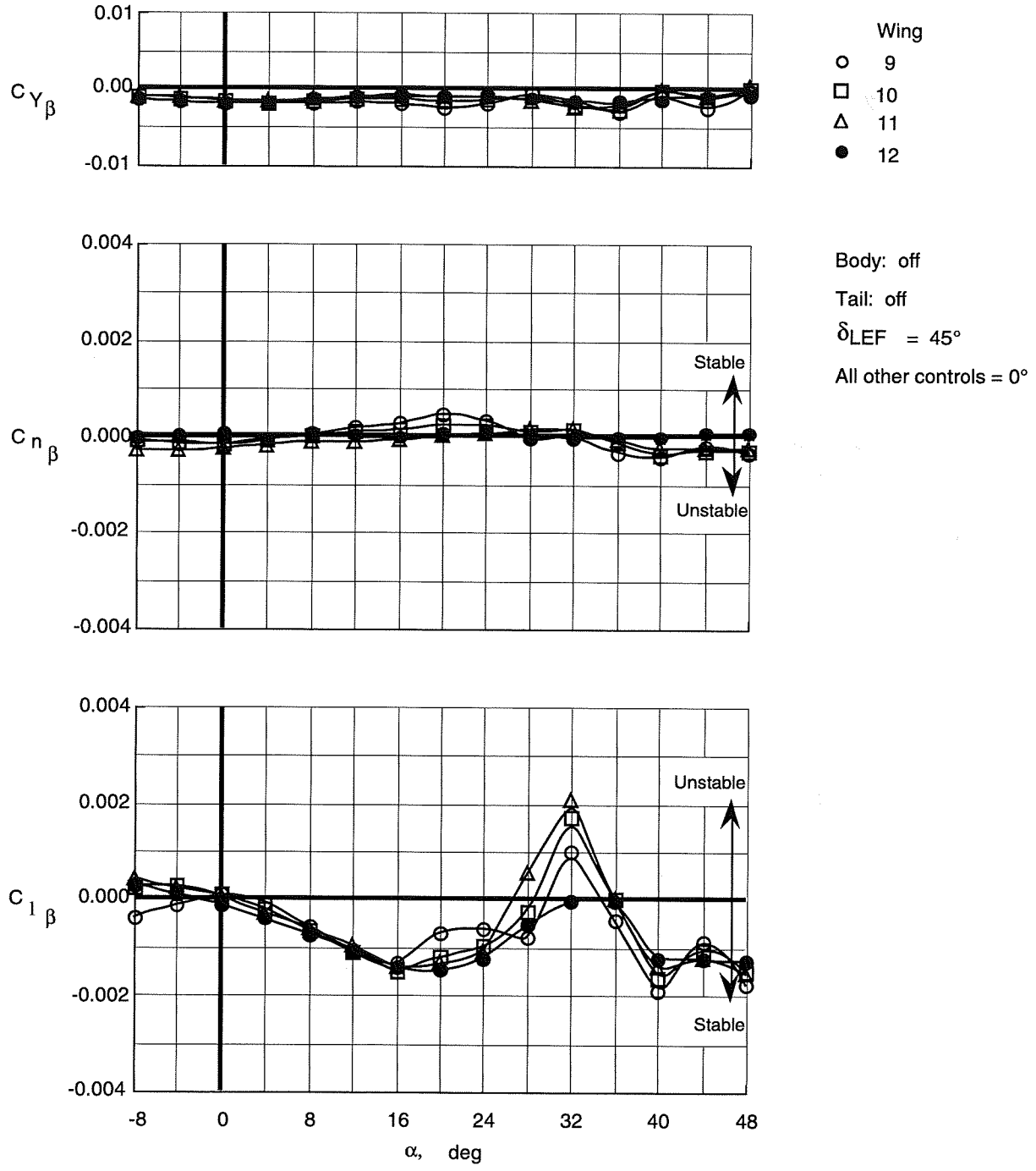

Figure 77. Lateral-directional stability characteristics of wing planforms with top body off and leading-edge flaps deflected.

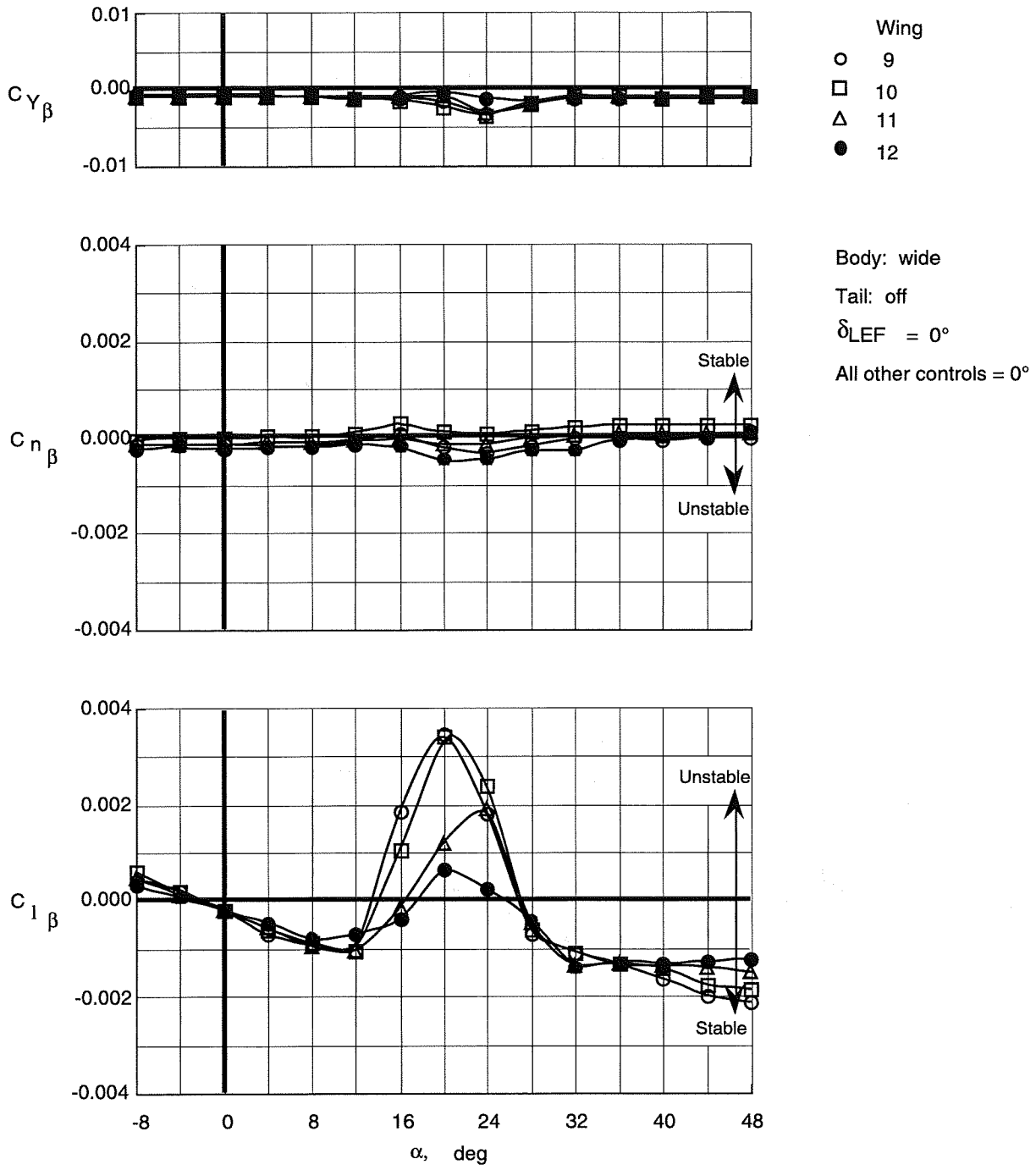

Figure 78. Lateral-directional stability characteristics of wing planforms with wide top body on.

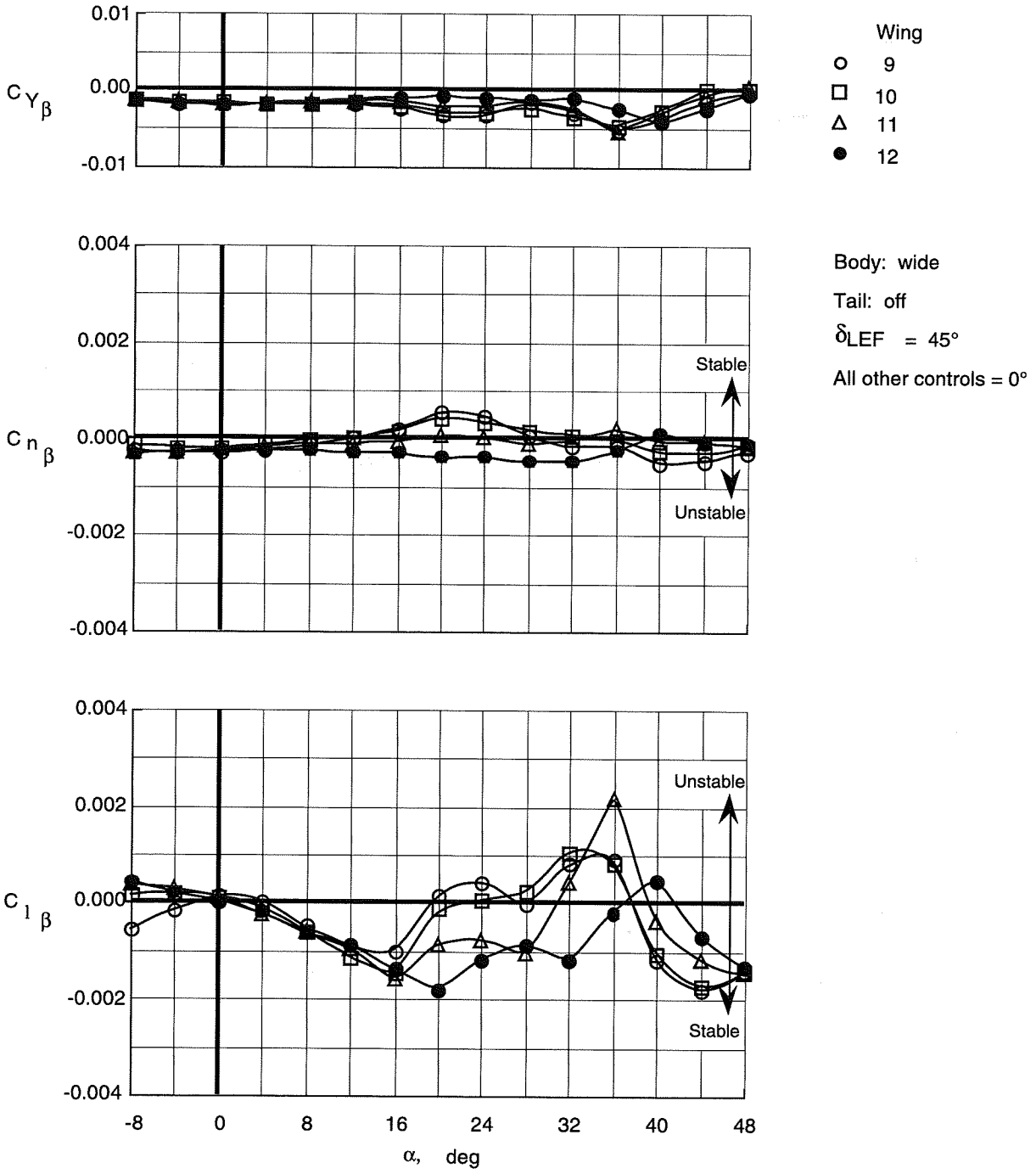

Figure 79. Lateral-directional stability characteristics of wing planforms with wide top body on and leading-edge flaps deflected.

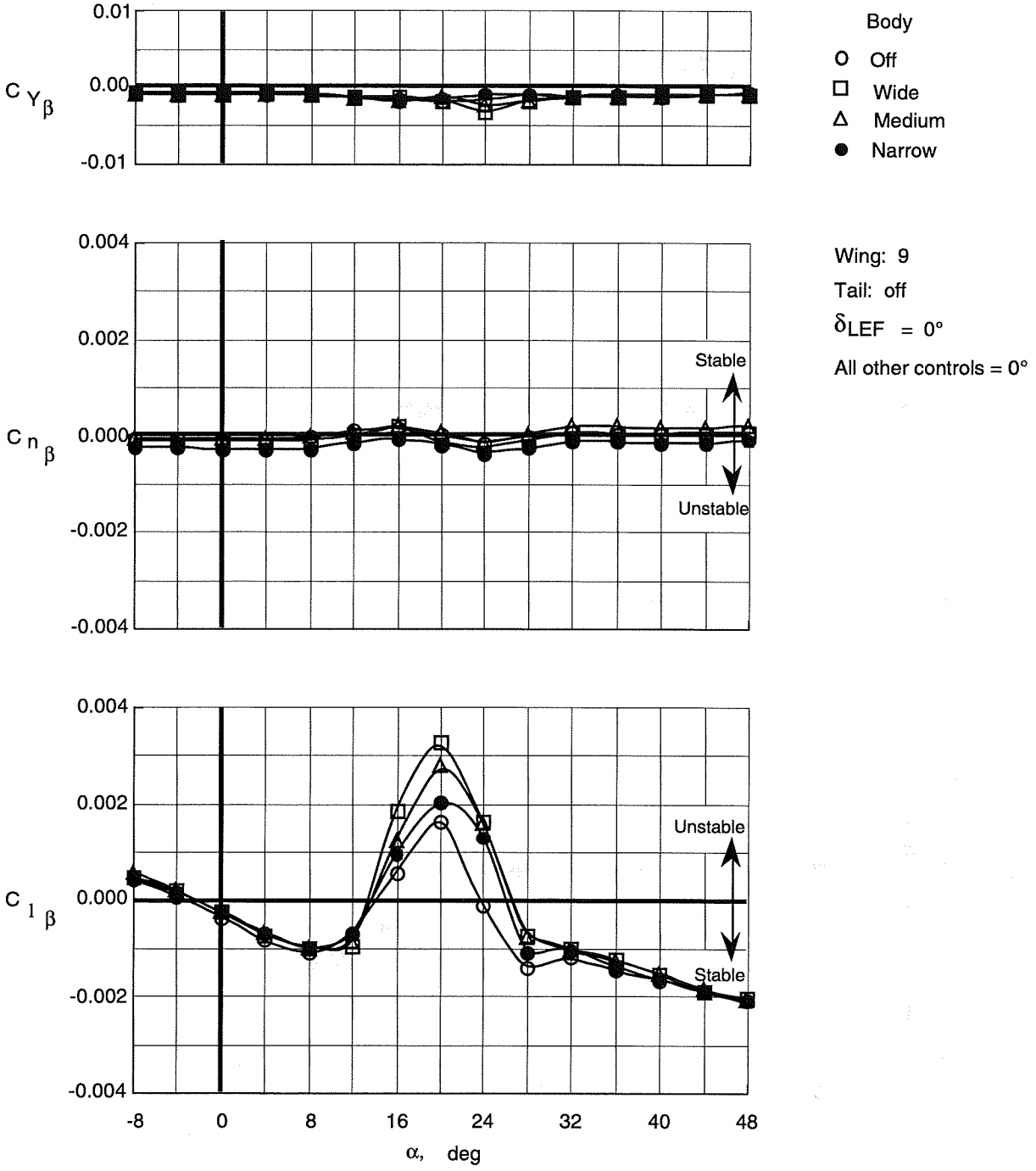

Figure 80. Effect of top body width on lateral-directional stability characteristics of Wing 9.

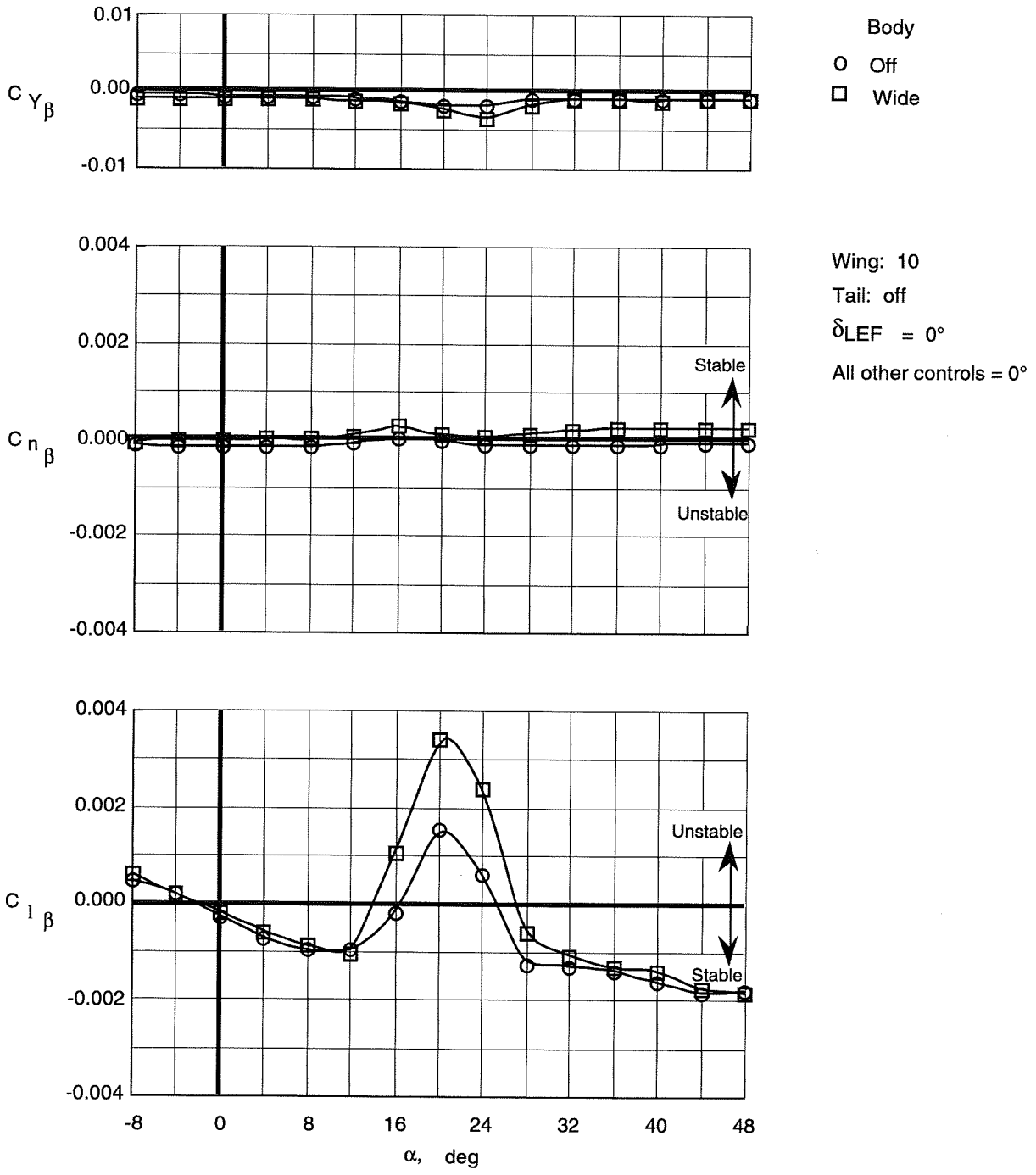

Figure 81. Effect of wide top body on lateral-directional stability characteristics of Wing 10.

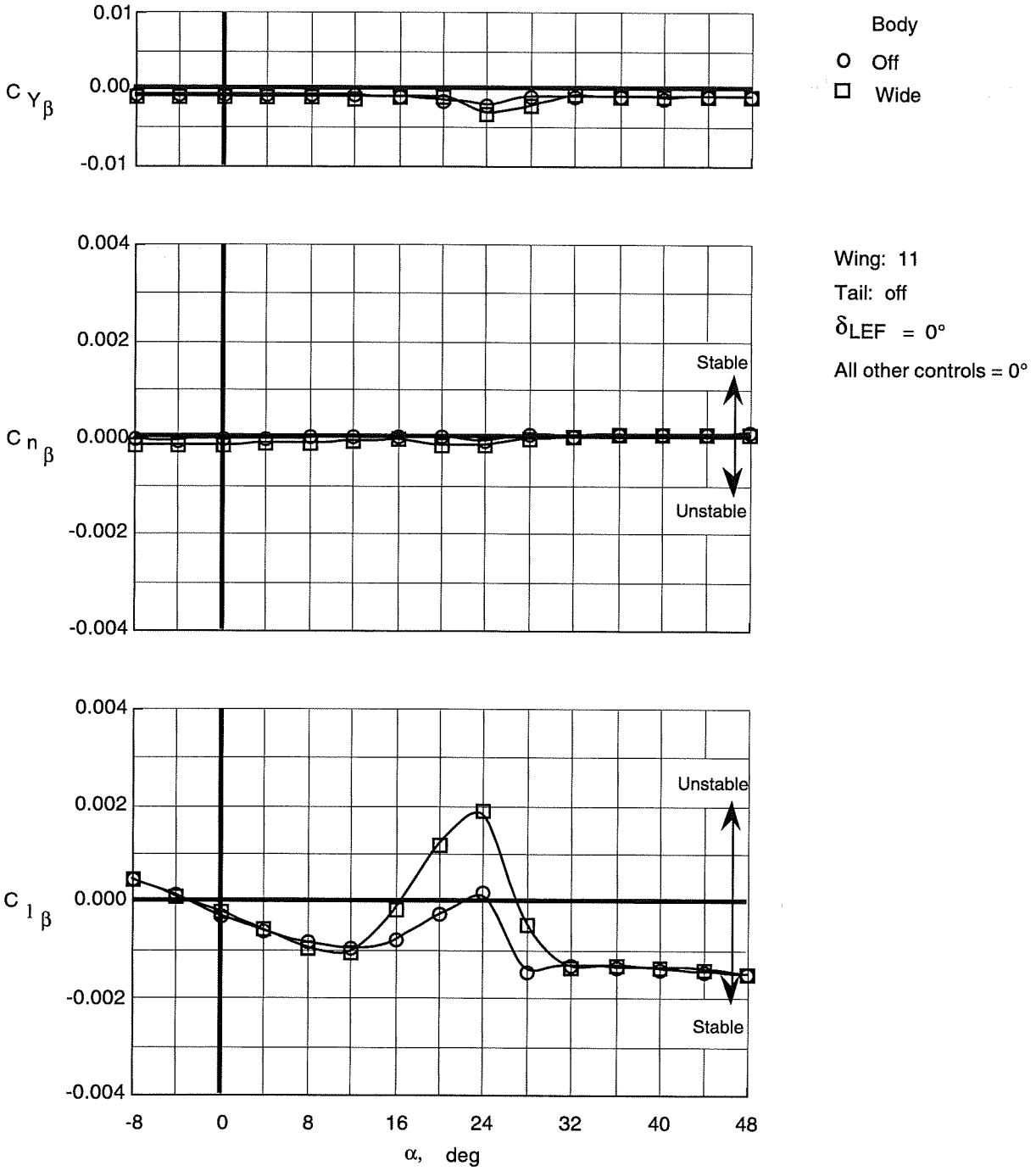

Figure 82. Effect of wide top body on lateral-directional stability characteristics of Wing 11.

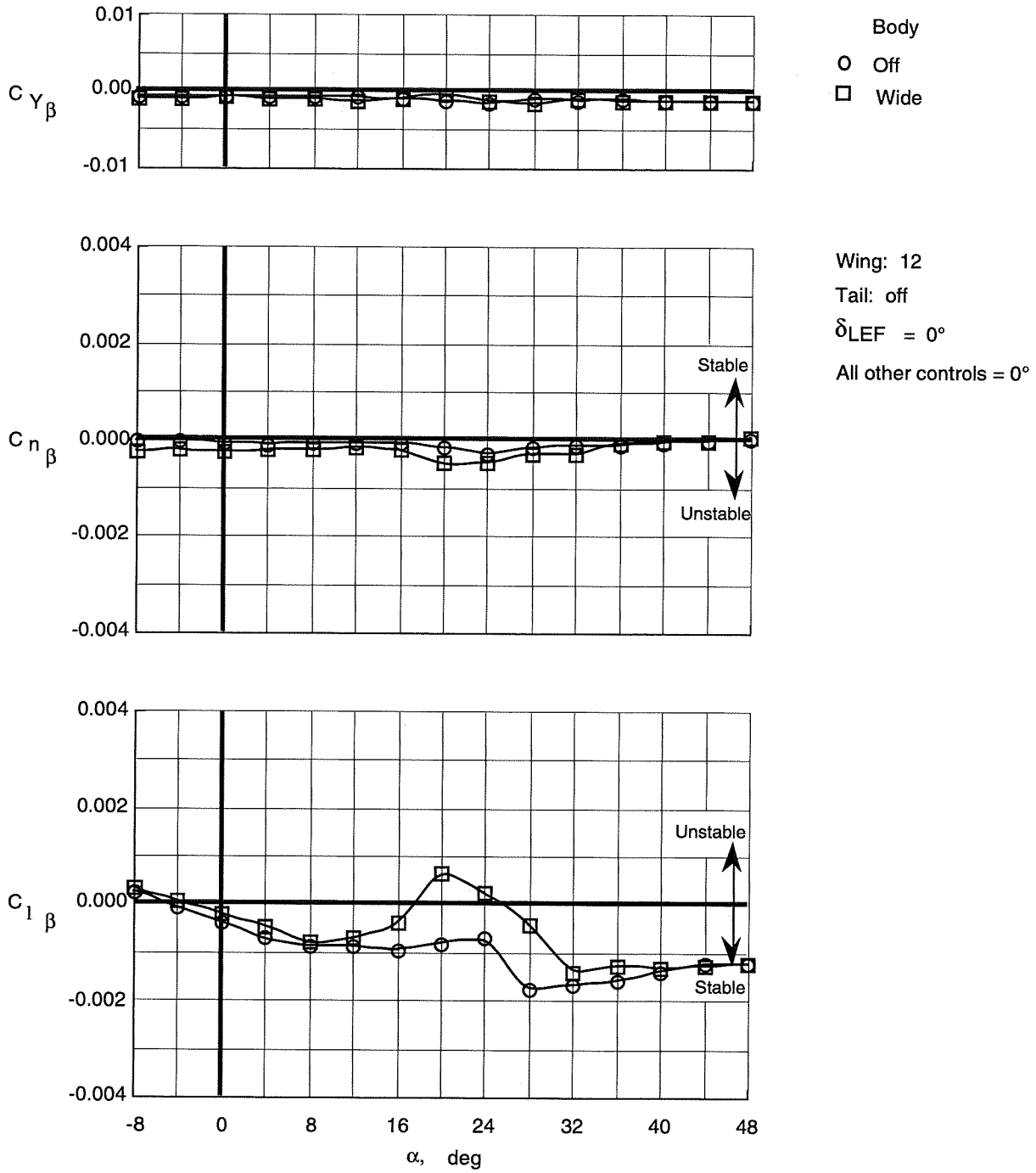

Figure 83. Effect of wide top body on lateral-directional stability characteristics of Wing 12.

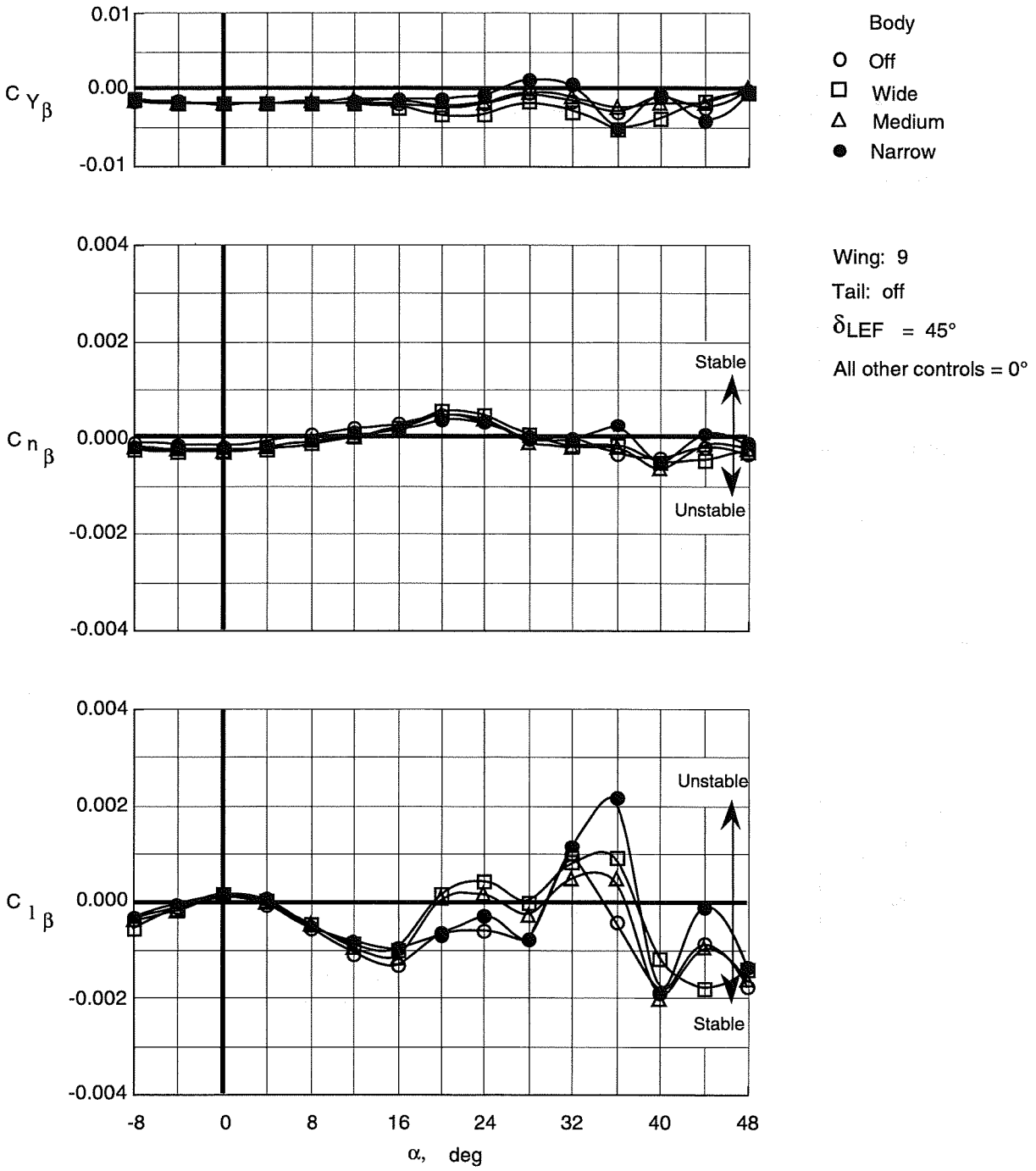

Figure 84. Effect of top body width on lateral-directional stability characteristics of Wing 9 with leading-edge flaps deflected.

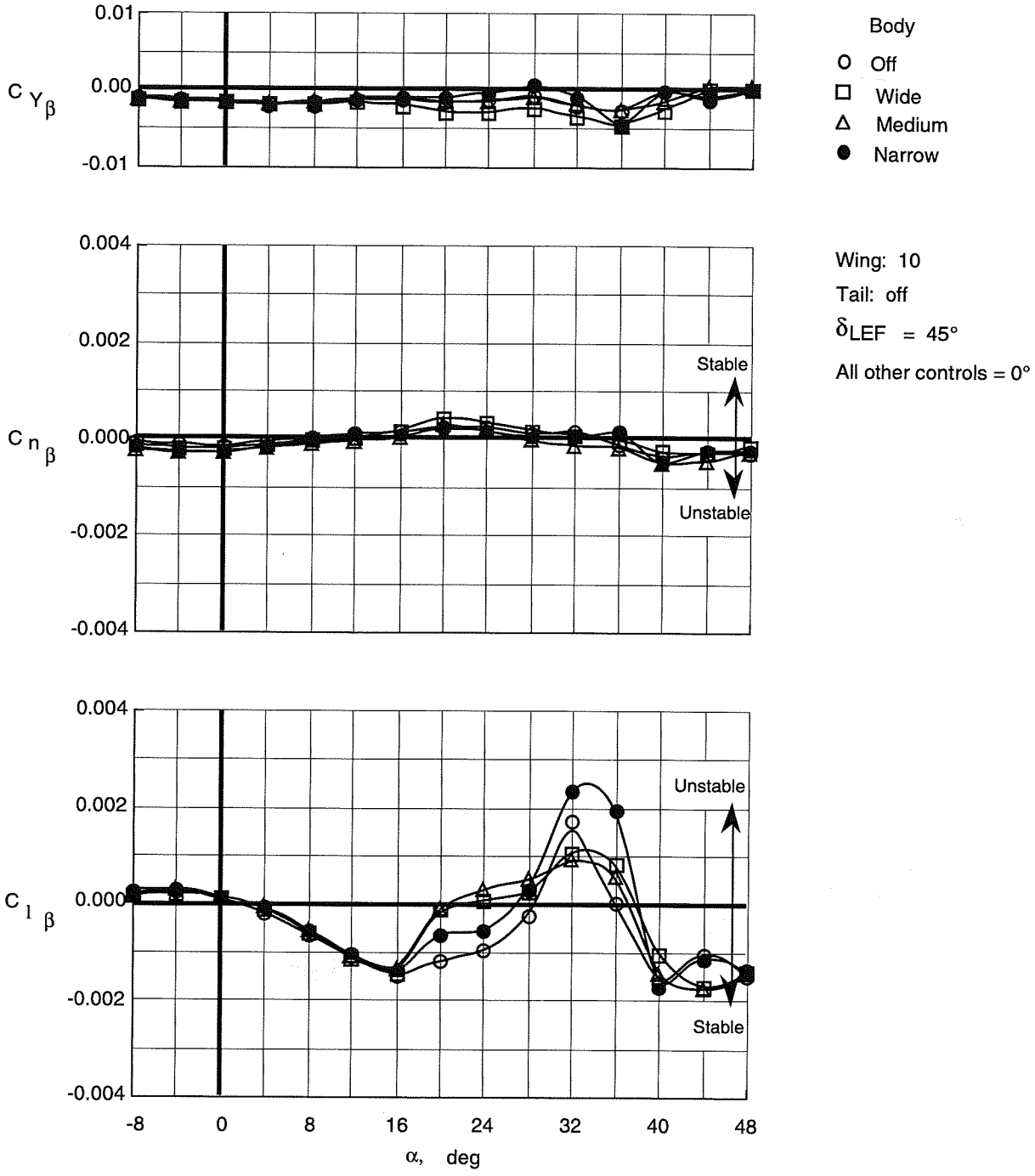

Figure 85. Effect of body width on lateral-directional stability characteristics of Wing 10 with leading-edge flaps deflected.

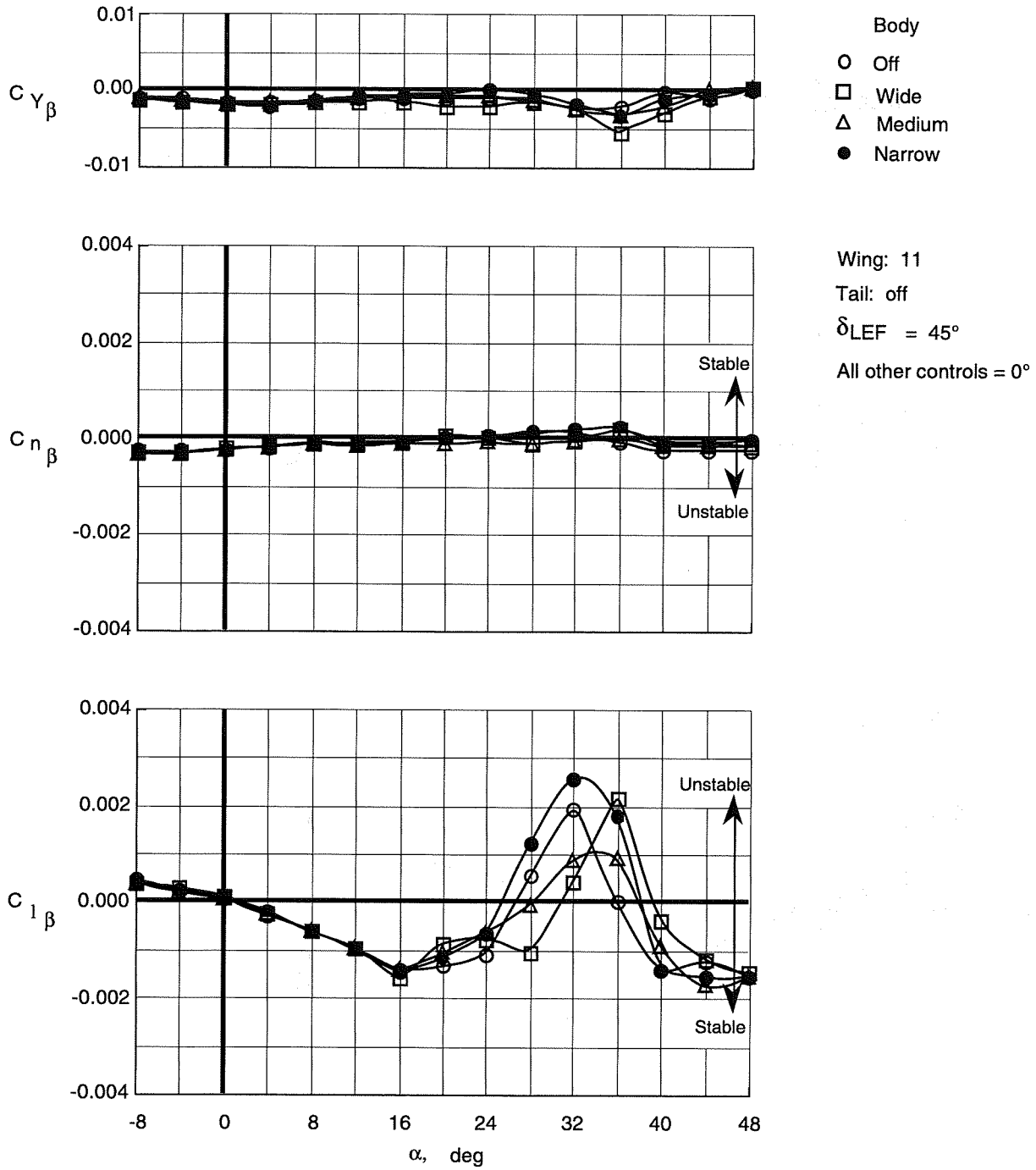

Figure 86. Effect of body width on lateral-directional stability characteristics of Wing 11 with leading-edge flaps deflected.

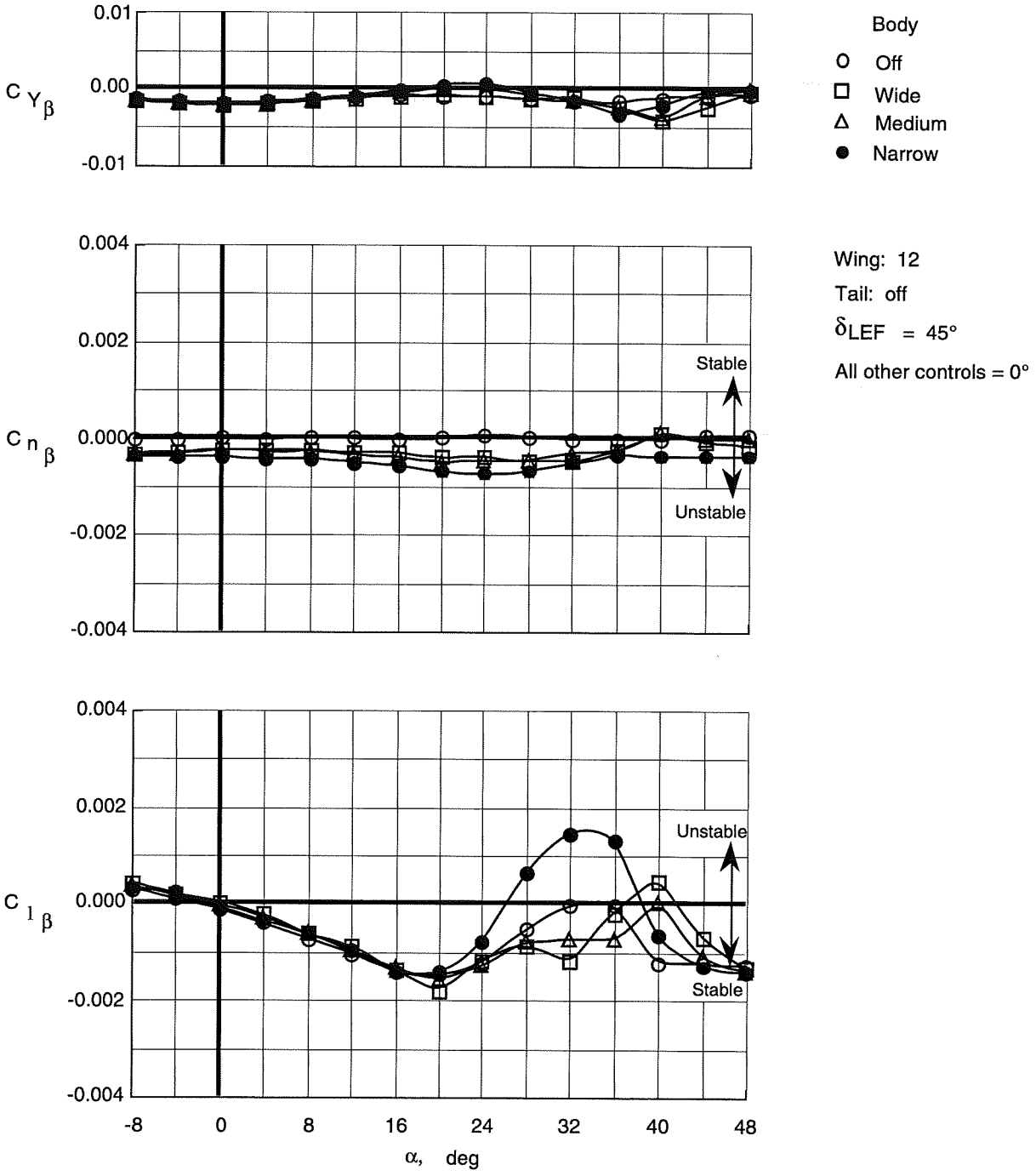

Figure 87. Effect of body width on lateral-directional stability characteristics of Wing 12 with leading-edge flaps deflected.

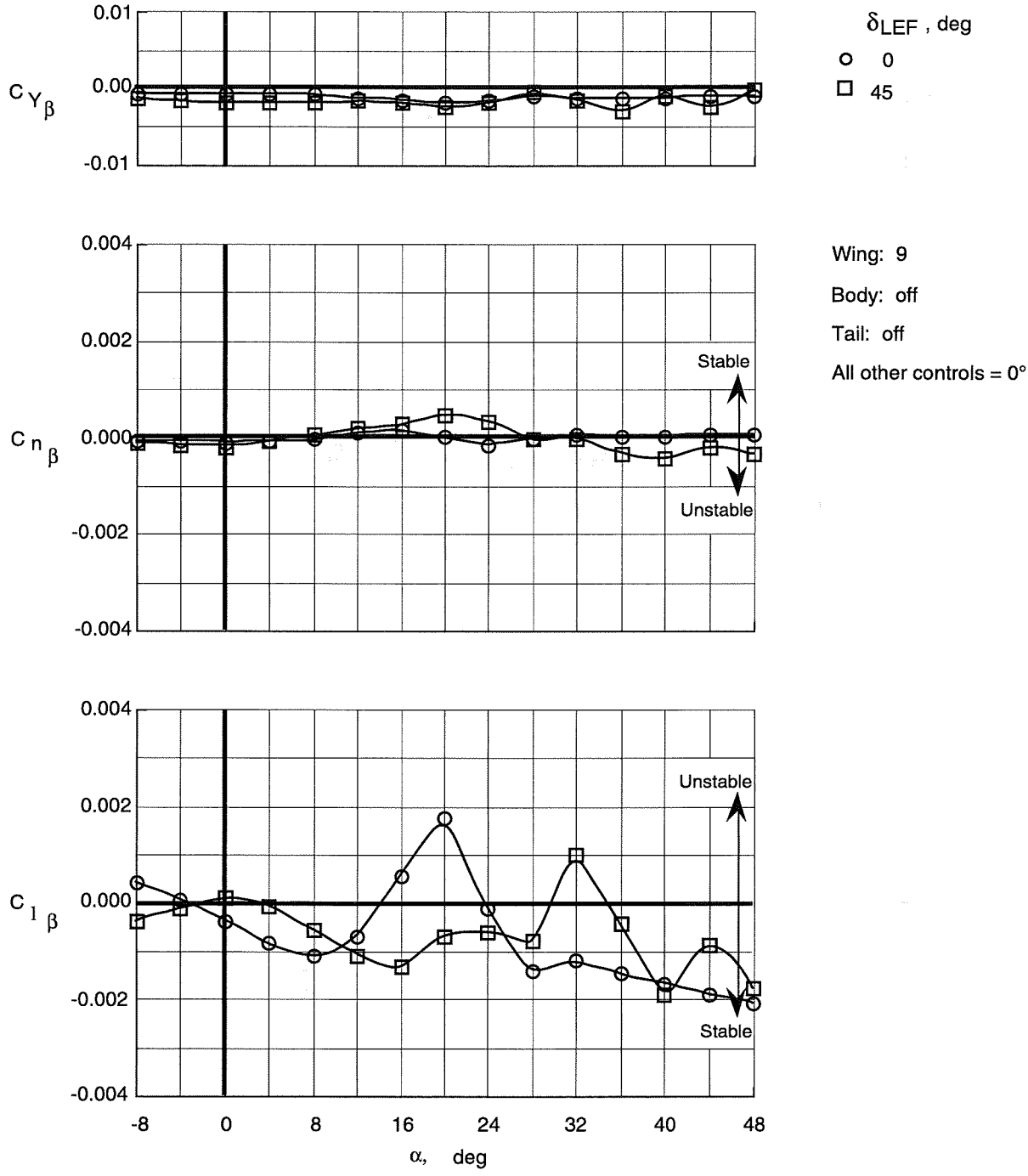

Figure 88. Effect of leading-edge flap deflection on lateral-directional stability characteristics of Wing 9 with top body off.

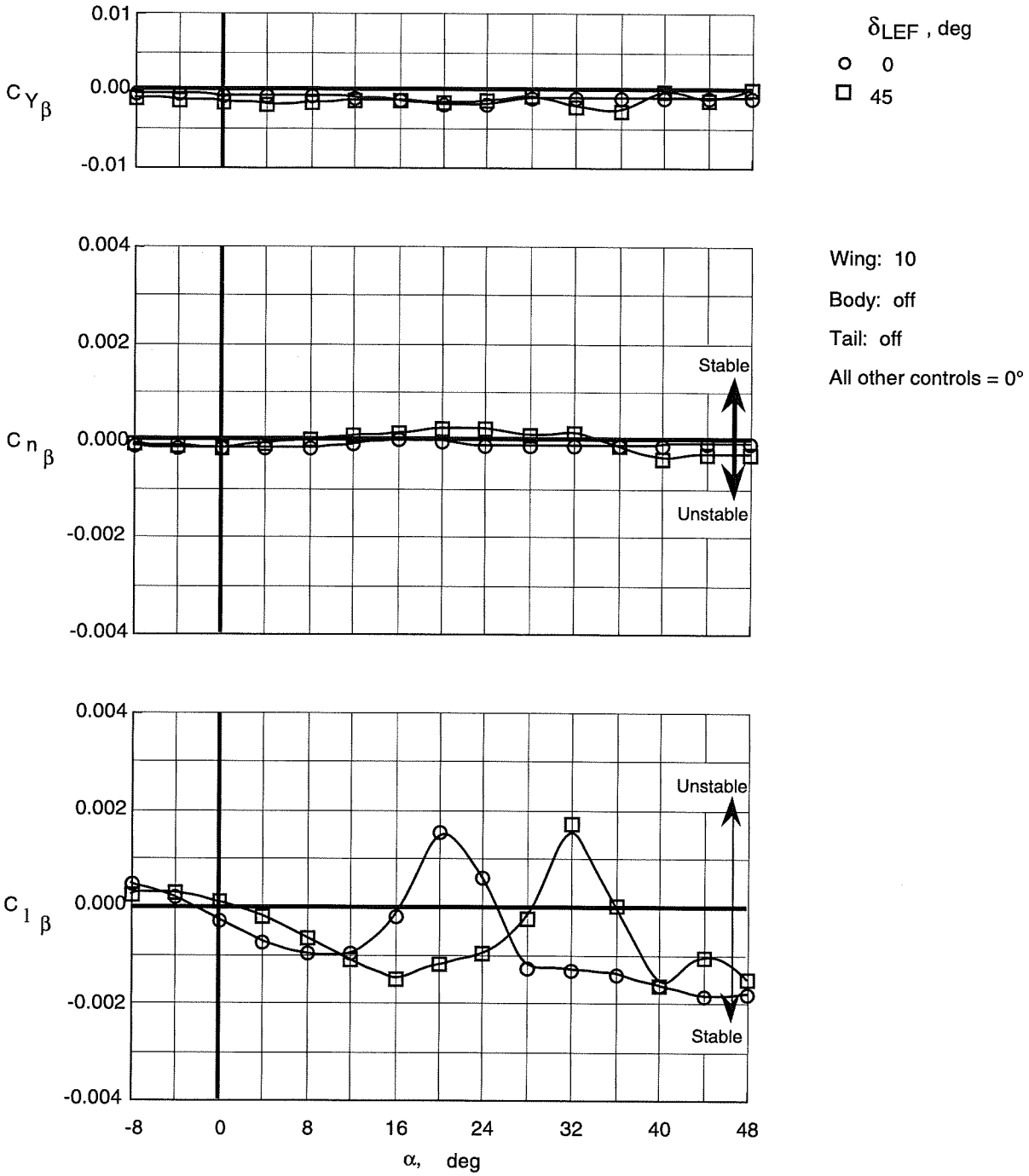

Figure 89. Effect of leading-edge flap deflection on lateral-directional stability characteristics of Wing 10 with top body off.

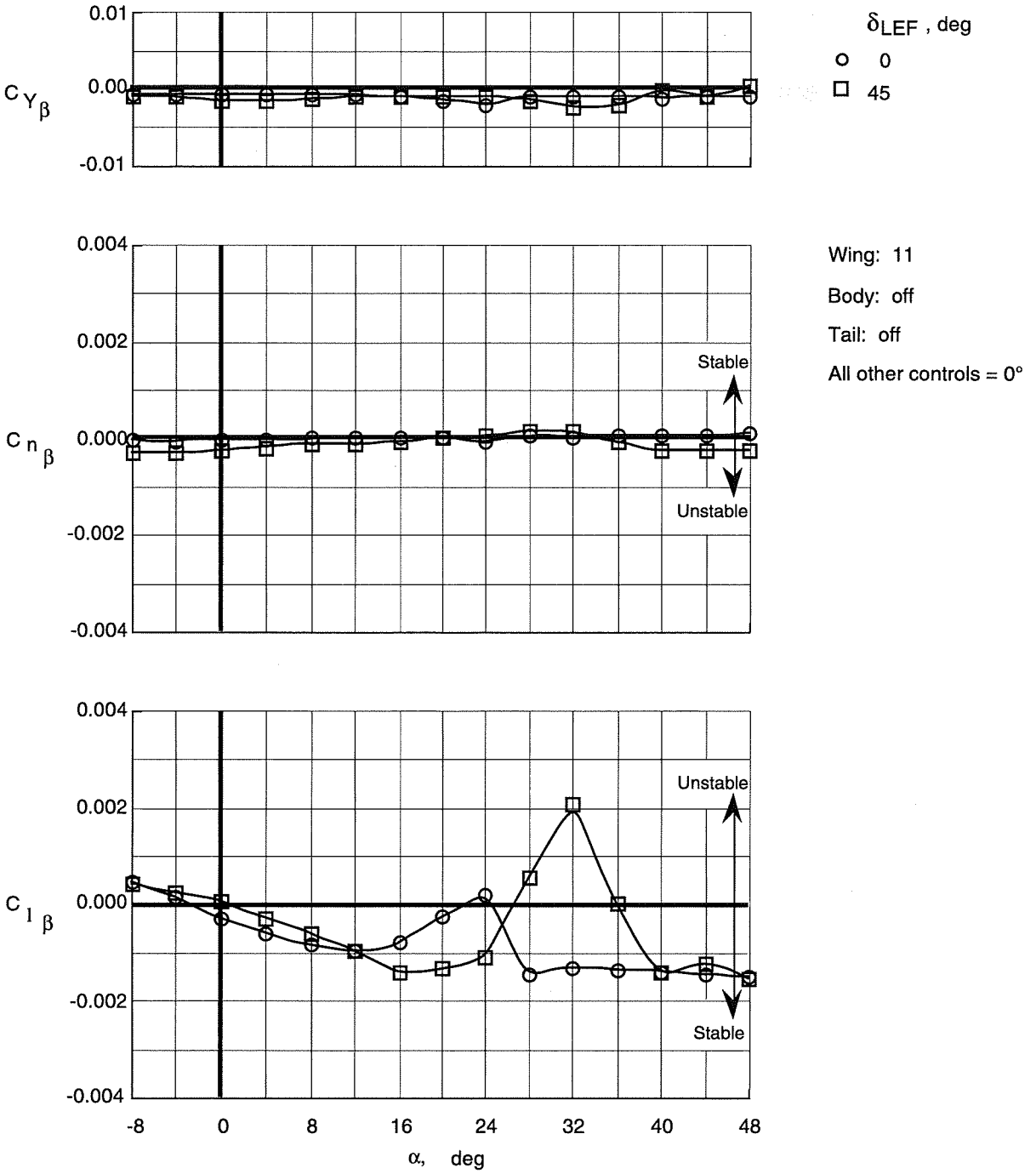

Figure 90. Effect of leading-edge flap deflection on lateral-directional stability characteristics of Wing 11 with top body off.

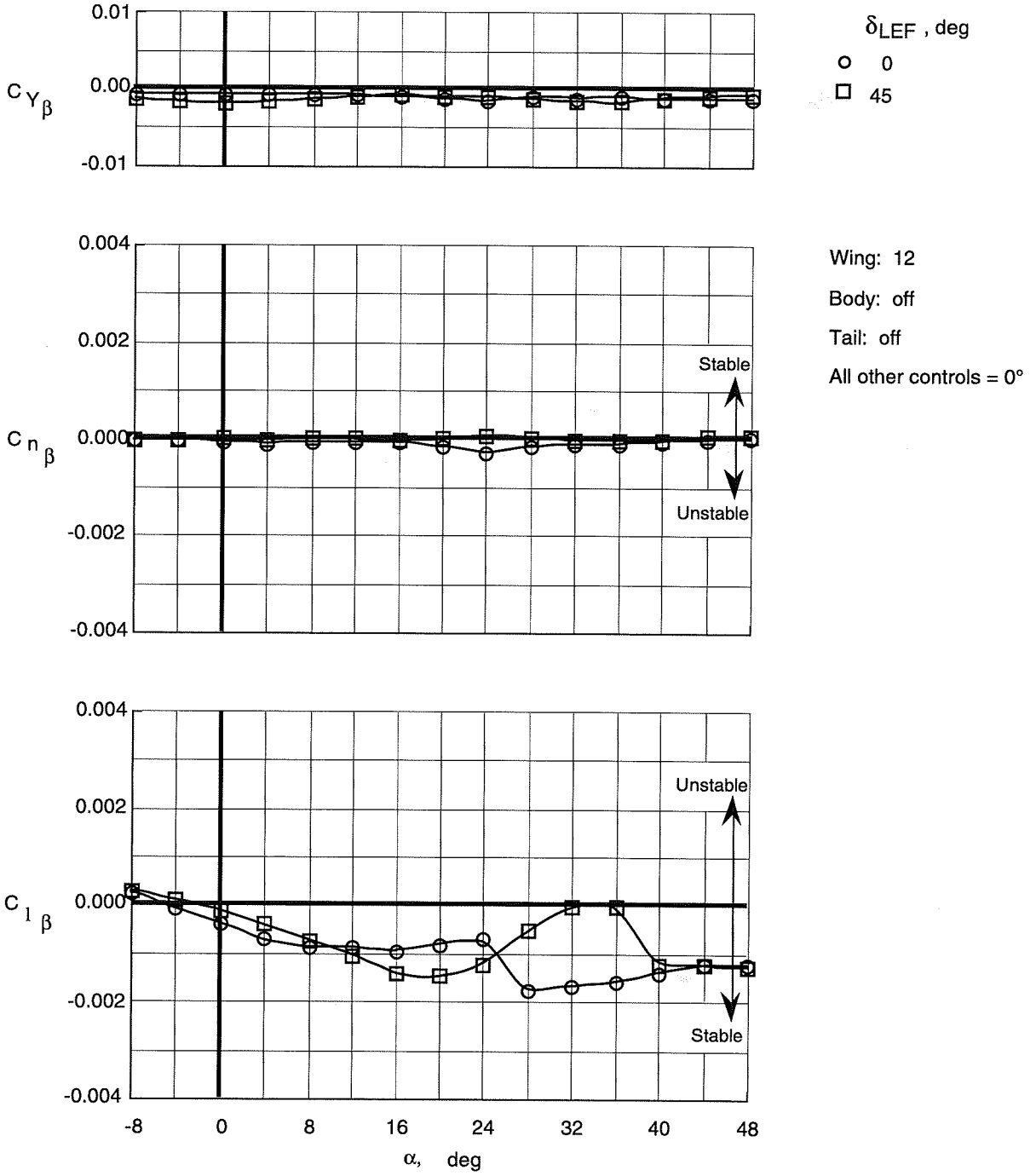

Figure 91. Effect of leading-edge flap deflection on lateral-directional stability characteristics of Wing 12 with top body off.

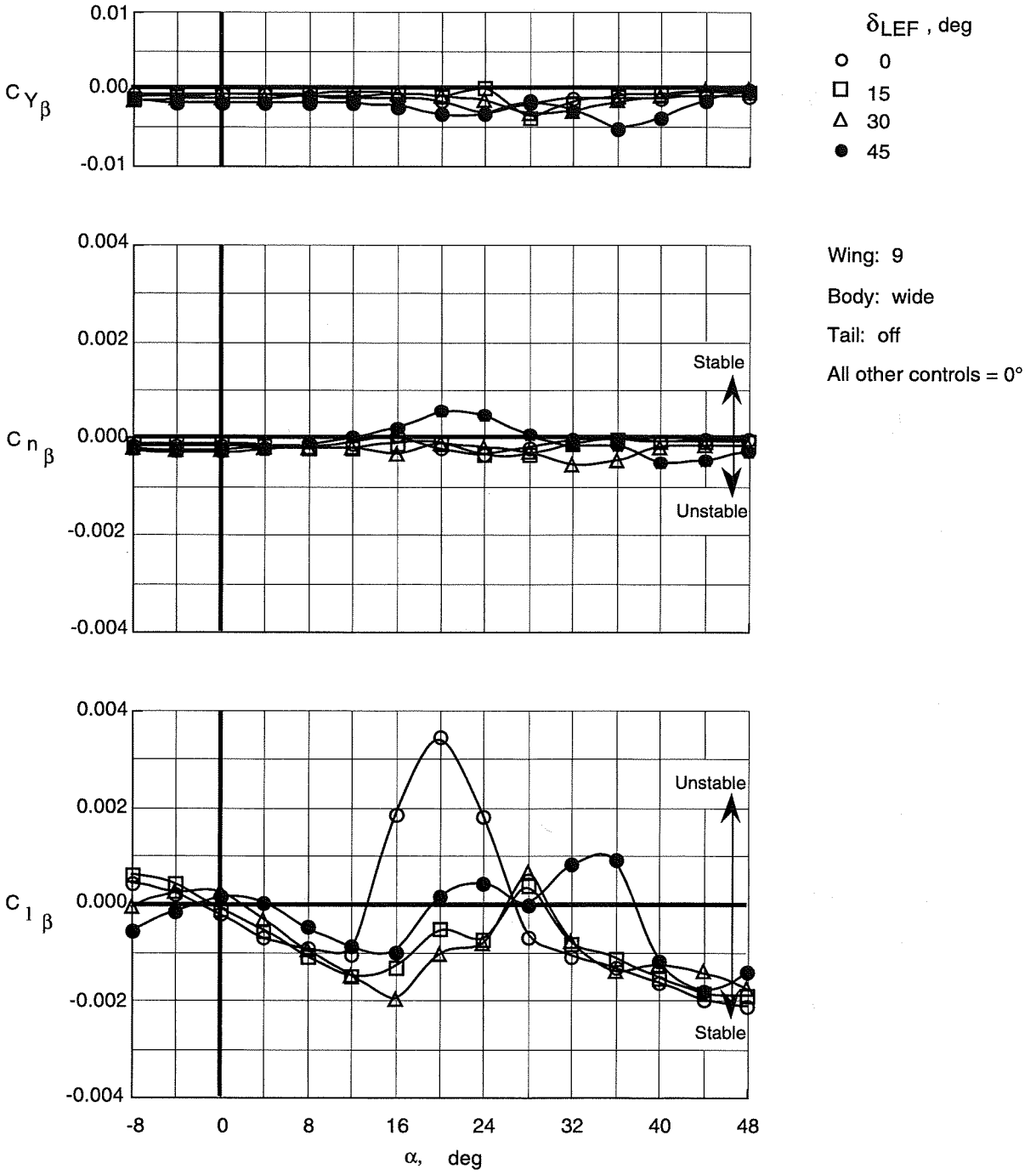

Figure 92. Effect of leading-edge flap deflections on lateral-directional stability characteristics of Wing 9 with wide top body on.

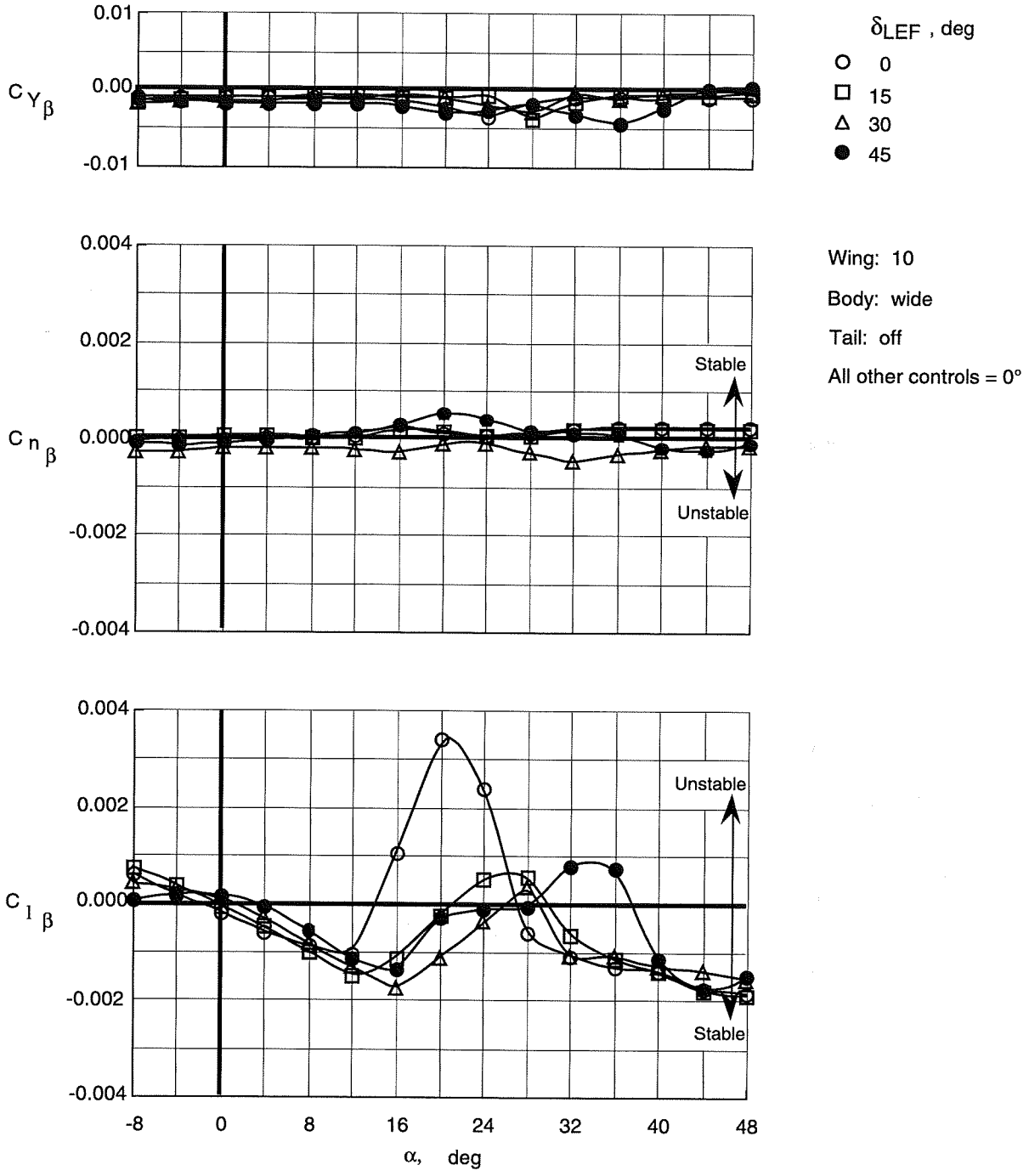

Figure 93. Effect of leading-edge flap deflections on lateral-directional stability characteristics of Wing 10 with wide top body on.

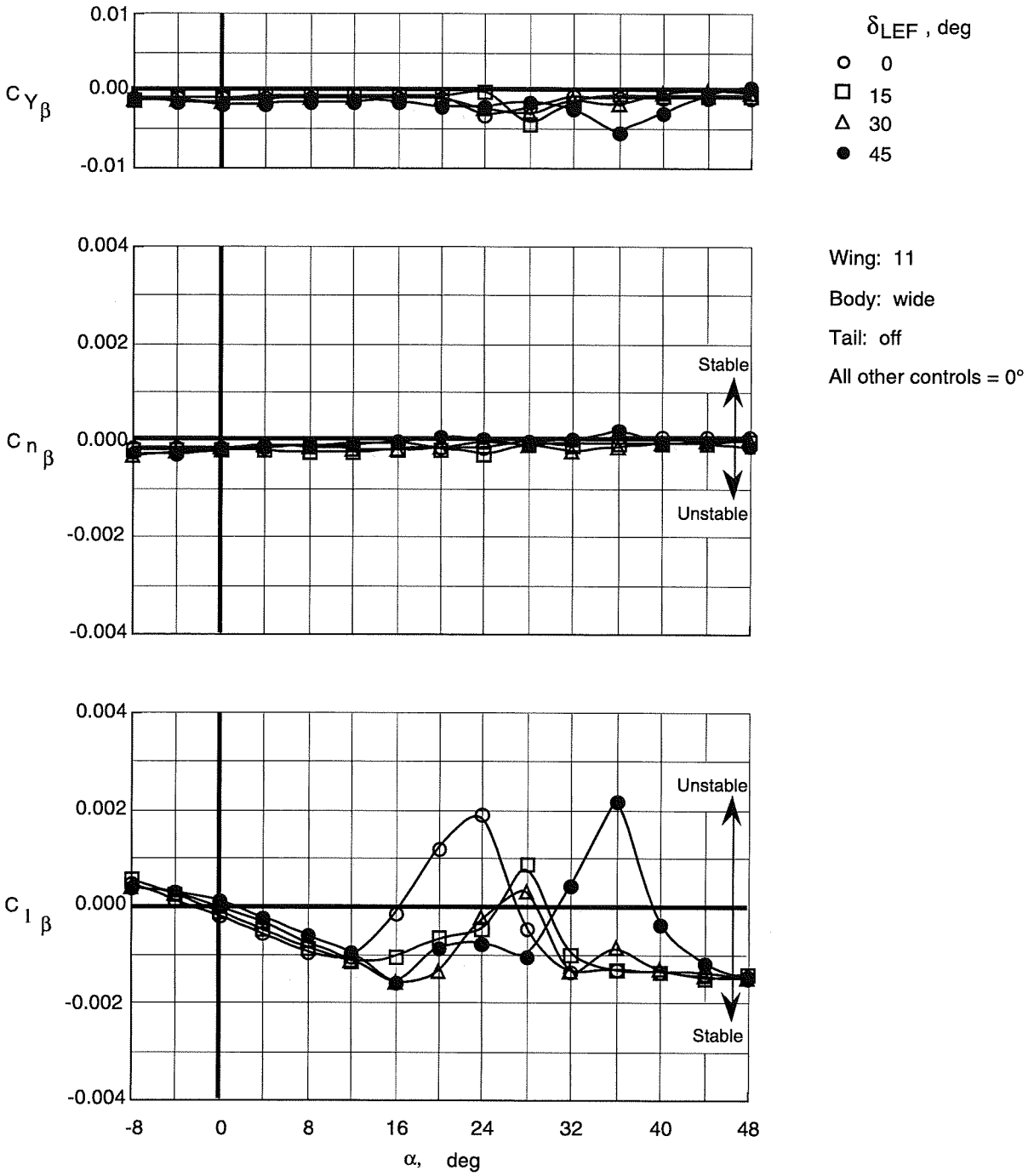

Figure 94. Effect of leading-edge flap deflections on lateral-directional stability characteristics of Wing 11 with wide top body on.

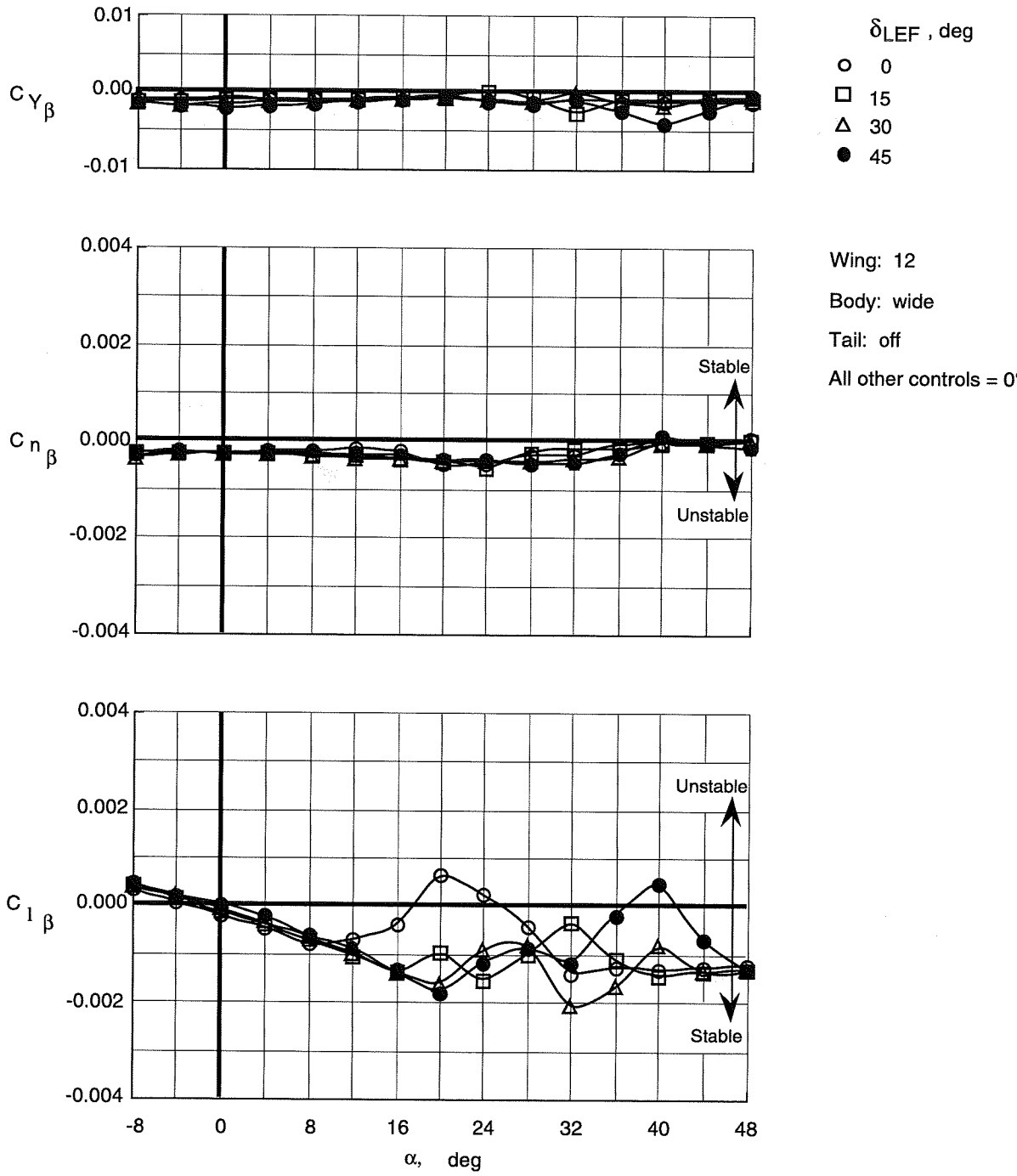

Figure 95. Effect of leading-edge flap deflections on lateral-directional stability characteristics of Wing 12 with wide top body on.

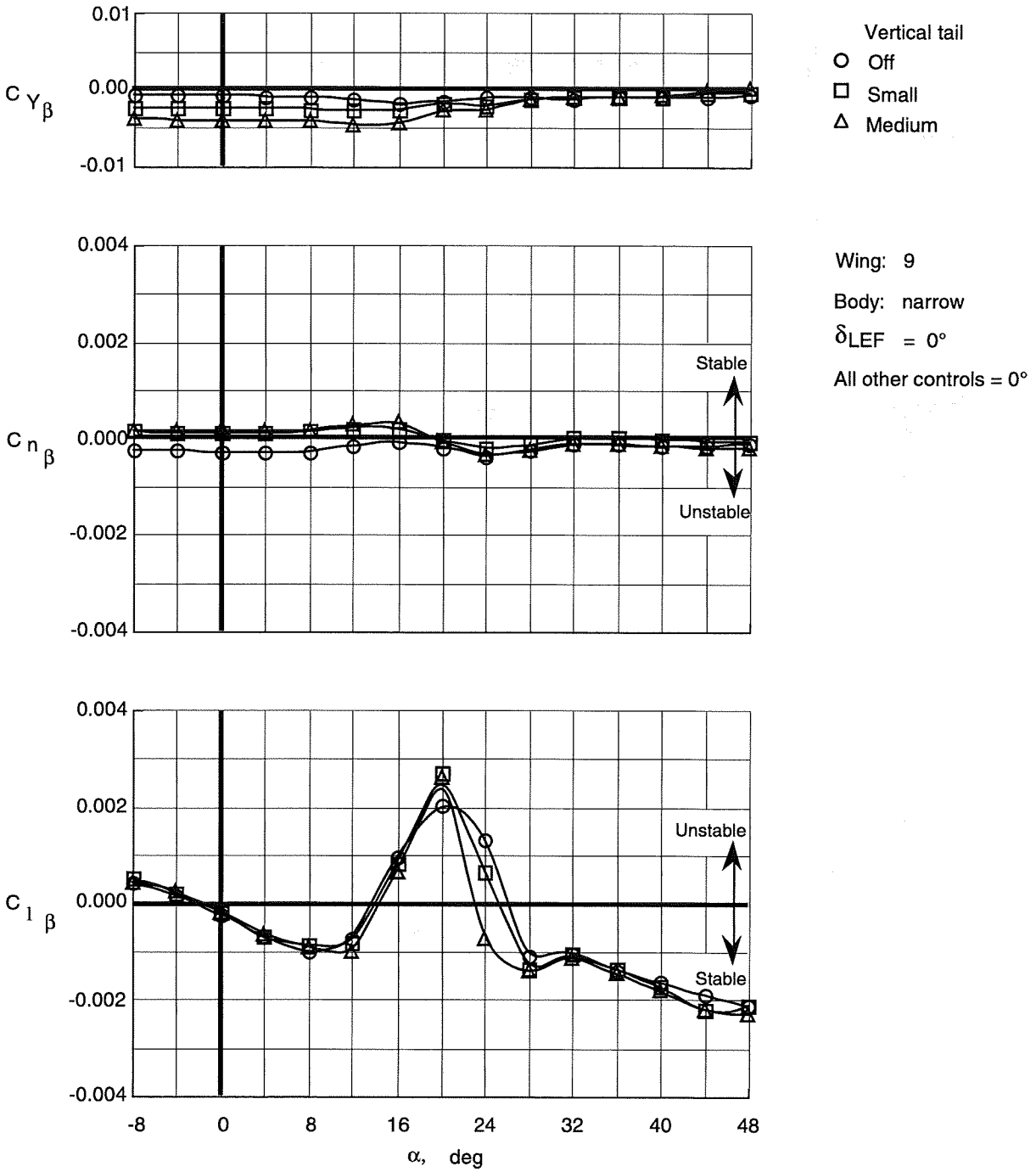

Figure 96. Effect of vertical tails on lateral-directional stability characteristics of Wing 9 with narrow top body on.

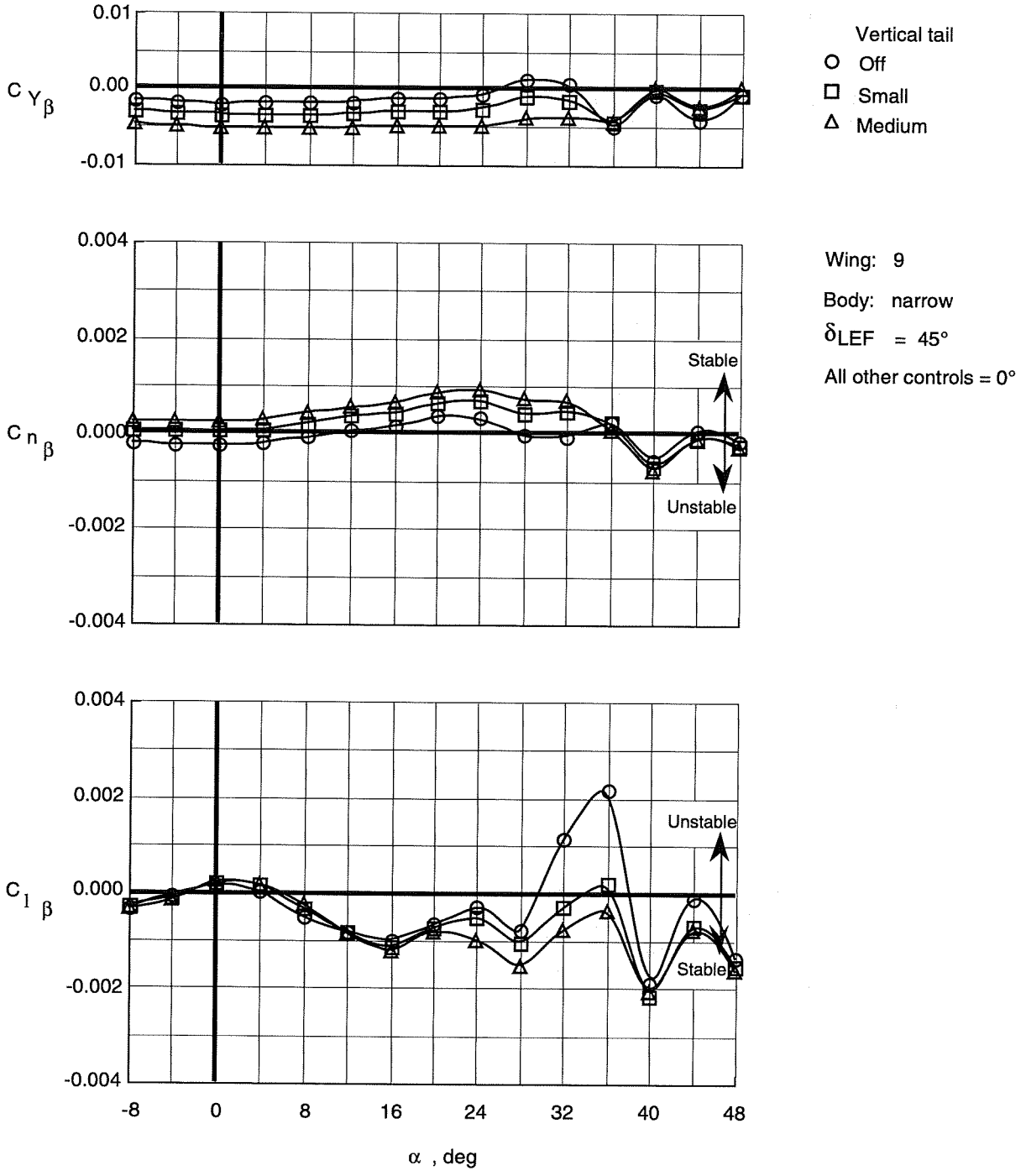

Figure 97. Effect of vertical tails on lateral-directional stability characteristics of Wing 9 with narrow top body on and leading-edge flaps deflected.

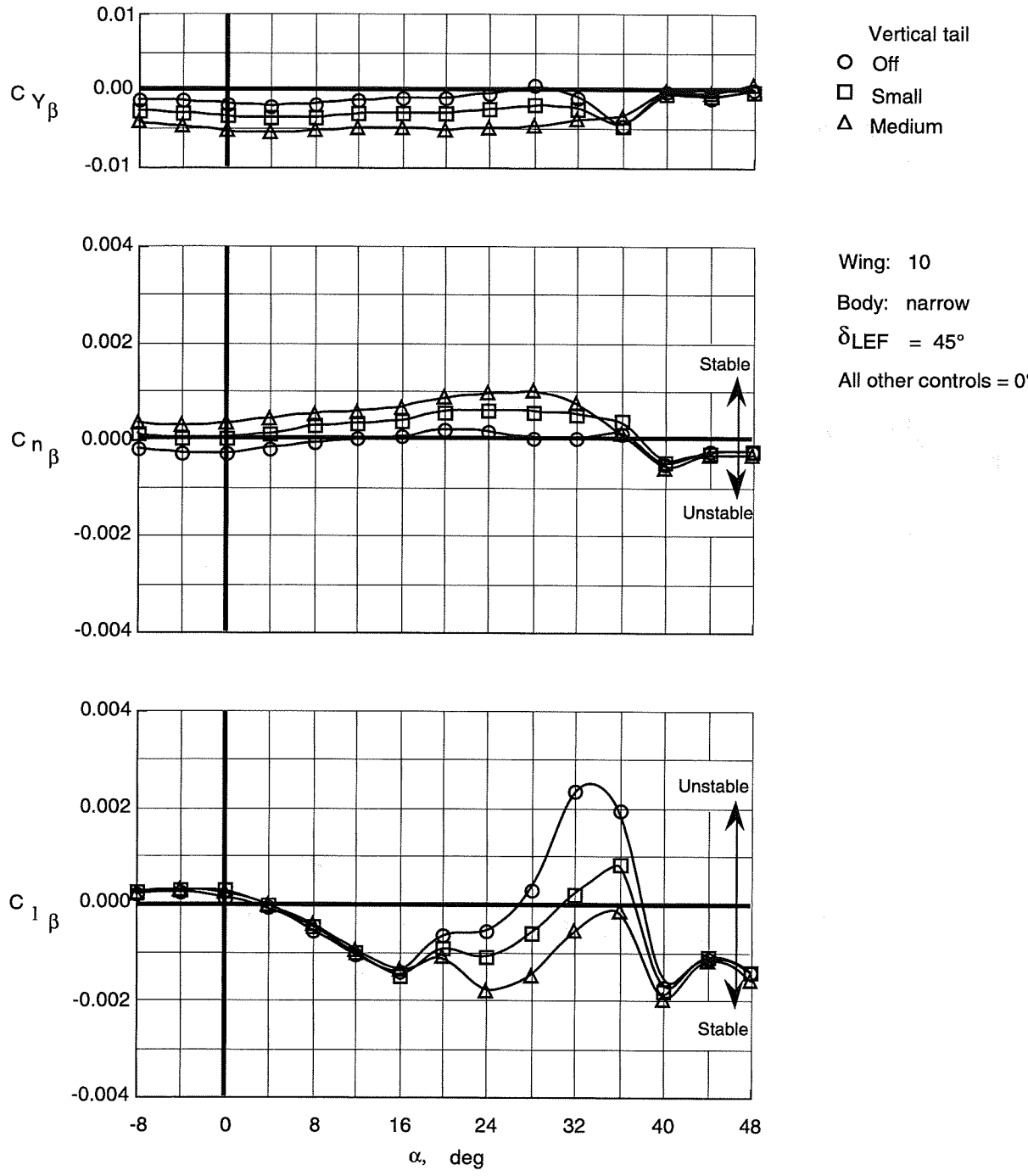

Figure 98. Effect of vertical tails on lateral-directional stability characteristics of Wing 10 with narrow top body on and leading-edge flaps deflected.

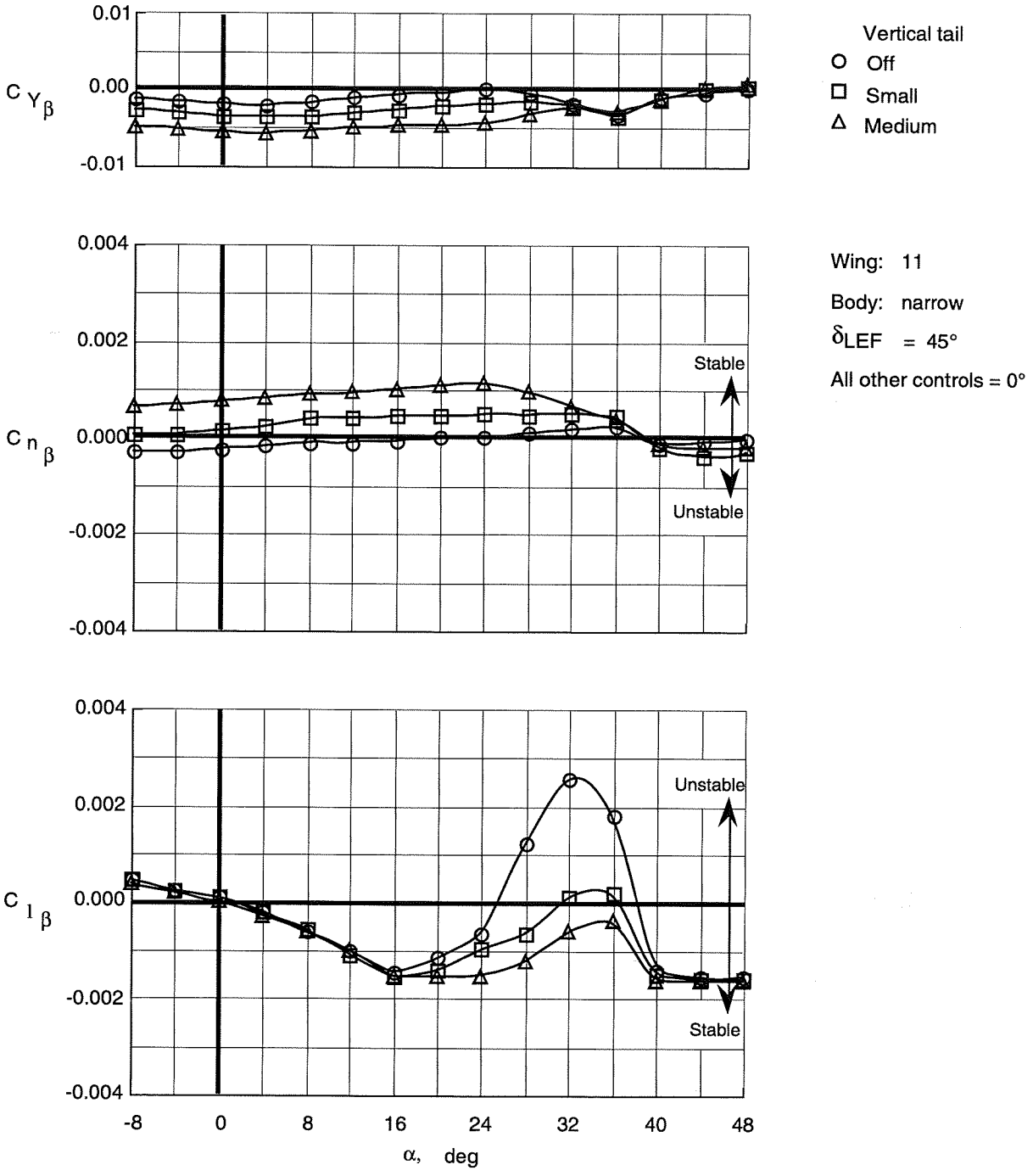

Figure 99. Effect of vertical tails on lateral-directional stability characteristics of Wing 11 with narrow top body on and leading-edge flaps deflected.

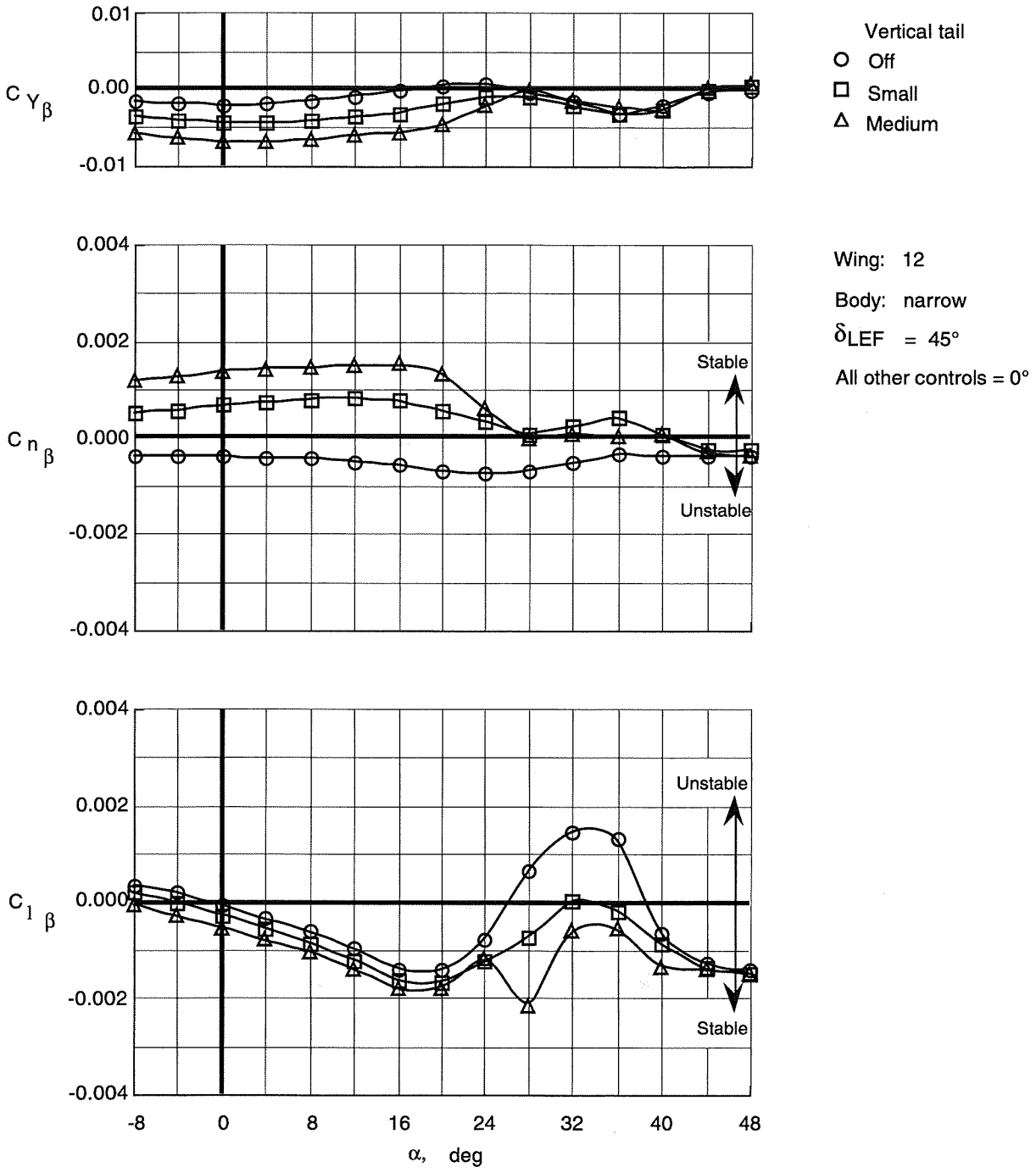

Figure 100. Effect of vertical tails on lateral-directional stability characteristics of Wing 12 with narrow top body on and leading-edge flaps deflected.

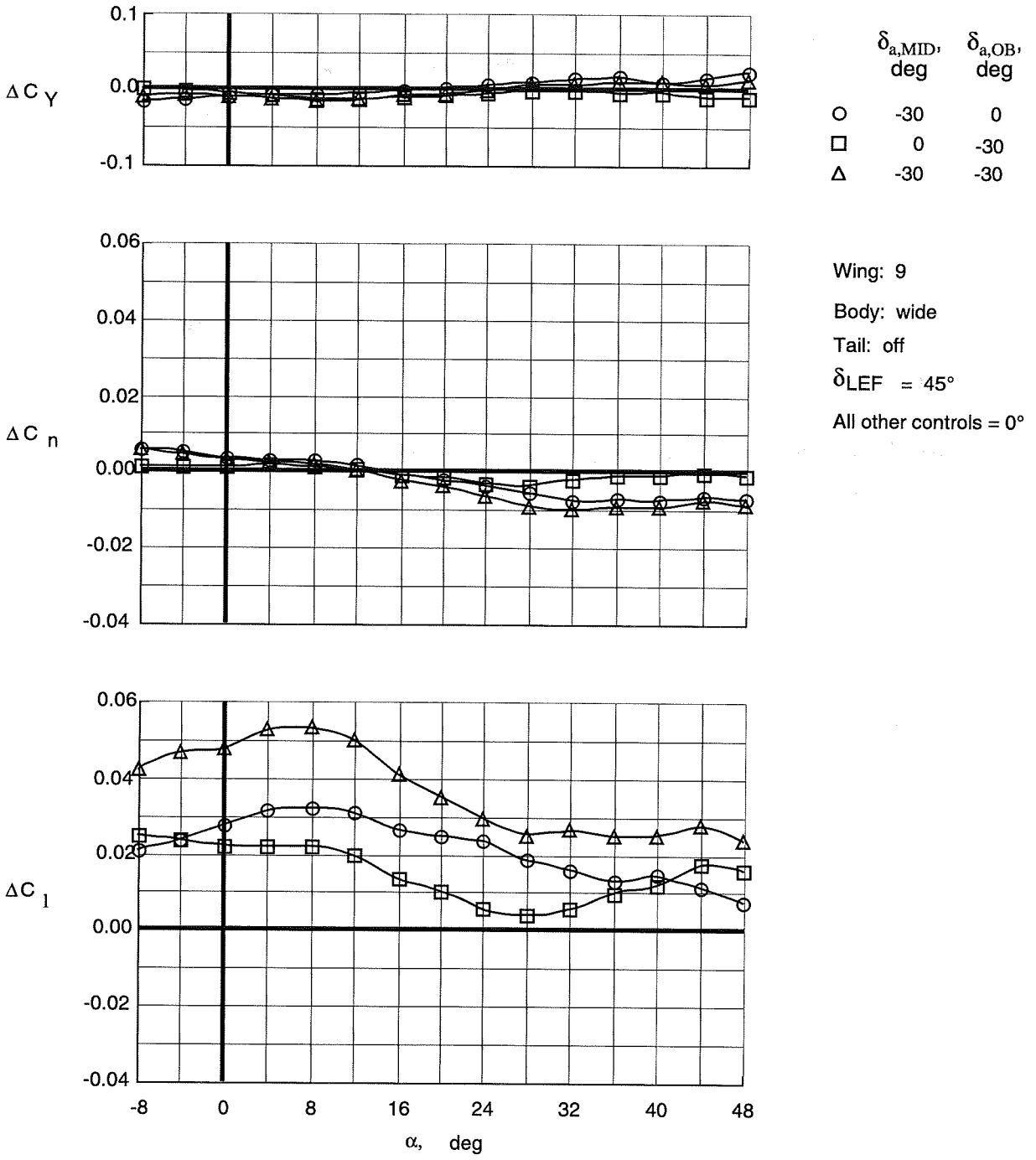

Figure 101. Control effectiveness of differential deflections of trailing-edge flaps on Wing 9 with wide top body on and leading-edge flaps deflected.

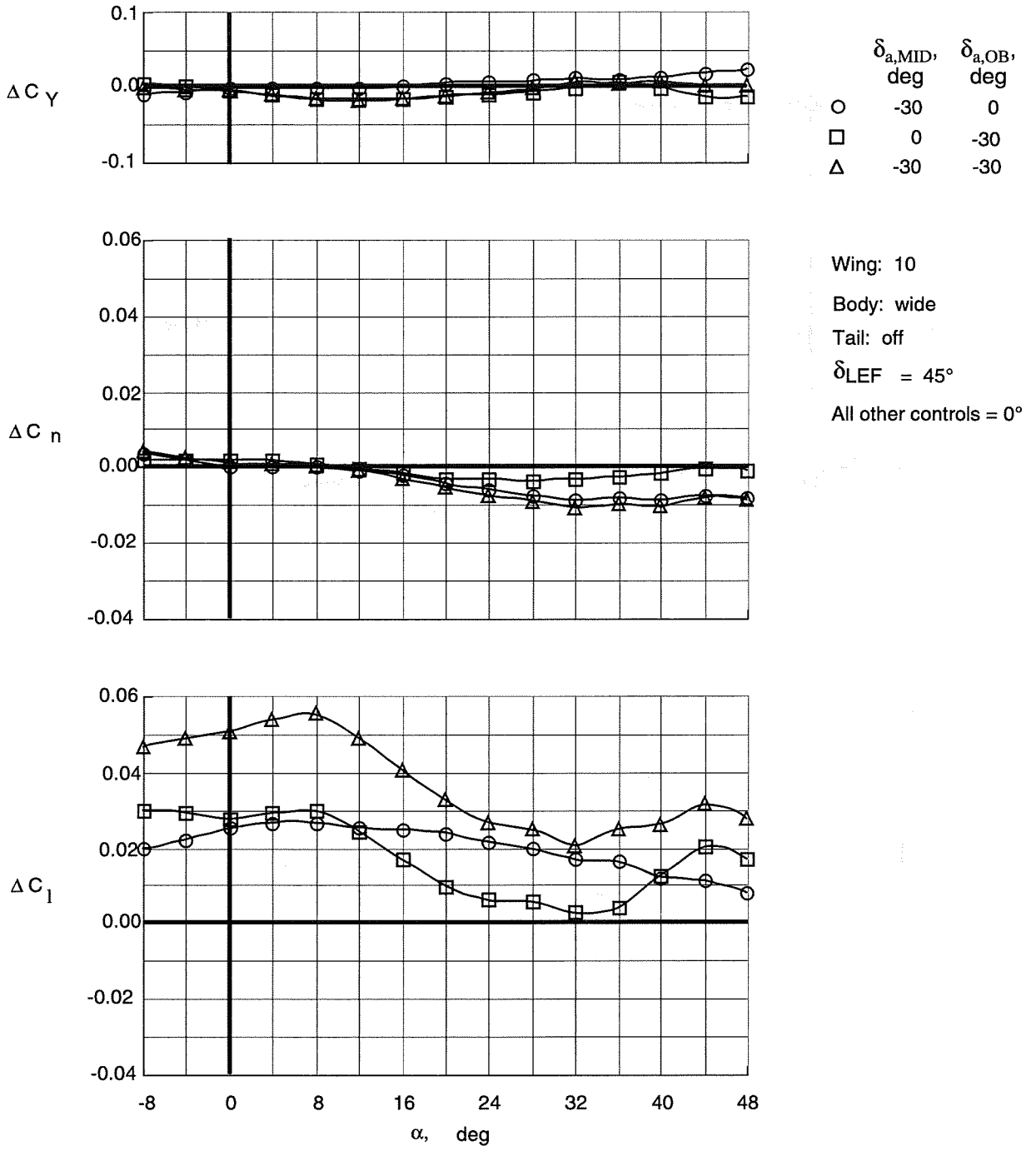

Figure 102. Control effectiveness of differential deflections of trailing-edge flaps on Wing 10 with wide top body on and leading-edge flaps deflected.

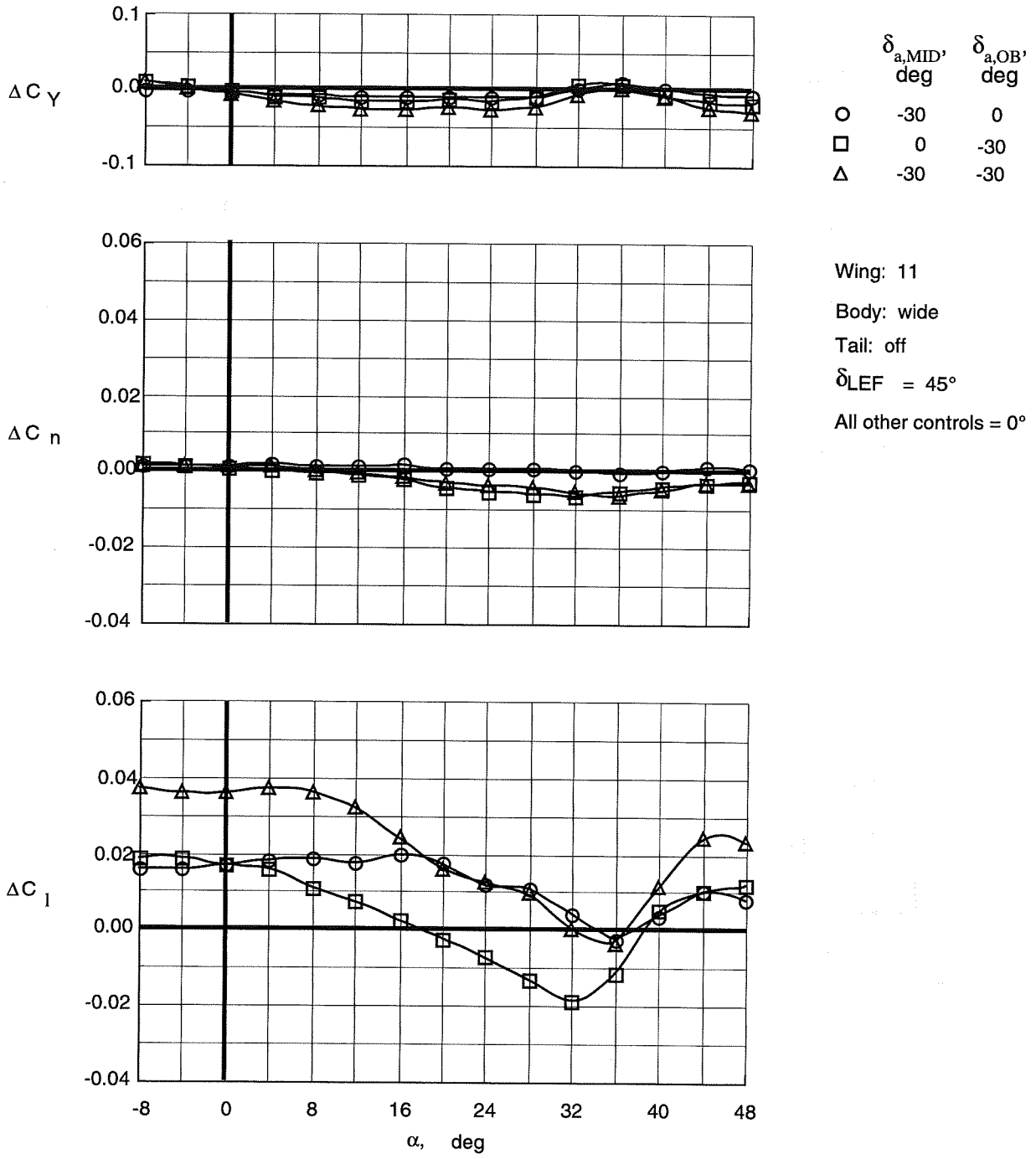

Figure 103. Control effectiveness of differential deflections of trailing-edge flaps on Wing 11 with wide top body on and leading-edge flaps deflected.

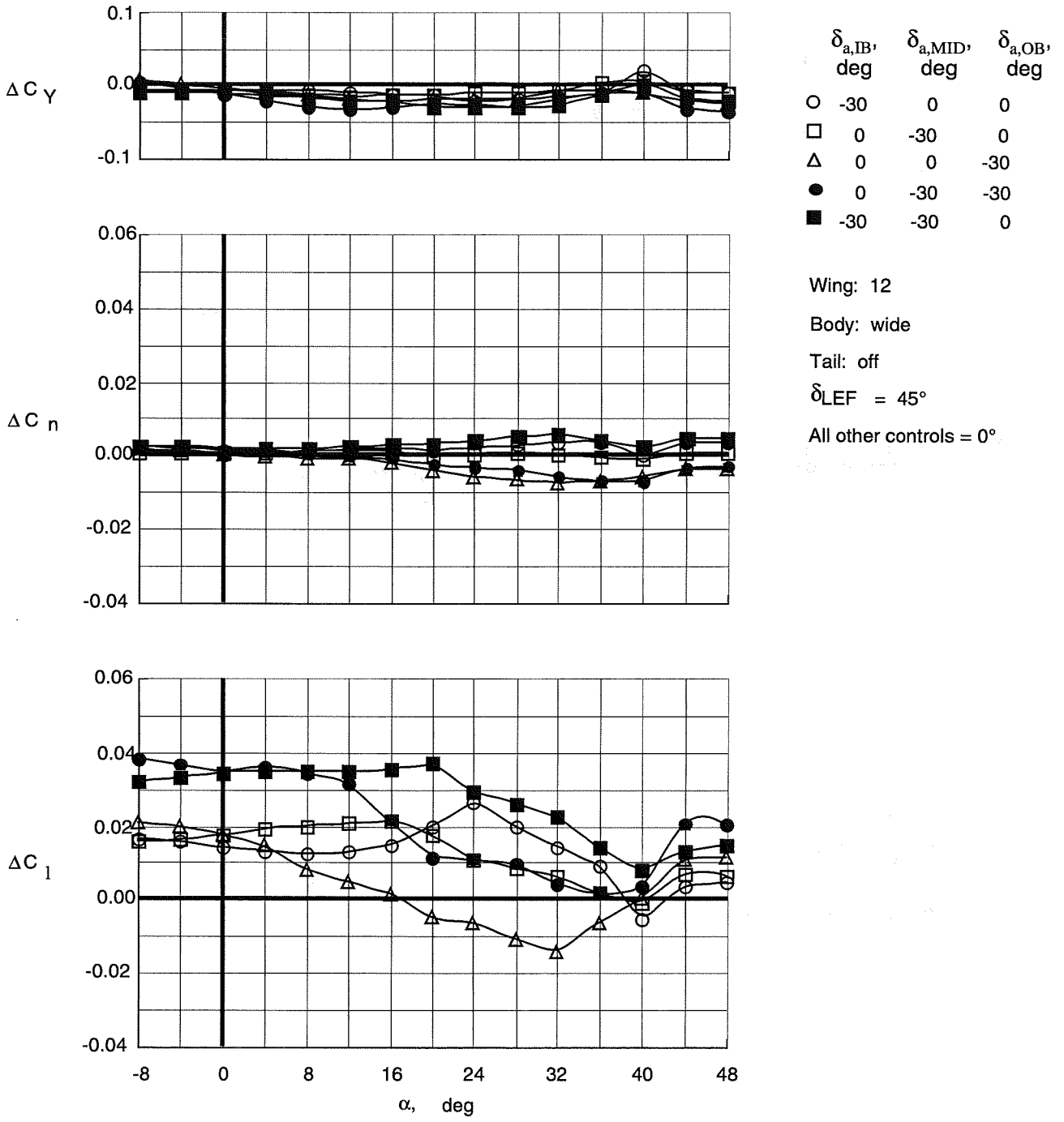

Figure 104. Control effectiveness of differential deflections of trailing-edge flaps on Wing 12 with wide top body on and leading-edge flaps deflected.

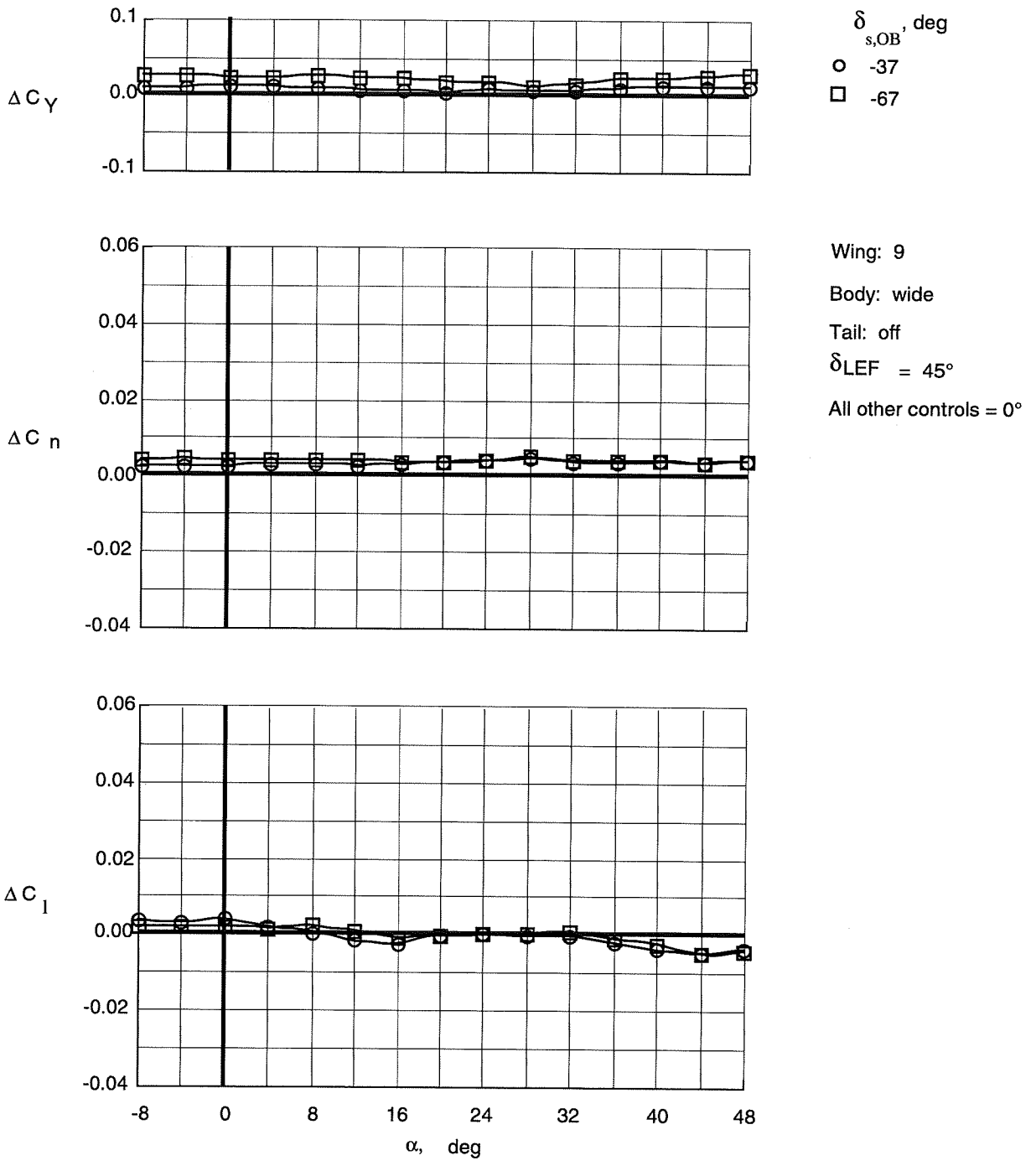

Figure 105. Control effectiveness of split deflections of right outboard trailing-edge flap on Wing 9 with wide top body on and leading-edge flaps deflected.

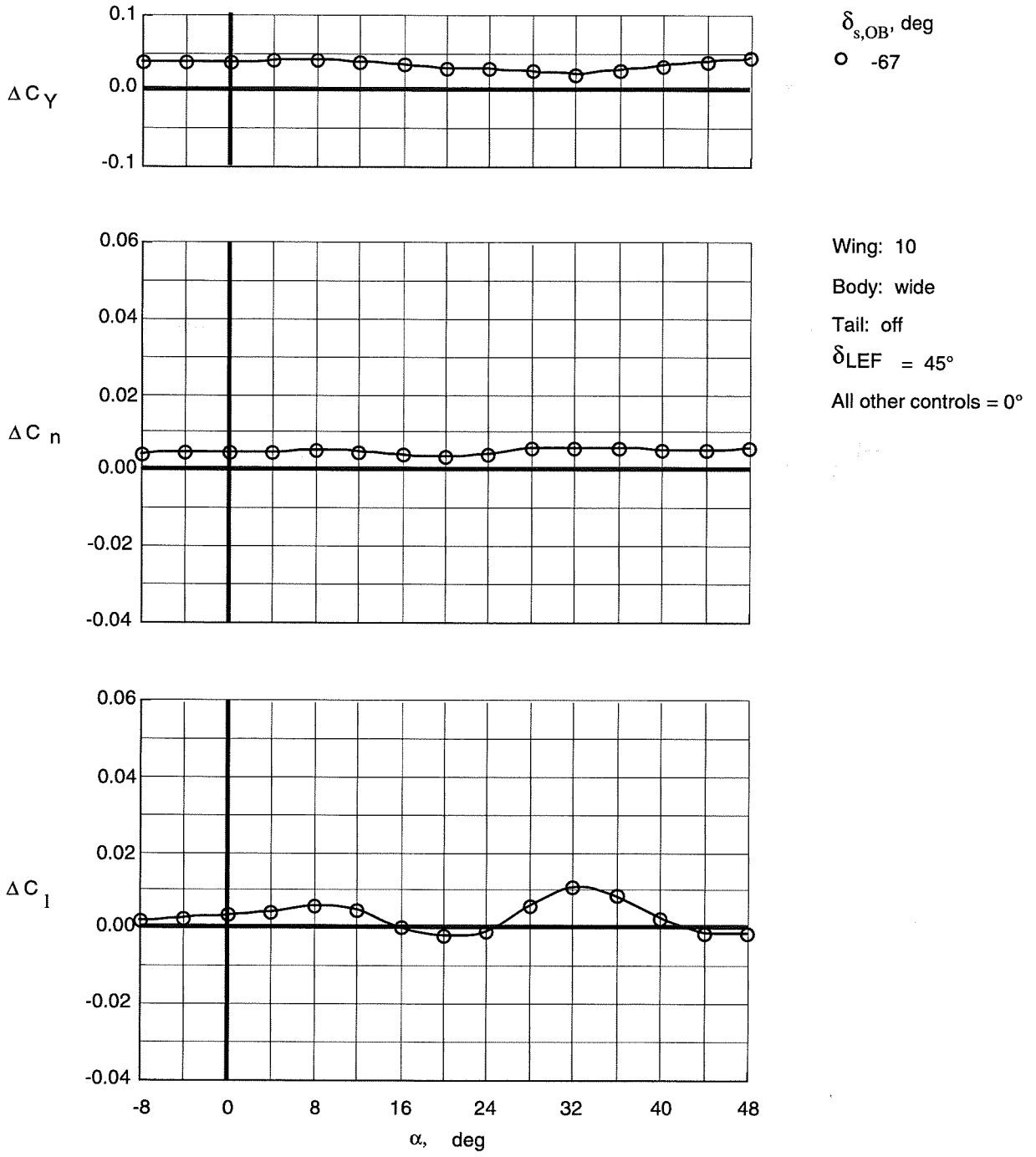

Figure 106. Control effectiveness of split deflection of right outboard trailing-edge flap on Wing 10 with wide top body on and leading-edge flaps deflected.

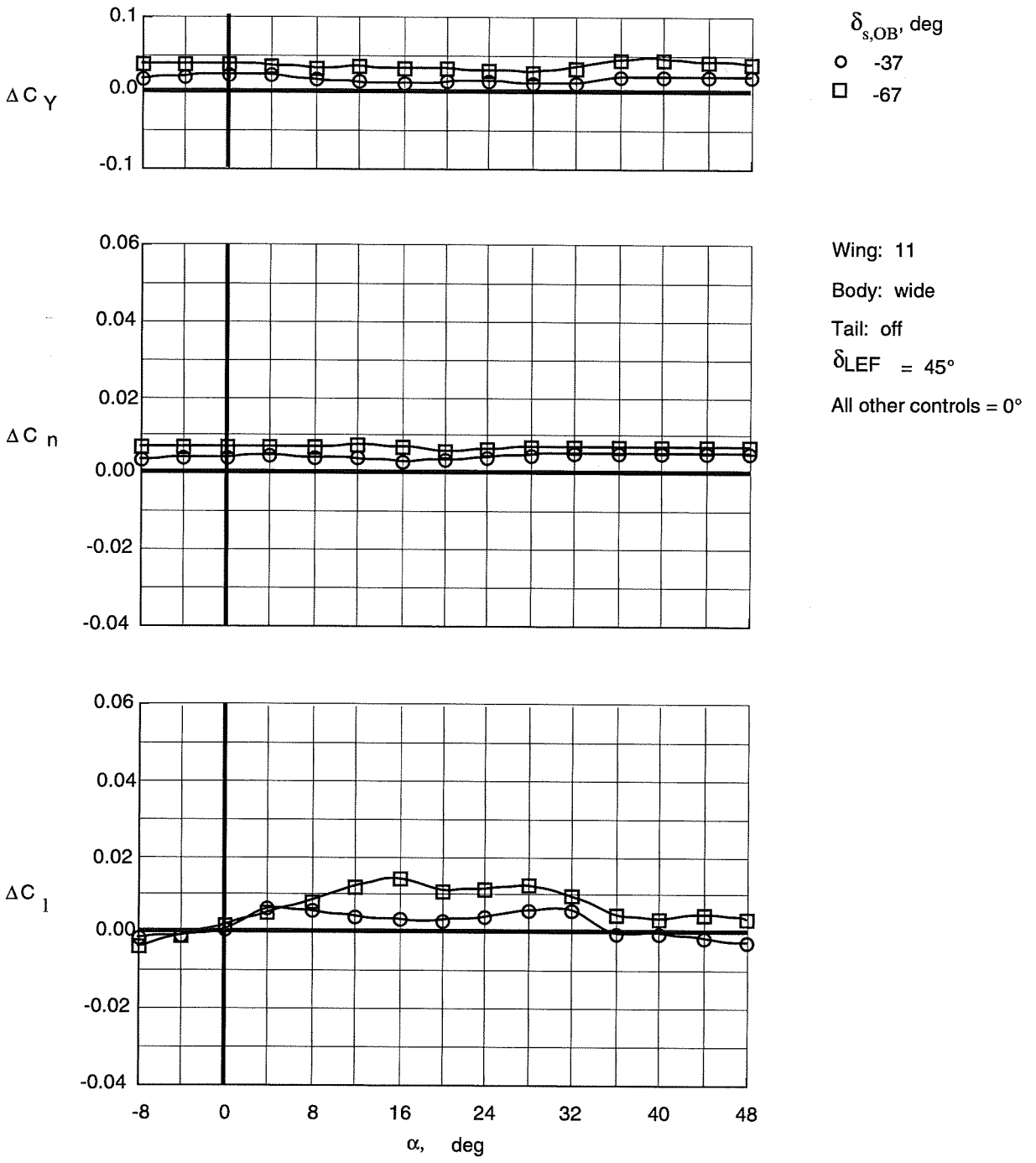

Figure 107. Control effectiveness of split deflections of right outboard trailing-edge flap on Wing 11 with wide top body on and leading-edge flaps deflected.

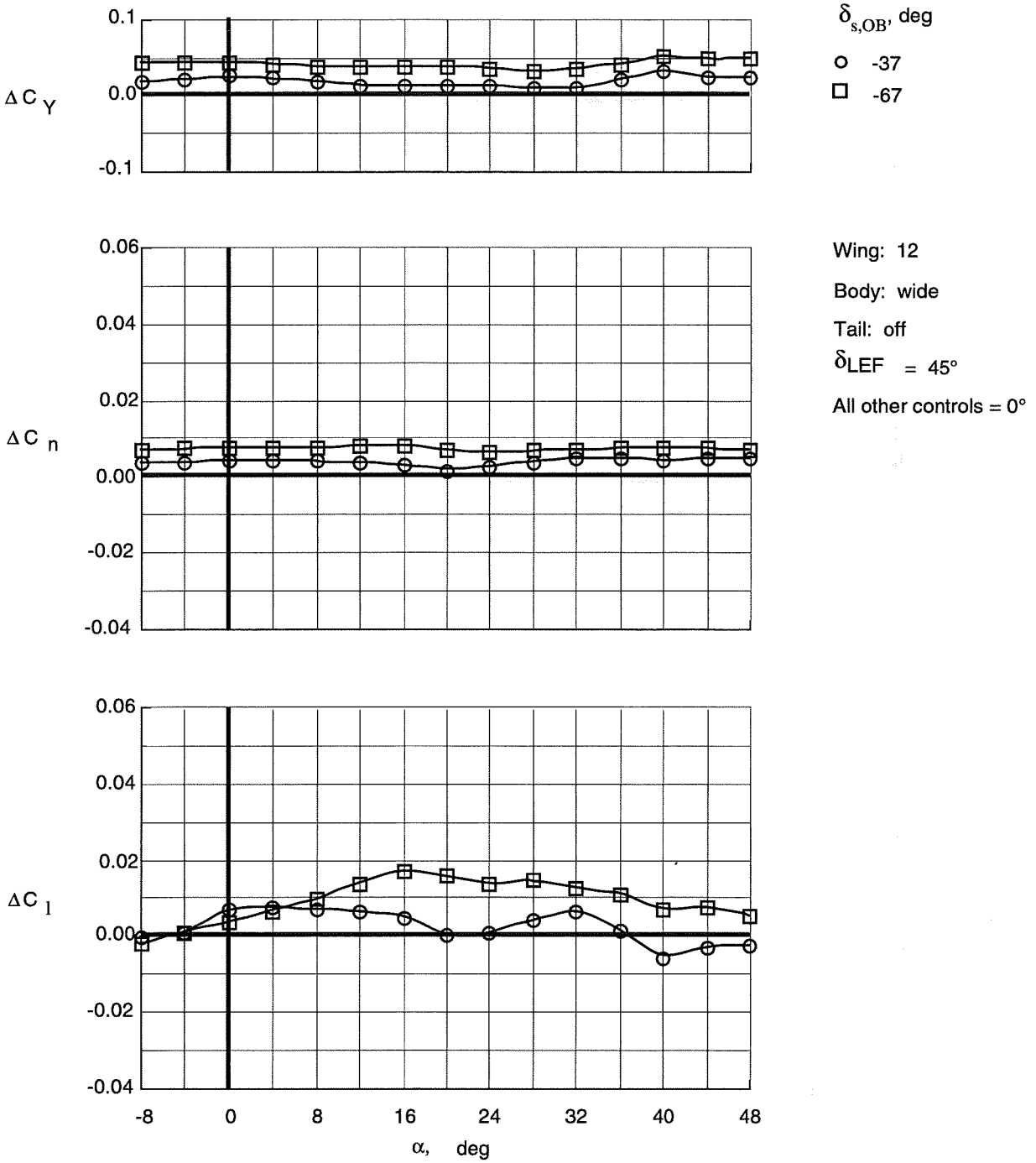

Figure 108. Control effectiveness of split deflections of right outboard trailing-edge flap on Wing 12 with wide top body on and leading-edge flaps deflected.

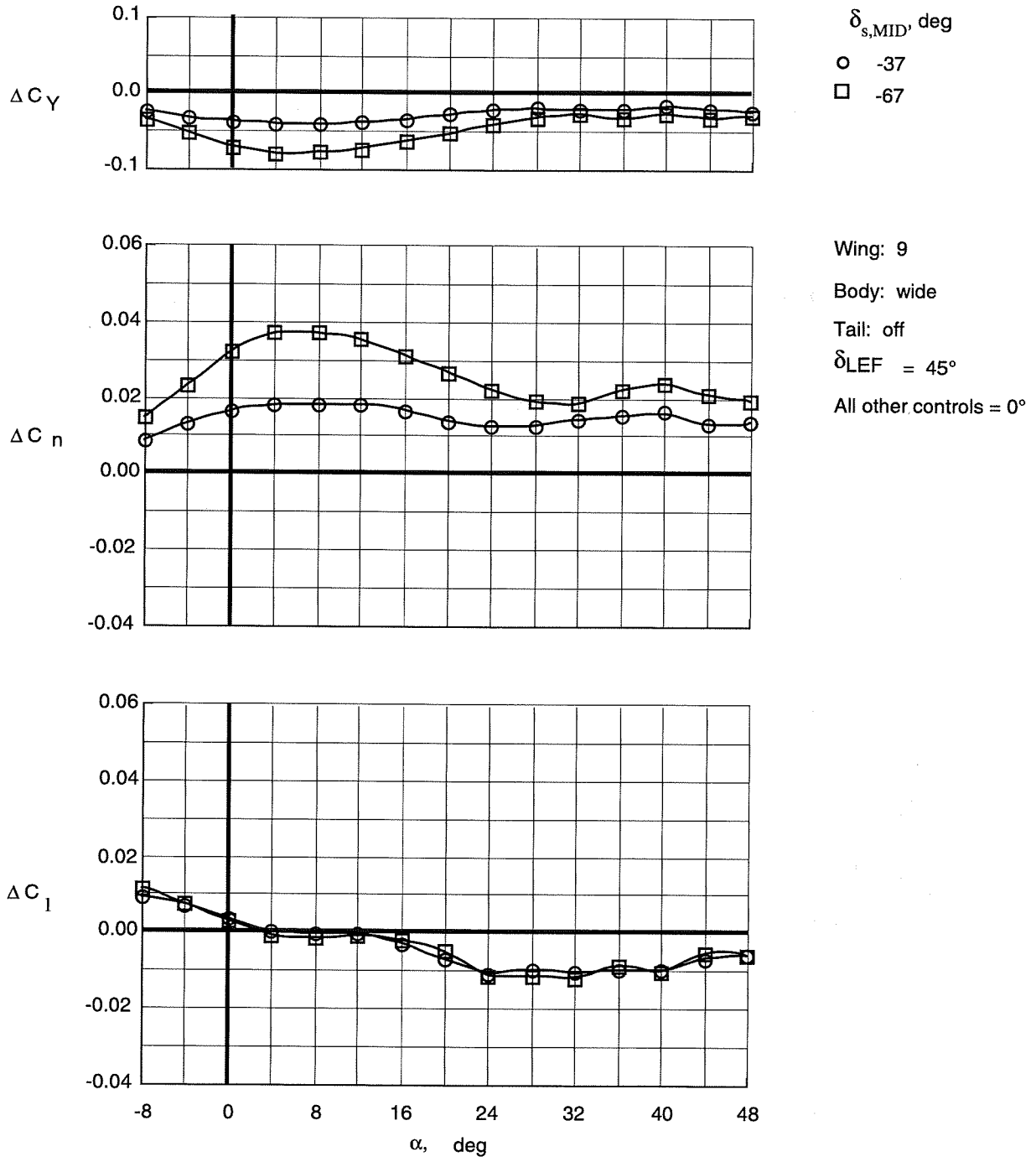

Figure 109. Control effectiveness of split deflections of right middle trailing-edge flap on Wing 9 with wide top body on and leading-edge flaps deflected.

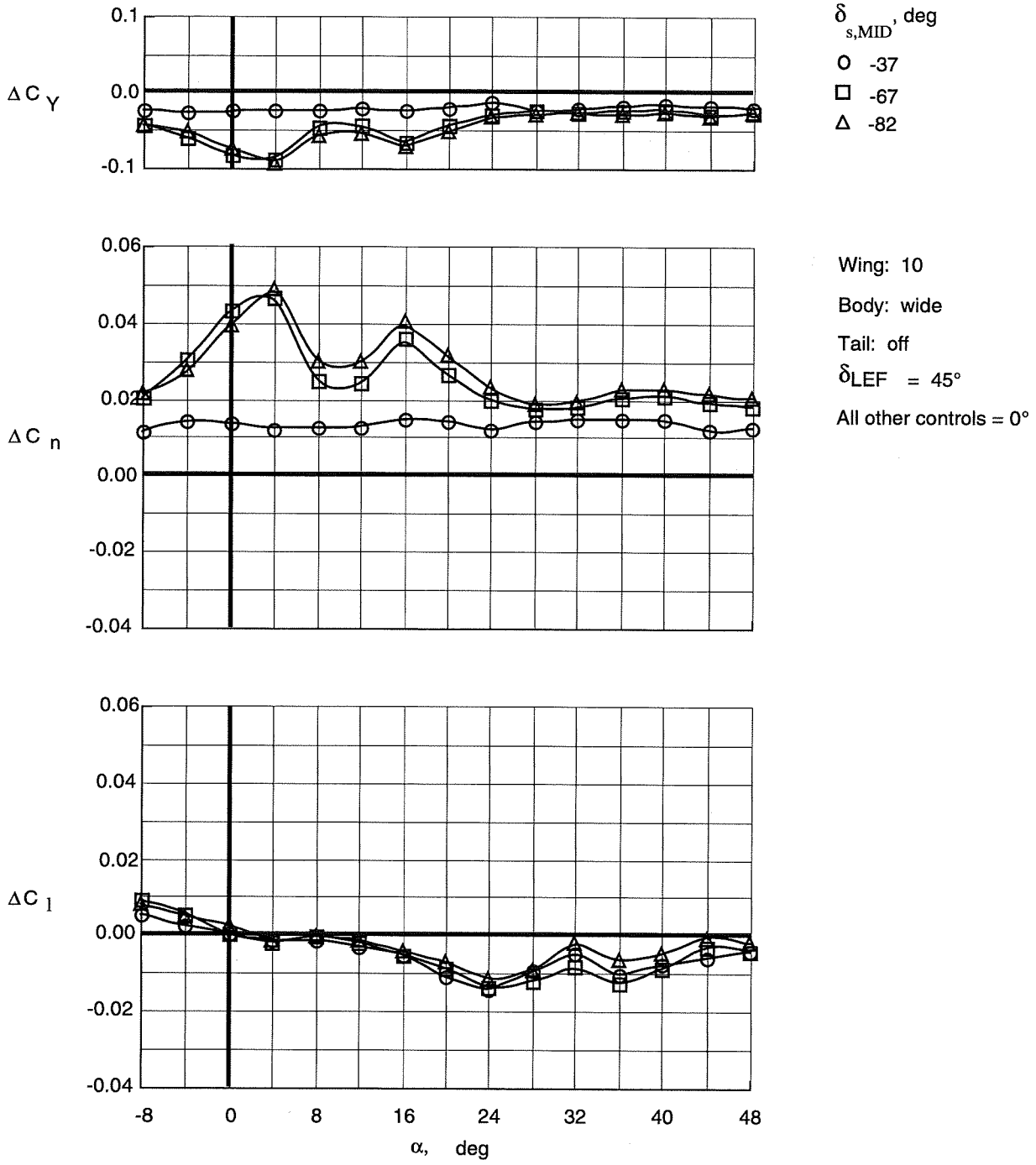

Figure 110. Control effectiveness of split deflections of right middle trailing-edge flap on Wing 10 with wide top body on and leading-edge flaps deflected.

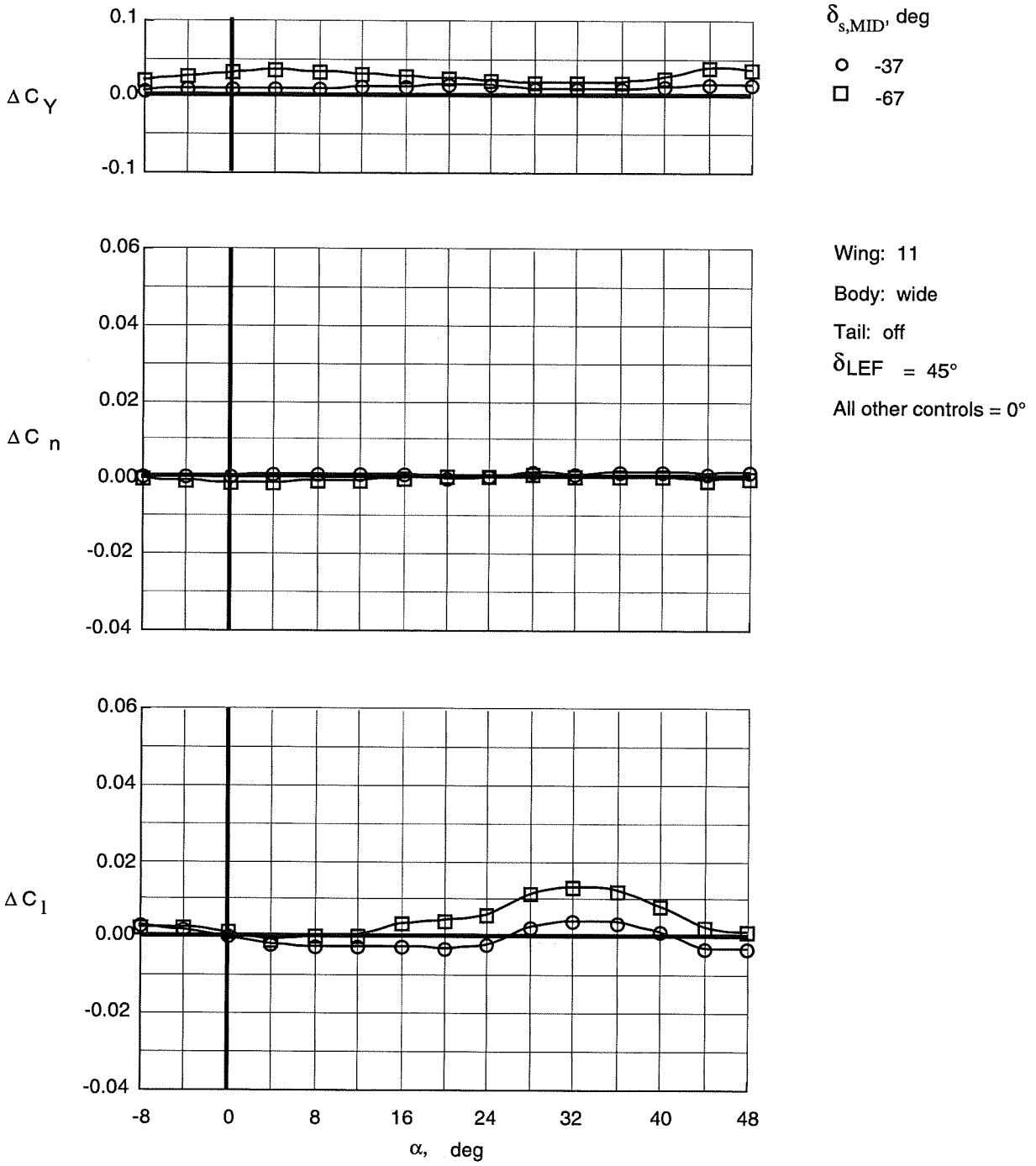

Figure 111. Control effectiveness of split deflections of right middle trailing-edge flap on Wing 11 with wide top body on and leading-edge flaps deflected.

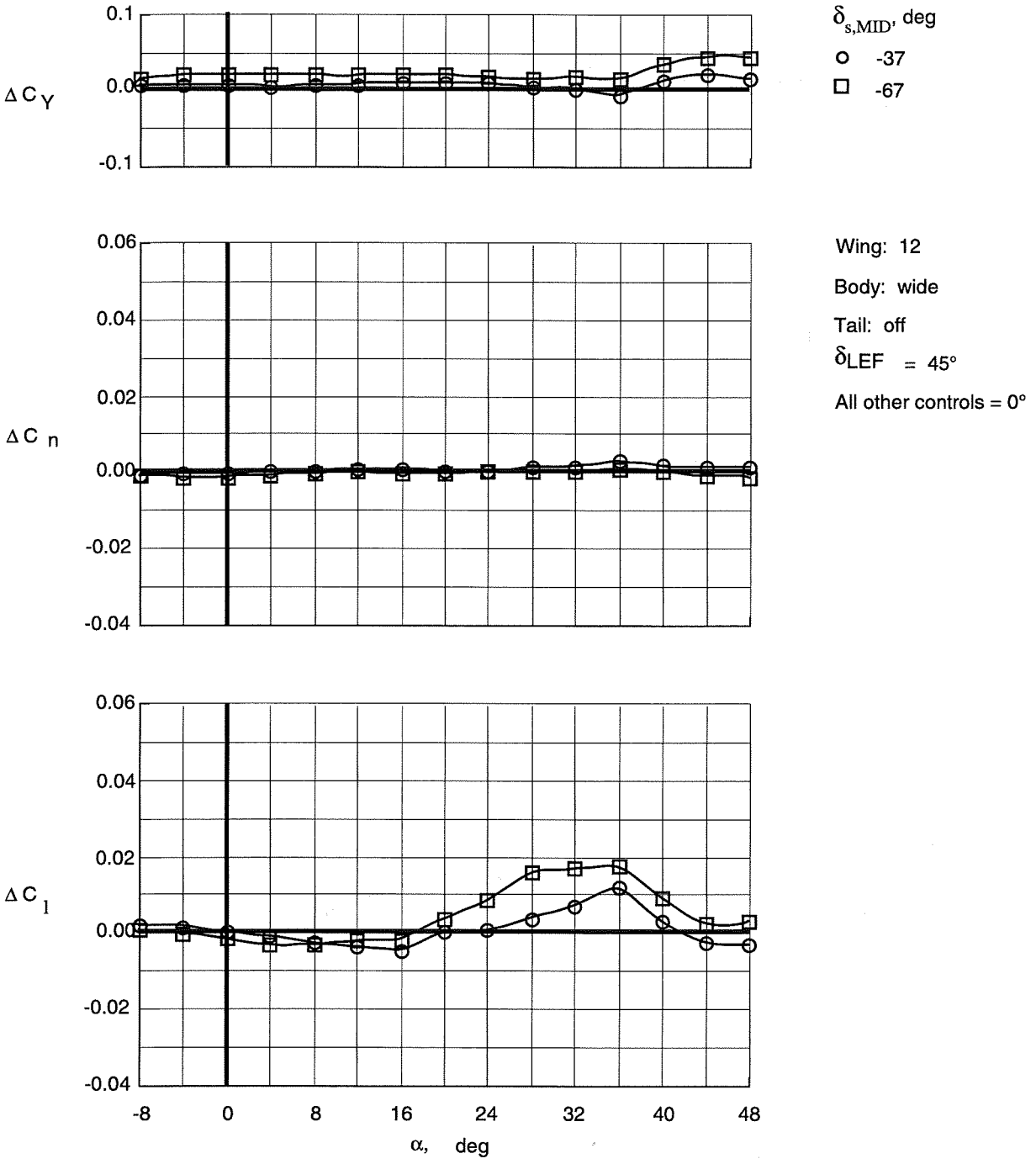

Figure 112. Control effectiveness of split deflections of right middle trailing-edge flap on Wing 12 with wide top body on and leading-edge flaps deflected.

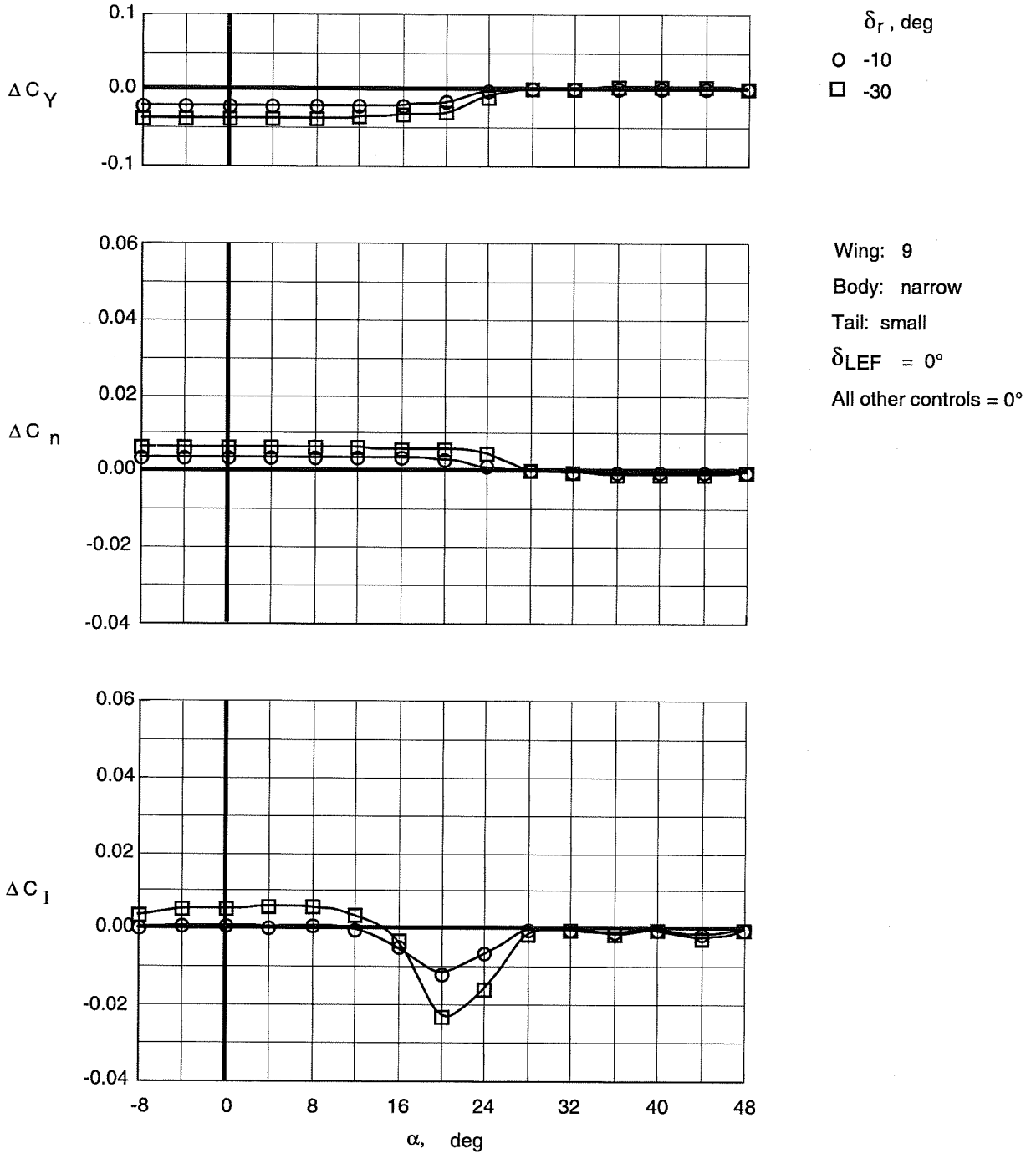

Figure 113. Control effectiveness of deflections of small vertical tails on Wing 9 with narrow top body on.

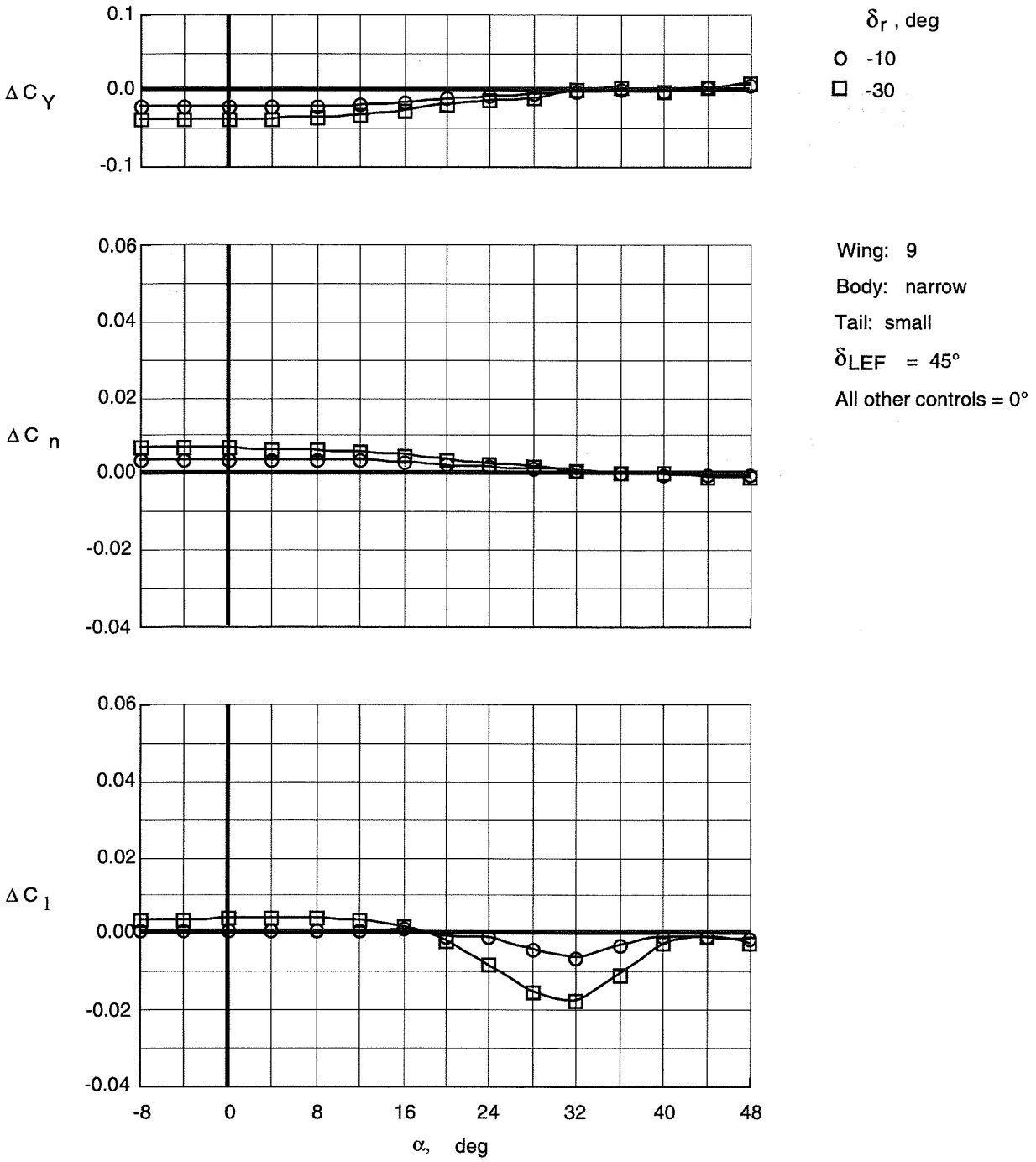

Figure 114. Control effectiveness of deflections of small vertical tails on Wing 9 with narrow top body on and leading-edge flaps deflected.

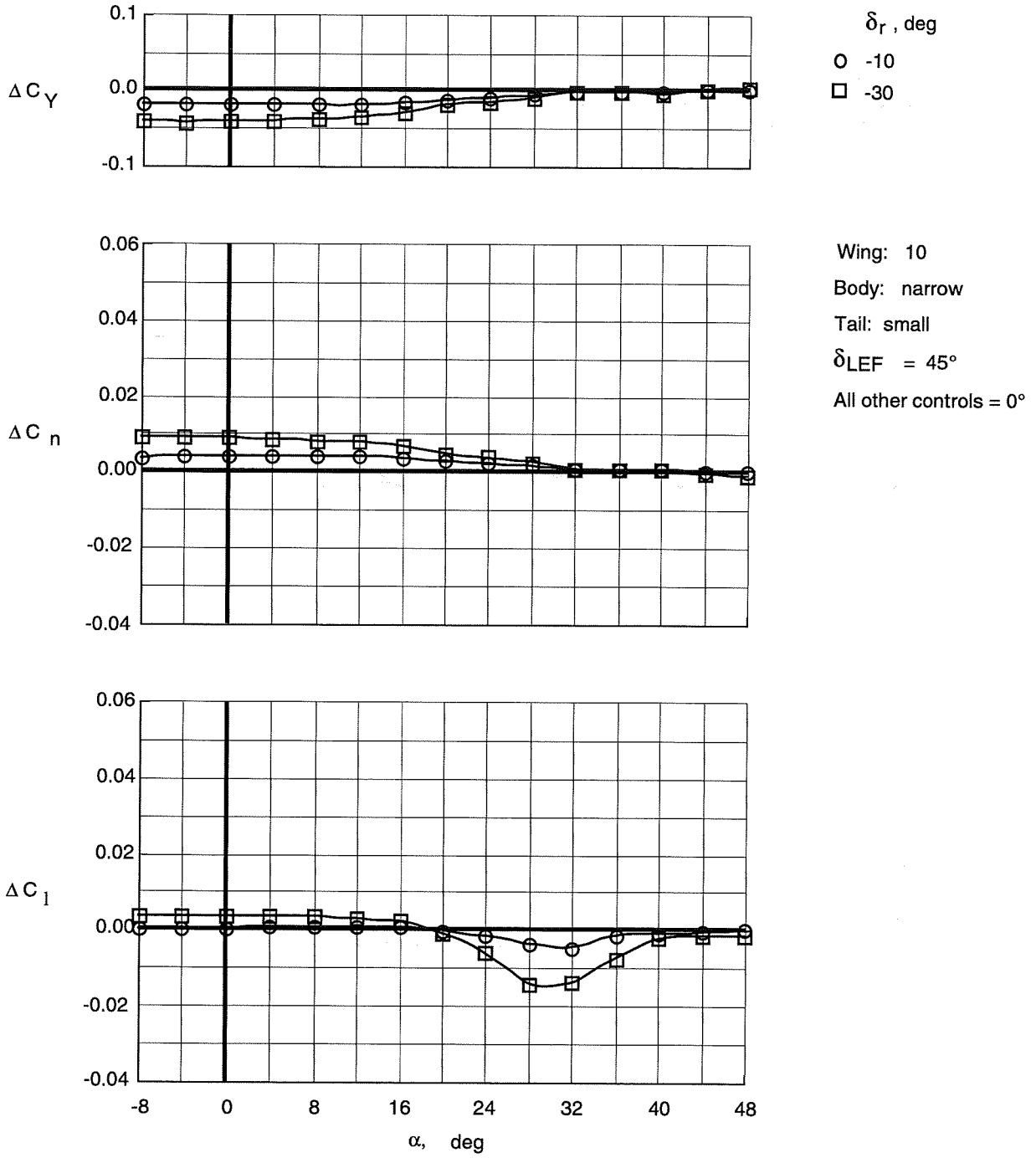

Figure 115. Control effectiveness of deflections of small vertical tails on Wing 10 with narrow top body on and leading-edge flaps deflected.

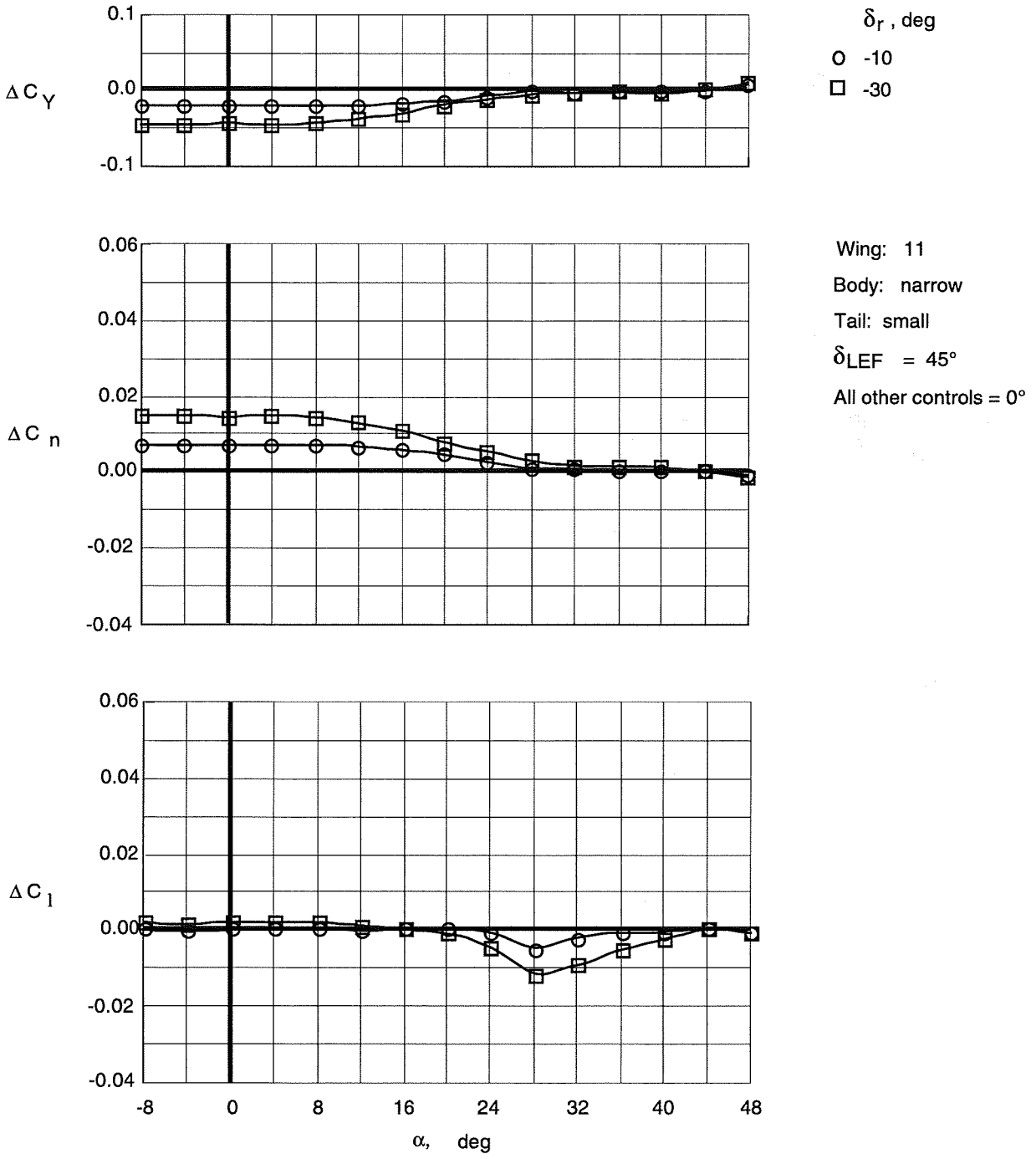

Figure 116. Control effectiveness of deflections of small vertical tails on Wing 11 with narrow top body on and leading-edge flaps deflected.

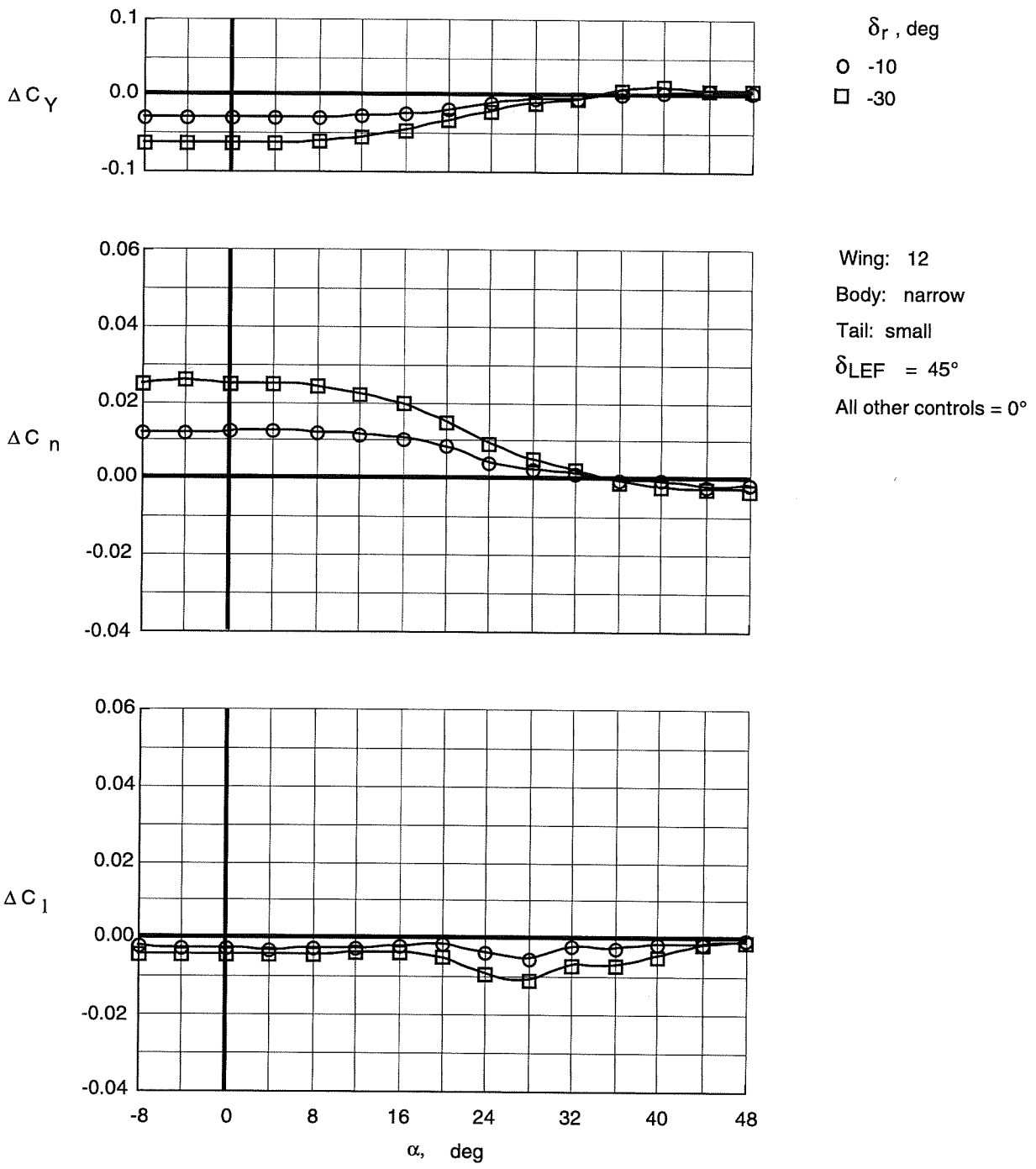

Figure 117. Control effectiveness of deflections of small vertical tails on Wing 12 with narrow top body on and leading-edge flaps deflected.

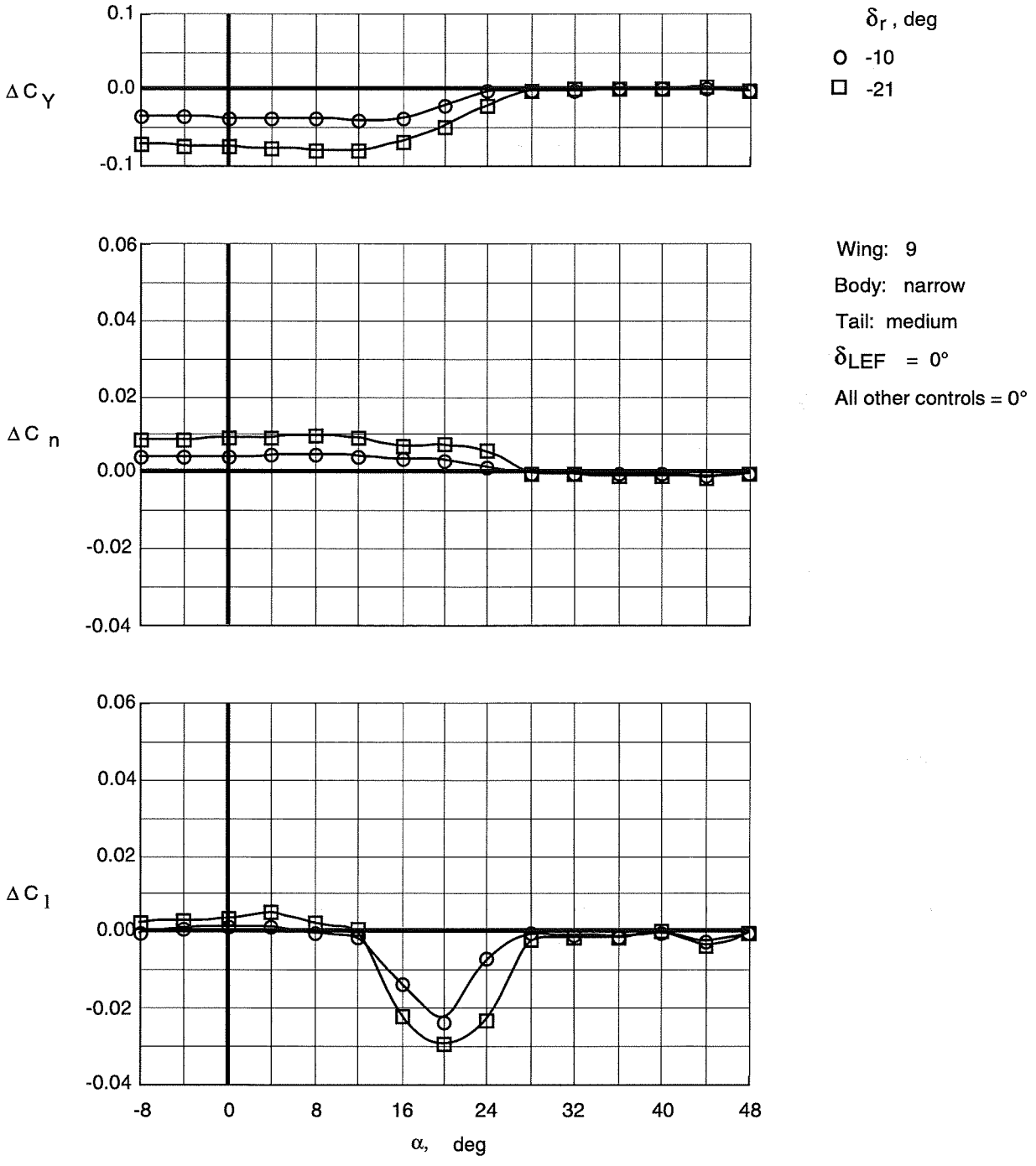

Figure 118. Control effectiveness of deflections of medium vertical tails on Wing 9 with narrow top body on.

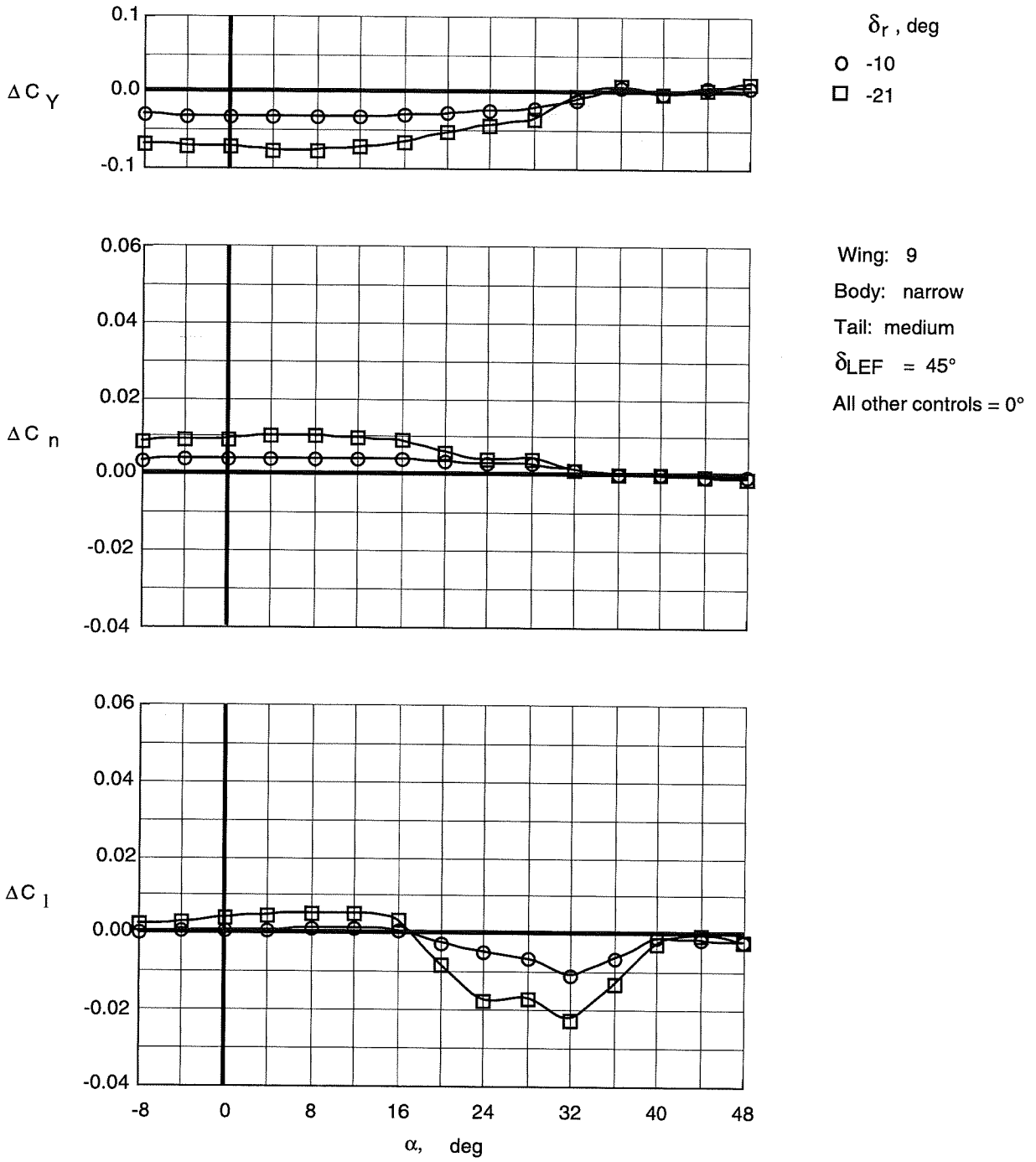

Figure 119. Control effectiveness of deflections of medium vertical tails on Wing 9 with narrow top body on and leading-edge flaps deflected.

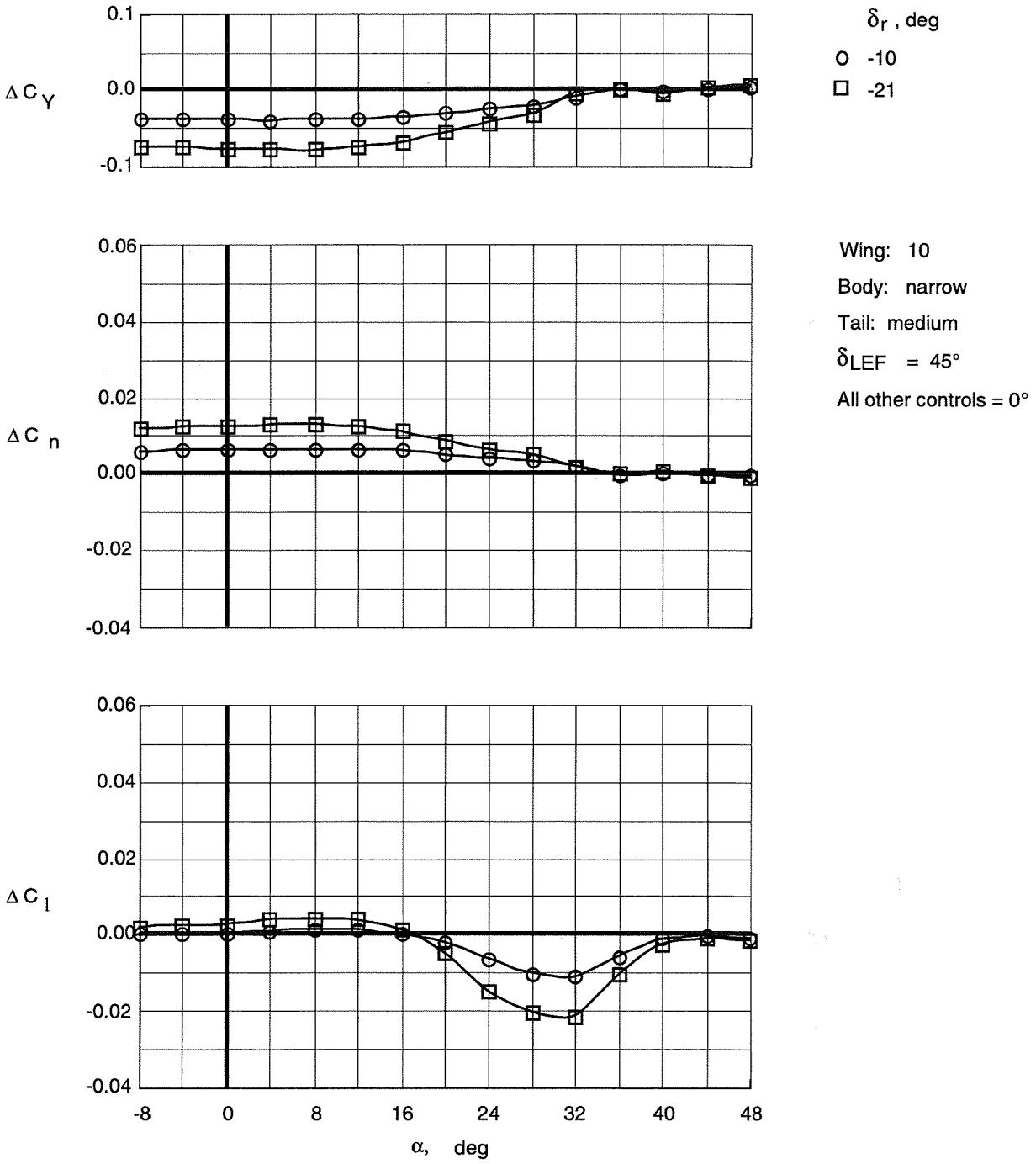

Figure 120. Control effectiveness of deflections of medium vertical tails on Wing 10 with narrow top body on and leading-edge flaps deflected.

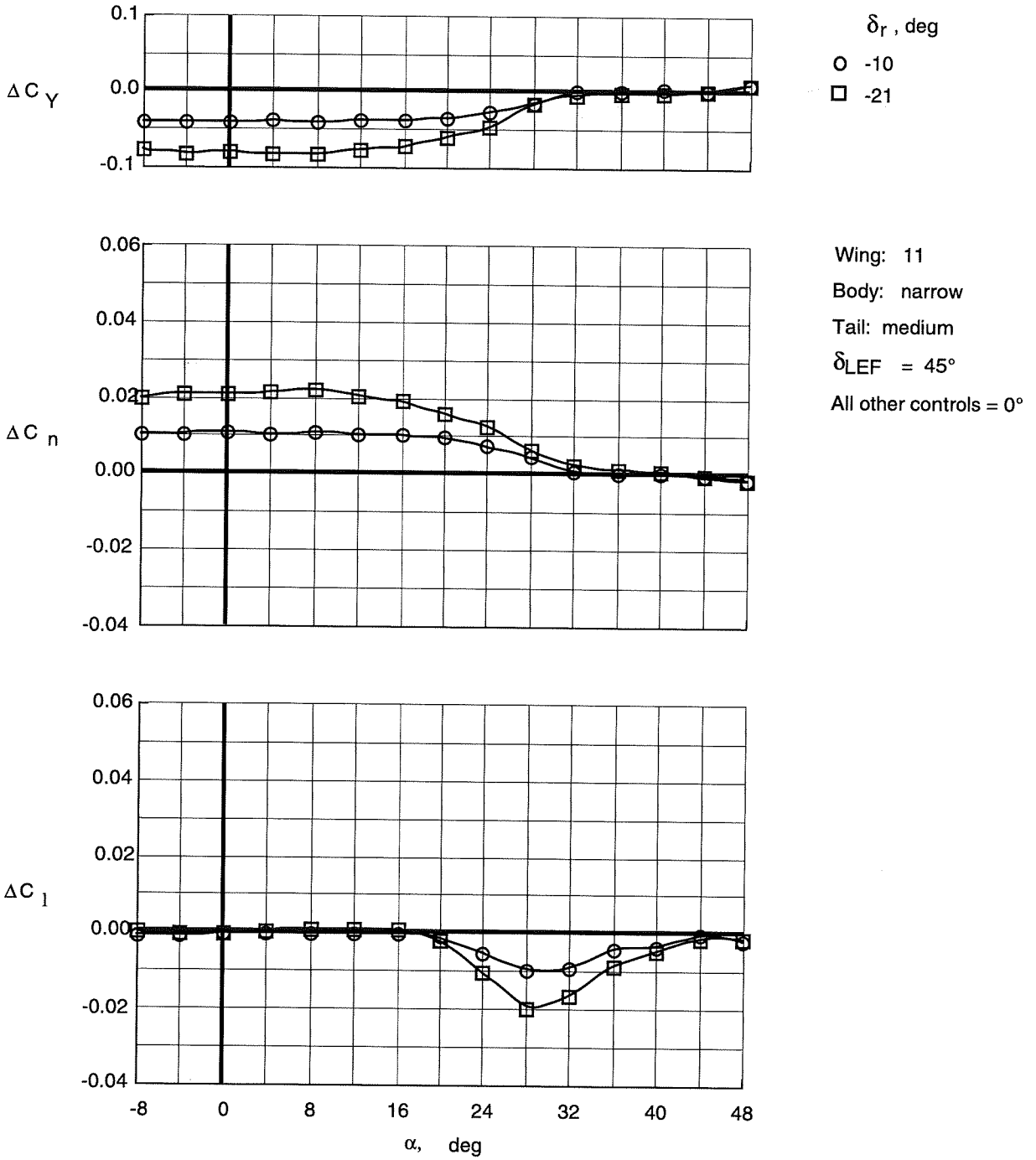

Figure 121. Control effectiveness of deflections of medium vertical tails on Wing 11 with narrow top body on and leading-edge flaps deflected.

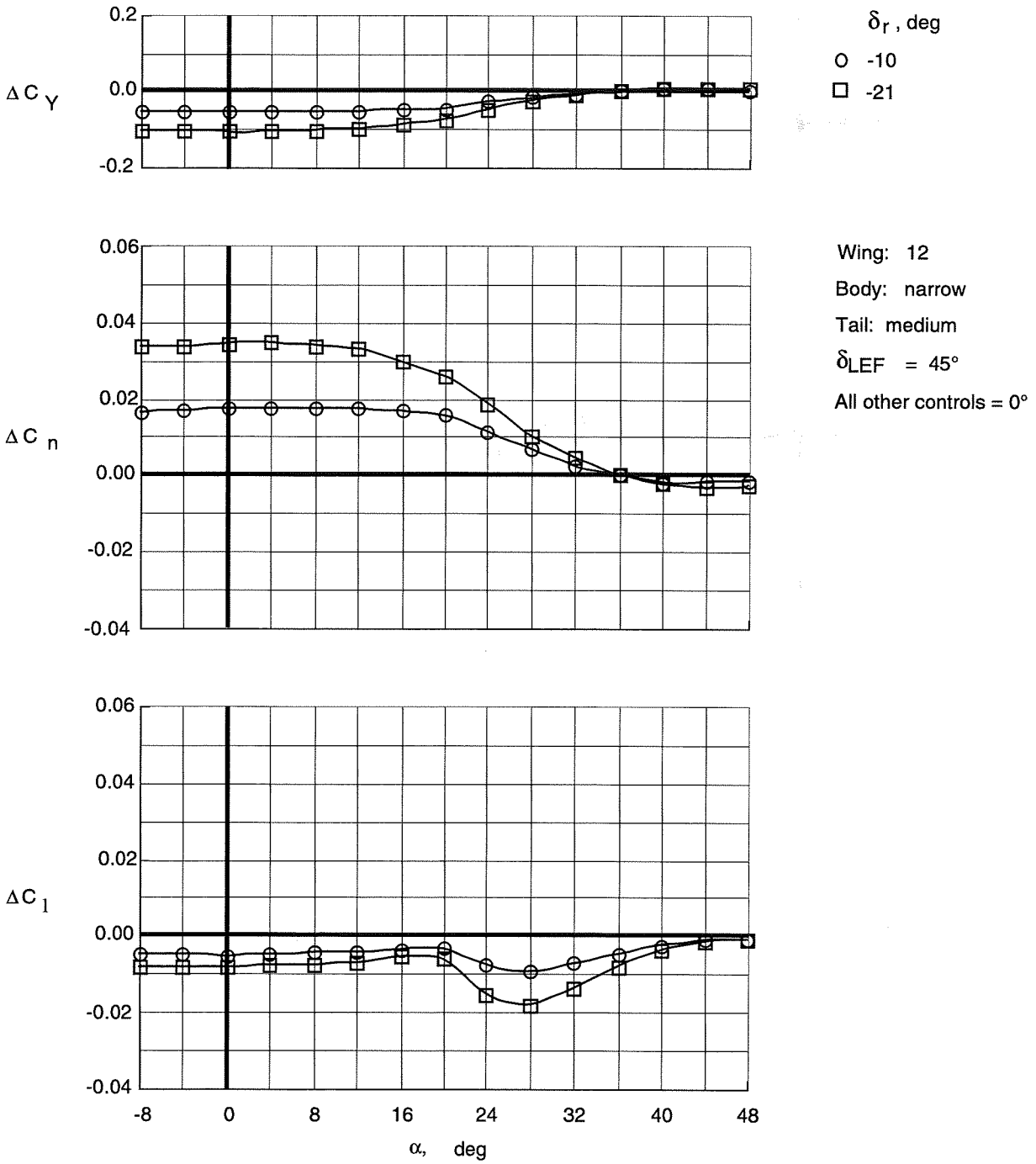

Figure 122. Control effectiveness of deflections of medium vertical tails on Wing 12 with narrow top body on and leading-edge flaps deflected.

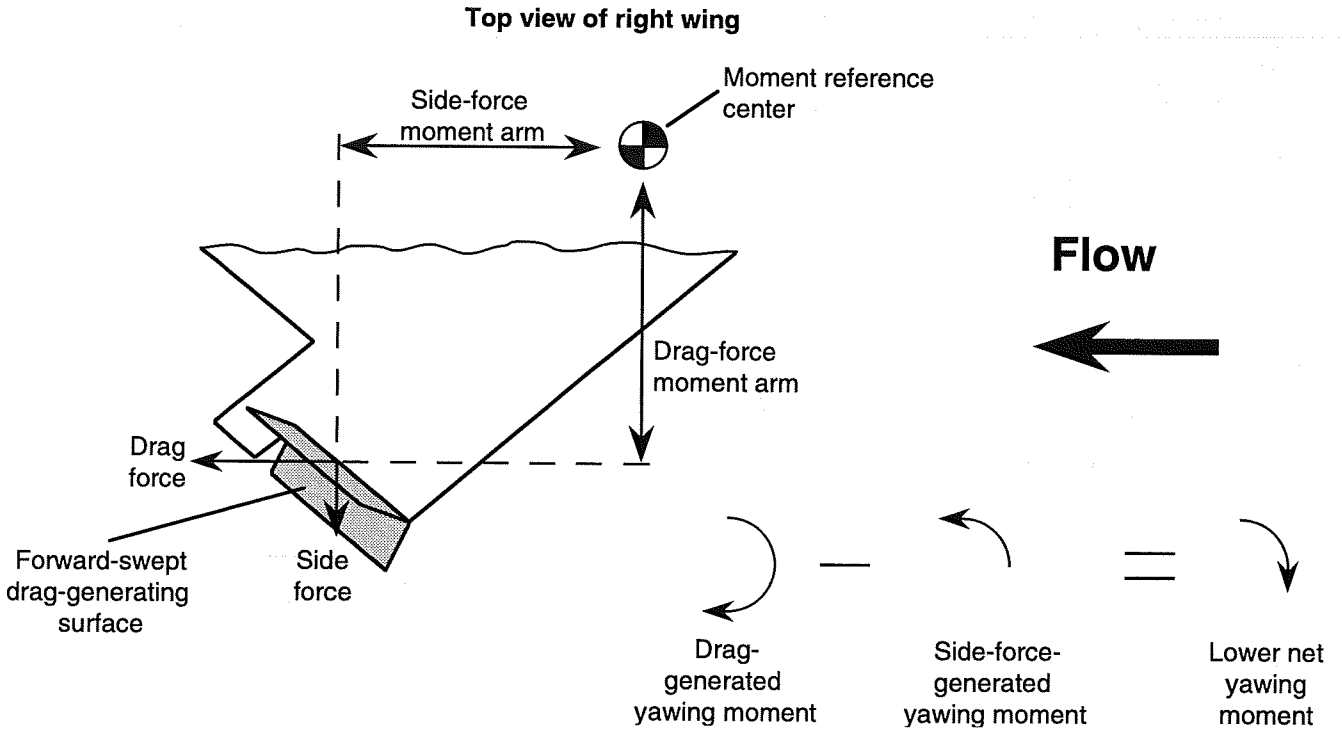

(a) Forward-swept drag-generating surface.

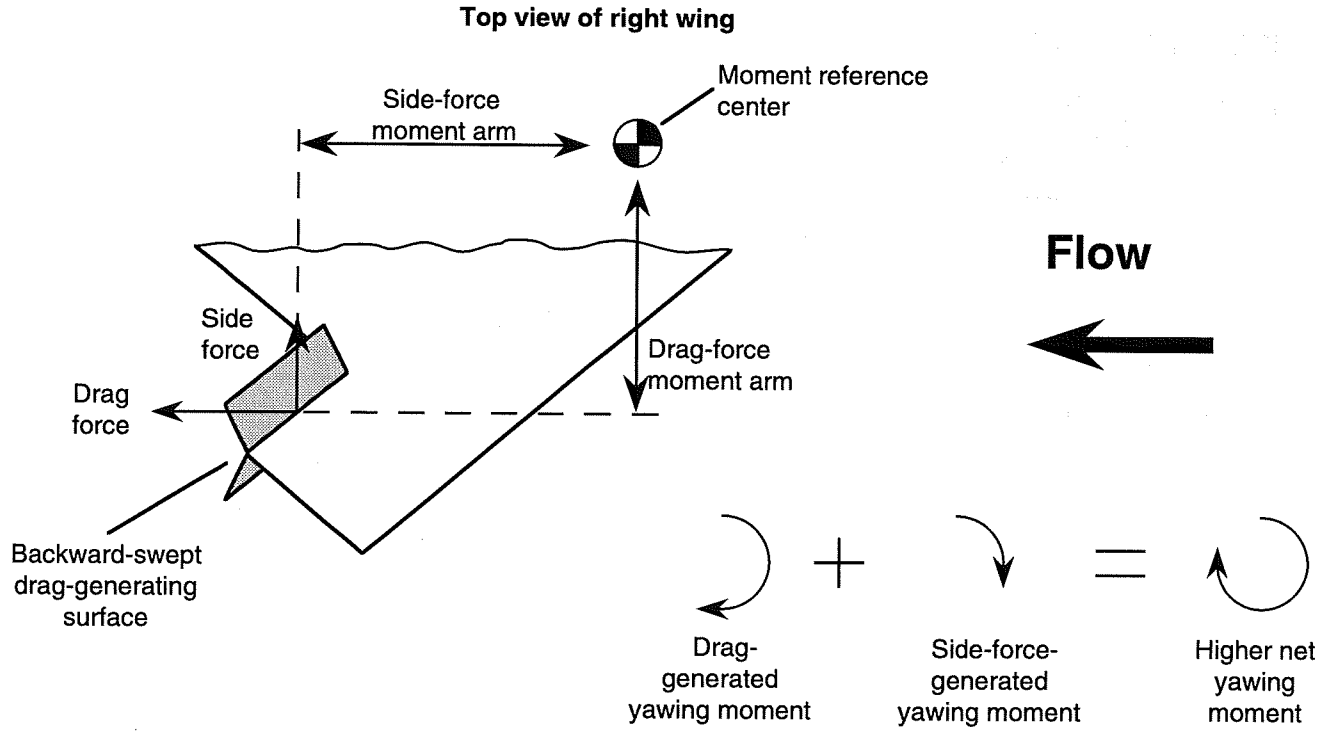

(b) Backward-swept drag-generating surface.

Figure 123. Effects of hinge line sweep of drag-generating yaw control on side force and associated yawing moment generated by control deflection.

REPORT DOCUMENTATION PAGE

Form Approved
OMB No. 0704-0188

1. AGENCY USE ONLY *(Leave blank)*	2. REPORT DATE	3. REPORT TYPE AND DATES COVERED
	June 1995	Technical Memorandum

4. TITLE AND SUBTITLE
Low-Speed Wind-Tunnel Investigation of the Stability and Control Characteristics of a Series of Flying Wings With Sweep Angles of 50°

5. FUNDING NUMBERS
WU 505-68-30-01

6. AUTHOR(S)
Scott P. Fears, Holly M. Ross, and Thomas M. Moul

7. PERFORMING ORGANIZATION NAME(S) AND ADDRESS(ES)
NASA Langley Research Center
Hampton, VA 23681-0001

8. PERFORMING ORGANIZATION REPORT NUMBER
L-17427

9. SPONSORING/MONITORING AGENCY NAME(S) AND ADDRESS(ES)
National Aeronautics and Space Administration
Washington, DC 20546-0001

10. SPONSORING/MONITORING AGENCY REPORT NUMBER
NASA TM-4640

11. SUPPLEMENTARY NOTES
Fears: Lockheed Engineering & Sciences Company, Hampton, VA; Ross and Moul: Langley Research Center, Hampton, VA.

12a. DISTRIBUTION/AVAILABILITY STATEMENT
Unclassified–Unlimited
Subject Category 05
Availability: NASA CASI (301) 621-0390

12b. DISTRIBUTION CODE

13. ABSTRACT *(Maximum 200 words)*

A wind-tunnel investigation was conducted in the Langley 12-Foot Low-Speed Tunnel to study the low-speed stability and control characteristics of a series of four flying wings over an extended range of angle of attack (–8° to 48°). Because of the current emphasis on reducing the radar cross section (RCS) of new military aircraft, the planform of each wing was composed of lines swept at a relatively high angle of 50°, and all the trailing-edge lines were aligned with one of the two leading edges. Three arrow planforms with different aspect ratios and one diamond planform were tested. The models incorporated leading-edge flaps for improved longitudinal characteristics and lateral stability and had trailing-edge flaps in three segments that were deflected differentially for roll control, symmetrically for pitch control, and in a split fashion for yaw control. Three top body widths and two sizes of twin vertical tails were also tested on each model. A large aerodynamic database was compiled that could be used to evaluate some of the trade-offs involved in the design of a configuration with a reduced RCS and good flight dynamic characteristics.

14. SUBJECT TERMS	15. NUMBER OF PAGES
Flying wings; Arrow wings; Diamond wings; Reduced radar cross section; Stability and control; High angle of attack	146
	16. PRICE CODE: A07

17. SECURITY CLASSIFICATION OF REPORT	18. SECURITY CLASSIFICATION OF THIS PAGE	19. SECURITY CLASSIFICATION OF ABSTRACT	20. LIMITATION OF ABSTRACT
Unclassified	Unclassified	Unclassified	